INTEGRATED MODELING AND HARDWARE-IN-THE-LOOP STUDY FOR SYSTEMATIC EVALUATION OF HYDRAULIC HYBRID PROPULSION OPTIONS

by

Young Jae Kim

A dissertation submitted in partial fulfillment
of the requirements for the degree of
Doctor of Philosophy
(Mechanical Engineering)
in The University of Michigan
2008

Doctoral Committee:

Research Associate Professor Zoran S. Filipi, Chair
Professor Dionissios N. Assanis
Professor Huei Peng
Associate Professor Jing Sun

To my parents,

To my beloved wife and daughter

ACKNOWLEDGMENTS

I sincerely thank to Professor Zoran Filipi for his unlimited support, instruction, and encouragement. His thorough guidance kept me on track throughout the research. I would also like to express my special appreciation to Professor Dennis Assanis. He accepted me in this great laboratory and gave me the inspiration for the doctoral study on the hybrid system. I also give my special thanks to Professor Huei Peng for invaluable lessons on the vehicle system control and allowing me to have the chance to study on the hybrid system control strategy and control optimization. I heartily appreciate Professor Jing Sun for allowing me to discuss about my humble study.

I also like to give my special thanks to Dr. Dohoy Jung for advising me how to study and live abroad. I would like to thank to hybrid team members. Especially, Dr. Fathy inspired me with his profound expertise on the hardware control. Jonathan and Ashwin did many Engine-in-the-Loop experiments with me. I would like to thank Jinming for sharing his broad knowledge and experience on the hybrid system and control and Rahul for his kind help in the vehicle modeling. I would also like to thank Fernando and Rajit for their sincere efforts and kindness when I need their support. And I specially thanks to Aris, Chris, Jason, Bruno, Hoon, Byungchan, Sangseok, Kyoungjun, Manbae, Taekyoung, Seunghwan, Sungjin, Chaitanya, Shriram, Hiro and all other Autolab members for me to live a happy laboratory life during the study.

I would like to give my special thanks to Keumjung Yoon, Taewoo Choi, Hyunjun Hong, Jerok Chun and other team members of Hyundai Motor Company in Korea.

My parents, they offered me their continuous love, support and encouragement throughout my study. I thank them for everything that they have done for me. Finally yet importantly, I must express a special word of appreciation to my wife, Hyounkyoung Yoon. Her love and sacrifice for me were the source of my research. Especially, my daughter, Hyunsoo, always gave me love and happiness.

TABLE OF CONTENTS

LIST OF FIGURES

LIST OF TABLES

LIST OF ABBREVIATIONS

4x4	4-wheel drive
a, b, c, α , γ , A_0, B_0, C_0, R	constants in Benedict-Webb-Rubin equation
A-ECMS	adaptive ECMS
AHS	GM-Allison hybrid system
APMS	aerosol particle mass spectrometer
β	oil bulk-modulus of elasticity [Pa]
BSFC	brake specific fuel consumption [g/kWh]
$BSNO_x$	brake specific NO_x [g/kWh]
BSsoot	brake specific soot [g/kWh]
BWR	Benedict-Webb-Rubin
CAD	crank angle degree
c_f	specific heat of foam [kJ/kgK]
C_f	coefficient of friction
CFD	computational fluid dynamics
C_h	coefficient of hydrodynamic loss
CO	carbon monoxide
CO_2	carbon dioxide
C_s	coefficient of laminar leakage
C_{st}	coefficient of turbulent leakage
c_v	constant volume specific heat of gas [kJ/kgK]
C_v	coefficient of viscous drag
CVT	continuously variable transmission
D	maximum P/M displacement per radian [m^3/rad]
DDP	deterministic dynamic programming
DMS	differential mobility spectrometer
DOE	design of experiment
ΔP	pressure difference between the accumulator and reservoir [Pa]
D_p	particle diameter
DP	dynamic programming
ECMS	equivalent consumption minimization strategy
ECU	engine control unit
EGR	exhaust gas recirculation
EMT	electro mechanical transmission
ESS	energy storage system
EIL	engine-in-the-loop
EPA	environmental protection agency
FE	fuel economy
FHS	Ford hybrid system

FSN	AVL smoke meter number
FUDS	federal urban driving schedule
g_k	cost incurred at time
HEV	hybrid electric vehicle
HHV	hydraulic hybrid vehicle
HIL	hardware-in-the-loop
HMMWV	high mobility multipurpose wheeled vehicle
HWFET	highway fuel economy test
ICE	internal combustion engine
J	minimized total cost
k	discrete time index
K_i	integral gain
K_p	proportional gain
LHV	low heating value
μ	oil dynamic viscosity [Ns/m^2]
m_f	foam mass [kg]
m_g	gas mass [kg]
$\dot{m}_{air}$	mass flow of air [kg/s]
$\dot{m}_{fuel}$	mass flow of fuel [kg/s]
$\dot{m}_{NO_x}$	mass flow of NO_x [kg/s]
M/G	motor/generator
MPG, mpg	mile per gallon
MPH, mph	mile per hour
MW_{NO_x}	molar mass of NO_x
$MW_{exhaust}$	molar mass of exhaust gas
N	horizon or number of times
NLSQP	non-linear sequential quadratic programming
NO_x	oxides of nitrogen
NYCC	New York city cycle
O_2	oxygen
π^*	optimal policy
PHH	parallel hydraulic hybrid
p_g	gas absolute pressure [kPa]
PM	particulate matter
P/M	pump/motor
PCM	powertrain control module
PSHH	power-split hydraulic hybrid
Q_a	actual flow rate [m^3/sec]
ρ	oil density [kg/m^3]
RTCS	real-time control strategy
SC03	part of the US EPA's supplemental federal test procedure
SDP	stochastic dynamic programming
SHH	series hydraulic hybrid
SMPS	scanning mobility particle sizer

SOC	state of charge
SOF	soluble organic fraction
SQP	sequential quadratic programming
T	absolute gas or foam temperature [K]
T_a	actual torque [Nm]
THC	total hydrocarbons
THS	Toyota hybrid system
T_w	accumulator wall or bladder temperature [K]
UDDSHDV	EPA urban dynamometer driving schedule for heavy-duty vehicles
v	gas specific volume [m^3/kg]
VESIM	vehicle engine simulation
ω	angular velocity [rad/sec]
$\omega_{eng,ref}$	demand engine speed [rad/sec]
$\omega_{eng,current}$	engine speed measurement [rad/sec]
U	set of the plausible controls
u_k	control or decision variable to be selected at time k
VGT	variable geometry turbocharger
w_k	random parameter (also called disturbance or noise)
WVUCITY	West Virginia city driving schedule
WVUINTER	West Virginia interstate driving schedule
WVUSUB	West Virginia suburban driving schedule
x	displacement factor
x_k	state of the system

ABSTRACT

The fuel economy benefits of any given hybrid technology depend greatly on the vehicle type, size, supervisory control and driving schedule. The main goal of this work is to develop a comprehensive methodology for up-front strategic assessments of the best hybrid system for a given vehicle platform, and to explore the impact of vehicle driving schedules on the final decision. Several other objectives enabled achieving the main goal, including modeling, optimization of design and power management of several hydraulic hybrid systems developed for a 4x4 light truck.

The parallel, series and power-split hybrid configurations are modeled and analyzed. The unique issues related to matching of components and interactions in the system with a high-power density of pump/motors and the energy storage (accumulator), but relatively low energy density of the storage and limited motor speed range are investigated. The design optimization is carried out to maximize the fuel economy while satisfying vehicle performance constraints. An Engine-in-the-Loop capability is developed for each of the hybrid architectures, integration issues are resolved and the EIL is subsequently used for validation of simulation predictions and studies of the impact of hybrid system configuration and control on diesel emissions.

For the power management optimization, the deterministic dynamic programming technique provides the fuel economy benchmark. Stochastic dynamic programming technique is explored next, in order to develop an implementable sub-optimal supervisory control policy based on the vehicle power demand probability distribution sampled from various driving schedules. The simulation results obtained over the wide range of driving schedules from aggressive city cycles to mild highway cycles provided fuel economy trends and comparison of hybrid propulsion options. Fuel economy improvements of ~80% (up to 150% with engine shutdowns) are shown for aggressive city-cycles, while the gains diminish for high-speed highway driving. Verification of the emission reduction potential is enabled by synergistic experiments using a newly developed

engine-in-the-loop capability. The results provide insight into the effects of the hybrid power management on transient emissions of soot and nitric oxides from a diesel, and provide guidance for the development of strategies for achieving both clean and efficient hybrid propulsion.

CHAPTER 1

INTRODUCTION

1.1. Motivation

Designing high fuel economy cars and trucks is one of the most challenging goals for automotive engineers. Fossil fuel reserves are globally limited, but total consumption for transportation keeps increasing, as do fuel prices. As a result, fuel economy becomes one of the most important factors in the market. In addition, fuel economy corresponds directly to greenhouse gas amounts, such as CO_2, which causes global warming, and that has recently become a significant societal issue. Through increasing fuel economy, the possibility of reducing total emissions also increases. However, the automotive manufactures need to maintain high vehicle performance that consumers expect.

One of the solutions to overcome such intense challenges is the hybridization of vehicles. Hybrid vehicles use secondary energy storage, e.g., battery, hydraulic accumulator and flywheel, and a secondary power device, e.g., electric motor/generator (M/G) and hydraulic pump/motor (P/M). Efficient power management of these secondary power devices provides an additional degree of freedom to operate the engine, so that the engine operation can be designed to improve the fuel economy, emission reduction or vehicle performance. Moreover, the ability to choose specific engine operation range allows engineers to focus on the smaller engine range in the process of engine system development and calibration. However, the vehicle system becomes more complicated when it is hybridized.

Hybridizing light-duty trucks including Sports-Utility-Vehicles (SUVs) can be more beneficial than hybridizing passenger cars in the long run. Firstly, because the number of trucks purchased is increasing, their total fuel consumption rate is increasing; whereas the number of passenger cars purchased remains stable, as does the total fuel consumption (see Figure 1. 1). Therefore, the fuel-saving effects are larger in the case of trucks. Finally, an additional factor in truck applications is the fact that trucks operate long hours

and therefore accumulate many miles during the year; hence, the savings per vehicle can have a relatively larger impact than in the case of passenger cars. Commercial trucks spend a lot of time on the road, hence their annual fuel consumption per vehicle is very large and impact of fuel economy reduction is magnified.

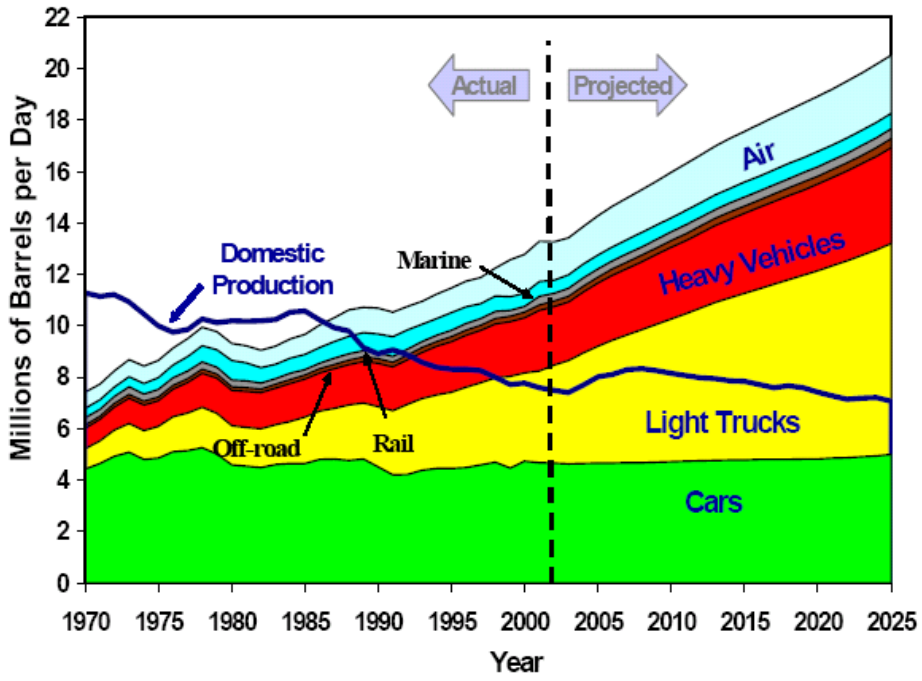

Figure 1. 1. Transportation petroleum use by mode and production [1]

However, improving the fuel economy is very limited in the case of truck. Thus, the powertrain hybridization might be the only way to achieve significant gains. The internal combustion engines that most trucks are already very fuel-efficient diesel engines. Hybridization, however, can optimize the system by orchestrating the diesel power and secondary power, e.g., electric and hydraulic. Thirdly, the payload dictates truck weight. In addition, lightweight structures are not usually considered as a way to reduce fuel consumption, as they are with cars, because of safety reasons. There are also limits to reducing the aerodynamic drag of trucks to improve fuel economy and vehicle performance. However, large vehicle mass implies large amounts of kinetic energy that can be recuperated during braking and this is a huge opportunity for hybrid concepts.

Consequently, hybrid powertrains promise significant improvement in the fuel economy of light-duty trucks. Many carmakers are already adding hybrid vehicles, mostly electric, to their existing line-ups of conventional vehicles. To the contrary, the

truck market is largely untapped, and yet it offers a chance for a huge impact with new hybrid systems and hybrid devices. A number of research questions need to be answered before the best technology for the truck market emerges. The questions include, firstly, what architectures and energy conversion options are the most promising for truck application and, secondly, how we can determine the true potential of any given option in order to be able to provide realistic quantitative comparisons.

In this study, the potential of the hydraulic hybrid will be determined for the various configurations with design and power management optimization. Even though the hydraulic hybrid has so far received less attention, the hydraulic hybrid application can capture more regenerative braking with better efficiency and provides the same vehicle power demand with relatively less mass addition due to its inherently high power density and comparatively high energy-conversion efficiency in comparison with electric hybrid. This is why the focus is on hydraulic energy conversion and storage option.

This provided a wide un-explored area of research, since the application of the hydraulic device into the vehicle hybridization is not widespread. With the development in the high-speed valve and electronic control system, the hydraulic hybrid becomes viable. Designs of prototype vehicles that have been pursued by the environmental protection agency (EPA) indicate a strong potential for fuel economy improvement [2].

1.2. Objectives and Scope

This study proposes to develop a comprehensive methodology for design, optimization and analysis of three main hybrid systems, parallel, series and power-split hydraulic hybrid powertrain. The study demonstrates the methodology including the optimization of supervisory powertrain control strategy or power management on case studies covering the most relevant hydraulic hybrid propulsion concepts. Applying the methodology for up-front strategic assessment of the best hybrid system for a given vehicle platform will yield guidance related to selection of the preferred hybrid system for different dominant duty cycles. More details about candidate architectures are also given.

The main objective of this study requires a number of advanced modeling and simulation capabilities, as well as methodologies for optimization of design and finding globally optimal power management strategies. In addition, the methodologies for

coupling the real engine to the hybrid system simulation is deemed necessary for validation of simulation result with the engine-in-the loop (EIL) setup and generating insight into the impact on transient diesel emissions.

In any hydraulic hybrid system, the propulsion hydraulic system and energy storage are size based on the vehicle performance requirements. However, intuitive engineering decisions are difficult to make for the critical designs parameters affecting optimal fuel economy while satisfying all constraints regarding vehicle performance because the complexity and the degrees of freedom in vehicle system increase tremendously. An optimization algorithm is required to select the best combination of design parameters for a given objective. In case of the hybrid vehicle, a complete vehicle simulation is executed over the driving cycle in each function evaluation. The optimization using efficient gradient-based algorithms will be setup for each of the hybrid architectures considered.

Optimized design is only a first step in maximizing the fuel economy potential of a given hybrid system. The power management, i.e. a strategy for coordination and control of the multiple power sources on board, has a critical impact on the hybrid vehicle behavior and efficiency of propulsion. The techniques for global optimization and establishing the optimal benchmark will be explored. The vehicle studies under realistic driving conditions require robust, control strategies, implementable in real-time. Hence, possibilities for direct development of sub-optimal power management with full-state feedback are considered. In particular, the approach that incorporates the probability of driver action holds a promise of providing a strategy suitable for direct implementation, rather than requiring extraction of rules from the benchmark strategy.

Finally, the impact of the hydraulic hybrid system design and supervisory control on transient diesel emission will be investigated using synergistic experiments in the diesel engine test cell. The models of soot formation in diesel combustion with sufficient predictiveness and computational efficiency for system-level studies are not available. Hence, creating realistic transient operating condition in the test cell, and application of advanced emission analyzers is necessary to provide insight into emissions The Engine-in-the-Loop capability will be developed for this purpose and for in-depth validation of simulation predictions. The methodology of applying the EIL capability is valuable itself

because the EIL setup involves the profound understanding of the engine and transient dynamometer test cell environment. However, integration of the simulation and real hardware poses unique challenges for each of the hydraulic hybrid configurations, and those will be addressed systematically in order to provide safe and reliable methodology supported by real-time models. After challenges regarding the EIL setup are overcome, this innovative technique will be capable of shedding light on transient phenomena of a diesel engine regarding fuel consumption and emissions. Power management strategies will be evaluated in terms of real-world controllability and driver's comfort through observed real engine behavior through the EIL test in the future study. The different engine behaviors in hydraulic hybrid system from those of conventional vehicles, e.g., frequent engine speed and load changes, may cause noise and vibration problems and make drivers feel uncomfortable.

In summary, this study demonstrates the complete methodology in case studies of parallel, series and power-split hydraulic propulsion system for a Class IIB truck, such as the High Mobility Multipurpose Wheeled Vehicle (HMMWV): a dual-use medium-duty truck, including optimal design and power management strategy and validation with EIL tests. This study confirms the value of a comprehensive methodology for quantifying the benefits of hybrid systems using hydraulic propulsion systems.

1.3. Background

Brief literature survey on four core concepts on the hydraulic hybrid, hybrid system architecture, supervisory control and Engine-in-the-Loop setup is presented below.

1.3.1. Hydraulic Hybrid

Hydraulics is a mature technology, due to its extensive use in construction machinery, but it has not gained popularity yet as means of propulsion [4]. The hydraulic hybrid propulsion system uses fluid power to propel vehicles, exclusively or in conjunction with the mechanical transmission according to the hybrid architecture [3].

Of the many hybridization options, the hydraulic hybrid application can be advantageous for heavier vehicles due to their high-power density and energy-conversion efficiency. Heavy vehicles especially have significant amounts of braking energy, and the power flow is very high. Accordingly, hybridizations of heavier vehicles have more

advantages than lighter vehicles, as heavy vehicles need to find a more efficient way to store and use the high power flow.

The energy storage in the hydraulic accumulator is achieved via the highly compressed gas working like a pneumatic spring. Thus, the accumulator has typically higher power density than its electric counterpart, battery. As a result, the possible rate of capturing the braking energy can be very high and a large amount of power assist can be realized in hydraulic hybrid vehicles in comparison with battery-powered vehicles [5]. In other words, the charging and discharging rates in hydraulic accumulators are much higher than those of batteries are because batteries depend on relatively slow chemical reactions. Exceeding the limits in the case of batteries, at particularly high frequencies, leads to overheating and battery destruction.

The power density of hydraulic accumulators is over ten times higher than that of batteries [2], [10] as shown in Figure 1. 2. However, the low energy density of the hydraulic accumulator is a huge drawback of the hydraulic accumulator in comparison with the battery's high-energy density because high-power discharging is maintained for only short time. This low energy density also brings the packaging problem to install in the limited room of a vehicle because the accumulator volume must be larger to capture regenerative braking energy as much as possible but the accumulator mass also increases.

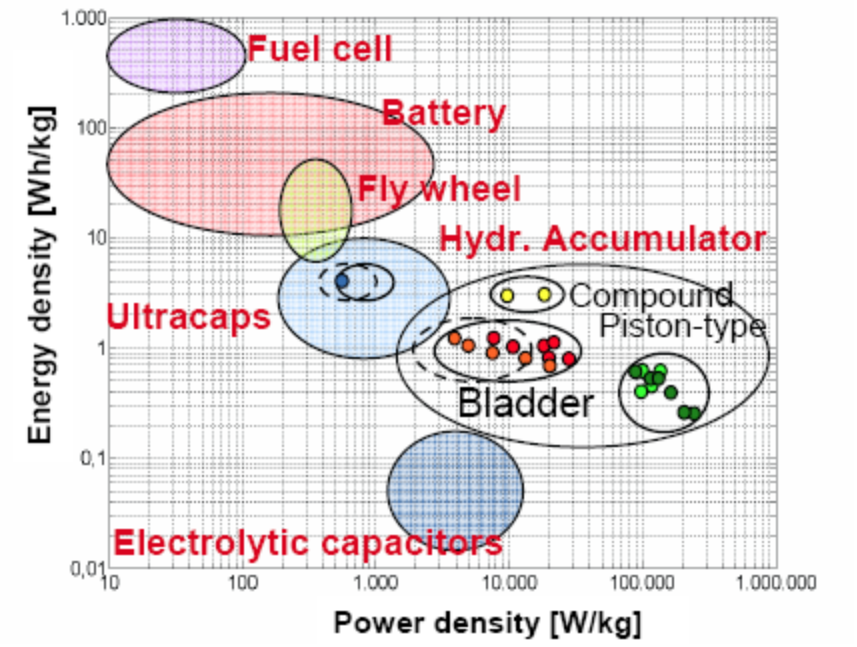

Figure 1. 2. Energy vs. power density of different energy storage systems

Because a practical limit exists for increasing the accumulator size, power management must be carefully designed and reliable to handle the state-of-charge (SOC) in proper level according to vehicle conditions. Since power management determines the rate and amount in storing energy during hybrid-propulsion operation, not only the design of hydraulic components but also power management should be carefully developed. Otherwise, the depletion of the hydraulic energy for the propulsion may affect the drivability especially in the case of series or power-split hybrid system.

The hydraulic accumulator has the high charge/discharge cycle efficiency, which is the ratio of input flow-energy to output flow-energy. The efficiency of the hydraulic accumulator reaches up to 98% in the case of the accumulator specially made for the vehicle propulsion [2]. The methods for realizing such high efficiencies will be presented in the section modeling the accumulator in Chapter 2.1. In contrast, the efficiency of battery becomes lower when the inverter efficiency is considered together. For example, the Li-ion battery discharge efficiency changes from 97% to 78% when the capacity rate (the time for total discharge in an hour unit) changes from 1 to 10 [5]. In the case of the inverter efficiency, Williamson et al. showed that the average efficiency of about 90% during cycle simulations [6]. In addition, an electric battery must operate at the limited window of SOC to be efficient and durable but the hydraulic accumulator can be used from zero to full SOC in charging and discharging without severe performance changes.

With a secondary power source, such as a P/M or generator/motor, engine downsizing is favored in hybrid systems. However, in hydraulic systems, the low-energy density of energy storage may limit our ability to downsize the engine due to the needs of mobility and drivability (such as for towing in high speed or cruising on the graded road) because the stored energy depletes much faster than it does in electric hybrid system. As a result, engine downsizing needs careful considerations in hydraulic hybrid applications.

The hydraulic P/M is used as a pump when it pumps the fluid into the accumulator and compresses the inert gas. It can be reversed and used as a motor when the inert gas expands and the fluid flows out of the accumulator. In the case of a variable displacement axial P/M, a swash plate controls the pump or motor output from zero to maximum. The swash plate angle is adjusted so that the instantaneous pump output flow is exactly enough to maintain a designated pressure. The specific power of the hydraulic

P/M is more than one order higher than that of the electric M/G. Therefore, the mass of the hydraulic P/M can be only one tenth of the electric M/G's mass with the same power output (see Figure 1. 3). In addition, the polar moment of inertia of the hydraulic P/M is much smaller than the inertia of electric M/G, so hydraulic P/M can respond faster than the electric M/G. Therefore, high bandwidth actuators are needed for controlling hydraulic hybrid systems.

The maximum power of the hydraulic P/M is limited by the maximum accumulator gas pressure and maximum rotational speed of hydraulic P/M. Modern hydraulic P/Ms can withstand 350 bar or even up to 420 bar [4]. As the maximum pressure is higher, the more energy can be stored with same volume, so increasing pressure is a solution for the low energy density of accumulator and packaging problem in the hydraulic hybrid system. As manufacturing technologies improve, the maximum speed and pressure of hydraulic P/M may increase, and the efficiency, which converts flow energy into rotation energy or vice versa, may increase. However, the noise, vibration, and sealing problems in the case of using the high-pressure system will not be easy to conquer in the near future and a breakthrough is needed for progress [4].

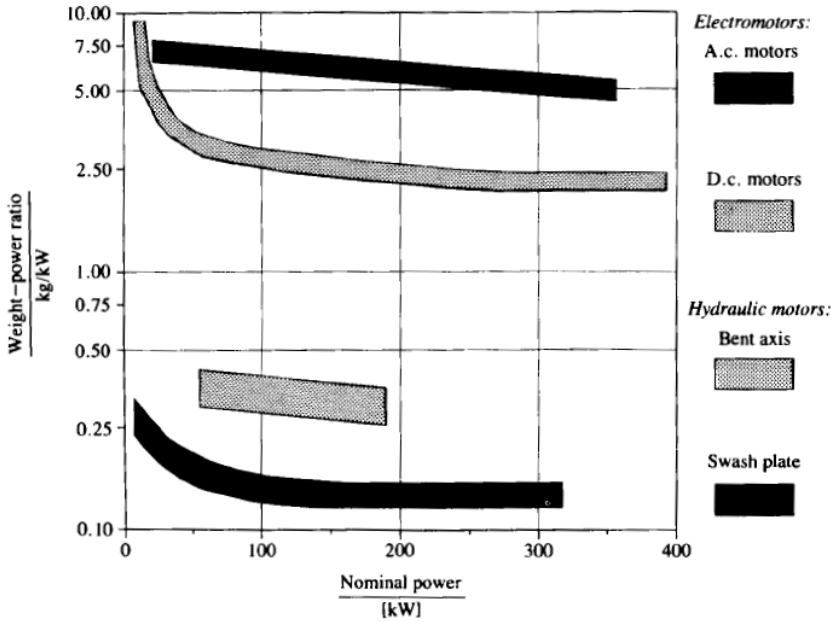

Figure 1. 3. Specific power density of electric and hydraulic motors [4]

Another advantage of using a P/M is its high efficiency in wide operating ranges. Its peak efficiency can be over 95%, and over 90% efficiency is possible in more than 60% of its operation range in the case of vehicle-propulsion P/M [2]. In that case, the total

efficiency (round-trip) of the hydraulic hybrid system is reported as high as 82% in the case of using regenerative braking energy to drive the wheel in Figure 1. 4.

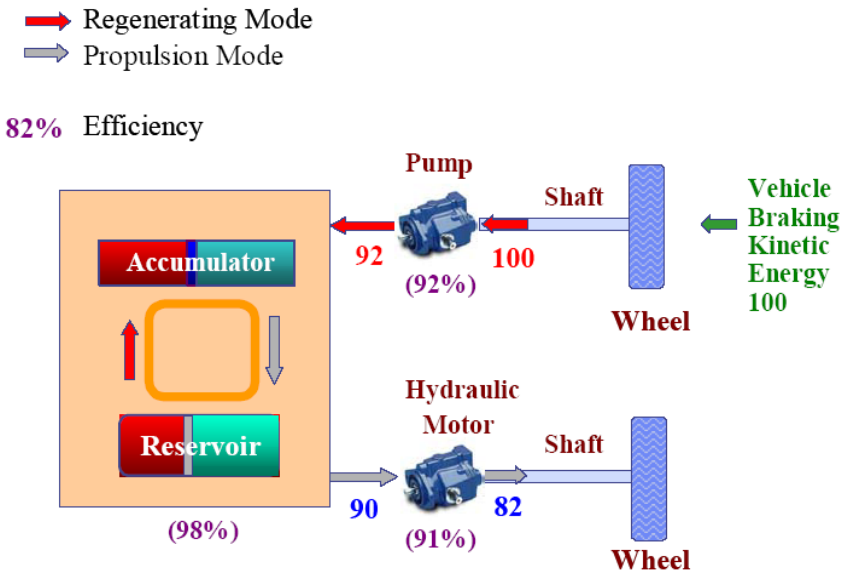

Figure 1. 4. Example of round-trip efficiency of hydraulic hybrid vehicle system [2]

1.3.2. Hybrid Architectures

The basic hybrid architectures can be classified as parallel, series and power-split hybrid systems, according to the connection of the main conventional power source-the engine and secondary power source to the wheel. Extensive variations of architectures and system components are proposed until now under this broad categorization [5]. Each hybrid system including a conventional system is shown in Figure 1. 5. Hybrid systems feature hydraulic components, but similar systems can be built using electric devices, e.g., the battery replacing the accumulator and reservoir and the motor/generator replacing the hydraulic P/M. In the case of a HEV, the inverter is usually located between the battery and motor/generator.

First, the parallel hybrid system is also called a “mild hybrid” system because the secondary power source, M/G or P/M, has usually small capacity or called a “power-assist hybrid” system because only the engine can drive the vehicle and P/M (or M/G) is mostly used for assisting the engine power and regenerative braking. In a parallel hybrid system, a P/M (or M/G) is connected to the input or output shaft of the transmission and most parts of the conventional powertrain are carried over. Because the parallel system can perform as a conventional vehicle with the hybrid system failure, this system is more reliable than other hybrid systems that depend on hybrid components for proper engine

operation. The engine can charge the accumulator (or battery) according to power management strategy to maintain specific SOC level. If there are rare chances of regenerative braking like highway driving, the fuel economy should be the same as that of conventional vehicle in the case of charge sustaining power management.

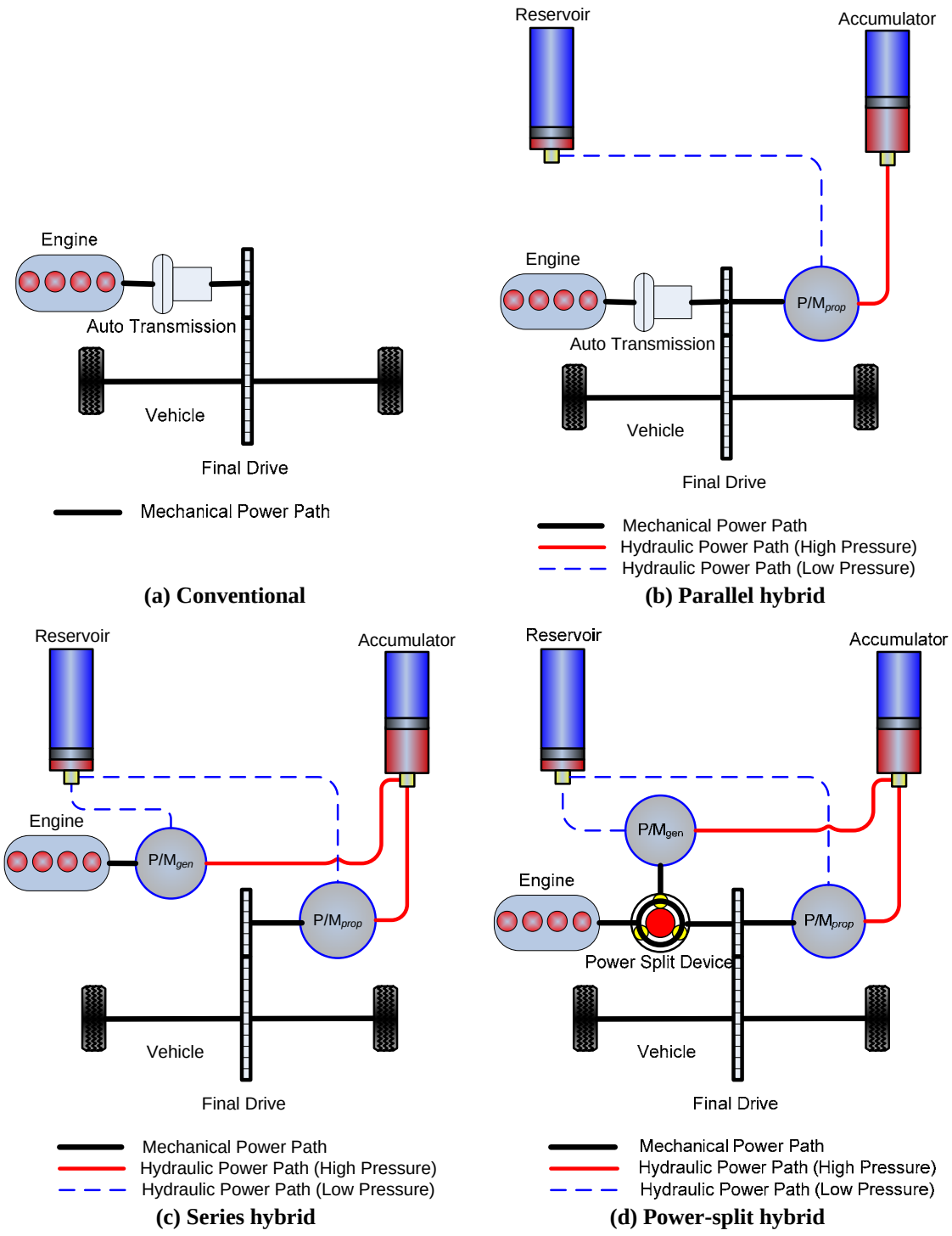

Figure 1. 5. Typical hybrid system configurations with hydraulic components

Second, the series hybrid system is always a "full hybrid" because all the propulsion or traction is supplied by the M/G or P/M and there is no mechanical connection between the engine and the wheels. In the series hybrid system, the engine is directly connected to the P/M_{gen} (or M/G_{gen}), so the engine operation is independent of the wheel. As a result, the engine operation area can be designed according to the manufacturer's policy, e.g., fuel economy-oriented and emission-reduction oriented. In SHH system, the engine energy is always converted to the hydraulic flow energy and the energy needs to be converted again to mechanical energy at P/M_{prop} (or M/G_{mot}). If the hydraulic fluid is charged into the accumulator and then discharged, the accumulator efficiency also affects the system efficiency. Thus, the overall system efficiency depends on the energy conversion efficiencies of the P/M and accumulator. In addition to the fuel economy benefit, the vehicle performance can improve because the maximum engine power can be used at any vehicle operating condition. Without the connection between the engine and wheel, the conventional transmission, transfer case and drive shaft can be removed, so the system configuration becomes relatively simple.

Third, the power-split hybrid system has both characteristics of the series and parallel hybrid systems. The meaning of power-split in a system classification is that the engine power is split by the power-split device. It is not related with the split of the vehicle power demand among multiple power devices. In the power-split hybrid system, the classification of P/M_{gen} and P/M_{prop} becomes ambiguous because both P/M can be used for the propulsion or generation. The energy generation and propulsion of each P/M depend on the control strategy. In this study, the notation of P/M_{gen} and P/M_{prop} is still used, indicating that P/M_{gen} works mostly as a pump controlling engine speed and P/M_{prop} works mostly as a motor assisting the engine for propulsion.

In comparison with power-split HEV, the hydraulic power-split system has much lower inertia so the response can be fast during acceleration or deceleration [96] but the low maximum speed of hydraulic P/M is a significant constraint in realizing the hydraulic power-split system.

1.3.3. Supervisory Powertrain Control – Power Management

The hybrid vehicle system needs not only a proper architecture design but also a proper supervisory powertrain control to orchestrate the multiple power sources, e.g., an

engine, battery and accumulator. The supervisory powertrain control is also called power management. Therefore, power management is a system level control and determines the power demand for each power device from the vehicle power demand in real time. From the given power demand, the lower level controller takes a control of speed and torque of each power device. This study assumes that the lower level control (or servo-loop) is acceptable to achieve the power demand and we concentrate on the study of the high-level power management. However, the lower level control is also a challenge to overcome in the actual vehicle application or EIL test.

There are three representative power-management strategies: rule-based power management, equivalent consumption minimization strategy (ECMS) and dynamic programming (DP).

First, Rule-based power management uses threshold values and if-then-else structures to implement the control logic. Thus, a heuristic control technique, based on load leveling, [11], [33], fuzzy logic [81] and genetic algorithm [95] are examples of rule-base power management. The set of thresholds can be tuned from engineering intuition or experiments based on trial-and-error method. The analysis of a benchmark power management such as dynamic programming can also provide implementable rule-based power management [11], [12], [33].

Second, ECMS is a popular approach that minimizes the total equivalent fuel consumption. The ECMS is an implementable and semi-optimal power management that is relatively cheap in terms of computation cost. However, the weakest point of the ECMS is that it is not a global optimization technique but an instantaneous optimization of arbitrarily assuming equivalent fuel consumption that depends on the system states at the current time. In addition, the ECMS technique is based on the static optimization, so it does not consider system dynamics during optimization.

Third, dynamic programming (DP) approach is a control optimization technique that can be applied to a non-linear dynamic system, such as a complex automotive powertrain [77]. Deterministic DP (DDP) finds the optimal trajectory of state variable and control inputs for a given disturbance, e.g., driving schedule in finite-horizon. However, it cannot be implemented in a real time application because of its preview nature that derives from the backward minimum cost sweep. In contrast, stochastic DP (SDP)

technique is an implementable sub-optimal power-management based on probability distribution that is extracted from pre-selected driving schedules [79], [80] and is a full-state feedback control algorithm in infinite horizon. The SDP algorithm has not been tested before for a series hybrid configuration, and in particular not for a hydraulic hybrid series configuration. The definition of a problem is very different from the case of a parallel system, since the power generation and propulsion are two functionally independent systems in a SHHV, and the ability of SDP to uncover new opportunities for fuel savings has yet to be proven for this configuration.

1.3.4. Engine-in-the-Loop

An Engine-in-the-Loop (EIL) test is a branch of the Hardware-in-the-Loop (HIL) simulation that integrates the physical device and virtual model in the closed loop system to take synergetic advantage of each other [105], [106]. To have a successive validation and development tool, the HIL simulator should capture the system characteristics based on the fidelity of the model and the high bandwidth of the actuator and sensor [107]. There have been many studies on the necessary enablers for the HIL [35], [36], [108], [109], [110], [111], [112], [113], [114], [115].

An internal combustion engine model is used to predict and optimize the fuel economy under vehicle performance constraints for the conventional and hybrid vehicle [11], [12], [33], [41], [43], [44]. However, the accurate predictions of transient emissions are still a challenge even with highly complex and slow computational fluid dynamics (CFD) models and chemical kinetics models [116], [117]. In addition, the computation load of such sophisticated simulation is too much to be used for system assess and in the optimization process. As a result, the direct application of the real engine into the simulation is the most viable alternative for accurately assessing the impact of the powertrain designing and control on emissions [105].

Nabi et al. [118] used the EIL setup in the design and calibration of the transmission and engine controller. Fleming et al.[119] presented the development work of Powertrain-in-the-Loop setup for the controller design and implementation on a parallel HEV. Shidore et al. [120] tested various powertrain components in connection with the virtual vehicle environment. Argonne National Laboratory (ANL) developed and utilized the HIL setup to investigate the impact of control and the relationship among fuel

economy and cumulative NO_x emissions in a parallel diesel hybrid vehicle with a CVT [121]. The goal of this experiment was to investigate and demonstrate the potential of diesel engines for hybrid electric vehicles (HEVs), and it did not focus on transient emissions of particulates, or alternative architectures and energy conversion options.

1.4. Contributions

The success in pursuing the overall objectives of the study critically depends on the original contributions pertaining to following areas:

- Representative series and power-split hydraulic hybrid vehicle systems are modeled by the integration of hydraulic components and sub-system models: This task involves additional modeling of sub-systems such as 4x4 options, simple transmissions and the speed reduction mechanism with additional planetary gear trains.
- Alternative modulated SOC control power management is developed and tested for representative series and power-split hydraulic hybrid vehicle systems: The low energy density of the hydraulic accumulator causes transient engine operation in traditional power managements and presents a particular challenge for the controller design. The modulated control aims to reduce the target SOC and enable effective regeneration of the braking energy. The smooth engine operation with the modulated SOC control and its impact on the fuel economy improvement and emission reduction is explored the Engine-in-the-Loop test.
- The power management optimizations for series and power-split hydraulic hybrid systems are carried out by applying the dynamic programming algorithm. The deterministic dynamic programming establishes the benchmark for the potential of the fuel economy improvement and gives an insight into mechanisms for improving the efficiency on the system level. However, the strategy is fully optimal only for a driving schedule used in the optimization, and the DDP has to be followed by a rule extraction or a stochastic dynamic programming algorithm needs to be setup based on the probability of driver action derived from analyzing several driving schedules. The ability of the SDP to provide an implementable sub-optimal power management policy for real-time application to advanced hydraulic configurations such as power-split and series configurations is investigated for the first time.

- The methodology of running the real engine in the loop by connecting a virtual hybrid vehicle modeling is developed to represent the parallel, series and power-split hydraulic hybrid vehicle systems: Integration requirements and challenges are investigated for the Engine-in-the-Loop setup in each hydraulic hybrid configuration. Particularly, issues related to the causality of the Engine-in-the-Loop setup and stability issues on engine speed and torque control are resolved through the modifications of the simulation model and modeling causality-reversed modules in series hydraulic hybrid system.
- The Engine-in-the-Loop capability is pursued for validation of the simulation model and for characterization of transient soot and NOx emission from a diesel engine used in the parallel, series and power-split hydraulic hybrid vehicle systems. The development of the EIL capability for a series and power-split HHV requires assessing the model causality in the context of dynamometer control, modifications of models to enable faster than real-time execution, and investigation of signal-noise and communication speed issues. In addition to typical research-grade engine instrumentation, the test-bed is equipped with ultra-fast emission analyzers in order to obtain deep insight into the engine system behavior while running coupled to a virtual hydraulic hybrid powertrain. The goal is to establish a link between the power management and transient NO_x and soot emissions and provide guidance for developing strategies capable of meeting a combined fuel economy-emission objective.

As supportive works for this study, the calibrations of the adjustable constant coefficients in the physics-based models of the hydraulic components were done for the optimization study and systematic design optimization was carried out. The optimization of the system design from the baseline ensured the fuel economy improvement while meeting all performance constraints.

CHAPTER 2

MODELING OF HYDRAULIC SYSTEM

The physics-based hydraulic accumulator and pump/motor (P/M) are modeled in this chapter. The hydraulic accumulator modeling is based on the thermodynamic equation with a real gas state equation and the elastomeric foam, used to increase the charge/discharge efficiency of the accumulator, is considered.

The hydraulic P/M model is based on the "black box" model that calculates the actual torque and fluid flow by multiplying the ideal torque and volumetric flow with torque and volumetric efficiencies accounting for physical losses. The constant coefficients in P/M efficiency equations are calibrated according to the actual experimental data and assumed constant while the P/M size changes during the design optimization.

The mass estimation of the hydraulic device and vehicle powertrain is carried out through the first order curve fitting results that are based on the actual hydraulic hybrid system data [17]. As a result, the vehicle mass change is reflected on every optimization run when the size of the system component changes.

2.1. Accumulator and Reservoir Modeling

As secondary energy storage, the hydro-pneumatic accumulator system is composed of a high-pressure inert gas container called accumulator, and a low-pressure inert gas container called reservoir. The accumulator is mainly used to store the energy, and the reservoir provides the pressure that prevents cavitations inside the hydraulic system. The pressure difference between the accumulator and reservoir produces the torque to rotate the hydraulic P/M.

The hydraulic P/M works as a motor for vehicle propulsion, when the fluid from the accumulator flows to reservoir through the P/M. Reversely, when the fluid flows from reservoir to accumulator through the P/M, it works as a pump, for example, regenerative braking or pumping by the engine. In modeling the accumulator and reservoir, thermodynamic energy conservation equation is used assuming that the charged gas in

the accumulator is exchanging work with hydraulic fluid and heat with both the elastomeric foam and accumulator wall in the closed system. A piston or bladder is used to separate the inert gas from the fluid inside the reinforced shelled container. The example of the bladder-type accumulator and its components are shown in Figure 2. 1.

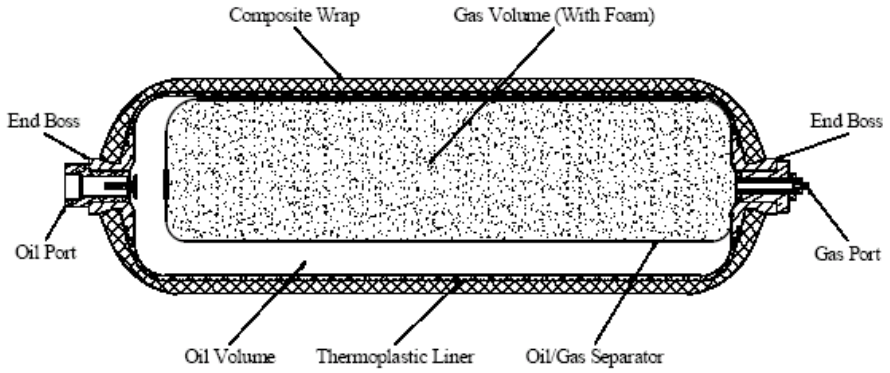

Figure 2. 1. Bladder-type accumulator and its components [17]

The accumulator's high efficiency depends on the ratio of heat capacity of the charge over heat loss by using the elastomeric foam [18]. The elastomeric foam, which is sealed by a piston or bladder, improves the charge and discharge efficiencies by reducing heat loss during the compression and expansion process. Because the elastomeric foam has a large surface area and a large specific heat, the foam can act as a heat sink with negligible temperature changes, which allows the heat to be transferred from the gas to the foam and vice versa. In addition, there are several advantages in using the elastomeric foam [18]: firstly, the accumulator efficiency becomes independent of pre-charge pressure, holding time and rate of charge and discharge. Secondly, the elastomeric foam insulates the gas from the accumulator wall, so it reduces the temperature variations and increases the energy storage capacity in the case of the same maximum pressure. Thirdly, the elastomeric foam makes the accumulator temperature lower by absorbing the heat, so the foam increases the durability of the accumulator. Fourthly, the gas pressure becomes an accurate indicator of SOC with nearly constant temperature.

A schematic diagram of energy transfer to the accumulator gas is shown in Figure 2. 2 and the governing equation for the ideal gas in the accumulator is Equation (2.1) [27], [28] and validated by experiments [29].

$$m_g \frac{du}{dt} = -p_g \frac{dv}{dt} - m_f c_f \frac{dT}{dt} - hA_w \left(T - T_w\right) \tag{2.1}$$

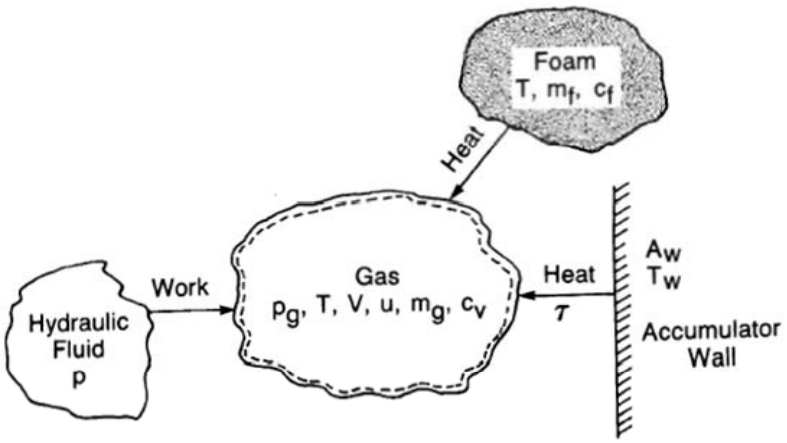

Figure 2. 2. Schematic diagram of energy transfer to the accumulator gas [28]

The internal energy of real gas is given by

$$du = c_v dT + \left[T\left(\frac{\partial p_p}{\partial T}\right)_v - p_g \right] dv \tag{2.2}$$

From Equation (2.1) and Equation (2.2), the thermodynamic energy equation can be simplified given below.

$$\left[1 + \frac{m_f c_f}{m_g c_v}\right]\frac{dT}{dt} = \frac{T_w - T}{\tau} - \left[\frac{\partial p_g}{\partial T}\right]_v \frac{dv}{dt} \tag{2.3}$$

with time constant: $\tau \equiv \dfrac{m_g c_v}{hA_w}$

where

m_f : Foam mass [kg]

c_f : Specific heat of foam [kJ/kgK]

m_g : Gas mass [kg]

T : Absolute gas or foam temperature [K]

T_w : Accumulator wall or bladder temperature [K]

c_v : Constant volume specific heat of gas [kJ/kgK]

p_g : Gas absolute pressure [kPa]

v : Gas specific volume [m^3/kg]

Benedict-Webb-Rubin (BWR) equation relates the real gas pressure to the gas temperature and specific volume as Equation (2.4).

$$p_g = \frac{RT}{v} + \left(B_0 RT - A_0 - \frac{C_0}{T^2} \right) / v^2 + \left(bRT - a \right) / v^3 + \frac{a\alpha}{v^6} + \left(c \left(1 + \frac{\gamma}{v^2} \right) e^{-\gamma / v^2} \right) / v^3 T^2 \quad (2.4)$$

where

$R, A_0, B_0, C_0, a, b, c, \alpha, \gamma$ are constants in BWR equation.

The volume specific heat of gas, c_v, varies according to both the pressure and temperature, and it is calculated by Equation (A-3) in [27].

As for a foam-filled accumulator, the thermal constant, τ is in the order of several minutes so that the gas temperature can be assumed almost constant for a short time and quasi-steady condition [28], [30]. Therefore, the pressure can be used to calculate SOC in real vehicle application because measuring the gas volume inside the accumulator is not easy.

In addition to the thermal loss, the internal frictional loss is also considered in the accumulator modeling. Thus, the overall frictional loss is assumed as 4% of the input energy. The pressure drops in the connecting lines including hoses, unions, fittings, and bends, etc., are estimated by assuming the equivalent hose length. The pressure drop is calculated for both the case of laminar and turbulent flow [28].

N_2 is used as inert gas in this study. The gas mass is directly related with the minimum and maximum gas pressure range and accumulator size. The gas mass is calculated to satisfy the conditions in Table 2. 1 with modest maximum pressure [4], [11], [12]. In this study, SOC is defined as the ratio of instantaneous fluid volume in the accumulator over the maximum fluid capacity. In a real vehicle application, the accumulator pressure may be easy to measure for estimating SOC, assuming gas temperature change is not so large with elastomeric foam.

Table 2. 1. Accumulator pressure boundary condition (at 298 K)

Accumulator pre-charge pressure (SOC = 0.0)	145 bar
Accumulator maximum pressure (SOC = 1.0)	350 bar
Reservoir pre-charge pressure (SOC = 0.0)	5 bar
Reservoir maximum pressure (SOC = 1.0)	10 bar

The foam mass is selected to keep the overall accumulator efficiency over 90 % during the federal urban driving schedule (FUDS) and highway fuel economy test

(HWFET). The characteristics of the accumulator used in this study, e.g., energy density, are provided in Appendix A. 4. In contrast with hydraulic accumulator, the internal resistance of battery is the function of the charging or discharging rate, the temperature and SOC [31]. Thus, it is hard to define overall battery efficiency because it changes as the battery operation condition changes and the inverter efficiency also needs to be considered but it also changes according to its types as battery does.

However, the foam-filled accumulator's instantaneous charging and discharging efficiency is almost constant and independent of pre-charge pressure, holding time, rate of charge and discharge as described above. The overall accumulator efficiency, which is the ratio of the hydraulic energy output to the hydraulic energy input during the general cycle simulation, is about 92~96% by using elastomeric foam, and this overall efficiency is close to the test result of EPA [2].

2.2. Hydraulic Pump/Motor Modeling

The axial-piston hydraulic pump/motor (P/M) is modeled according to updated Wilson's P/M theory [28]. Schematics of a swash-plate type, inline axial-piston hydraulic P/M and a bent-axis type, axial-piston hydraulic P/M are shown in Figure 2. 3(a) and Figure 2. 3(b), respectively.

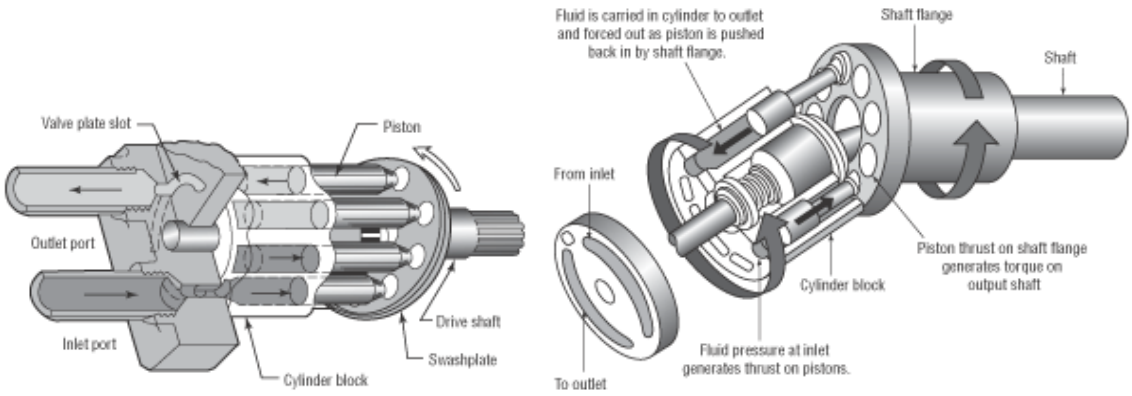

(a) Swash-plate type, inline axial-piston type **(b) Bent-axis type, axial-piston type**

Figure 2. 3. Axial-piston type hydraulic P/Ms [32]

A swash-plate type, axial-piston, variable-displacement P/M is modeled in Equation (2.5)~Equation (2.10). The torque and hydraulic fluid flow are controlled by the displacement factor that corresponds to the swash plate angle [28] and validated by experiments [29].

Ideal leak-free volumetric flow rate of P/M:

$$Q_i = x\omega D \tag{2.5}$$

Ideal frictionless torque of P/M:

$$T_i = x\Delta pD \tag{2.6}$$

x is displacement factor that is the ratio of the current P/M displacement to the maximum P/M displacement. Its sign is negative for pump operation and positive for motor operation; ω is angular velocity [rad/sec]; D is maximum P/M displacement per radian [m^3/rad]; and ΔP is the pressure difference between accumulator and reservoir [Pa].

The difference between actual volumetric flow (Q_a: Actual flow rate [m^3/sec]) and actual torque (T_a: Actual torque [Nm]) are defined by accounting for flow and torque losses, respectively. Flow losses include laminar leakage loss, turbulent leakage loss and the loss due to the fluid compressibility. From Equation (2.7) and Equation (2.8), volumetric efficiency is the function of displacement factor, rotational speed, maximum displacement and pressure difference.

$$\eta_{v,gen} = \frac{Q_a}{Q_i} = 1 - \frac{C_s}{|x|S} - \frac{\Delta P}{\beta} - \frac{C_{st}}{|x|\sigma} \tag{2.7}$$

$$\eta_{v,motor} = \frac{Q_i}{Q_a} = \frac{1}{1 + \frac{C_s S}{|x|} + \frac{\Delta P}{\beta} + \frac{C_{st}}{|x|\sigma}} \tag{2.8}$$

$\frac{C_s}{|x|S}$, $\frac{\Delta P}{\beta}$ and $\frac{C_{st}}{|x|\sigma}$ represent laminar leakage loss, loss from fluid compressibility and turbulent leakage loss, respectively; coefficients in these terms are C_s for laminar leakage and C_{st} for turbulent leakage. β is oil bulk modulus of elasticity [Pa].

$S \equiv \frac{\mu\omega}{\Delta P}$ and $\sigma \equiv \frac{\omega D^{1/3}}{\left(2\frac{\Delta p}{\rho}\right)^{1/2}}$ are dimensionless numbers in which μ is oil dynamic viscosity [Ns/m^2] and ρ is oil density [kg/m^3].

Torque losses include fluid viscosity loss, mechanical friction and hydrodynamic loss. From Equation (2.9) and Equation (2.10), torque efficiency is the function of displacement factor, rotational speed, maximum displacement and reciprocal of pressure difference.

$$\eta_{T,gen} = \frac{T_i}{T_a} = \frac{1}{1 + \frac{C_v S}{|x|} + \frac{C_f}{|x|} + C_h x^2 \sigma^2} \tag{2.9}$$

$$\eta_{T,motor} = \frac{T_a}{T_i} = 1 - \frac{C_v S}{|x|} - \frac{C_f}{|x|} - C_h x^2 \sigma^2 \tag{2.10}$$

$\frac{C_v S}{|x|}$, $\frac{C_f}{|x|}$ and $C_h x^2 \sigma^2$ represent fluid viscosity loss, mechanical friction loss and hydrodynamic loss, respectively; coefficients in these terms are C_v for viscous drag, C_f for friction and C_h for hydrodynamic loss.

The total efficiency (instantaneous ratio of energy output to energy input), that is calculated from multiplication of the volumetric efficiency and the torque efficiency, indicates instantaneous ratio of output energy to input energy in Equation (2.11) and Equation (2.12). It is the function of displacement factor and rotational speed for given pressure difference.

$$\eta_{totoal,motor} = \frac{E_{shaft}}{E_{flow}} = \frac{T_a \dot{\omega}_{shaft}}{\Delta P Q_a} = \frac{T_a \dot{\omega}_{shaft}}{\frac{\Delta P Q_i}{\eta_{v,motor}}} = \eta_{v,motor} \times \eta_{t,motor} \tag{2.11}$$

$$\eta_{totoal,gen} = \frac{E_{flow}}{E_{shaft}} = \frac{\Delta P Q_a}{T_a \dot{\omega}_{shaft}} = \frac{\eta_{v,gen} \Delta P Q_i}{\frac{T_i \dot{\omega}_{shaft}}{\eta_{T,gen}}} = \eta_{v,gen} \times \eta_{t,gen} \tag{2.12}$$

The coefficients, which are used to calculate volumetric and torque efficiencies in this study, are calibrated to match coefficients of a particular P/M for vehicle-propulsion use [17] and are different for motor case and pump case. The coefficients are assumed constant while scaling maximum P/M displacement, *D*.

The effects of individual parameters on the total P/M efficiency are shown in Figure 2. 4. Even though the calibration of coefficients cannot exactly match real P/M efficiencies, efficiency trend and characteristics of P/M can be derived. P/M maps that are used in this study are calculated in Figure A. 2. The best P/M efficiency is located at high load and low-medium rotational speed region. Characteristics of hydraulic P/M used in this study, e.g., power density, are provided in Figure A. 3.

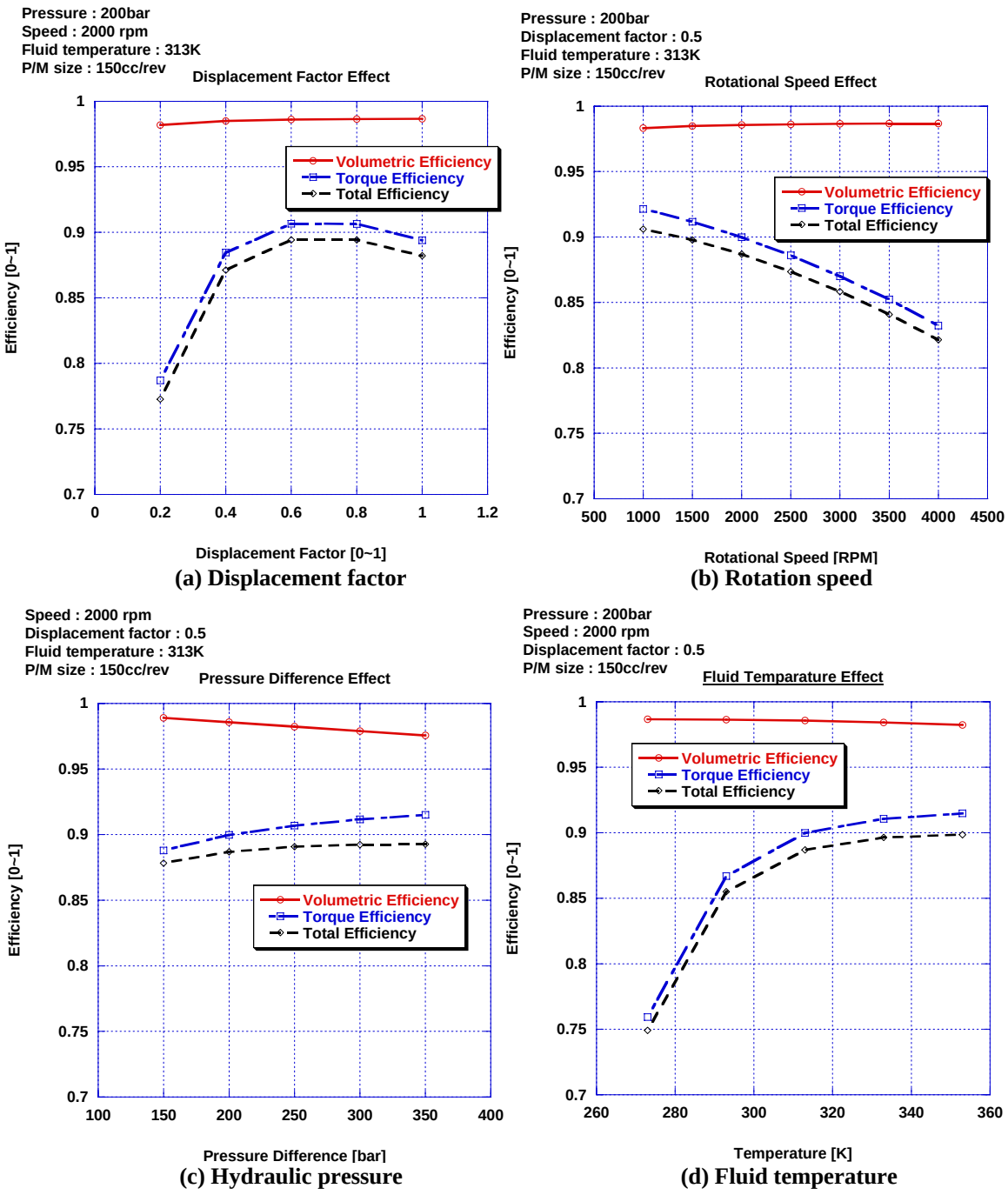

Figure 2. 4. Effects of individual parameters on the P/M efficiency

2.3. Hydraulic System Mass Estimation

The mass estimation of the hydraulic system is critical to determine total vehicle mass and optimize hybrid system design. The mass estimation is mostly first order curve fitting of reference data based on the design specifications of SHH vehicles [17].

The hydraulic hybrid vehicle mass can be represented in Equation (2.13).

Vehicle mass = Vehicle shell mass + Engine mass + Hydraulic system mass + Payload (2.13)

where

Engine mass = Baseline engine mass × Engine power scaling factor (2.14)

Hydraulic system mass = Accumulator mass + Reservoir mass + P/M mass + Hydraulic oil & circuit (including hose and conditioner) mass + Gear box mass (if exists) (2.15)

Accumulator or reservoir mass = Shell mass + Foam mass + Gas mass + Fitting & bladder mass (2.16)

Hydraulic oil & circuit mass = Oil mass + Hose mass + Conditioner mass (2.17)

Gear box = Gear box mass× Total number of gear box (2.18)

The number of P/M_{prop}s is same to the gear box number in the case of 4x4 architecture. Coefficients of the curve fitting are given in Table 2. 2. In the case of SHH system, the conventional transmission and transfer case including drive shaft and transmission oil can be removed. In the case of PHH system, conventional powertrain components cannot be removed. In the case of PSHH system, only the conventional transmission can be removed. The engine-mass scaling factor is also used as an engine power scaling factor in a small range, e.g., ± 10% of the nominal value [12] and it also effect the transmission mass estimation.

Table 2. 2. Hydraulic hybrid component mass estimation

Component mass [kg]	Mass calculation method
Accumulator shell mass [kg]	Maximum gas volume [Liter] / 56.8 [Liter] × 43.3 (fitting, bladder, etc)
Reservoir shell mass [kg]	Maximum gas volume [Liter] / 56.8 [Liter] × 18.0 (fitting, bladder, etc)
Foam mass [kg]	Maximum gas volume [m^3] × foam density (0.096 [kg/m^3])
Accumulator oil mass [kg]	Maximum gas volume × 0.5×fluid density (0.84 [kg/m^3])
Hose + conditioner mass [kg]	Estimated equivalent length × 2.2 ([kg/m], high pressure) or 1.2 ([kg/m], low pressure) + 41.9 (conditioner, etc)
P/M mass [kg]	Maximum displacement [cc/rev] × 0.338
Planetary gear box mass [kg]	15 × conventional vehicle mass / 2585.5
Transmission, transfer case and shaft, etc [kg]	Dried T/M mass × 1.9

CHAPTER 3

MODELING OF A SERIES HYDRAULIC HYBRID SYSTEM, OPTIMAL DESIGN AND INITIAL POWER MANAGEMENT STUDY

Even though the hydraulics is a mature technology, the studies on the series hydraulic hybrid are rare. Most of the previous work on series hybrid systems considered electrical propulsion and storage, while previous attempts at optimizing hydraulic hybrid system design focused on the parallel architecture [12]. The SHH vehicle simulation is developed, and hydraulic device modules are integrated with the engine and the vehicle dynamics. The initial power management study assesses the application of the traditional thermostatic control logic, and then provides an alternative based on the SOC sustaining idea, but with a much more sophisticated controller. This establishes a comprehensive understanding of the interactions in the series hydraulic hybrid system, and paves the way for subsequent applications of algorithms for optimization of supervisory control in Chapter 4.

A series hybrid system is also called a "full hybrid" system because the series hybrid system uses only the large M/G or P/M for traction without mechanical connection between the engine and wheel. Without the connection between the engine and wheel, the conventional transmission, transfer case and drive shaft can be removed and the system configuration becomes relatively simple. In case of hydraulic hybrid systems, the "pure hydrostatic" hybrid system is another name for the series hybrid system [3].

In the series hybrid system, the engine operation is independent of the wheel. Thus, the engine energy is always converted to the hydraulic flow energy (or electric current), so the flow energy (or electric energy) should be converted again to mechanical energy at P/M_{prop} (or M/G_{mot}). If charging or discharging the accumulator (or battery), the accumulator or battery efficiency is included in system efficiency. Therefore, the overall system efficiency depends on efficiencies of the P/M and accumulator or the M/G and battery. In the case of HEV, the inverter efficiency needs to be considered, too. As a

result, series hydraulic hybrid system is more advantageous than series electric hybrid system in terms of overall system efficiency.

The vehicle performance can improve because the maximum engine power can be used at any vehicle condition and series hydraulic hybrid can take advantage of the high power density of accumulator. However, the low energy density of accumulator is one of the significant challenges that series hydraulic hybrid has to overcome.

A common approach to the power management of a series hybrid configuration was based on the load leveling. In the case of load leveling, the engine power is maintained at the pre-designated level by charging the accumulator if the vehicle power demand is lower than the pre-designed power level.

In the case of the series HEV, the thermostatic power management using a constant engine power at the best BSFC area, i.e., sweet spot, is generally accepted as an optimal power management for the fuel economy improvement with the high energy density energy storage, battery. However, this study shows that the low energy density of the hydraulic accumulator causes very transient engine operation with the thermostatic power management. In addition, the "sweet spot" cannot be a best point any longer for the constant engine power demand. As an alternative power management, the modulated SOC control is introduced to keep the energy level as low as possible during normal vehicle propulsion conditions. This guarantees highly effective regenerative braking, as the accumulator capacity to store energy increases if the starting SOC is low. In addition, the modulated control prevents direct charging of the accumulator by the engine. In addition, the smooth engine operation is expected to reduce transient emissions. The transient effects on exhaust emissions and fuel consumption are shown by the Engine-in-the-Loop test in Chapter 5.

3.1. Series Hydraulic Hybrid Vehicle Modeling

Previously, HMMWV with conventional powertrain was modeled by a bond graph model [34]. The conventional HMMWV model is updated for Engine-in-the-loop test [35] as a point-mass model balancing the fidelity and simplicity and this new HMMWV model is used as a baseline platform for the vehicle simulation and design optimization. The powertrain model including the torque converter and automatic transmission is also updated to match the high performance V8 engine that is tested in the Lay Autolab at the

University of Michigan. This conventional vehicle model, namely "super-HMMWV", is used as the baseline for the fuel economy and vehicle performance. The engine and vehicle specification are presented in Appendix A.1.

The new baseline HMMWV model is integrated in a complete forward-looking vehicle engine simulation (VESIM) model in MATLAB/Simulink environment. The high-fidelity VESIM model of the conventional truck has been validated by actual vehicle test on the proving ground [41]. A parallel HEV truck model [33] and a PHH medium-truck model [11] have adopted the VESIM model for optimal power management study. The design and power-management optimization for PHH heavy-duty truck was carried out with the VESIM model, too [12]. The typical schematic of a conventional and SHH vehicle with 4x4 capability are given in Figure 3. 1.

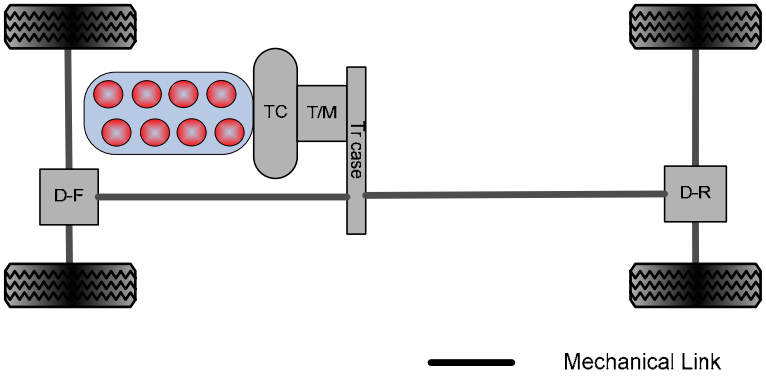

(a) Conventional 4x4 system

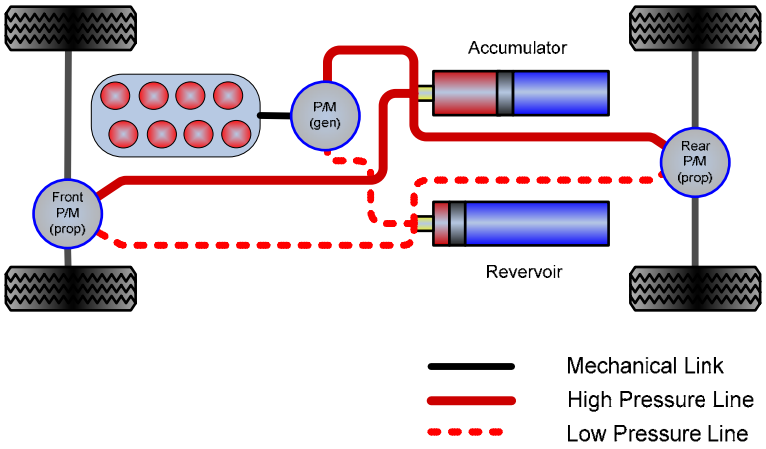

(b) Series hydraulic hybrid 4x4 system

Figure 3. 1. 4x4 configurations of conventional and SHH vehicles

In the case of conventional 4x4, a transfer case divides the transmission output torque into front and rear driveshafts. The torque division ratio can be controlled according to the road condition. However, it is assumed that the same torque is transferred to the front and rear driveshafts in this study. In SHH 4x4, the engine connected only to the P/M_{gen} and two P/M_{prop}s can propel the vehicle with 4x4 capability. Even though two P/M_{prop} s are connected to front and rear driveshafts through a differential gear respectively (not shown here) in Figure 3. 1 (b) but one large P/M_{prop} with a transfer case architecture is also possible. P/M_{prop} is used for propulsion and used for regenerative braking. If the regenerative braking torque is not enough to stop the vehicle, the frictional brake assists the braking of P/M_{prop}.

In SHH, the driver's power demand is directly transferred to the P/M_{prop} and hydraulic energy that comes from the accumulator or from the P/M_{gen} driven by the engine or both is used by P/M_{prop} according to hybrid power management. The power management determines engine power demand corresponding to various input state variables, e.g., SOC, vehicle speed and vehicle power demand. The engine operation is independent of the wheel so engine speed and torque can be controlled along pre-designed path for a given engine power demand. In terms of fuel economy, vehicle performance and emissions, the SHH system have advantages over the conventional or PHH vehicle with more degrees of freedom in controlling the engine according the developer's concerns, e.g., fuel economy and emissions.

The complete forward-looking vehicle-engine simulation model of SHH is integrated in MATLAB/Simulink environment (see Figure 3. 2). From the input of the driving schedule, the vehicle power demand is calculated by the driver model. The engine, P/M_{gen} and P/M_{prop} power demands are calculated from the power management block. The vehicle speed is fed back to the driver model to calculate the next vehicle power demand at every time step.

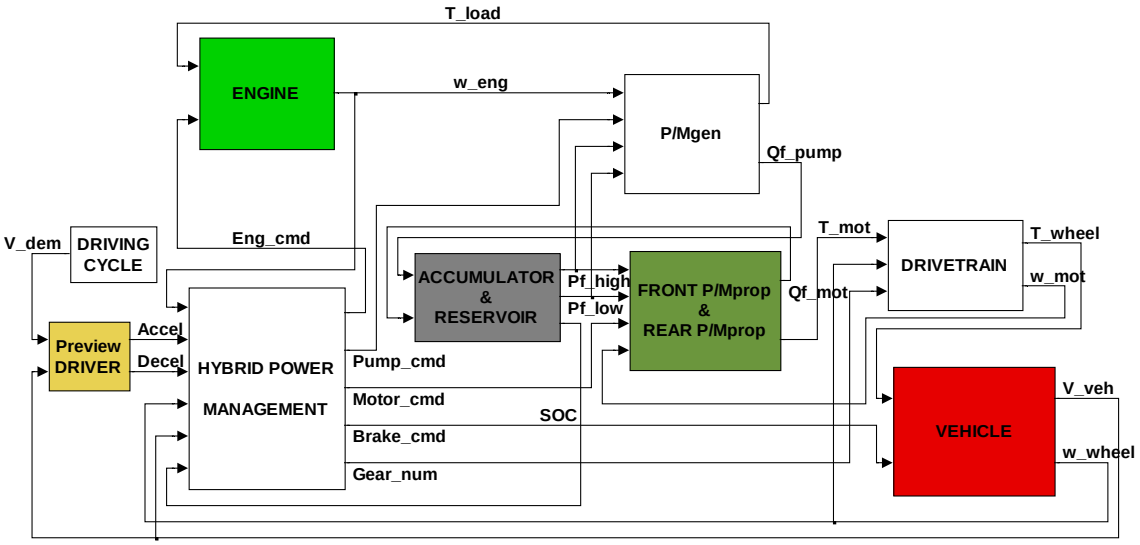

Figure 3. 2. Integrated forward looking SHH vehicle simulation in SIMULINK

3.1.1. Engine Modeling

The engine model used for the simulation is based on the test results of a 6.0 L, V8, direct-injection diesel engine at the Lay Automotive Lab at the University of Michigan and the engine specification is presented in Appendix A.1. The steady-state engine maps of BSFC, NO_x and soot are drawn from test results as shown in Figure A. 1.

In the simulation, instead of using a high-fidelity thermodynamic engine model [41], a map-based engine model is used to reduce the calculation time because the design optimization study will run the driving schedule repeatedly. However, the engine model has a carefully calibrated fuel governor with first-order delay simulating a turbo-lag during the transient engine operation. From the engine speed and fuel delivery per cycle, the engine brake-torque output is calculated from the look-up table, based on the BSFC engine map.

The fuel consumption and emissions are calculated assuming the quasi-steady engine operation because the look-up table is generated from steady-state engine test results. Because transient engine effects may not be captured from the engine model, the fuel economy and emission results from the simulation may be optimistic in comparison with the real world SHH application data. The validations of simulation results with a real engine in the loop test are presented in Chapter 5.

The idle-stop and start capability occupies a large portion in fuel economy gains in the hybrid vehicle application. In the series hybrid system, the idle-stop and start can be

done much easier than any other hybrid system because the engine and wheel are totally disconnected. Thus, starting the engine with P/M_{gen} in the motor mode can be accomplished in any vehicle condition. To estimate the starting torque, the motoring torque of the real engine was measured at several engine speeds and the starting torque is extrapolated between zero and idle speed assuming no fuel delivery until engine speed reaches the idle speed. The P/M_{gen} torque to rotate the engine from the engine stop condition to the idle speed in 0.5 second is found to be around 120 Nm. However, this value is when the engine is fully warmed up, so the starting torque may change according to actual engine conditions, e.g., oil temperature. The simulation of the idle-stop-and-start mechanism is modeled and the result is shown in Figure 3. 3.

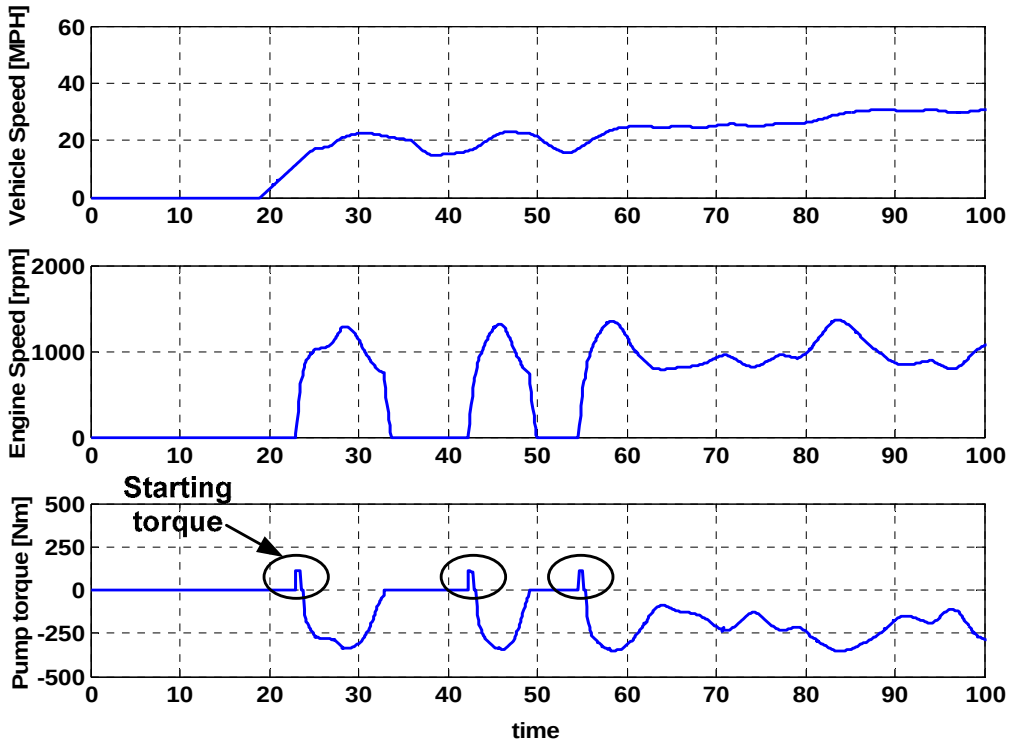

Figure 3. 3. Idle-stop and start simulation in SHH

However, the idle-stop and start may affect the exhaust emissions and driver's comfort in the actual vehicle application. Thus, various engine control strategies are possible and actual idle-stop and start strategies may change according to the engine and vehicle condition. Therefore, to be more consistent in predicting fuel economy with the idle-stop capability, simulations are carried out without idle-stop and the estimation of the fuel consumption with idle-stop is post-processed by removing the fuel consumption while

the engine power demand is zero. Thus, fuel economy with the idle-stop represented in this study may be an optimistic value without applying the actual engine start-and-stop model.

3.1.2. Preview Driver Modeling

The driver model is a PI speed-feedback controller with a preview feature, as shown in Figure 3. 4. This driver model is originally developed for a stable output of the vehicle power demand in the EIL setup [36]. This virtual driver has a low-pass filer to attenuate measuring noise and 1-, 2- and 3- second previews with proportional gains that are necessary for ensuring desired dynamic performance. Even though this complicated driver model is not necessary for the simulation, this preview driver model is used in the simulation to be consistent with the EIL test presented in Chapter 5.

The driver model has an anti-windup to prevent the integration-error saturation. The outputs of the driver model are accelerator and braking pedal position signal that are normalized between zero and one. In the series hybrid system, these pedal-position signals are directly sent to the P/M_{prop} and used as a displacement factor for the propulsion or regenerative-braking.

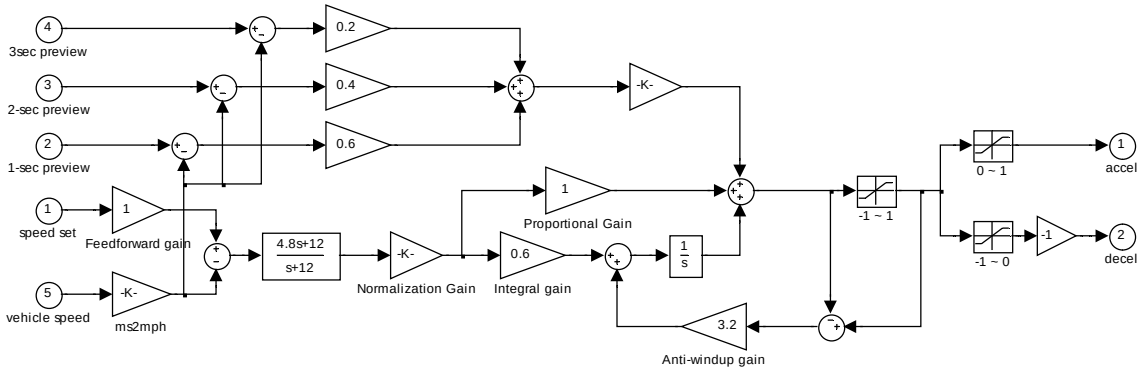

Figure 3. 4. Forward-looking preview driver model in Simulink

3.1.3. Driving schedule

Driving schedule critically affects fuel economy and emissions because the driving schedule defines the vehicle power demand at every time step. Instead of the special driving schedule of the military vehicle, FUDS is selected as a baseline driving schedule to measure fuel economy of SHH light-duty vehicle. If the vehicle speed deviation of more than 2 mph from the reference vehicle speed continues over 1 second, the cycle simulation is considered a failure.

3.2. 4x4 Architecture

Conventional SHH 4x4 architecture is composed of one P/M_{prop} with a transfer case or two small P/M_{prop}s located at front and rear driveshafts generating same torque. The fuel-economy advantage is explored by applying various 4x4 architectures in SHH system.

3.2.1. Operating models for a 4x4 powertrain – simultaneous operation

Conventional 4x4 operation is divided into 1-P/M_{prop} and 2-P/M_{prop} case. First, the 1-P/M_{prop} case uses a transfer case to divide P/M torque into the front and rear wheels. Second, in two P/M_{prop} case, two small P/M_{prop}s are located at front and rear driveshaft respectively producing the same torque. In the 1-P/M_{prop} with a transfer case, the half of the P/M_{prop} torque is provided to the front and rear driveshaft ideally without mechanical losses. The 4x4 configuration of 1-P/M_{prop} with a transfer case for SHH is shown in Figure 3. 5.

In simultaneous operation with 2-P/M_{prop}, output torque to both the driveshafts is the same because the two propulsion P/M_{prop}s receive the same displacement factor command. In the case of braking, the same regenerative braking energy is absorbed with the same displacement factor command in both front and rear P/M_{prop}s. The simultaneous operation with 2-P/M_{prop} case is shown in Figure 3. 6.

Figure 3. 5. A 4x4 configuration of 1-P/M_{prop} with a transfer case

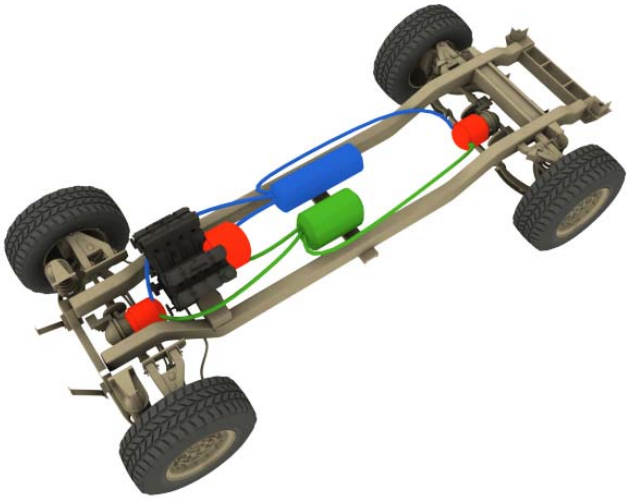

Figure 3. 6. A 4x4 configuration of simultaneous operation with 2 P/M$_{prop}$s

Figure 3. 7(a) represents visiting points of one P/M$_{prop}$ with a transfer case or simultaneous operation with two P/M$_{prop}$s on the P/M map of 200bar during FUDS. The P/M displacement factor rarely reaches high load area, where the efficiency of energy conversion is high in both the cases of acceleration and deceleration. The histogram of P/M displacement factor clearly shows that how long a particular interval of displacement is used during FUDS in Figure 3. 7(b). The accumulated time when the displacement is zero is not counted to avoid adding vehicle stop time to propulsion time. During acceleration, the displacement factor is mostly below 0.4, and during deceleration, the displacement factor is mostly over -0.6. However, P/M$_{prop}$ size cannot be easily reduced to increase P/M$_{prop}$ efficiency because the P/M$_{prop}$ needs to be oversized for the up-hill and acceleration performance. If the P/M operation is mostly part load, then the low overall P/M$_{prop}$ efficiency results in lower fuel economy. If P/M$_{prop}$ operation points can be moved to the high-load range for the same power demand, overall P/M$_{prop}$ efficiency improves, and the fuel economy will improve. As a solution to this problem, a sequential operation is applied in the next section. Figure 3. 7(c) and (d) show the cycle simulation examples of 1 P/M with a transfer case and simultaneous operation with two P/Ms during FUDS, respectively. Both P/M operation strategies show almost similar displacement and SOC predictions because the total P/M size of 2 P/M case is the same to that of one-P/M case with slight difference in P/M$_{prop}$ efficiency.

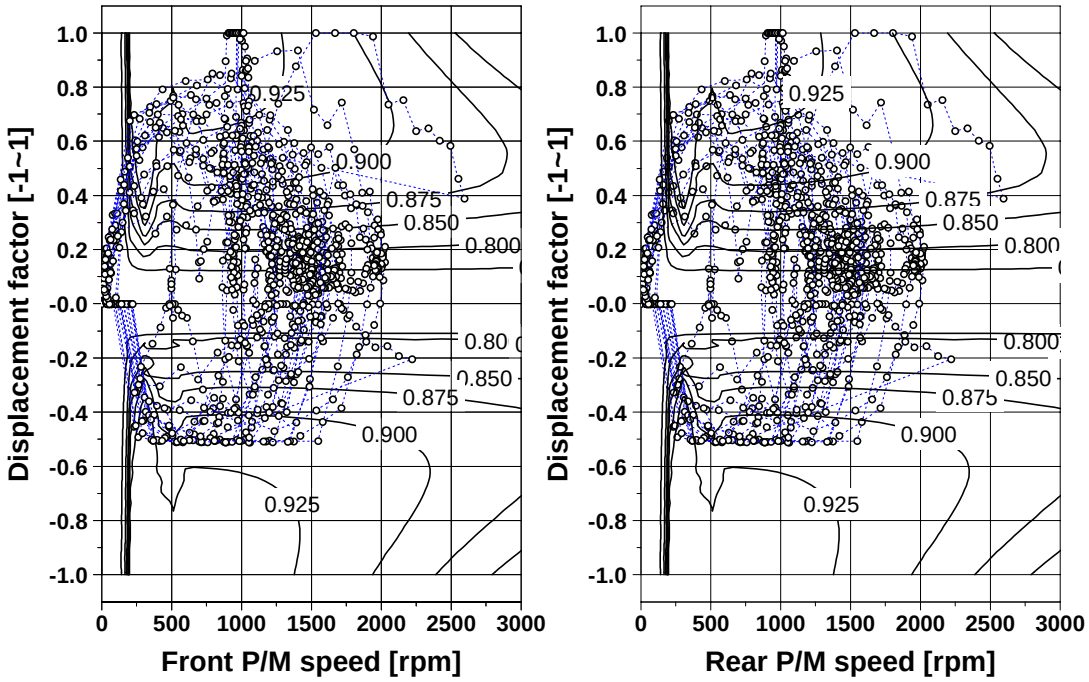

(a) Displacement factor prediction on P/M map (at 200 bar) with conventional 4x4 operation

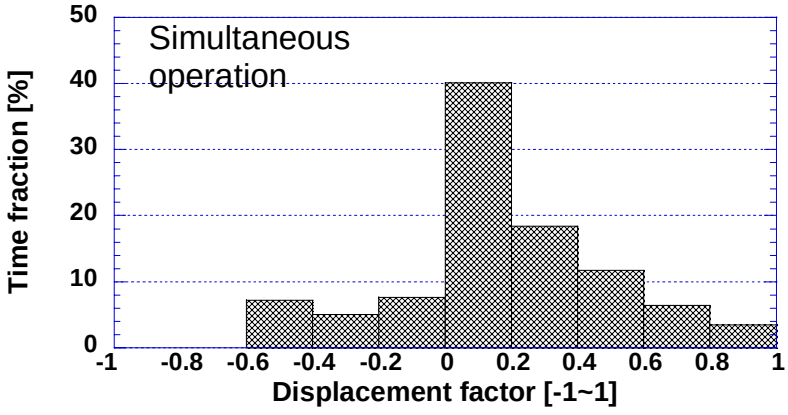

(b) Histogram of time fraction of front and rear P/M$_{prop}$ displacement factor

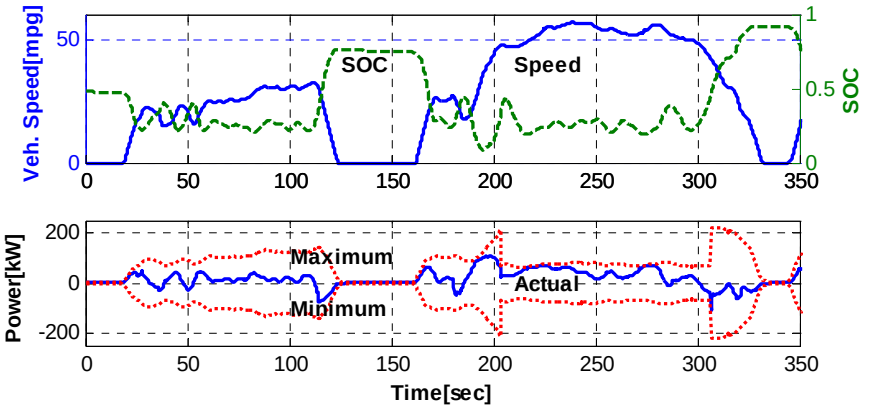

(c) 4x4 operation with 1 P/M$_{prop}$ during FUDS

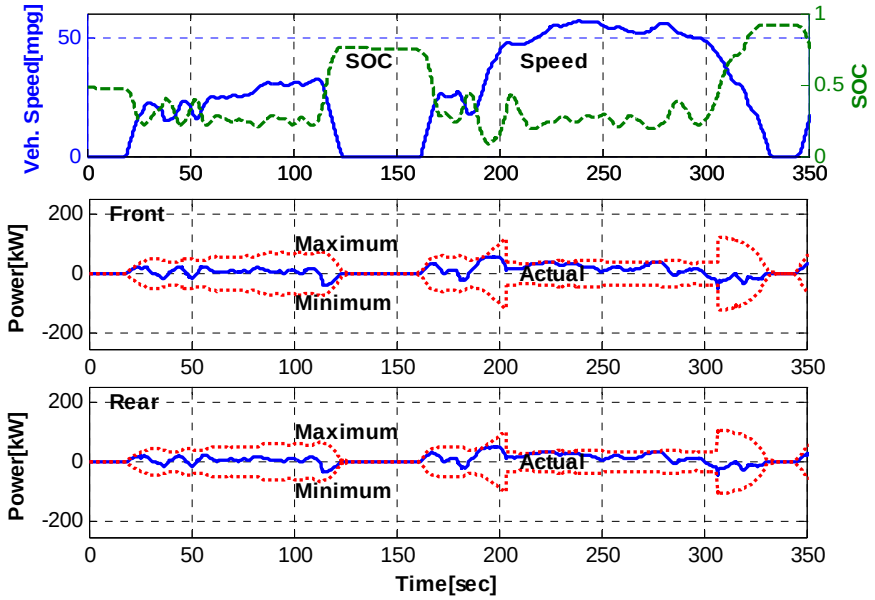

(d) Simultaneous 4x4 operation with 2 P/M$_{prop}$s during FUDS

Figure 3. 7. Illustrations of conventional 4x4 operation with 1 P/M$_{prop}$ and 2 P/M$_{prop}$s

3.2.2. Sequential 4x4 Operation with 2 P/Ms

Sequential 4x4 operation with two P/M$_{prop}$s is suggested to improve the low overall P/M efficiency of conventional 4x4 operation. In sequential 4x4 operation, the rear P/M$_{prop}$ only delivers the traction torque in normal driving condition. The front P/M$_{prop}$ starts to add the torque when the rear P/M$_{prop}$ reaches its maximum torque. The front P/M$_{prop}$ delivers negative braking torque in normal braking condition and the rear P/M$_{prop}$ starts to assist the braking after the front P/M$_{prop}$ reaches its maximum negative torque.

Figure 3. 8(a) shows the visiting points of sequential 4x4 operation with two P/Ms on the P/M map of 200bar during FUDS. The P/M$_{prop}$'s operation points moves to the high load area in both acceleration and deceleration cases, so the overall P/M efficiency increases. Figure 3. 8(b) and (c) represent histograms of displacement factor for front and rear P/M$_{prop}$s during FUDS. The front P/M$_{prop}$ displacement factor frequently reaches the high negative load below -0.6 during deceleration and reaches over 0.8 assisting the rear P/M$_{prop}$ during acceleration. The rear P/M$_{prop}$ displacement factor reaches more than 0.8 for about 30% of total operation time and most of deceleration is done by front P/M$_{prop}$. Figure 3. 8 (d) shows the cycle simulation result of sequential 4x4 operation with two P/Ms and slight higher SOC when vehicle stop in sequential operation. Because of high efficiency of P/M$_{prop}$, the amount of consumed flow energy is smaller in

sequential operation due to more efficient P/M$_{prop}$ operation than conventional 4x4 operation and reduces the engine work as shown in Table 3. 8.

The sequential 4x4 operation with 2 P/Ms is used as baseline 4x4 architecture because of higher fuel economy for the same hydraulic system. After finding the optimal sizes of front and rear P/M$_{prop}$ s, the effect of 4x4 architecture on the fuel economy will be evaluated. The sequential 4x4 operation with 2 P/Ms is a fuel economy-oriented 4x4 operation, so simultaneous 4x4 operation with 2 P/Ms will be used by just switching control logic in the powertrain control module in case of the off-road or slippery condition.

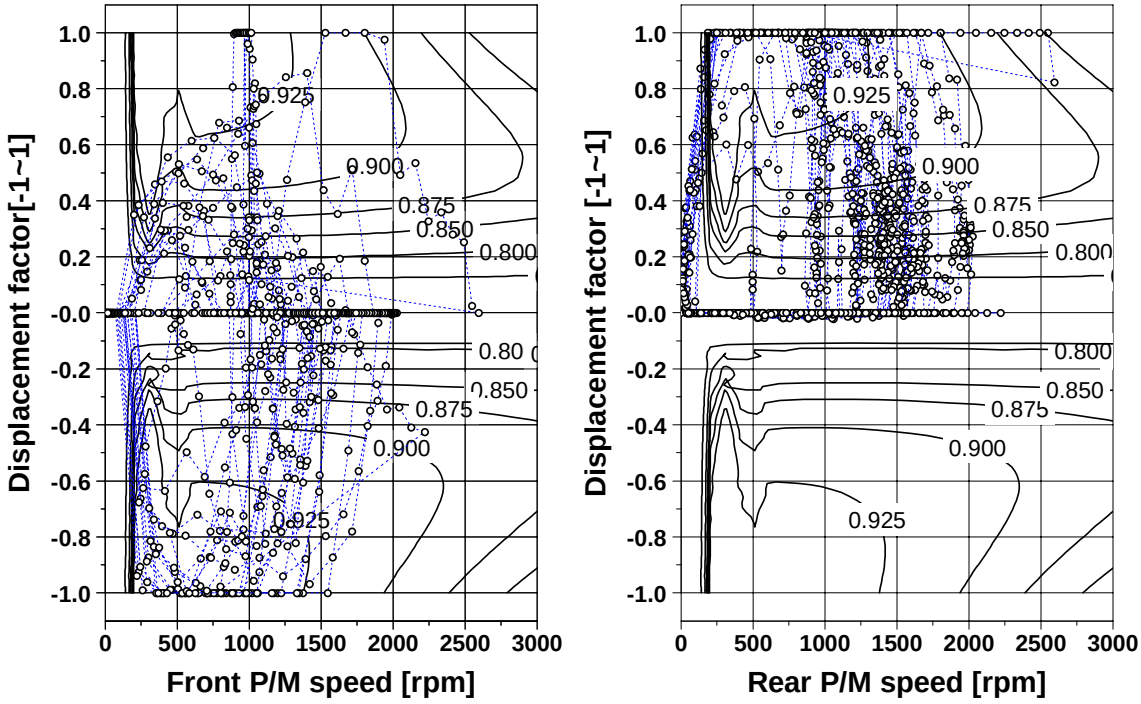

(a) Sequential 4x4 Operation points with 2 P/M$_{prop}$s on P/M$_{prop}$ map (at 200 bar)

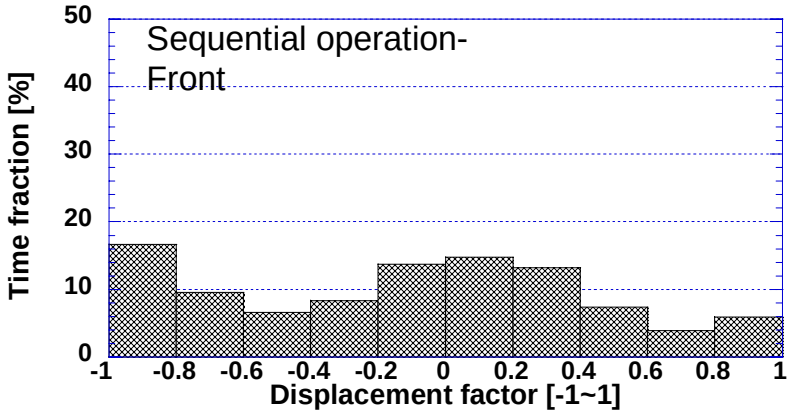

(b) Histogram of time fraction of front P/M$_{prop}$ displacement factor

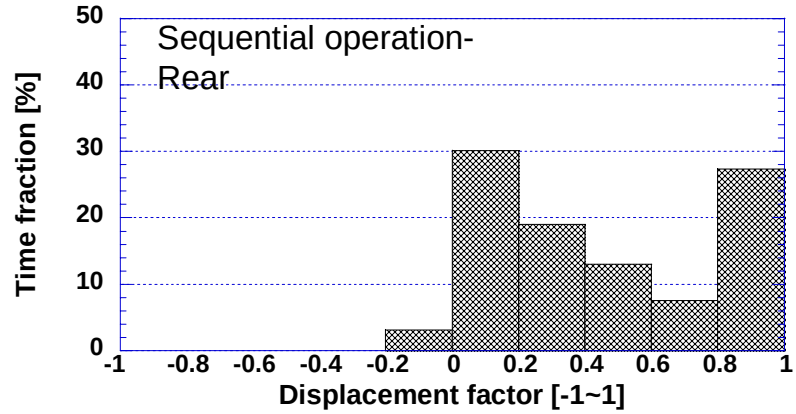

(c) Histogram of time fraction of rear P/M$_{prop}$ displacement factor

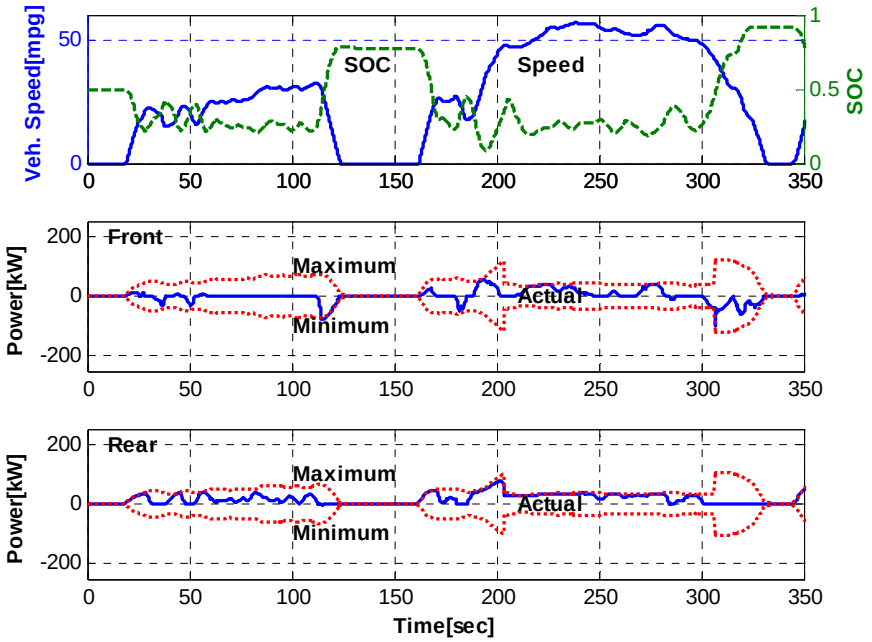

(d) Sequential 4x4 operation with 2 P/M$_{prop}$s during FUDS

Figure 3. 8. Illustration of sequential 4x4 operation with the 2 P/M$_{prop}$s

3.2.3. 2-Speed Transmission and Gear Shift Logic

In SHH, even though the conventional multiple-stage transmission may not be needed, at least two-stage transmission is needed to reduce the P/M$_{prop}$'s rotational speed at high vehicle speed assuming maximum P/M speed as 4000 rpm. The adoption of transmission can also improve the fuel economy because the P/M efficiency drops at high speed. As a result, the proper design of gear ratios and gearshift logic are necessary to improve the vehicle performance and fuel economy. A planetary gear train can be used as a two-stage transmission, and it has three different modes, e.g., low, high and neutral stages [17]. The sun gear is connected to the P/M$_{prop}$ and the carrier is connected to the differential

gear. The low gear ratio is selected as 3:1, being the lowest practical gear ratio [45] and the high gear ratio is selected as 1:1, i.e., direct connection. The clutch dynamics is not considered in this study, and hence, the gearshift occurs without time delay and the vehicle speed does not change during the gearshift. Neglecting clutch dynamics may show slightly optimistic vehicle performance and fuel economy.

Figure 3. 9 (a) and (b) represent the prediction of vehicle speed and pedal position of baseline SHH HMMWV on the gear shifting logic map during FUDS and HWFET.

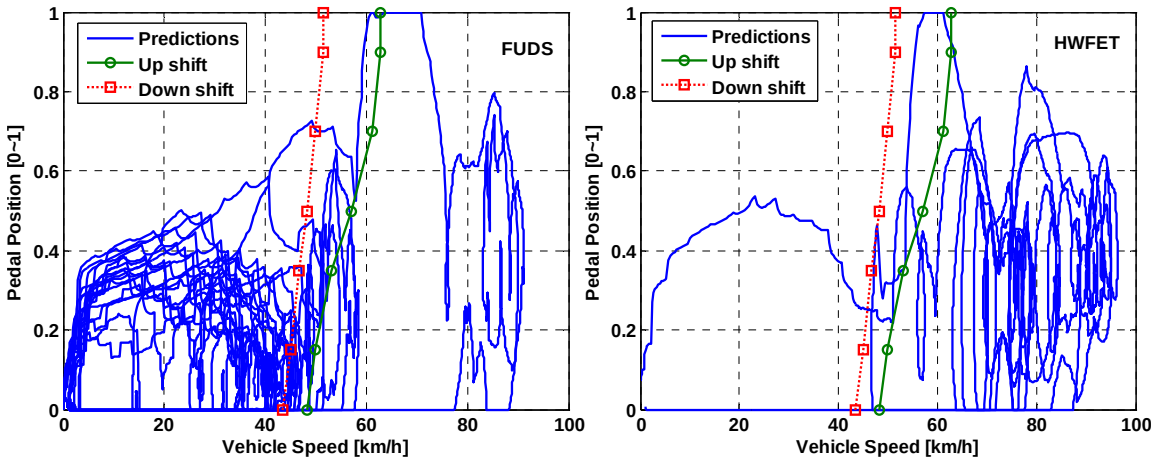

(a) FUDS **(b) HWFET**

Figure 3. 9. Pedal position trajectories on the gear shift map during FUDS and HWFET

This baseline gear shifting logic is designed to shift up to the higher gear at 3000rpm of P/M$_{prop}$ speed at maximum pedal position, assuming the P/M efficiency drops critically after 3000rpm. As the final gear ratio increases, the vehicle acceleration at the low speed range improves but the vehicle maximum speed decreases.

In addition, the P/M efficiency improves by engaging higher gear at the low pedal position by moving the P/M$_{prop}$'s operation points to the high load and low speed range. However, the gap between up-shift and downshift line should be carefully designed to prevent the shifting oscillation.

3.3. Series Hydraulic Hybrid Power Management

The hybridization of vehicle propulsion system has an inevitable challenge on how to manage the engine and secondary power source. As a high-level supervisory powertrain control algorithm, the power management should assure that regenerative braking energy is absorbed as much as possible and the engine and P/Ms operate most efficiently. Even though the objective is to improve fuel economy in this study, the power management

influences transient emissions and drivability, too. In SHH, driver's power demand is used as the power demand of P/M_{prop} for acceleration and regenerative braking. Other state variables, for example, SOC, vehicle speed and vehicle power demand, can used to calculate the engine power demand.

For the engine power demand calculation, the thermostatic SOC control scheme (on-off engine operation) has been traditionally used for its simplicity and reliability in controlling the engine power for both HEV and HHV application, even though the actual applications were different case by case. Especially, the low energy density is a significant challenge for the power management of SHH.

Most papers regarding series hybrid-vehicle simulations also have been concentrated on HEV power management strategies. Common series hybrid power managements are based on (a) power tracking that calculates the total power to propel the vehicle from the engine or (b) load leveling that maintains engine power at the pre-designated level by charging the accumulator if the vehicle power demand is lower than the pre-designed power level.

Hochgraf et al. [98] applied a thermostatic, on-off power management with a load-leveling concept based on SOC. The thermostatic power management was proven the relatively simple, efficient, and robust for the series HEV control. Jalil et al. [23] and Caratozzolo et al. [20] introduced rule-based power managements for series HEVs. They used a power-split concept that divides the vehicle power demand into the generator power and the accumulator power with a thermostatic power management running in background. Rule-based power management operates the engine at the fuel-efficient region of the engine map. Barsali et al. [86] proposed the power management of series HEV using a forecast algorithm that calculates the average of the prime mover's (engine or micro-gas turbine-generator) fuel consumption. They used a SOC-sustaining algorithm with thermostatic power management for the prime mover and considered the losses of the various system elements and costs related to the start-up of the prime mover. Barsali et al. [87] proposed power management of series HEV that determines whether the engine is in on-off operation mode or continuous operation mode by forecasting the average power request during the optimization period. Optimized power management calculates the engine power demand in both engine operation modes. Liang et al. [94]

proposed rule-based series HEV power management. They used engine-power compensation function to maintain the SOC at a reasonable level with a power-split concept. Pre-selected charging power is multiplied by the SOC deviation from the average SOC that is between low and high SOC levels.

Pisu et al. [85] developed an ECMS for a series HEV with two secondary-energy storages – a battery and ultra capacitor. By introducing a power-split concept – dividing vehicle power demand into the generator power and the battery or ultra capacitor power, the semi-optimal instantaneous power-split ratio is pre-calculated and saved in a multi-dimensional map with three input variables – SOC, number of energy storage, and torque needed at the wheel.

He et al. [76] introduced an optimal power management for a series hybrid HEV that is real-time implementable and it compensates for transient effects. They proposed a two-stage optimization method that, firstly, produces a pre-computed static instantaneous optimization map from the ECMS and, secondly, calculates the engine power and the rate of engine power, assuming a quasi-steady state. The time constant of a diesel engine is derived from a transient fuel-consumption model and is given as a time step for cost function minimization. Charge-sustaining function is added as a linear penalty in the cost function.

Brahma et al. [19] and Perez et al. [89] used DDP technique to find optimal energy managements of series HEVs. With the power-split concept between the electric energy generation path and electric energy storage path, they presented benchmark power management of electrical energy generation and storage. Their power managements sustain SOC with a tunable weight penalizing the amount of electrical energy consumption. However, both DDP studies were based on pure mathematical equations and the actual system dynamics used for the optimization was not provided. In addition, the cost function is total energy consumption such that the minimum fuel consumption depends on the tuning factor of the electric energy consumption and the charge sustaining is not easily guaranteed after the optimization.

Wu et al. [9] showed the potential of fuel economy improvement by refining the initial simulation result with parametric studies of the passenger-car series hydraulic hybrid (SHH) system. They used thermostatic power management dividing the accumulator

energy level into two parts; energy level reserved for regenerative braking and energy level for power decoupling according to the vehicle speed. If the vehicle power demand is higher than the level needed for power decoupling, the shut-off valve isolated the accumulator and only the engine would drive the vehicle. Kapellen et al. [13] presented PHH and SHH heavy refuse-collection truck simulations and showed significant fuel economy improvements using on-off power managements, even though the simulation did not account for the electrometric foam effects. Beachley et al. [25] proposed a thermostatic SHH power management with pre-designed energy levels that is determined by the vehicle speed as Wu et al [9] did.

This study introduces two rule-based power-management strategies: the traditional thermostatic SOC control that includes scheduled SOC control when the vehicle power demand is high and modulated SOC control as an alternative SOC control. The fuel economy potential of two power managements will be compared and the transient emission effects will be explored with the EIL test.

3.3.1. Thermostatic SOC Control Scheme

The thermostatic SOC control scheme is a traditional approach used for the series HEV and HHV power managements. Because of the low energy density of accumulator, the scheduled SOC control portion is indispensable instead of the typical thermostatic SOC control of only engine on/off.

The basic idea of the thermostatic SOC control scheme is shown in Figure 3. 10(a) and examples of actual engine power prediction are shown in Figure 3. 10(b). Engine power demand becomes zero or threshold power at the threshold SOC with a dead-band that prevents frequent engine on-offs. If the vehicle power demand increases and the threshold power is not enough to maintain the threshold SOC, engine power demand increases up to the maximum engine power according to pre-designed schedule. In normal driving condition, the SOC is maintained around the threshold SOC with engine on and off. If the threshold SOC is set lower, the room for storing the regenerative braking energy increases but if it is set too low, hydraulic energy buffer decreases. The assist from hydraulic power stops when the SOC becomes zero. To increase the reliability of maintaining SOC over zero, the maximum power SOC should be high. However, if the maximum power SOC is too close to the threshold SOC, the engine

operation becomes sensitive to SOC change below threshold SOC. The example of the thermostatic SOC control result is shown in Figure 3. 10(c). In contrast to the series HEV, the engine on/off happens frequently because of the low energy density of the accumulator and frequent engine on/offs may aggravate exhaust emissions and the driver's comfort.

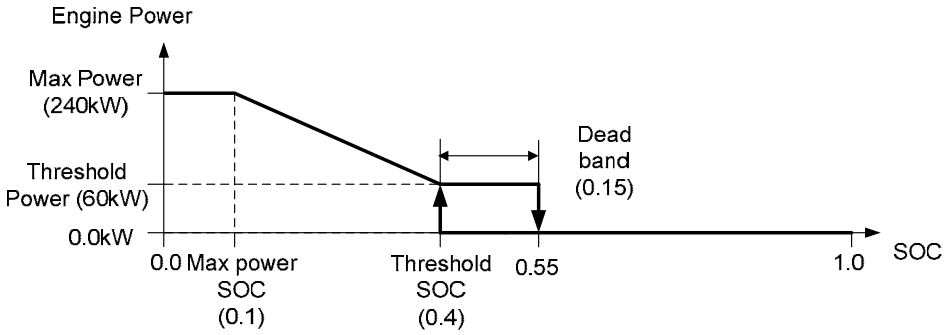

(a) Design parameters of thermostatic SOC control

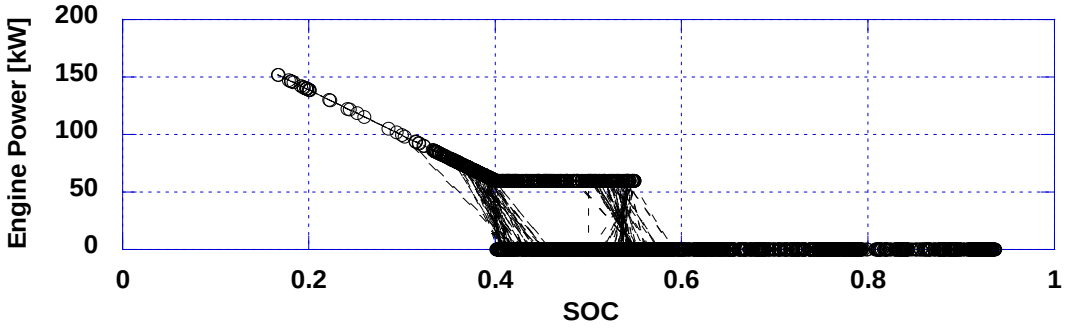

(b) Actual engine power prediction according to SOC

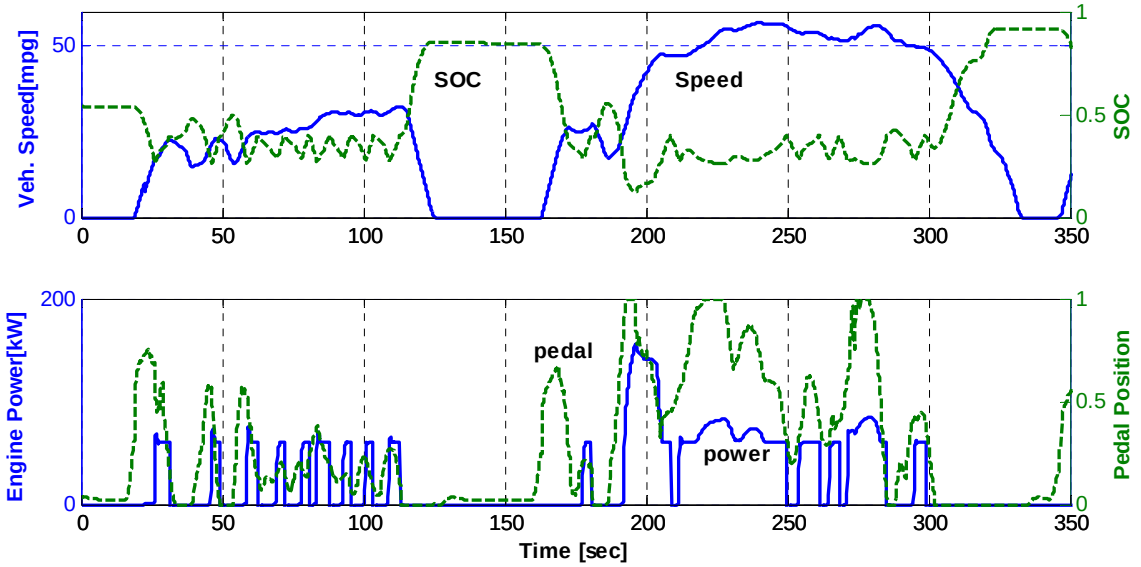

(c) System behavior

Figure 3. 10. Design parameters and system behavior of the thermostatic SOC control in SHH

3.3.2. Modulated SOC Control Scheme

The modulated SOC control scheme originated from the idea that maintaining the SOC at the constant level will improve fuel economy by preventing the engine from charging the accumulator to avoid unnecessary energy conversions and storing the regenerative brake energy effectively by keeping SOC at the pre-designed low level before the braking event. With this power management, the energy generated by engine can flow directly to the P/M_{prop} bypassing the accumulator and maintain the constant SOC. In other words, the modulated SOC control uses the load-tracking concept but the integration feature of hydraulic accumulator filters the high frequency vehicle power demand so the engine operation becomes smooth.

Especially, the power management of the SHH system have been mostly done by thermostatic power management, but, the engine operation becomes very transient by frequent on-and-off's because of the low energy density of the hydraulic accumulator. In addition, the frequent on-and-off's of the engine result in the extra transient fuel consumption and exhaust emissions and aggravate the driver's comfort. In addition, it will reduce the durability of the engine and other system components.

As a result, as an alternative power management, the modulated SOC control prevents the charging of an accumulator with the extra engine power and ensures enough room for the regenerative braking energy. Because the engine power is only used to maintain the target SOC, the regenerative braking mostly does the charging of the accumulator. A similar approach to the power management of PHH system was derived from optimal power management studies, which showed that reducing the recharging of the accumulator with the engine power is advantageous for fuel economy because the inefficient energy conversion process lowers the system efficiency [11].

The accumulator power can assist the engine power in the case of the high vehicle power demand with the stored energy at the constant level, SOC_{target}, and SOC_{target} works as a buffer improving the drivability. The assist of stored hydraulic energy at SOC_{target} is especially useful for the diesel engine operation because of the turbo-lag during the severe acceleration.

The modulated SOC control uses a PI feedback controller to maintain the SOC_{target}. The SOC_{target} needs to be high enough to guarantee the vehicle mobility. However, it

also needs to be low enough to maintain the SOC as low as possible before the braking event to absorb the regenerative braking energy as much as possible for a given accumulator size and duty cycle. Accordingly, the design value of target SOC highly depends on the accumulator size and the driving schedule, i.e., the energy buffer size and regenerative braking potential.

The vehicle power demand is the sum of the engine power and accumulator power in Equation (3.1). In SHH system, the engine operation is independent of the wheel so the engine power is only related to the P/M_{gen} power in Equation (3.2). Because the accumulator power is composed of the P/M_{gen} and P/M_{prop} powers in Equation (3.3), the vehicle power demand is just the P/M_{prop} power in Equation (3.4).

$$\text{Vehicle power demand} = \text{Engine power} + \text{Accumulator power} \tag{3.1}$$

$$\text{Engine power} + P/M_{gen}\ \text{power} = 0 \tag{3.2}$$

$$\text{Accumulator power} = P/M_{gen}\ \text{power} + P/M_{prop}\ \text{power} \tag{3.3}$$

$$\text{Vehicle power demand} = P/M_{prop}\ \text{power} \tag{3.4}$$

The control input of the modulated SOC control is ΔSOC, which is $SOC_{target} - SOC_{current}$ and the controller output is the normalized engine power level that is between zero and one. The engine power demand is calculated by multiplying the maximum engine power by the normalized engine power level in Equation (3.5). The anti-windup scheme is used to remove the saturation of the integration error.

$$P_{eng,demand} = P_{eng,max} \times \left[K_p \left(SOC_{target} - SOC_{current} \right) + K_i \int \left(SOC_{target} - SOC_{current} \right) dt \right] \tag{3.5}$$

where $P_{eng,demand}$ is the engine power demand, $P_{eng,max}$ is the rated engine power, SOC_{ref} is the target SOC, K_p is a proportional gain and K_i is an integral gain. The controller performance is tuned by proportional gain and integration gain but finding suitable gains is not an easy task. The proper proportional gain and integral gain are selected from the EIL test with the baseline SHH model because the EIL test is more demanding condition than the pure simulation case with a relatively simple engine model. These final gains show quite robustness that changes in the hydraulic device sizes do not affect much on the controller performance. Therefore, final gains can be used for the design optimization process that changes system parameters at each run of the cycle simulation. The feed forward control can be added to reduce the load of feedback

control and to increase control gains for the better control performance in this feedback control logic but it is not applied in this study. The actual control block of the engine power demand in MATLAB/Simulink environment is shown in Figure 3. 11. The engine can be idle or idle-stop when the engine power demand is zero. To prevent the oscillation of the engine power demand near zero, a relay function is added at the end of the controller.

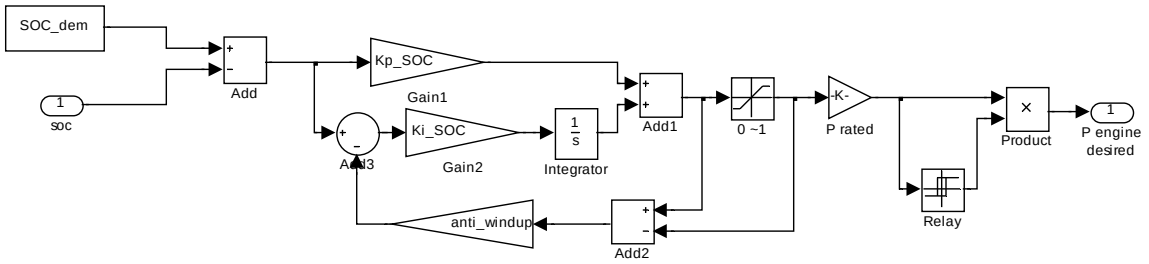

Figure 3. 11. Modulated SOC control in SIMULINK

This modulated SOC control in SHH system is observed to have four different modes in Figure 3. 12. Firstly, when the accumulator SOC is high enough, only accumulator energy is used to drive the vehicle. Usually, the accumulator is charged after the braking, so this mode always happens when the vehicle starts. The engine power and P/M_{gen} power are zero and the P/M_{prop} only propels the vehicle consuming the accumulator energy in Figure 3. 12(a).

Secondly, as the accumulator SOC is close to the SOC_{target}, the engine starts to provide the part of vehicle power demand in Figure 3. 12(b). The start of this mode is tuned by the gain control in Figure 3. 11. As the gains increase the hydraulic-assist mode starts earlier. The engine power is transferred to the P/M_{prop} through $P/M_{gen.}$ This mode is the transition from the hydraulic-only drive to the hydrostatic drive.

Thirdly, when the SOC is maintained at SOC_{target}, only the engine power is used to drive the vehicle. The fluid flow generated from P/M_{gen} is equals to the consumption in P/M_{prop} in hydrostatic equilibrium in Figure 3. 12(c). The hydraulic energy stored at SOC_{target} is used as buffer when the driver needs sudden accelerations compensating system delays, e.g., turbo-lag.

Fourthly, if the driver needs more power than the maximum engine energy, the accumulator energy of SOC_{target} is used until it reaches the pre-designed SOC_{min}, which is set as the minimum SOC, to prevent the cavitation inside the hydraulic path in Figure 3.

12(d). Instead of using the shut-off valve, the power management is designed to reduce the vehicle power demand to maintain the SOC_{min}. As a result, the cavitation and durability issues can be avoided. When the SOC reaches SOC_{min}, the engine power maintains the rated condition at the hydrostatic equilibrium. The example of the modulated SOC control during FUDS clearly shows how the modulated SOC control scheme works according to the vehicle power demand and SOC in Figure 3. 12(e).

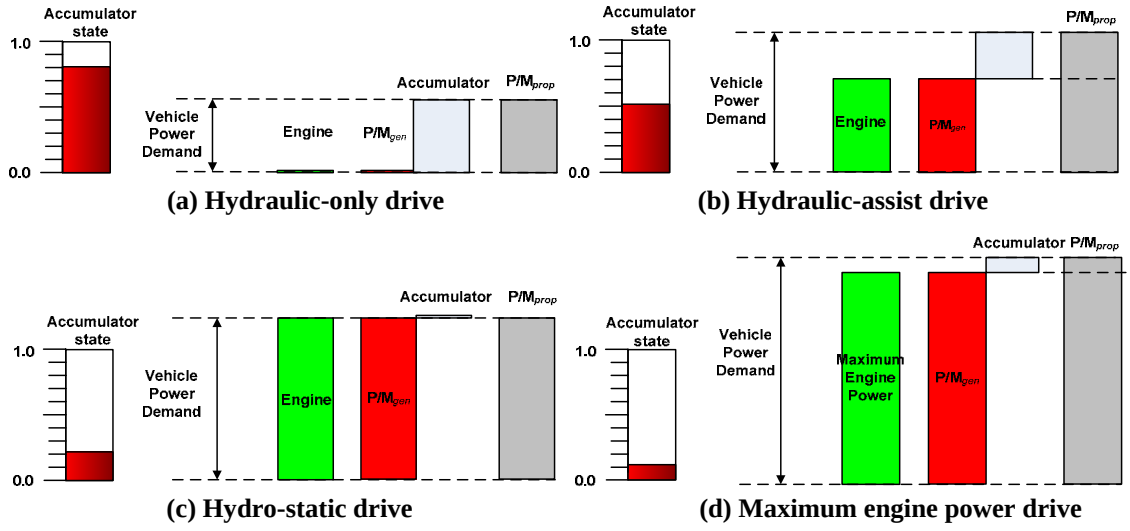

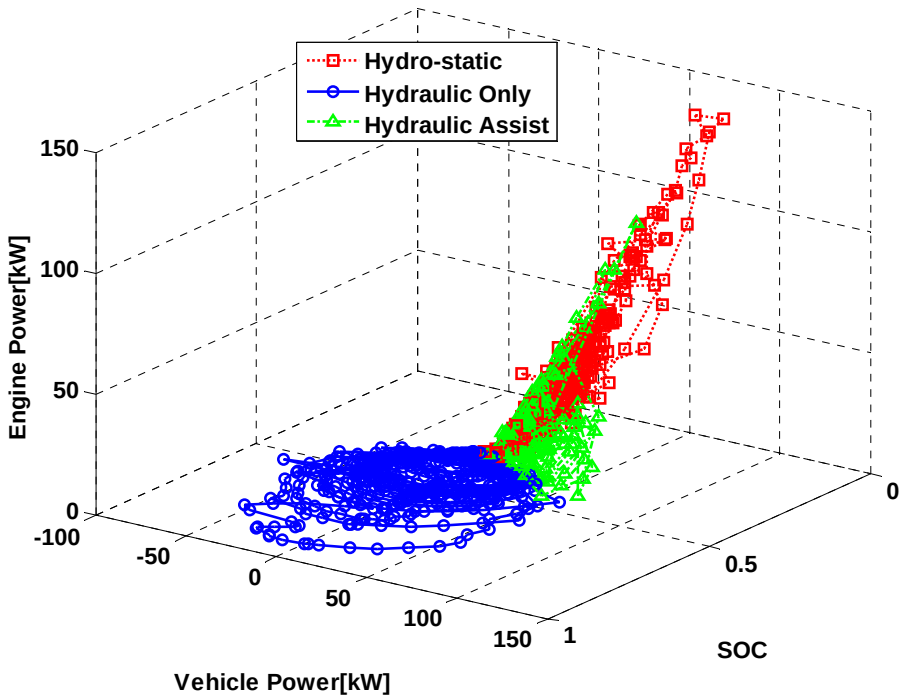

(e) Engine power, SOC, and vehicle power demand relation (SOC_{target} = 0.25, FUDS)

Figure 3. 12. Four modes of the modulated SOC control scheme

The example of the modulated SOC control is shown in Figure 3. 13. The modulated SOC control scheme controls the engine power demand smoothly because the accumulator works as an energy buffer. Therefore, the modulated SOC control can reduce transient exhaust emissions and improve the driver's comfort in the actual vehicle application. In the modulated SOC scheme, the controller gains must be selected to be reliable not to deplete the SOC even at the most severe acceleration point in the given driving schedule and not to oscillate the engine power.

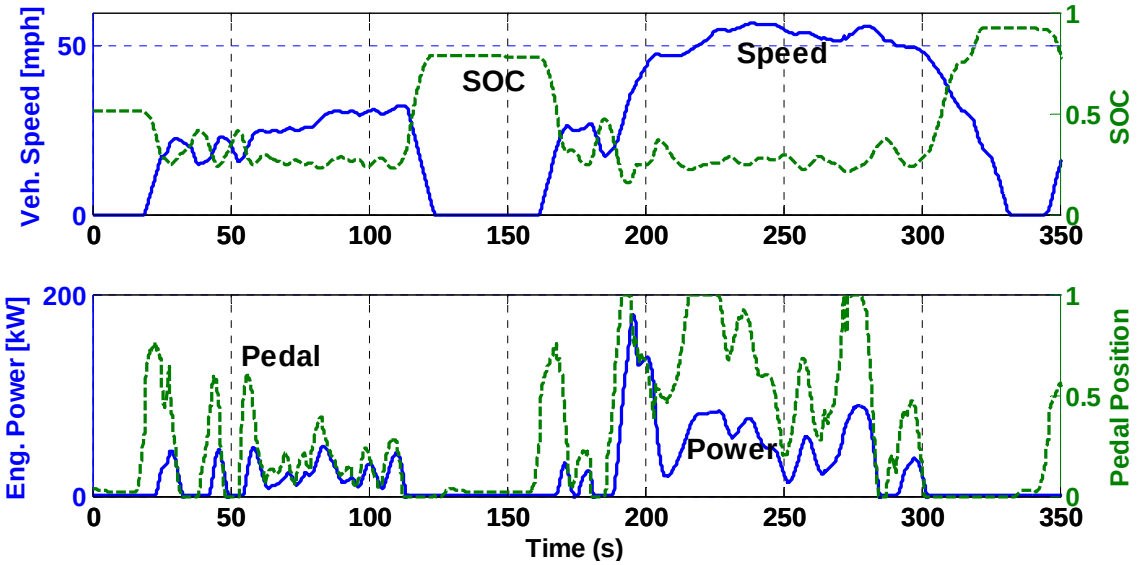

Figure 3. 13. SHH system behavior of the modulated SOC control scheme

3.3.3. Engine Speed and Torque Control

The engine speed and torque can be independently controlled in series hybrid systems for a given engine power demand. Thus, the desired engine speed and torque are pre-designed according to the specific objective. In this study, the objective is fuel economy improvement, so the engine speed and torque are controlled along pre-selected minimum BSFC line on the engine map shown by the dotted line in Figure A. 1. However, optimizing only engine operation does not guarantee the system level optimization and this will be discussed again at power management optimization in Chapter 4.

The engine speed is controlled by the P/M_{gen} torque and the engine torque is controlled by the engine rack signal that determines the fuel delivery to the engine. Speed deviation from the reference speed is input to the PI feedback controller and the displacement factor of P/M_{gen} is the normalized output from -1 to 0 in Equation (3.6). The anti-windup scheme is used to remove the saturation from the integration.

$$x_{P/M_{gen}} = K_p\left(\omega_{eng,ref} - \omega_{eng,current}\right) + K_i\int\left(\omega_{eng,ref} - \omega_{eng\_current}\right)dt \quad (3.6)$$

where $\omega_{eng,ref}$ is demand engine speed, $\omega_{eng,current}$ is engine speed measurement, K_p is a proportional gain, and K_i is an integration gain.

The engine torque control is much harder than the speed control because the torque control is controlling the acceleration implicitly, so the torque signal is a higher order signal than the speed signal. As a result, the feedback control of the engine torque is not easy even with the simplified engine model and it needs the torque measurement that is expensive and noisy in real vehicle applications. Therefore, the open-loop torque control is applied with pre-measured engine rack values corresponding to the pre-set torque values for given engine power demands. The main assumption of the open loop control is as follows. Firstly, the speed control is fast and reliable. Secondly, the calibrated rack position for the given torque is repetitive. Thirdly, the transient effect in the torque build-up, e.g., turbo-lag, is not significant. As a result, the actual engine speed can synchronize the torque output as the pre-set point on the engine map. This open loop torque control works better when the engine power demand is controlled smoothly. These engine speed and torque control strategy is proven to work by successful EIL validation tests presented in Chapter 5.

3.4. Series Hydraulic Hybrid Design Optimization

The system-design optimization methodologies for the parallel hybrid system have been proposed for the HEV [24], [42], [100] and the HHV [12]. Rahman et al. [26] presented design studies of series HEV with simulation model based on the performance target without conjunction of the optimization objective, such as fuel economy or emission or both. This section presents the design optimization of SHH system with fuel economy objective under performance constrains.

3.4.1. SHH Design Optimization Setup and Result

The design optimization of a SHH vehicle starts with the selections of initial design parameters, and the initial design parameters are derived from the following criteria. Firstly, accumulator size should be large enough to provide propulsion energy until the engine reaches the power demand as a buffer and absorb the full braking energy from given duty cycle. However, it should be small enough for the packaging and reducing heat transfer loss. Secondly, the P/M_{gen} size should be large enough to absorb the

maximum engine power and match the maximum engine torque at minimum SOC to control engine speed at any condition. P/M_{gen} is directly connected to the engine, assuming maximum speed of P/M is higher than the rated engine speed, 3300rpm. Thirdly, P/M_{prop} size should be large enough to satisfy vehicle performance constraints. Fourthly, the final gear ratio guarantees maximum vehicle speed within maximum P/M_{prop} speed that is assumed as 4000 rpm in this study.

With initial design values, parametric studies show the effects of designs variables on fuel economy and vehicle performance and refines initial design values for baseline SHH in Figure 3. 14. The increase of accumulator size improves the fuel economy and vehicle performance until the fuel economy saturates because regenerative energy is limited and heat loss increases in Figure 3. 14(a). The increase of P/M_{prop} decreases the fuel economy because the increase of P/M_{prop} makes system efficiency lower by reducing average displacement factor. The 0-50 mph acceleration time starts to increase at a certain point as the P/M_{prop} size increases in Figure 3. 14(b). This is because larger P/M_{prop} depletes the accumulator energy fast and the lower displacement factor of larger P/M_{prop} decreases the system efficiency during hydrostatic condition. The increase of target SOC decreases the fuel economy because the room for regenerative braking energy in accumulator deceases as shown in Figure 3. 14(c). However, the low SOC_{target} reduces the accumulator's capability of assisting engine power during engine power delay so the low target SOC reduces the drivability.

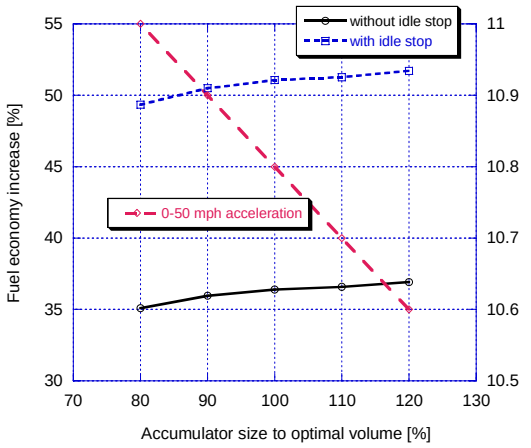

(a) Effect of accumulator size

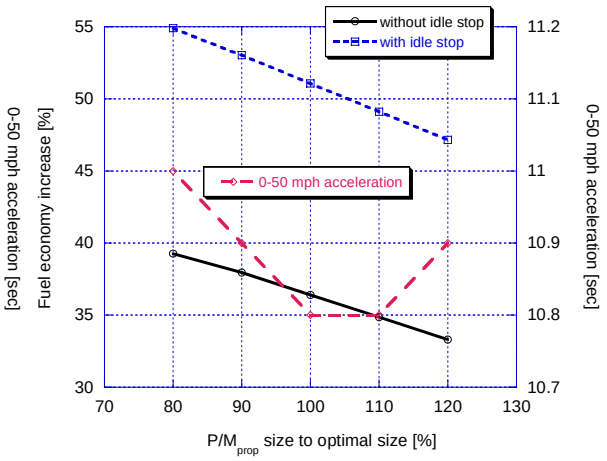

(b) Effect of P/M_{prop} size

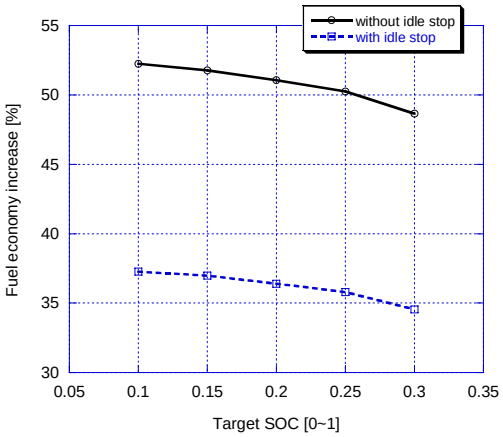

(c) Effect of SOC_{target}

Figure 3. 14. Effects of SHH design parameters on fuel economy and vehicle performance

The parametric study has a limitation to be used as a design optimization tool because it only shows one parameter effect at a time and the number of data points increases exponentially as the number of variables increases. Even though the parametric study finds a good baseline fuel-economy value, it dose not guarantee that the fuel economy value is the optimum and baseline design satisfies constraints. As a result, the optimization process uses the baseline design values for estimating the boundary of design parameters at the initial stage.

As a first step, the conventional HMMWV model simulation is carried out to find performance constraints and assess the baseline fuel economy. The aim of optimization is to improve fuel economy under vehicle performance constraints of the conventional vehicle and HMMWV operation standard as shown in Table 3. 1.

Table 3. 1. Performance constraints of the design optimization

Performance	Constraint
Gradeability @ 55 mph	> 2%
Gradeability @ 45 mph	> 3%
Acceleration: 0 – 50 mph time (initial SOC : 1.0)	< 10.8 second (of conventional)
Speed error lasting time (over 2 mph deviation)	< 1 second

The system design optimization uses the modulated SOC control scheme because the modulated SOC control scheme has only one variable, SOC_{target}. On the contrary, the thermostatic SOC control scheme has 4 variables (e.g., threshold power, threshold SOC,

max-power SOC and dead-band). The number of design variables increase the computation time exponentially. Therefore, after the device size for the performance constraints are found after the optimization, parameters of only thermostatic SOC control scheme will be optimized in the following section. Baseline SHH vehicle design parameters and boundaries of design optimization are shown in Table 3. 2.

Table 3. 2. Design parameters and boundaries of the design optimization in SHH

Design parameter	Baseline value	Upper and lower boundary
SOC_{target}	0.2	0.1~0.5
Front P/M_{prop} Size [cc/rev]	180	90~360
Rear P/M_{prop} Size [cc/rev]	180	90~360
P/M_{gen} Size [cc/rev]	300	240~360
Final gear ratio	2.67	1.34~4.05
Accumulator volume [Liter]	70	35~140

The design optimization adopts the general-purpose nonlinear sequential quadratic programming (NLSQP) to reduce the intensive computation time of optimization process because the NLSQP guarantees fast convergence [46], [100]. However, this gradient-based optimization technique does not guarantee the global optimal point, so the design optimization uses the multi-start method to increase the probability of finding the global optimal fuel economy [12], [42]. In doing multi-start method, the optimization process should start at random points and the random points should be distributed evenly in the design space, so the design of experiment (DOE) technique is used for the random-sampling of initial design values. The design optimization process uses the Latin-hypercube sampling to generate 50 points randomly in the total design space [47].

After cycle simulations and vehicle performance tests with 50 points, the optimization process picks five multi-start points, which show relatively better fuel economy and vehicle performance. Then, the optimization process applies the NLSQP for five multi-start points with iSIGHT optimizer [48]. The design optimization result of five starting points is shown in Table 3. 3.

Table 3. 3. Multi-start points and optimization result in SHH

No	Target SOC [0~1]	Front P/M_{prop} Size	Rear P/M_{prop} Size	P/M_{gen} size [cc/rev]	Final gear ratio	Acc. Volume [Liter]	0~50 mph time [sec]	Fuel economy* [mpg]
#1	0.10	107	118	389	2.86	78	11	17
Optimized	0.23	177	115	292	2.22	107	9.3	17.6
#2	0.15	173	156	563	1.99	129	7.9	16.4
Optimized	0.15	177	123	496	1.83	129	8.6	17
#3	0.19	299	96	481	2.10	84	9.1	16.3
Optimized	0.19	163	96	278	2.07	140	8.7	17.7
#4	0.26	343	211	346	5.01	54	10.5	16.1
Optimized	0.23	213	111	600	2.32	121	9.7	17.5
#5	0.34	140	167	279	1.88	56	9.1	17
Optimized	**0.26**	**159**	**130**	**250**	**1.92**	**82**	**8.8**	**17.6**

*** without idle-stop condition**

Finally, the optimization point from #5 is selected as final optimal point because the fuel economy is close to the best fuel economy with the smallest accumulator volume that is 20~40 % less than other optimized points. This finally designed accumulator's energy storage capacity is 800 kJ and the specific energy is 6.7 kJ/kg. The total P/M_{prop}'s maximum power is about 490 kW and P/M_{gen}'s maximum power is 440 kW at 4000 rpm and 350 bar. The specific power of rear P/M_{prop} is about 5.2 kW/kg and specific power of P/M_{gen} is 5.6 kW/kg. The system behavior during FUDS is shown in Figure 3. 15.

After design optimization, the fuel economy improves 42 % without idle-stop and 58 % with idle-stop in comparison with the fuel economy of the conventional vehicle during FUDS. In contrast to the case of the parallel hybrid system, this optimized SHH vehicle system shows the highway fuel economy gain around 10 % over that of the conventional vehicle. Even though the highway cycle has rare chance of regenerative braking, the efficient engine operation of SHH on the minimum BSFC line brings fuel economy gains and this means that the energy conversion efficiency of the SHH is

comparable with the mechanical efficiency of conventional vehicle, for example, auto transmission, etc.

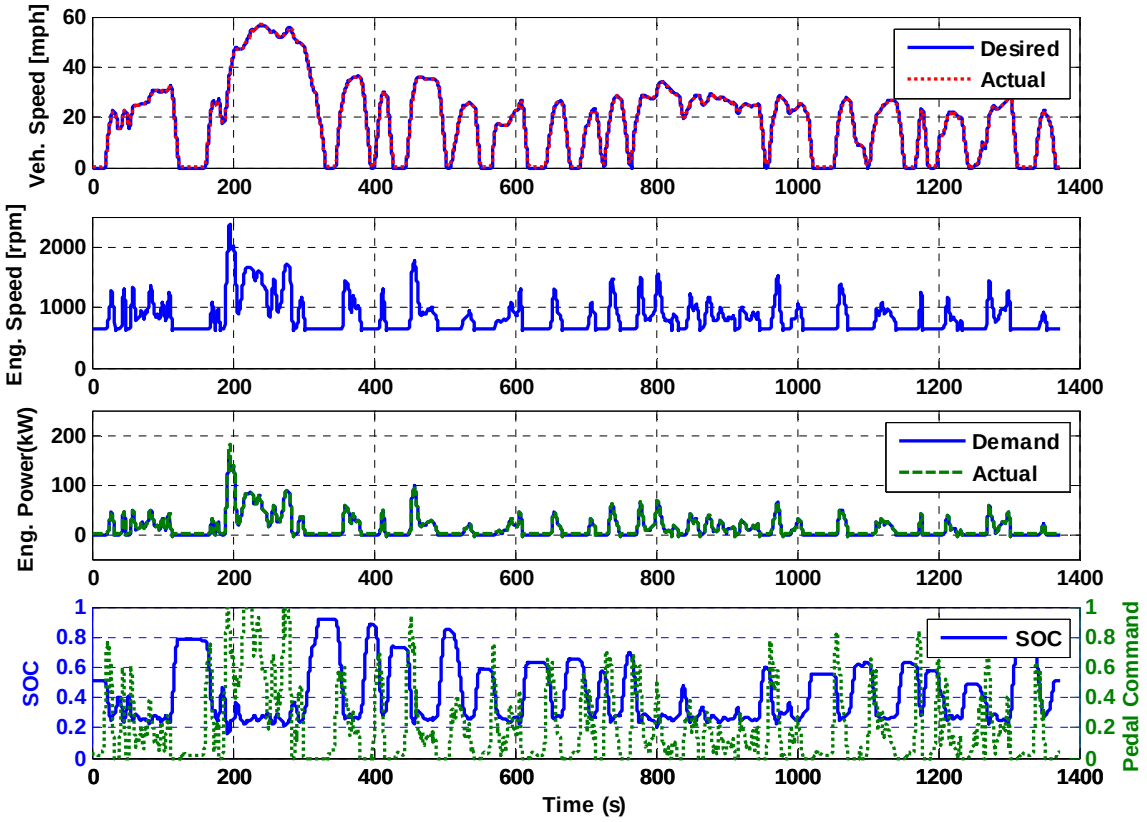

Figure 3. 15. SHH system behavior of the modulated SOC control during FUDS

Figure 3. 17 shows that the conventional vehicle uses higher engine speed and lower load in comparison to the SHH vehicle in Figure 3. 17 because the wheel speed determines the engine speed in the conventional vehicle even though the automatic transmission intervenes. In addition, Figure 3. 17 shows that the speed and torque are controlled well on the minimum BSFC line in the SHH. The fuel consumption in SHH is peak around the 80kW which is relatively lower than the "sweet spot" power, around 120kW. This implies that the engine is too large for the vehicle and the engine downsizing is possible if only the vehicle performance is not degraded. The engine downsizing case is represented at the end of this chapter.

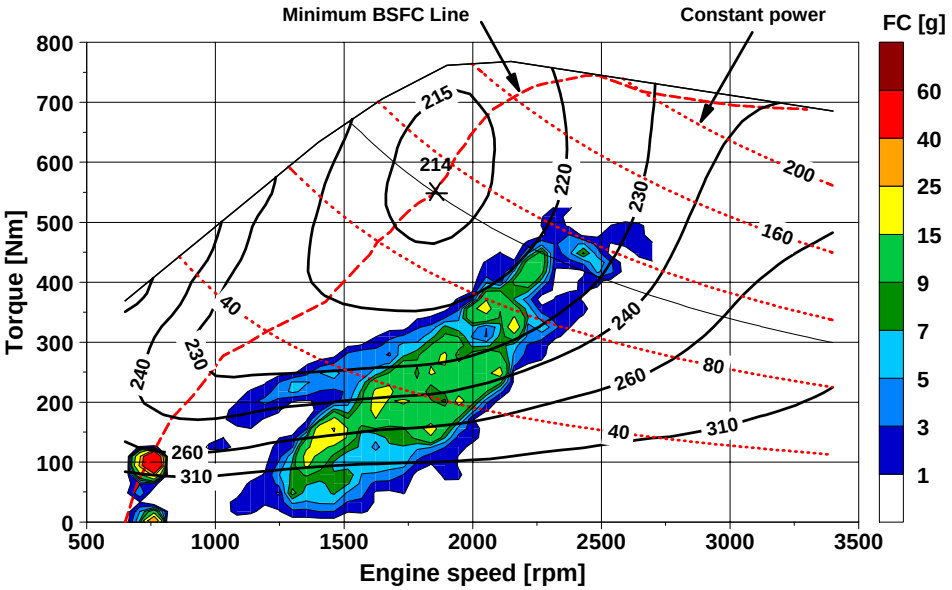

Figure 3. 16. Integrated fuel consumption of the conventional vehicle during FUDS

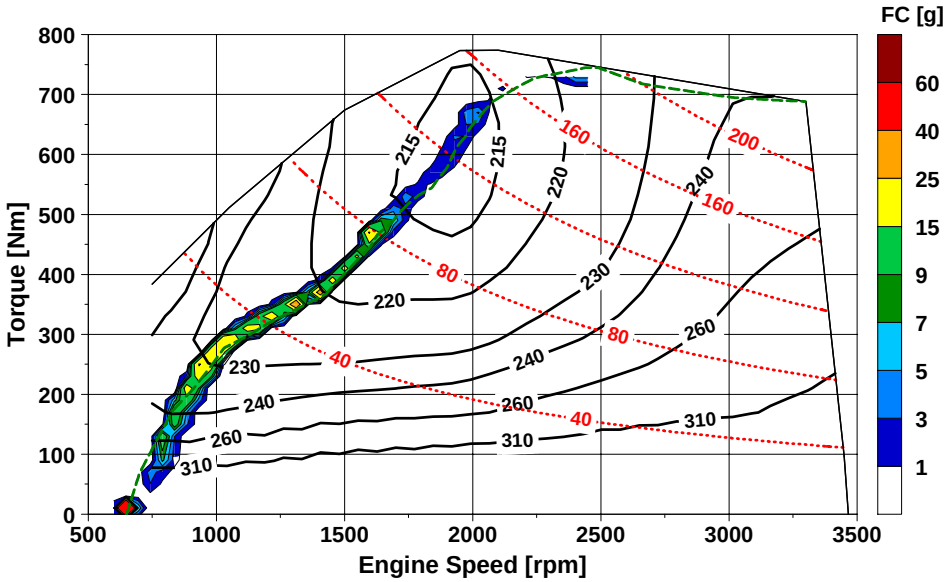

Figure 3. 17. Integrated fuel consumption of the SHH vehicle during FUDS

The overall energy flow and energy conversion efficiency of each hybrid system device during FUDS is represented in Table 3. 4. The accumulator efficiency is as high as 96 % and the P/M efficiency is almost 90 % during FUDS. The rear P/M$_{prop}$'s pump efficiency is only 17 % because it works only at part load during braking because of the sequential operation of P/M$_{prop}$s and the front P/M$_{prop}$ runs at higher load in regenerative braking. The energy flow through reservoir is less than 4 % of energy flow through the accumulator.

Table 3. 4. Overall energy flow and conversion efficiency of each hydraulic hybrid device

	Energy in [kJ]	Energy out [kJ]	efficiency [%]
Engine (with/without idle) (Diesel LHV : 42.8 MJ/kg)	57583/ 51677	19061	33.1 / 36.9
Accumulator*	8384	8025	95.7
Reservoir*	304	292	96.1
P/M_{gen} pumping	19061	16806	88.2
Front P/M_{prop} pumping	7327	6638	90.6
Front P/M_{prop} motoring	2958	2596	87.8
Rear P/M_{prop} pumping	85.3	14.7	17.2
Rear P/M_{prop} motoring	19955	17845	89.4

*** Bypassed energy is not counted after the accumulator pressure reaches the maximum.**

3.4.2. Thermostatic SOC Control Optimization

The thermostatic SOC control optimization uses the same design parameters found by design optimization with the modulated SOC control scheme because those parameters ensure to satisfy performance constraints. Thus, only thermostatic SOC control parameters are searched.

The parametric study shows that the threshold power is not simply the sweet-spot power because the engine operation becomes transient as the threshold engine power increases and the fuel consumption to push the engine power to the high threshold power increases (see Figure 3. 18). Interestingly, the idle fuel consumption increases as the threshold power increases so there exists a maximum fuel economy with idle-stop case at 60 kW because the fuel consumption to pushing engine power up to threshold power becomes larger than fuel reduction from the increase of idle-stop time (see Figure 3. 19). Fuel economy decreases continuously without idle-stop because increase of the threshold power also increase idle fuel consumption.

Fuel economy decreases as threshold SOC increases because the room for storing regenerative braking energy decreases. A similar parametric study sheds light on the effect of dead-band. The mechanism is straight forward, since increased dead-band extends charging events and reduces their frequency. Increased charging causes to

decrease the storage for regenerative braking and increase more energy conversion with low efficiency. Values between 0.1 and 0.15 yield the best fuel economy (see Figure 3. 20). Optimized thermostatic SOC control scheme shows comparable fuel economy with that of modulated SOC control scheme without idle-stop. However, optimized thermostatic SOC control scheme shows about 5 % better fuel economy improvement than that of modulated SOC scheme with idle-stop.

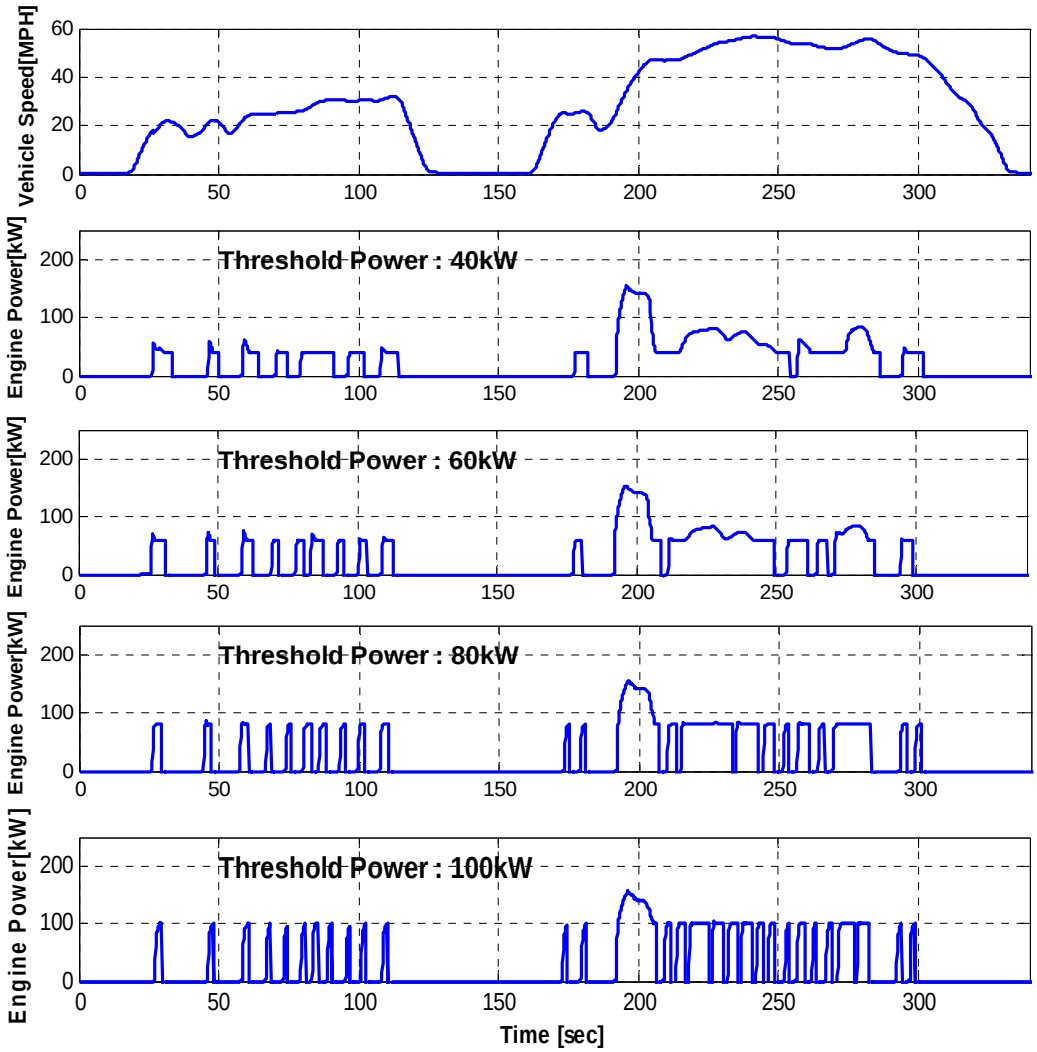

Figure 3. 18. Threshold-power effect on the engine power behavior

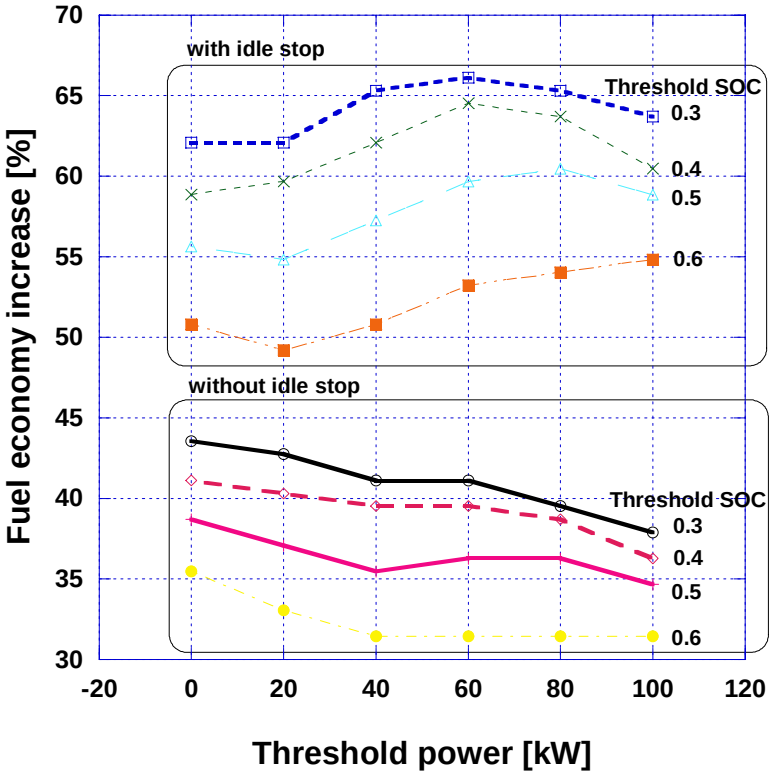

Figure 3. 19. Effects of threshold power and threshold SOC on the fuel economy gain

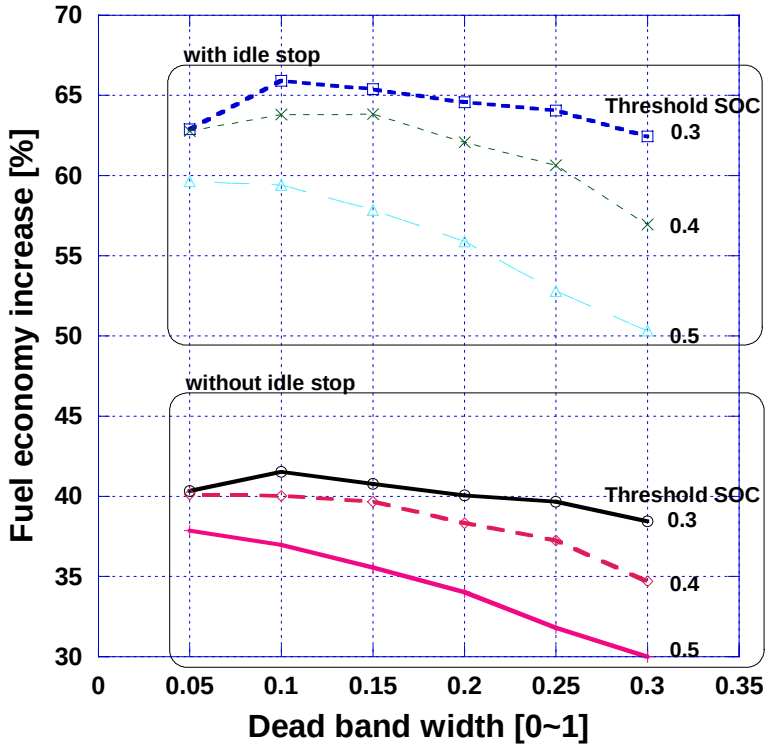

Figure 3. 20. Effects of dead-band width and threshold SOC on the fuel economy gain

Final parameters after the optimization of the thermostatic SOC control scheme are shown in Table 3. 5.

Table 3. 5. Optimized control parameters in the thermostatic SOC control

Threshold SOC	0.3
Max power SOC	0.1
Dead-band	0.1
Threshold Power (kW)	60

Even though the SOC control is reliable, the engine operation seems to be very transient during FUDS shown in Figure 3. 21. Therefore, this transient engine operation may cause system stability and durability problems. In addition, the transient emission and driver's comfort may be issues, too. EIL tests may show transient effects on the fuel economy and emissions with a real engine in Chapter 5.

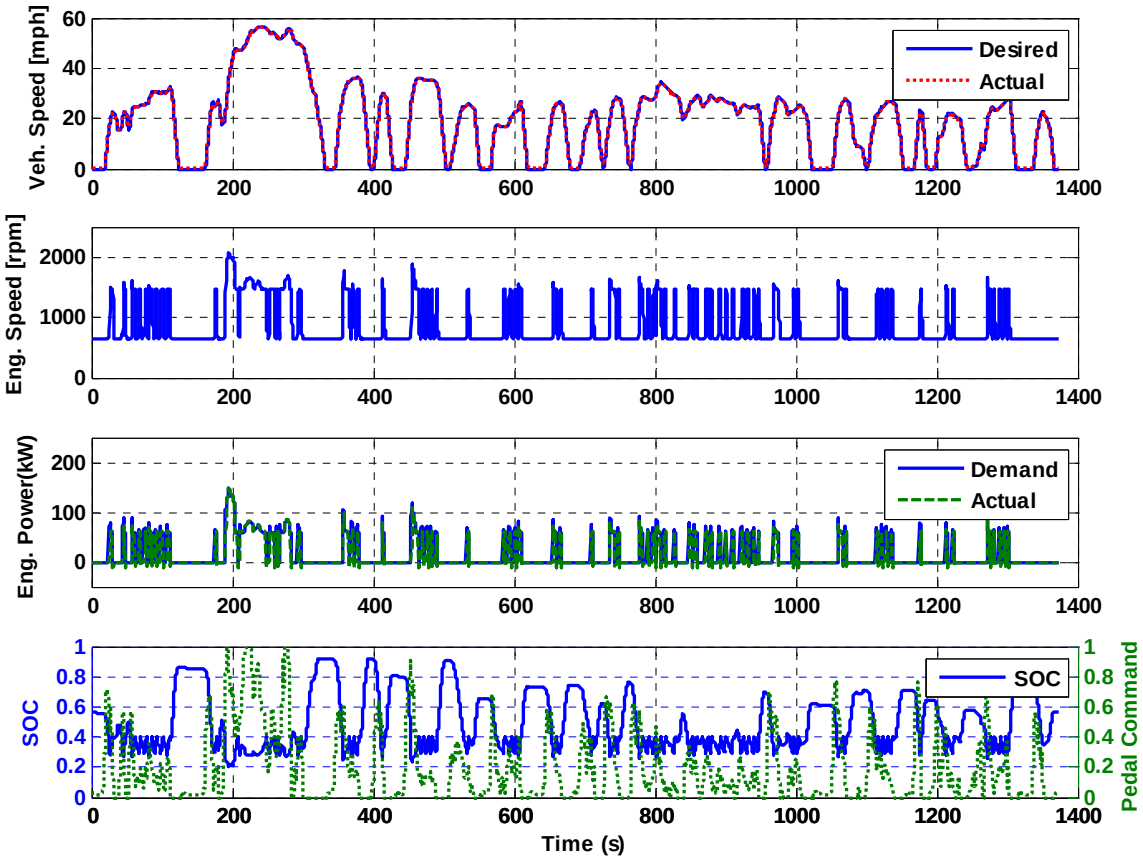

Figure 3. 21. SHH system behavior with thermostatic control during FUDS

The integrated fuel consumption during FUDS with thermostatic SOC control is shown in Figure 3. 22. The fuel consumption concentration clearly jumps from idle to

60kW of threshold power. Thus, the fuel consumption concentrates around 60kW and the fuel consumption at low BSFC decreases in comparison with that of modulated SOC control. However, the idle fuel consumption also increases so much in case of without idle-stop. As a result, it can be said that the success of thermostatic control heavily relies on idle-stop-and-start capability to improve fuel economy.

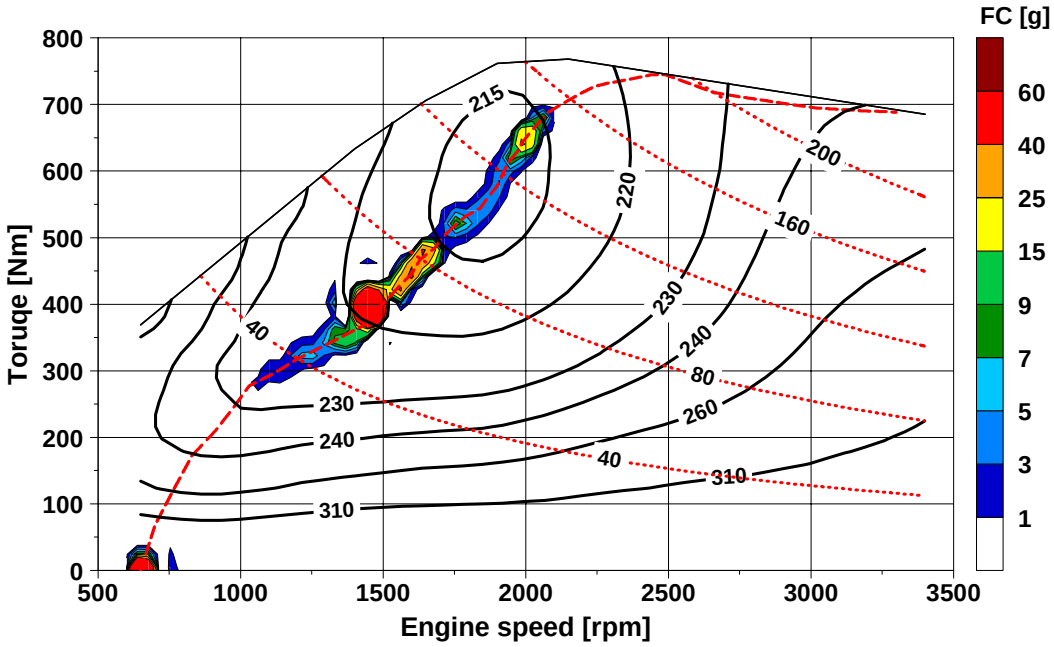

Figure 3. 22. Integrated fuel consumption with thermostatic SOC control (threshold power: 60 kW)

3.4.3. SHH Super-HMMWV Performance

The SHH super-HMMWV's 0~50 mph acceleration test result is shown in Figure 3. 23. The maximum engine power demand is input by step function with initial SOC of 1.0. The engine power reaches its maximum with small delay because it is independent of wheel speed. The SOC increases just after the gearshift at the P/M_{prop} speed of 3000 rpm because the P/M_{prop} speed decrease instantly and the discharging rate from the P/M_{prop} decreases with same pumping rate from P/M_{gen}. The vehicle reaches maximum speed keeping the hydrostatic equilibrium at pre-designated minimum SOC.

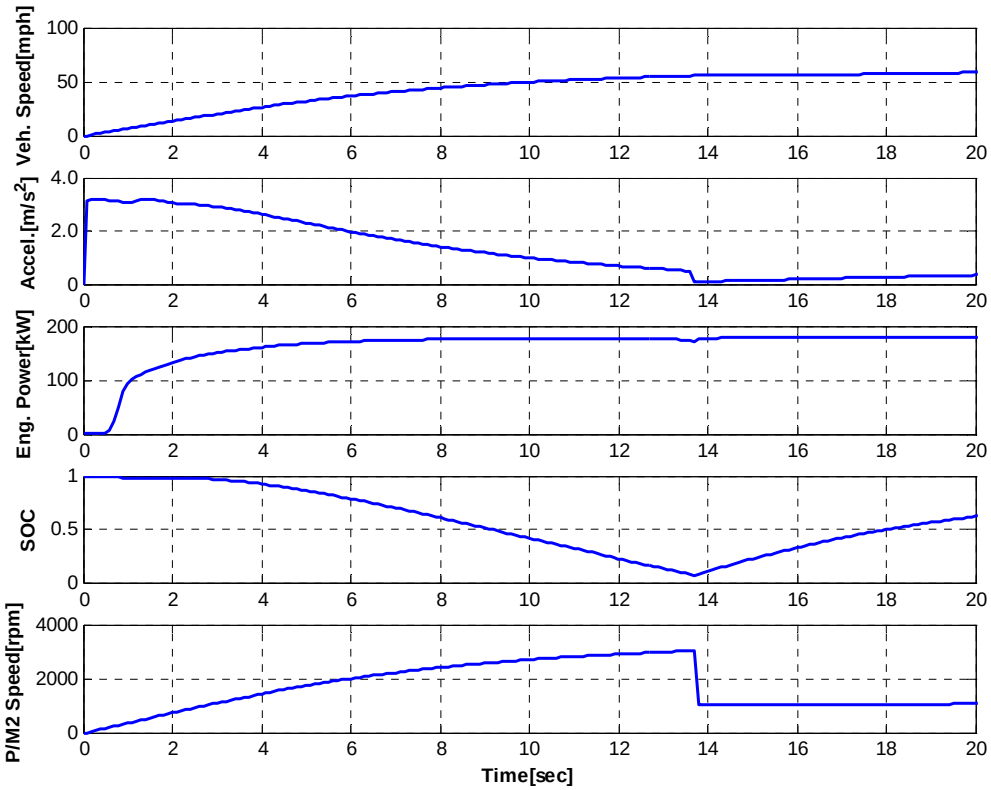

Figure 3. 23. 0-50mph acceleration test result in SHH

3.5. Design Optimization with Engine Downsizing

The engine downsizing is usual in hybrid application because the secondary energy storage and the secondary propulsion device exist. However, in hydraulic hybrid system, accumulator energy is consumed so fast because of its low energy density. When the SOC of the accumulator is at the minimum level in hydrostatic equilibrium, the vehicle uses only engine power, so engine downsizing means lowering the vehicle performance in hydraulic hybrid system.

As a result, in hydraulic hybrid, the engine downsizing is not favored for mobility and reliability of driving [11]. However, in SHH system, the engine operation is independent of the wheel, so the engine can produce maximum power regardless of the vehicle condition on the contrary to the PHH system.

Only 75% of the maximum engine power is enough to pass FUDS as shown in Figure 3.17. Given that the maximum speed is not the critically factor in HMMWV operation, the constraints become only acceleration and cruise on the graded road condition for vehicle performance. The V8 engine model is downsized to V6 engine assuming only decreasing the cylinder number from 8 to 6. Therefore, engine torque, total fuel

consumption and emissions are scaled down to 75% of original engine with same fuel delivery to each cylinder.

3.5.1. Design Optimization Setup and Result with a V6 engine

The design optimization process selects the component sizes and powertrain parameters under the same performance constraints of V8 SHH case. As a result, the engine downsizing can be possible with comparable acceleration and gradeability performance only if the maximum speed of the vehicle is not the critical constraint. The same design optimization approach of V8 case is used for the V6 case. The design optimization result with V6 is shown in Table 3. 6.

Finally, optimization point from #3 is selected as an optimal point because the fuel economy is close to the best fuel economy value, but the accumulator volume is 20~50 % less than the other optimization points. In comparison with the optimal point of V8 engine, this optimal point has similar parameters except reduced P/M_{gen} size, which is 76 % of V8 design, and it is close to the ratio of V8 to V6 engine size. It is reasonable that the P/M_{gen} size corresponds proportionally to the maximum engine torque because P/M torque is proportional to the maximum displacement. The accumulator size increases a little and seems to compensate the reduced maximum engine power. The sum of P/M_{prop} size and final gear ratio is close to those of V8 case satisfying the same acceleration constraint.

As a result, 0-50 mph acceleration time is 0.5 second faster than that of conventional even though the maximum speed decreases with engine downsizing. The fuel economy improves 7 % without idle-stop and 4 % with idle-stop in comparison with the fuel economy of the SHH V8 case during FUDS. The fuel consumption at idle is lower in the case of V6, so the idle-stop effect is relatively small.

The finally designed accumulator's energy storage capacity is 835 kJ and the specific energy is 6.7 kJ/kg. The total P/M_{prop}'s maximum power is about 490 kW and P/M_{gen}'s maximum power is 345 kW at 4000 rpm and 350 bar. The specific power of rear P/M_{prop} is about 5.2 kW/kg and specific power of P/M_{gen} is about 5.4 kW/kg.

Table 3. 6. Multi-start points and optimization result with V6 in SHH

No	Target SOC [0~1]	Front P/M_{prop} Size	Rear P/M_{prop} Size	P/M_{gen} size [cc/rev]	Final gear ratio	Acc. Volume [Liter]	0~50 mph time [sec]	Fuel economy* [mpg]
#1	0.198	156	178	269	2.64	80	12.3	17.5
Optimized	0.145	236	90	184	1.87	126	9.1	18.6
#2	0.263	305	107	536	1.83	127	8.7	17.0
Optimized	0.310	191	119	583	1.70	112	10.1	18.2
#3	0.361	173	167	233	3.62	52	12.2	17.6
Optimized	**0.248**	**154**	**134**	**194**	**1.87**	**86**	**10.3**	**18.5**
#4	0.427	321	250	214	1.34	137	7.8	17.3
Optimized	0.277	238	100	215	1.50	102	10.1	18.3
#5	0.500	332	101	187	2.53	95	12.2	17.2
Optimized	0.169	174	128	233	2.33	135	10.7	18.2

*** without idle-stop condition**

The system behavior of V6 SHH system during FUDS is shown in Figure 3. 24. In comparison with V8 case, the V6 engine produces almost the same amount of power but the relative torque level is higher with the downsized engine, so the chance to use better BSFC region increases.

The integrated fuel consumption of SHH with V6 engine is shown in Figure 3. 25. In comparison with the SHH with V8 engine, the engine operation points move to the higher load level especially around the “sweet spot” of the downsized engine, so more fuel is consumed at most efficient region. However, if the engine power demand over the “sweet spot” is needed, engine downsizing case results in lower engine efficiency.

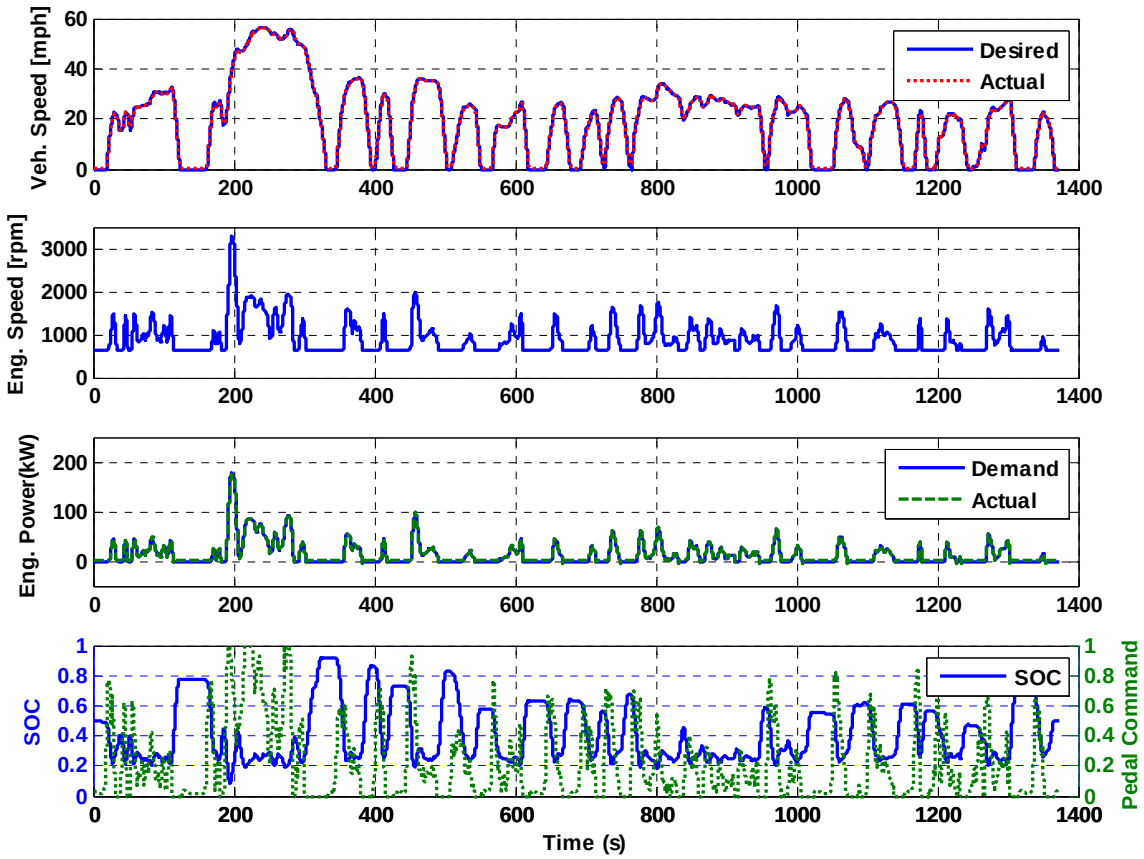

Figure 3. 24. System behaviors of optimized SHH super-HMMWV with V6 during FUDS

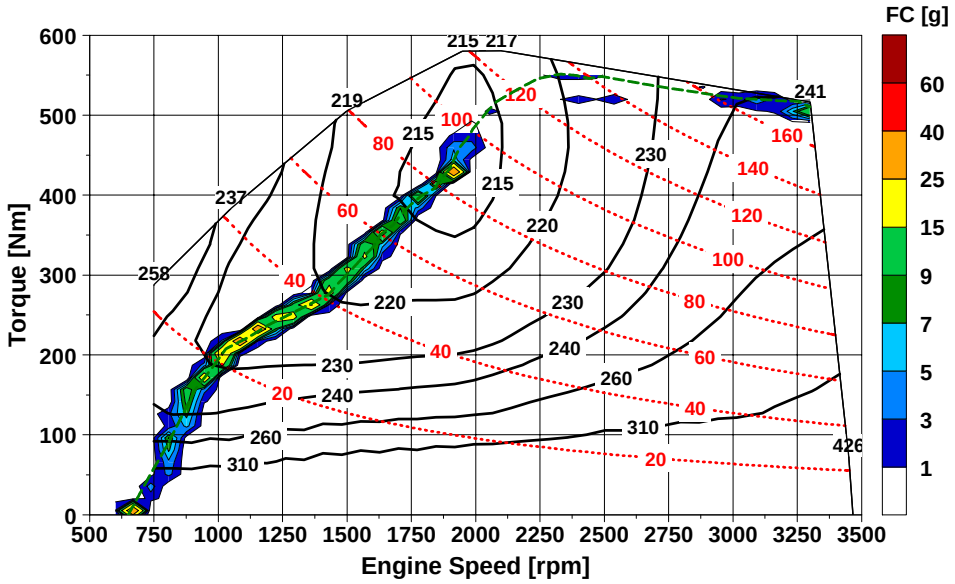

Figure 3. 25. Integrated fuel consumption of SHH with V6 during FUDS

The overall energy flow and energy conversion efficiency of each hybrid system device during FUDS are shown in Table 3. 7. The engine efficiency for V6 case increases by 0.4 and it is 1.2% higher in the case of with- and without idle-stop

respectively than those of V8 cases are because engine downsizing improves engine efficiency by moving the engine operation points close to “sweet spot”. Overall energy conversion efficiency of each hydraulic device during FUDS is similar with those of V8 case.

Table 3. 7. Overall energy flow and conversion efficiency of each hydraulic hybrid device with V6

	Energy in [kJ]	Energy out [kJ]	efficiency [%]
Engine (with/with out idle) (Diesel LHV : 42.8 MJ/kg)	54886/ 50444	18805	34.3 / 37.3
Accumulator*	9146	8756	95.7
Reservoir*	344	330	95.9
P/M_{gen} pumping	19061	16616	88.4
Front P/M_{prop} pumping	7400	6684	90.3
Front P/M_{prop} motoring	3444	3019	87.7
Rear P/M_{prop} pumping	50.8	5.5	10.9
Rear P/M_{prop} motoring	19325	17339	89.7

*** Bypassed energy after the accumulator pressure reaches the maximum is not counted**

The test result of the three 4x4 architecture options with the optimized design parameters with V6 are shown in Table 3. 8. Sequential operation with 2 P/Ms shows about 5% improved the energy conversion efficiency in front and rear P/M for regenerative braking and propulsion respectively. It leads to about 10% fuel economy gain in comparison to those of 1-P/M with a transfer case or simultaneous operation with 2 P/Ms.

The breakdown of fuel economy improvement over conventional vehicle is done for SHH V6 engine case in Figure 3. 26. The regeneration portion is the fuel economy difference between with and without regeneration and it results in 58 % of total fuel economy improvement. The engine shutdown effect is 21% assuming the most effective engine-shut down control. The hydraulic system-efficiency improvement effect includes the engine operation optimization on the minimum BSFC line and the gain is 21%. The engine downsizing effect by moving the engine operation points close to the “sweet spot” is around 12 %, almost half of total improved system efficiency. The improvement from the sequential 4x4 operation is also assessed. Sequential operation brings 8 % of gain

during propulsion and 9 % gain during braking. Interestingly, without engine downsizing and the sequential 4x4 operation, the gain from SHH system efficiency is only 1 %.

Table 3. 8. Fuel economy gains and hybrid system efficiencies of different 4x4 architectures with V6 during FUDS

	mode	1 P/M $_{prop}$	2 P/M$_{prop}$ Simultaneous	2 P/M $_{prop}$ Sequential
Fuel economy improvement [%]	without idle-stop	37.3	38.8	49.2
	with idle-stop	48.1	49.8	62.1
Accumulator efficiency [%]*		95.8	95.8	95.7
P/M$_{gen}$ pump efficiency [%]*		88.6	88.8	88.4
Front P/M $_{prop}$ efficiency [%]	motor mode	84.7	85.1	87.7
	pump mode	85.1	85.1	90.3
Rear P/M $_{prop}$ efficiency [%]	motor mode		85.1	89.7
	pump mode		85.1	10.9

*** Bypassed energy is not counted after the accumulator pressure reaches the maximum.**

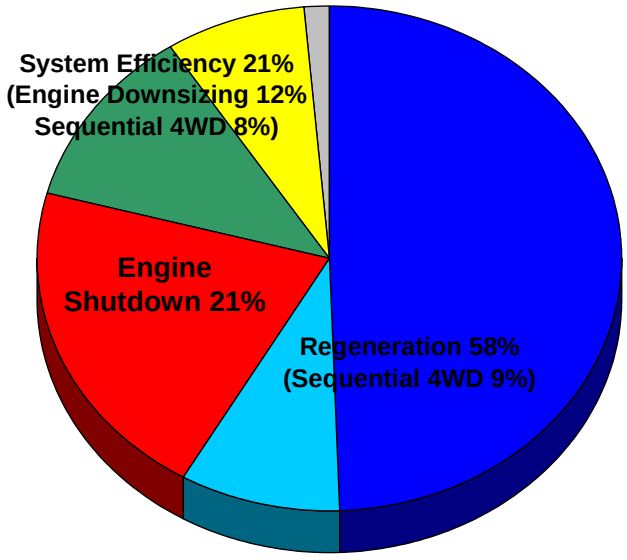

Figure 3. 26. Breakdown of fuel economy gains in SHH with V6

3.5.2. Thermostatic SOC Control Optimization with a V6 engine

For the optimization of thermostatic SOC control scheme with downsized V6 engine, the same procedure is used as the V8 engine case. The optimal threshold power is located at 60 kW same as V8 engine case with idle-stop and the idle-stop is also needed

to maximize the advantage of thermostatic control, Figure 3. 27. The optimal dead-band width is around 0.1~0.15, Figure 3. 28.

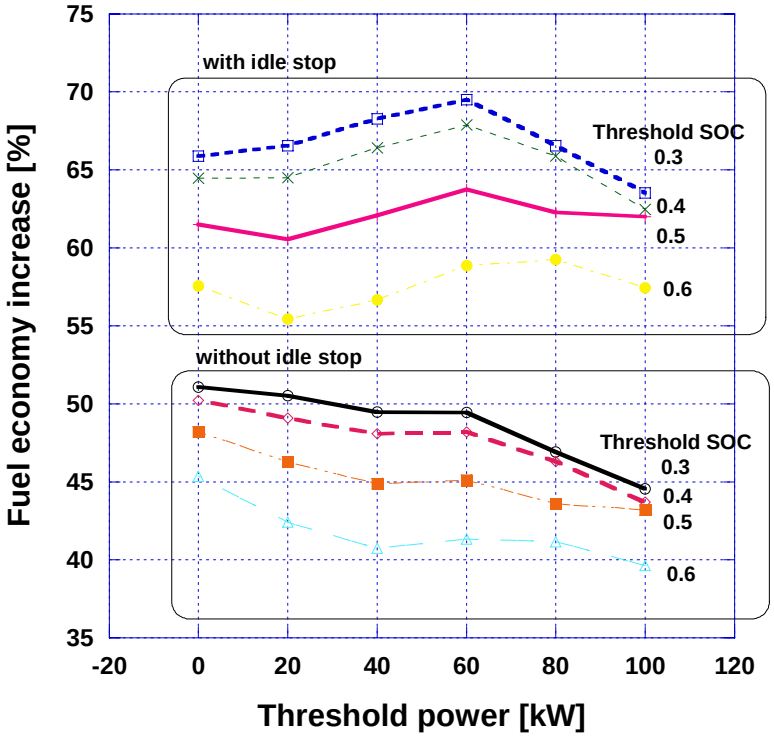

Figure 3. 27. Effects of threshold power and threshold SOC on the fuel economy gain with V6

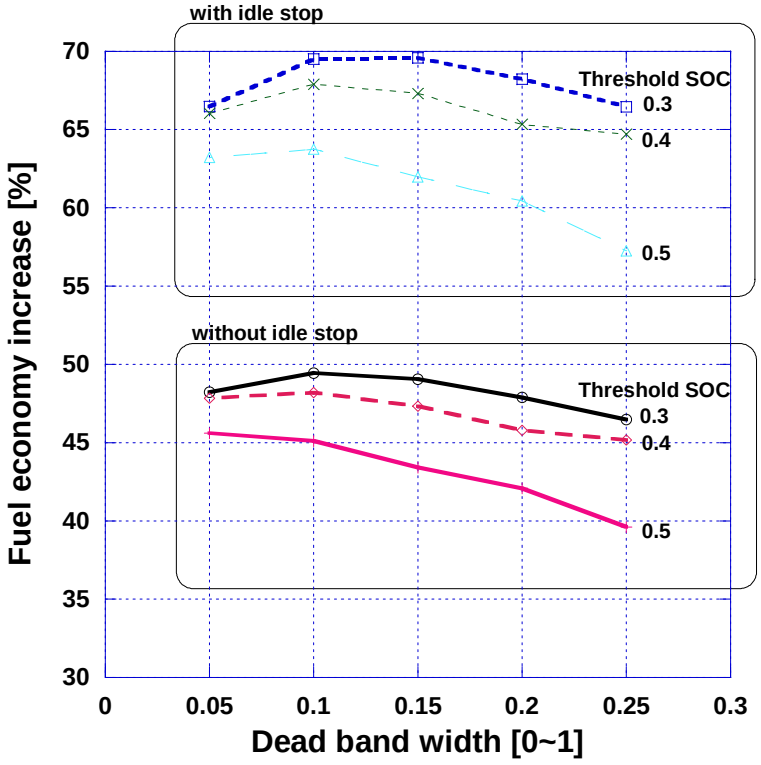

Figure 3. 28. Effects of dead-band width and threshold SOC on the fuel economy gain with V6

The system behavior with thermostatic SOC control with V6 during FUDS is shown in Figure 3. 29. The vehicle speed follows reference speed well with downsized engine. In comparison with V8 case, the engine speed is higher with same engine power demand and more transient engine operations are expected in the real engine application of the downsized engine case.

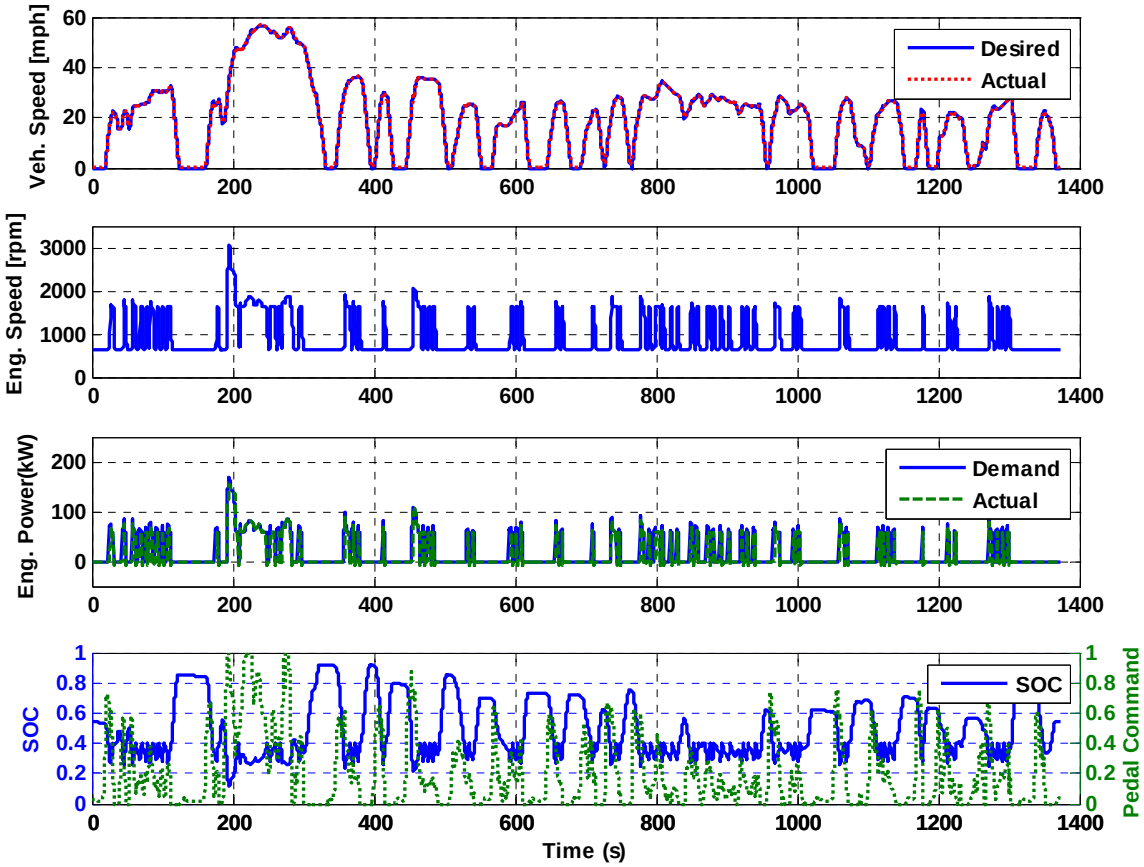

Figure 3. 29. System behavior of the thermostatic SOC control with V6 during FUDS

The modulated SOC control scheme and the thermostatic SOC control scheme show comparable fuel economy gain without idle-stop in Table 3. 9. With idle-stop capability, the thermostatic SOC control scheme shows about 6% of the fuel economy gain than the modulated SOC control scheme because it has longer idle time than the modulated SOC control. However, the step change of the engine power, which has overshoot and undershoot of the engine power in simulation, may cause control problem in the real engine application. In addition, the highly transient engine operation in the thermostatic SOC control scheme increases the transient emissions (e.g., NO_x and soot) much more than that of modulated SOC control scheme in the real engine operation and aggravates

the durability of system and driver's comfort. The EIL test will validate how the transient thermostatic control may affect fuel economy and emissions in Chapter 5.

Table 3. 9. Summary of fuel economy gains of the SHH super-HMMWV

		Conventional	Optimization (V8)		Optimization (V6)	
			Modulated control	Thermostatic control	Modulated control	Thermostatic control
		Fuel economy [mpg]	Fuel economy improvement [%]	Fuel economy improvement [%]	Fuel economy improvement [%]	Fuel economy improvement [%]
Without idle-stop	FUDS (City)	12.4	41.9	41.5	49.2	49.2
	HWFET (Highway)	14.3	10.3	9.6	12.6	11.2
With idle-stop	FUDS (City)	-	58.1	65.9	62.1	68.2
	HWFET (Highway)	-	11.1	11.7	12.6	12.5
0 – 50 mph Acceleration time [sec]		10.8	8.8		10.3	

3.5.3. SHH Super-HMMWV Performance with V6

The 0-50 mph acceleration test of V6 engine case with initial SOC of 1.0 shows 1.5 second delay in comparison with SHH with V8 but still 0.5 second faster than conventional vehicle because the maximum engine power is available instantly (see Figure 3. 30). Therefore, the V6 engine is enough to maintain the comparable vehicle performance of the conventional vehicle with V8 except maximum vehicle speed. The gradeability is also comparable with SHH V8 case because the gradeability is determined by P/M_{prop} torque, not by engine torque and the total size of P/M_{prop} of V6 case is almost the same to that of V8 case. The engine and vehicle behavior during 0-50 mph acceleration is represented in Figure 3. 30.

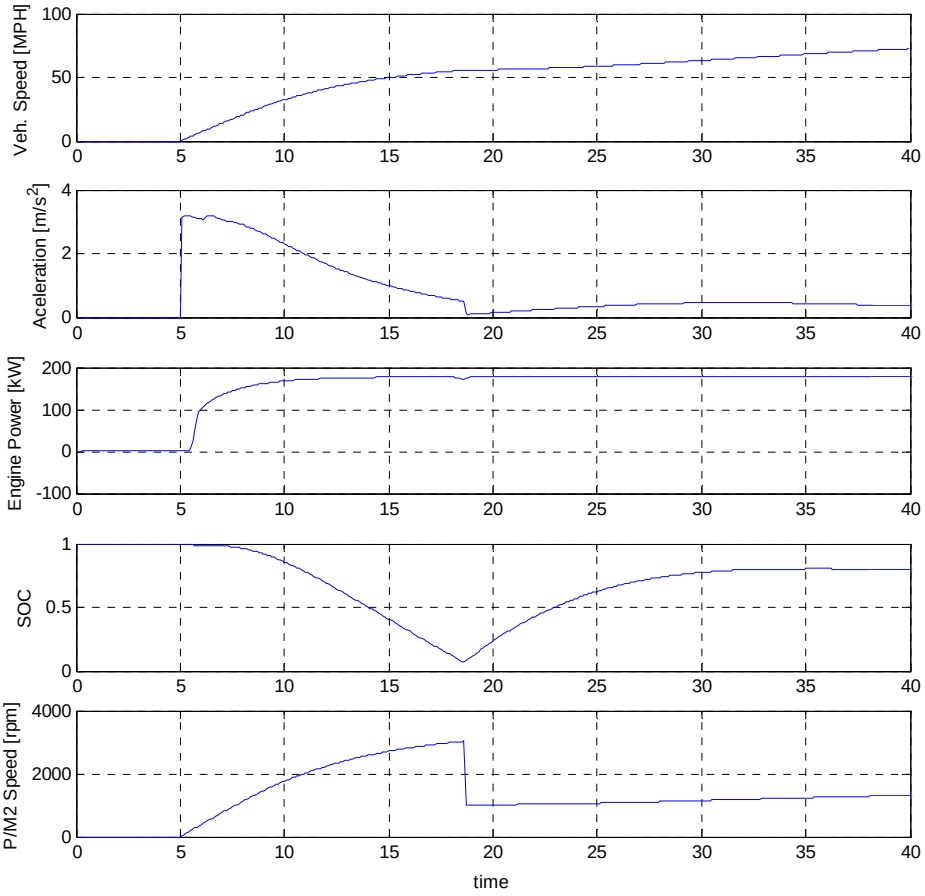

Figure 3. 30. 0-50mph acceleration test result of SHH, V6

CHAPTER 4

POWER MANAGEMENT OPTIMIZATION OF A SERIES HYDRAULIC HYBRID SYSTEM

Most of the power management optimizations of the series hybrid system have been concentrated on the series HEV system. Such as the studies on the sub-optimal implementable power management using the ECMS algorithm. The algorithms for optimizing the policy over a known schedule or using a probabilistic driver input have been successfully demonstrated before for parallel hybrids [11], [43], [44], but not the series configuration. In particular, the work on using the stochastic dynamic programming technique is almost non-existent even in series HEV studies. Therefore, the studies on the power management optimization of the SHH system are entering an uncharted territory, with particular challenges stemming from a low energy density of the energy storage device (accumulator).

In this study, the deterministic dynamic programming technique is applied to find out the optimal benchmark supervisory control and the fuel economy potential of the SHH system for a given driving schedule. Rather than attempting the rule extraction with subjective criteria, the stochastic dynamic programming technique is used to get the sub-optimal implementable supervisory control policy directly. The application of optimization algorithms for control strategy development of a series HHV raises interesting philosophical questions, as the problem cannot be distilled down to a traditional power-split decision. Instead, the policy needs to coordinate operation of two seemingly independent sub-systems, a power-generation and a propulsion unit, in a way that best fits the objectives for the complete vehicle.

4.1. Dynamic Programming Introduction

The supervisory powertrain control refers to the power management among multiple power devices, e.g., engine, generator/motor and hydraulic P/M, in the hybrid propulsion system. The lower-level powertrain control manages each power device control from the

given power demand. The power-management optimization is the optimization of the control strategy about the distribution of the vehicle power demand to each power device at the system level.

Power management optimization of shows how much the efficiency or performance of the hybrid propulsion system can improve given a hybrid vehicle specification. In addition, because each power device's operation range is limited by the optimal power management, the power device development and calibration can be focused on the specific operation range, and therefore the development cost can be reduced. In this chapter, the optimal power-management strategy is explored with a dynamic programming technique after the baseline hybrid system parameters have been found from the design optimization process.

The power management of the hybrid propulsion system can be generally divided into three categories [76]. Firstly, the rule-based power management is an implementable power management in real time, which uses power-demand calculation rules according to pre-set conditions. For example, the state variables, vehicle power demand, wheel speed, and SOC, are compared with the reference values and pre-designed control input signals are provided to power devices such as the power-split ratio. The rule-based power management is a heuristic control and generally depends on the engineering intuition or experience. The rule can also be learned from the benchmark optimized power management.

Secondly, the semi-optimized power management is divided into a static system power management optimization, e.g., equivalent consumption minimization strategy (ECMS) and a dynamic system optimization, e.g., stochastic dynamic programming (SDP). The ECMS is an implementable power management in real time based on the static optimization. The static system efficiency is calculated off-line simulations before the actual vehicle operation, and the control outputs are calculated according to state inputs from pre-designed power demand maps. The ECMS is based on the average efficiency of the power devices and the hydraulic or electrical energy is converted into the equivalent fuel consumption. The SDP is based on the dynamic model and a full-state feedback look-up table is generated with multiple state inputs and control outputs. The SDP technique is based on the stochastic probability function extracted from

predictions of the vehicle power demand during sampled cycles. Both the ECMS and SDP techniques have cost functions that need to be minimized and the cost can be fuel consumption, exhaust emissions, or any other property to be reduced.

Thirdly, the globally optimized power-management provides the trajectory of the control inputs minimizing the cost function during a pre-selected driving schedule. Because of its preview feature, the globally optimized power management cannot be implemented in a real-time application. However, the globally optimized power management can provide a benchmark power management that can be learned by the implementable power managements. The deterministic dynamic programming (DDP) is a technique to find a globally optimized power management and establish a benchmark. The optimal control inputs to power devices and corresponding state variables, e.g., SOC, are calculated from the given driving schedule, i.e., the vehicle power demand.

In this study, the power management optimization with DDP and SDP techniques for the SHH systems are carried out. A brief description of the DP algorithm is given below. For the nonlinear, multiple-input, and multiple-output dynamic system, the DP technique can find a globally optimized power management. The DP technique aims to minimize a cost, which is a mathematical expression of undesirable outcomes, and captures the trade-off relationship by systematically optimizing the current cost and expected future cost. The formulation of the DP algorithm assumes that the given problem can be described as a discrete-time dynamic system and that the cost function can be additive over time [70].

The dynamic system has to be represented in the discrete form

$$x_{k+1} = f_k\left(x_k, u_k, w_k\right), \qquad k = 0,1,...,N-1 \tag{4.1}$$

where

k indexes discrete time,

x_k is the state of the system and summarizes past information relevant to the future optimization,

u_k is the control or decision variable to be selected at time k,

w_k is a random parameter (also called disturbance or noise, depending on the context), and

N is the horizon or number of times that the control is applied.

The cost function is additive in that cost incurred at time k, denoted by $g_k(x_k, \mu_k(x_k), w_k)$, which accumulates over time, and the problem can be formulated as the optimization of the total cost

$$g_N(x_N) + \sum_{k=0}^{N-1} g_k(x_k, u_k(x_k), w_k) \tag{4.2}$$

where the optimization is over control u_k with random variable (disturbance), w_k.

The DP algorithm is based on Bellman's principle of optimality that states as follows [71].

"Let $\pi^* = \{\mu_0^*, ..., \mu_{N-1}^*\}$ be an optimal policy for the basic problem, and assume that when using π^*, a given state x_k occurs at time $k = i$ with positive probability. Consider the sub problem at x_k at time $k = i$ and wish to minimize the "cost-to-go" from time $k = i$ to time $k = N$,

$$E\left\{ g_N(x_N) + \sum_{k=i}^{N-1} g_k(x_k, u_k(x_k), w_k) \right\} \tag{4.3}$$

where E is the expectation and g_k is the instant cost at time $k = i$, then, the truncated policy $\pi^* = \{\mu_i^*, \mu_{i+1}^*, ..., \mu_{N-1}^*\}$ is optimal for this sub problem."

DP is divided into the deterministic dynamic programming (DDP) if the parameter w_k is a fixed value at time $k = i$ and the stochastic dynamic programming (SDP) if w_k is a random value at time $k = i$. Therefore, the DDP does not need the expectation and the SDP generates a probability function to calculate the expectation.

4.2. Series Hydraulic Hybrid Design Optimization Setup and Result

As a first step of the power management optimization, the design optimization of the SHH system is carried out. To make the DDP formulation simple and easy, a simultaneous 4x4 option with the same sizes of front and rear P/Ms is selected as the 4x4 architecture. For the speed reducing and torque multiplication, a 2-speed transmission, which has the shift ratio of 3:1 and 1:1, with the constant shift speed of the P/M_{prop} as a design parameter is considered. Modulated SOC control is used as the power management of the SHH system during the design optimization process. The 60 % gradeability is newly added to reflect actual HMMWV's performance expectations. The

vehicle is assumed to start at a level grade and the final speed should be over 5 mph at 60% grade to pass the constraint. FUDS is selected as a baseline driving-schedule for the design optimization. The design optimization setup is given below.

Objective: maximize fuel economy

Constraints:

0-50 mph acceleration time (initial SOC: 1.0) $\leq$ 10.8 second (of conventional vehicle)

Maximum speed $\geq$ 65 mph

Maximum grade $\geq$ 60% slope

Cruising grade (@ 50mph) $\geq$ 2% slope

Cruising grade (@ 40mph) $\geq$ 3% slope

Test-fail condition: continuous deviation of more than 2 mph from the reference speed over 1 second

The design-parameters and boundaries are set as shown in Table 4. 1 for the initial DOE sampling and design optimization process.

Table 4. 1. Design parameters and boundaries of the design optimization in SHH

Design parameter	Lower	Upper
Accumulator volume [Liter]	34.3	109.8
Target SOC	0.1	0.5
P/M_{prop} size [cc/rev]	90	270
P/M_{gen} size [cc/rev]	150	450
P/M_{prop} -shift speed [rpm]	2010	3990
Final-gear ratio	1.34	4.01

The optimization process follows the same as described in Chapter 3.4.1. Five multi-start points are selected after cycle simulations with randomly chosen 100 points selected by a DOE shown in Table 4. 2. The optimization procedure is shown in Figure 4. 1.

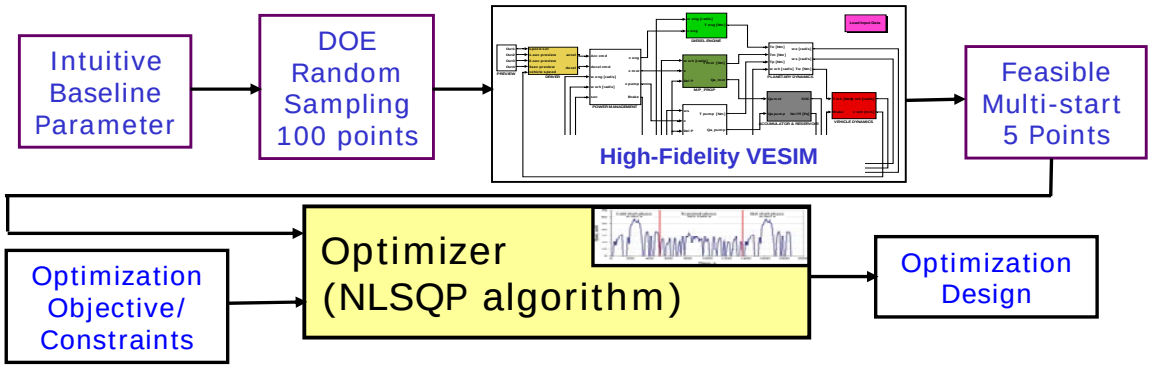

Figure 4. 1. Design optimization procedure of the SHH HMMWV

The optimal point from #2 is selected as an optimization point and will be used as a baseline SHH system design for the power management optimization as shown in Table 4. 2. With the same design parameters, the fuel economy reaches 17.9 mpg (9.2 % fuel economy increase) if the sequential 4x4 operation is applied.

Table 4. 2. Multi-start points and optimization result in SHH

No	Target SOC [0~1]	P/M_{prop} Size	P/M_{gen} size [cc/rev]	Shift speed [rpm]	Final gear ratio	Acc. Volume [Liter]	0~50 mph time [sec]	Fuel economy* [mpg]
#1	0.24	185	280	2727	5.00	108.3	7.1	15.4
Optimized	0.24	157	232	2502	4.5	100	7.9	16.3
#2	0.29	210	292	2211	4.70	102.9	7.0	15.2
Optimized	**0.28**	**168**	**227**	**2112**	**4.24**	**104**	**7.8**	**16.4**
#3	0.33	223	198	2169	2.07	109.8	8.8	15.1
Optimized	0.27	197	222	2076	2.15	110	9.2	15.9
#4	0.37	146	180	2766	4.26	64.8	8.5	15.9
Optimized	0.37	141	180	2690	4.36	76	8.4	16.2
#5	0.37	226	214	2091	5.14	107.5	6.6	14.7
Optimized	0.31	172	216	2064	4.21	108	7.7	16.3

*** without idle-stop condition**

The system behavior of the optimized design with the modulated SOC control during FUDS is shown in Figure 4. 2.

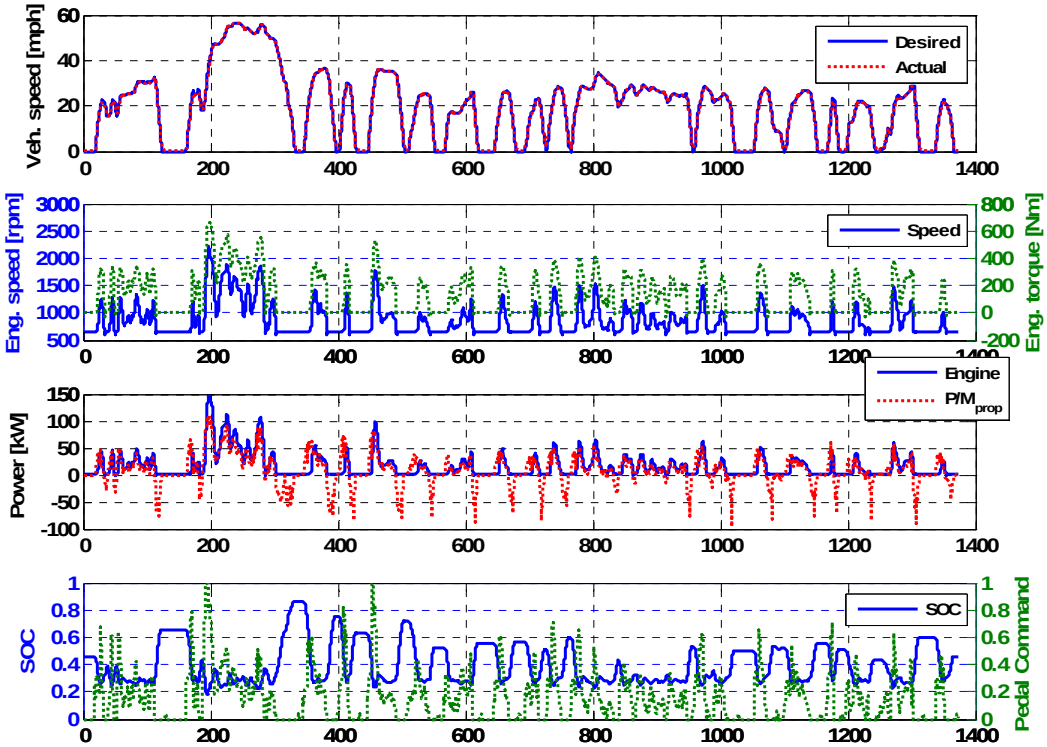

(a) System behavior during FUDS

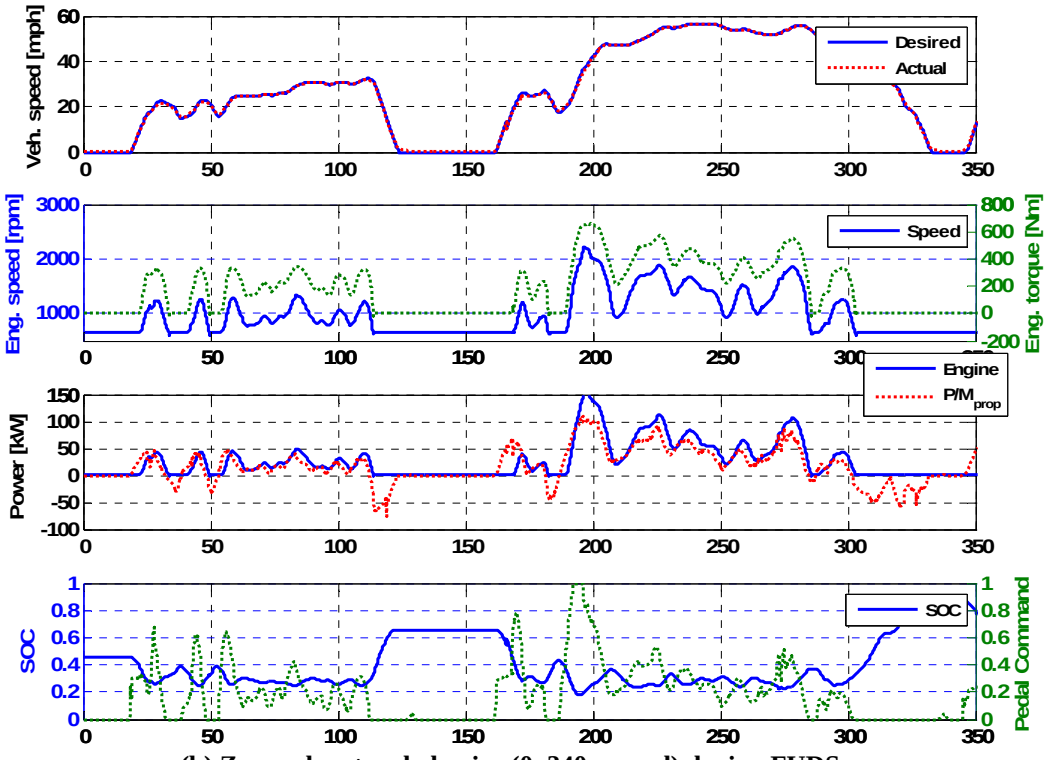

(b) Zoomed system behavior (0~340 second) during FUDS

Figure 4. 2. SHH system behavior during FUDS with modulated SOC control

4.3. Series Hydraulic Hybrid Power Management Optimization with Deterministic Dynamic Programming

As for the SHH system, studies using the DDP technique to find the optimal power management are none. The result of the DDP technique shows benchmark control inputs to power devices and corresponding state variables during a given driving schedule. In addition, the fuel economy from the DDP technique results indicates the theoretical maximum of the given design of the SHH system.

4.3.1. DDP Algorithm

The algorithm of the DDP technique is divided into three stages, generating the transition-cost table, backward minimization of sub-total cost and forward optimal-solution search. During the transition-cost table generating stage, the instant cost from the state transition with every possible initial state and control combination is calculated at each time step. At the stage of backward minimization of the sub-total cost, the accumulated cost-to-go is calculated in the backward time frame.

The minimized total cost J is

$$J = \min_{u \in U} \left[g_N\left(x_N\right) + \sum_{k=0}^{N-1} g_k\left(x_k, u_k, w_k\right) \right] \tag{4.4}$$

where U is the set of the plausible controls that satisfy the constraints of the dynamic system, so that the resultant state is physically meaningful. The backward minimization of the sub-total cost is carried out as follows.

Step N-1:

$$J_{N-1}^{*}\left(x_{N-1}\right) = \min_{u_{N-1}} g_{N-1}\left(x_{N-1}, u_{N-1}\right) + g_N \tag{4.5}$$

Step k, for $0 \le k < N-1$

$$J_k^{*}\left(x_k\right) = \min_{u_k} \left[g_k\left(x_k, u_k\right) + J_{k+1}^{*}\left(x_{k+1}\right) \right] \tag{4.6}$$

After the set of the plausible controls, U, is found from the backward cost minimization, the corresponding states and control inputs at each time, k, are searched by forward march in time horizon from a given initial condition.

4.3.2. SHH DDP Setup

With system design parameters found from the design optimization, the DDP technique is setup for the SHH system. To setup the DDP, states and controls are determined first. The vehicle power demand is extracted from the wheel power output of a high fidelity SHH VESIM and used as a pre-determined disturbance. From complex

actual states and controls in the SHH system, two states and two controls are selected to represent the SHH system and discretized as shown in Table 4. 3. Because, DDP is so expensive in terms of the computation time and memory occupation, it is critical to reduce the number of states and control inputs as much as possible. The grid sizes for the states and controls are selected after pre-DDP grid sensitivity tests. The grid sizes for the state and control inputs should be selected to be small enough to represent the reasonable system dynamics. However, DDP requires a large number of computations. Therefore, the grid size should not be too small. If the grid size is too large, the state does not change as the control changes.

The time step is also a critical factor in determining the computation time and memory usage. It is observed that if the time step is too small, the state does not change with different control inputs. Thus, the time step should be large enough but small enough to represent the system dynamics. The time step is also pre-tested with various values and determined as one second.

Table 4. 3. State and control variables and grid discretization in SHH DDP

State	Engine speed [rpm]	650 : 3300	40 grids
	SOC	0 : 0.025 : 1	40 grids
Control	Engine command	0 : 0.02 : 1	50 grids
	P/M_{gen} command	-1 : -0.02 : 0	50 grids

To reduce the computation time, the high fidelity SHH model is simplified such that it can shows the basic system dynamics of the high fidelity model. Firstly, the fast dynamics that is much faster than 1 Hz is neglected. Thus, the engine torque generation in the engine model is changed to a static look-up table. Secondly, the accumulator gas dynamics is changed to the polytropic state equation model where the gas volume is only a function of the gas pressure, instead of high fidelity real-gas dynamic model. The coefficients of the polytropic process are acquired from curve fitting the cycle simulation result of the high fidelity SHH vehicle model simulation. Thirdly, the high-fidelity vehicle model is changed to the simple road-load vehicle model. The rolling resistance coefficients of the simple vehicle model are calibrated to show almost the same vehicle

power demands, so the fuel economy is so close to that of high fidelity vehicle model with less than 1% difference.

In addition to the simplification of the SHH model, vectorization and an m-file approach are used to reduce the calculation time in generating the forward transition cost table. Firstly, the vectorization technique is especially advantageous for the multiple state and control problem with many grids. The vectorization enables the whole grids of a variable to be calculated at once instead one by one. This vectorization technique is known to reduce the calculation time dramatically [77], [83]. In this study, the SOC and the engine command are vectorized and they are input to the simulation as a matrix format not a single variable formant in the MATLAB environment.

Secondly, the m-file in MATLAB is directly used for the SHH system modeling instead of the MATLAB/Simulink model. By coding the SHH vehicle model in a m-file to calculate the transition cost table, the unnecessary time of running the Simulink model is removed and the calculation time can be reduced by a factor of 10 [83].

Physical constraints are given below and if the constraints are violated, an infinite penalty is given to the cost function.

$$0 \le SOC(k) \le 1 \tag{4.7}$$

$$\omega_{eng\_\min} \le \omega_{eng}(k) \le \omega_{eng\_\max} \tag{4.8}$$

$$T_{P/M_{prop}\_min} \le T_{P/M_{prop}}(k) \le T_{P/M_{prop}\_max} \tag{4.9}$$

The maximum P/M_{gen} speed is higher than the maximum engine speed so the P/M_{gen} speed is not added in the constraints. In contrast to the case of HEVs, the accumulator charge and discharge limits are not included because of the high-power density of the accumulator. In addition, the SOC can be from 0 to 1 in the hydraulic accumulator in comparison with the relatively narrow available SOC range of the battery. In addition to the physical constraints above, the engine operation is restricted at the low engine speed and high torque area because of the noise and vibration problem that occurs in a real vehicle application (see Figure 4. 7).

The cost function, $g(k)$, is calculated as follows.

$$g(k) = fuel\,consumption(k) + \beta\left((\omega_{eng,k+1} - \omega_{eng,k})/\omega_{eng\,max}\right)^2 \tag{4.10}$$

In addition to the pure fuel consumption, the penalty for the transient engine speed is added to the cost function by introducing the engine acceleration reduction factor, β. The square of the normalized engine acceleration is multiplied by β, assuming the engine operation may become too transient without the charging or discharging power constraint as HEVs has [44]. In the future studies, reasonable engine acceleration limits or engine power rate limits may be added as an infinite penalty by considering the transient exhaust emission restrictions or driver's comfort instead of an arbitrary engine acceleration penalty. For various values of the tuning factor, β, the DDP technique is applied in the following section. The idle-stop capability is not assumed so the idle fuel consumption is included in the cost function.

The final SOC needs to be equal to the initial SOC to simulate the charge sustaining capability. The penalty of the SOC deviation is given by the squared distance from the initial SOC in Equation (4.11) and added to the cost function in the final step.

$$g_N\left(x_N\right) = \alpha\left(SOC - SOC(0)\right)^2 \tag{4.11}$$

where α is a weighting factor for charge sustaining.

Finally, the total cost to be minimized is represented in Equation (4.12).

$$\begin{aligned}\min \sum_0^N g_k = \min \sum_0^{N-1} \Bigg(& \textit{fuel consumption}(k) + \beta\left(\left(\omega_{eng,k+1} - \omega_{eng,k}\right)/\omega_{eng\,max}\right)^2\Bigg) \\ & + \alpha\left(SOC\left(N\right) - SOC\left(0\right)\right)^2\end{aligned} \tag{4.12}$$

4.3.3. SHH DDP Result

The DDP technique is applied to the SHH system including the engine acceleration reduction factor, β, which can be seen to affect the fuel economy as shown in Table 4. 4.

Table 4. 4. Effect of β on the fuel economy

β	Fuel economy [mpg]	% to fuel economy of modulated SOC control
0	25.0	153
12.5	20.5	126
25	17.8	109
37.5	17.3	106
50	17.0	104

As β increases, the engine acceleration is suppressed as expected, but fuel economy decreases. Finally, fuel economy saturates when β is over 25 and the gain of the optimal power management was reduced to less than 10 % in comparison with that of the modulated SOC control case where the engine acceleration is relatively low.

The effect of β to the engine speed during FUDS is shown in Figure 4. 3. In the case of $\beta = 0$, the engine speed is highly transient, and it seems to act as an extreme thermostatic control case. However, the extremely transient engine operation seems unrealistic in the actual SHH application. The cases when $\beta \geq 25$ seem to have reasonable engine operation in an engineering sense. However, the study on the proper maximum engine acceleration is rare and a proper engine acceleration limits or other criteria, e.g., power rate limit, if exists, can be used as a penalty in a future study.

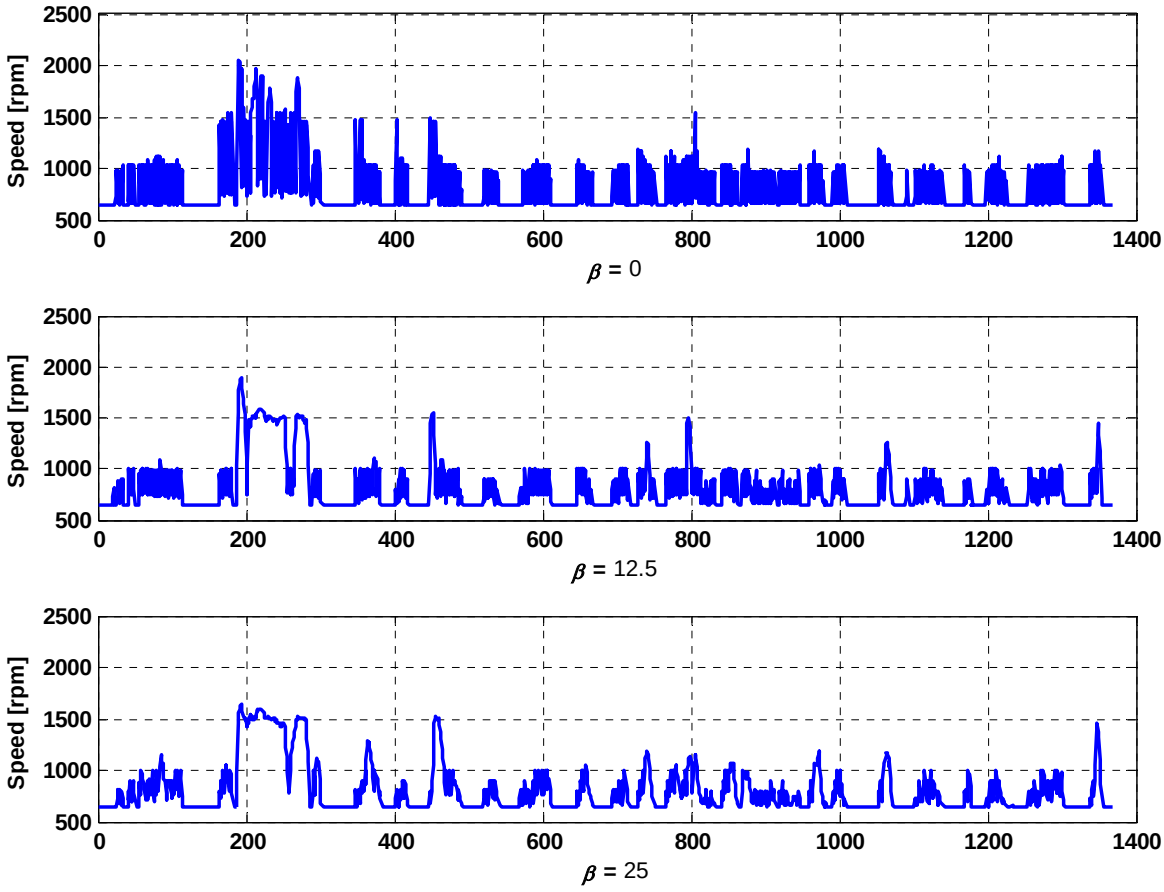

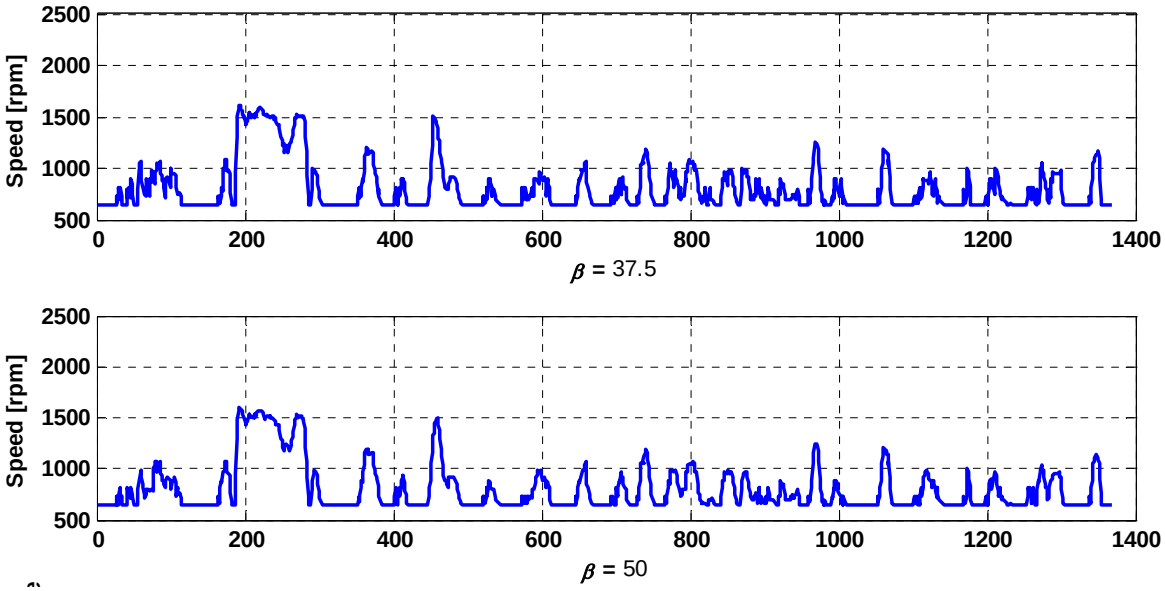

Figure 4. 3. Effect of β on the engine speed in SHH DDP during FUDS

The SHH DDP results are shown in Figure 4. 4(a) ~ (d), with β equals to 25. Interestingly, the SOC goes down to zero, fully utilizing the accumulator energy as shown in Figure 4. 4(a). With the SOC going down to zero, the stored energy can be fully used at each vehicle start and the accumulator has a room for the effective regenerative braking by maintaining the hydrostatic operation as much as possible at the low SOC. In addition, P/M_{gen} and P/M_{prop} use high displacement factors, so the system efficiency increases even though the high pressure is advantageous for P/M in Figure 2. 4. This trade-off relation may be reflected in the DDP solution. However, the vehicle propulsion operations at the low SOC can cause drivability problems in the real PSHH application so this benchmark power management may be possible because of the preview feature – backward solution search – of the DDP technique. Clearly, DDP uses the accumulator power at vehicle launch without engine assist because the engine efficiency is low when the power demand is low as shown in Figure 4. 4(b). When the vehicle speed is high and the high power is needed as it is the case in the second hill of FUDS (around 160~340 seconds), the engine starts early and maintains the high power such by load leveling.

Even though the transient engine speed is suppressed by the engine-acceleration reduction factor, β, the engine torque becomes highly transient especially when the vehicle power demand is low, during around the 20~125 seconds region in Figure 4. 4(c).

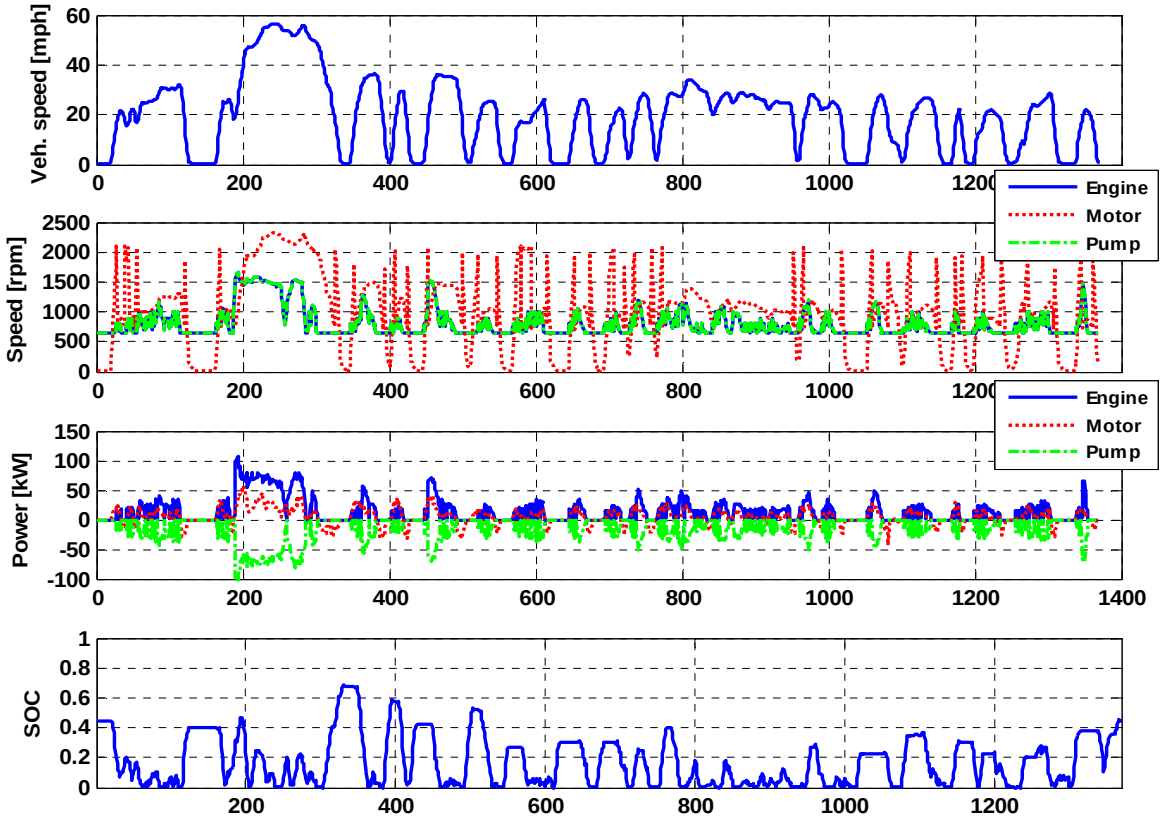

(a) SHH DDP result during FUDS

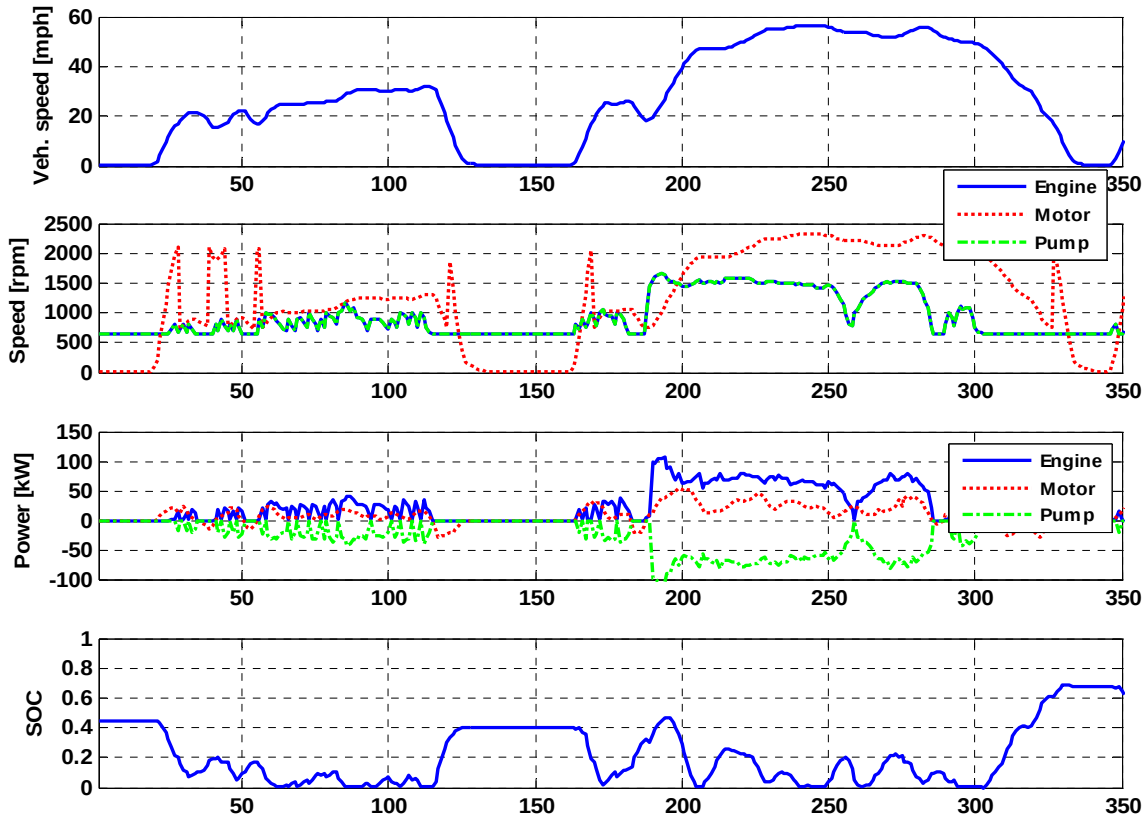

(b) SHH DDP result from 0 to 350 seconds

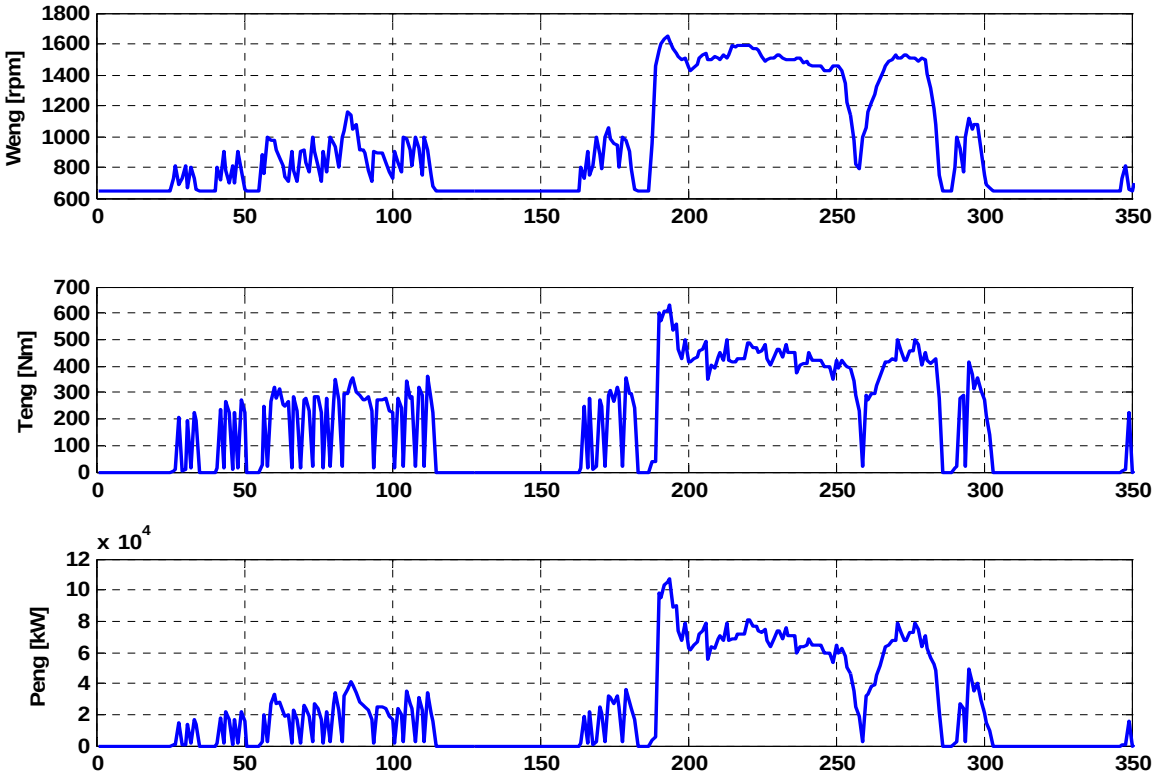

(c) Engine operation from 0 to 350 second

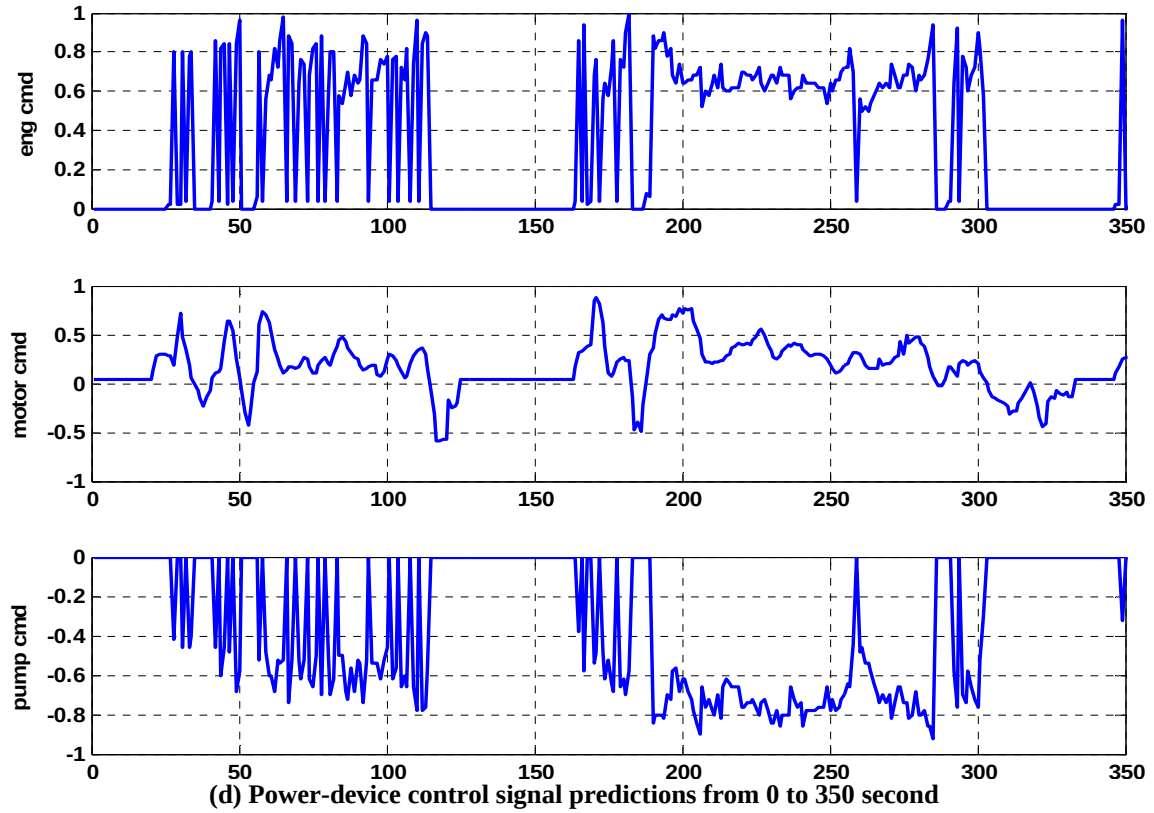

(d) Power-device control signal predictions from 0 to 350 second

Figure 4. 4. SHH DDP result during FUDS (β = 25)

The engine power also charges the accumulator at 180~280 second regions when the vehicle power demand is high. Thus, the engine can use the fuel-efficient high load area just like the load leveling. The charged energy is used for the vehicle propulsion later. With the SOC close to zero, the engine and P/M_{gen} uses the high load exclusively. The engine rack command and pump rack command can be high values especially when the engine power demand is low. As a result, the system efficiency improves but highly transient operations may cause excessive exhaust emissions and durability problems in the real SHH application as shown in Figure 4. 4(d). The parametric study of the minimum SOC effect is done by giving an infinite penalty when the SOC goes below an arbitrary pre-set SOC to simulate the real SHH application which needs a hydraulic energy buffer to compensate for system delays and improve driveability in Figure 4. 5.

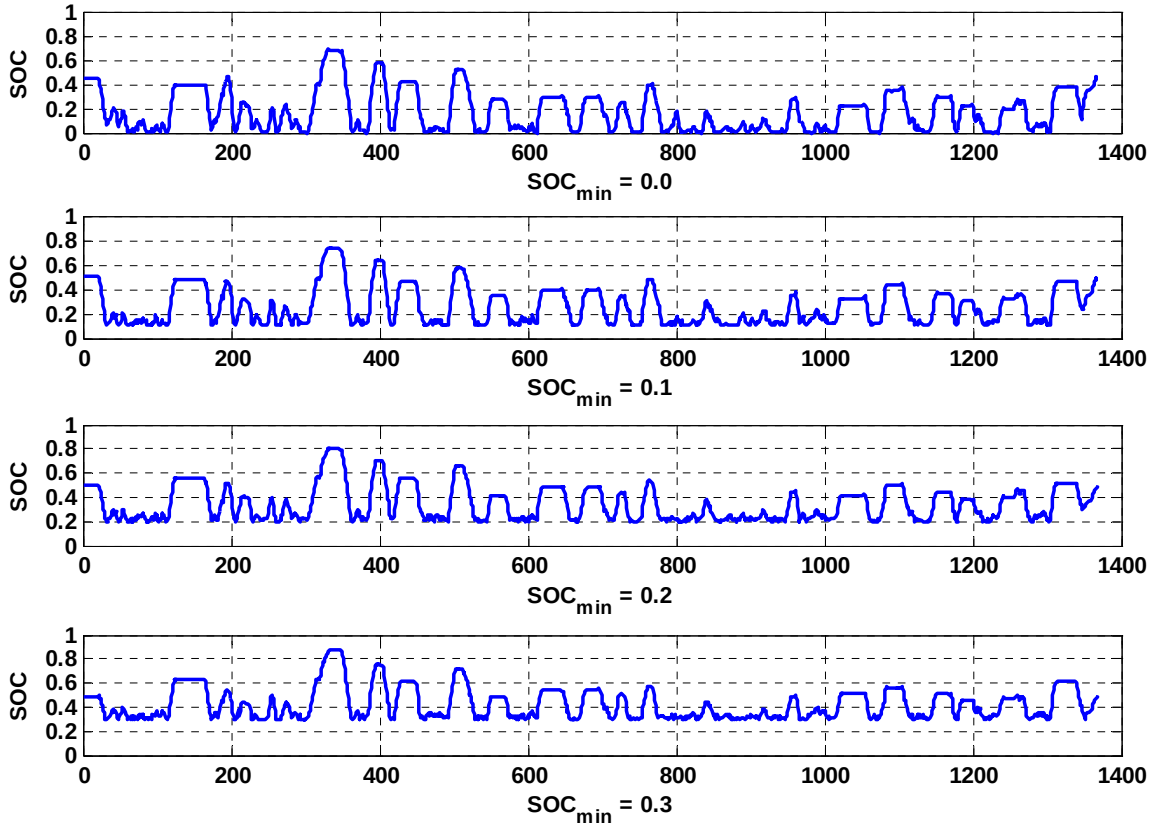

Figure 4. 5. Effect of SOC_{min} on the SOC prediction in SHH DDP (β = 25)

The fuel economy does not change until SOC_{min} is set to 0.2 and it decreases by 2% when SOC_{min} is 0.3. This result is reasonable because the accumulator size is pre-designed by the modulated SOC control with the target SOC of 0.28. As a result, the accumulator is large enough to hold the same regenerative braking energy without

bypassing the compressed fluid at the maximum accumulator pressure until the SOC_{min} is as high as 0.2. Therefore, the SOC_{min} below the SOC_{target} of the modulated SOC control does not affect the fuel economy result. The engine power versus vehicle power demand during FUDS is shown in Figure 4. 6. With the stored energy, the engine power can be zero realizing the hydraulic-only drive, even when the vehicle power demand is over 50 kW. The hydraulic-assist drive is observed when the engine power is lower than the 1:1 line as a transition between hydraulic-only and engine-only drive in Figure 4. 6 (a). Interestingly, the engine power vs. vehicle power demand in Figure 4. 6 (a) shows the constant engine power of around 15kW. This implies that the DDP tries to avoid the low engine-efficiency area by charging the accumulator with the engine. In addition, the engine power seems to be load leveling around 80 kW. Most of engine power demands are below the "sweet spot" power (~120 kW) and this implies that charging the accumulator for the optimal engine power management at the "sweet spot" power is avoided because the energy conversion loss is larger than the gains from the optimal engine operation at the "sweet spot".

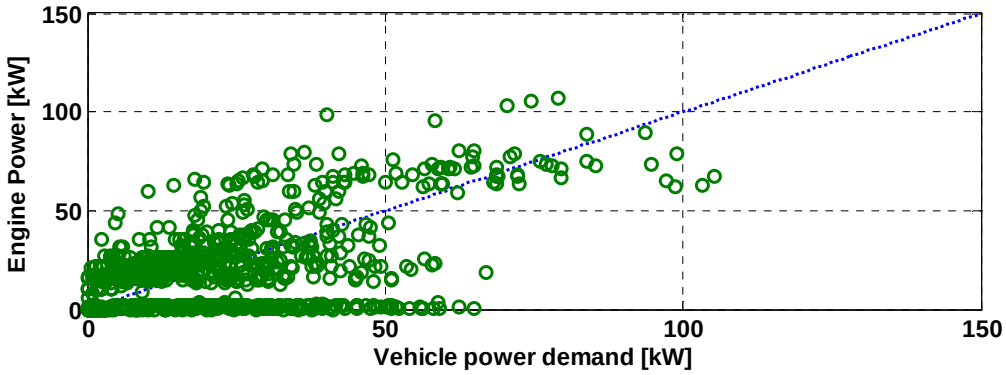

(a) Engine power vs. vehicle power demand

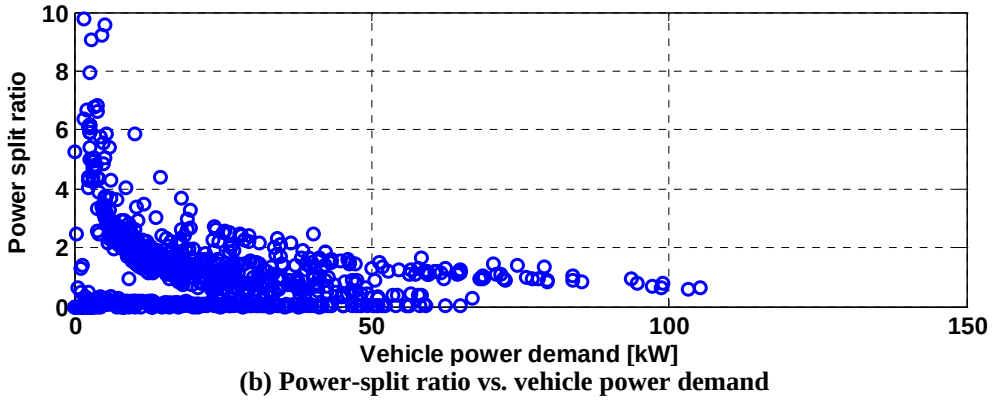

(b) Power-split ratio vs. vehicle power demand

Figure 4. 6. Engine power vs. vehicle power demand during FUDS (β = 25)

DDP finds the way to improve the fuel economy demand by charging the accumulator and severely transient engine operation when the engine power demand is small.

The integrated fuel consumption from DDP results is shown in Figure 4. 7. The fuel consumption is not on the minimum BSFC line contrary to engineering intuition. In the systematic perspective, this fact implies that the DDP finds more efficient power-generation area that is relatively at the low speed and high load area of the engine map.

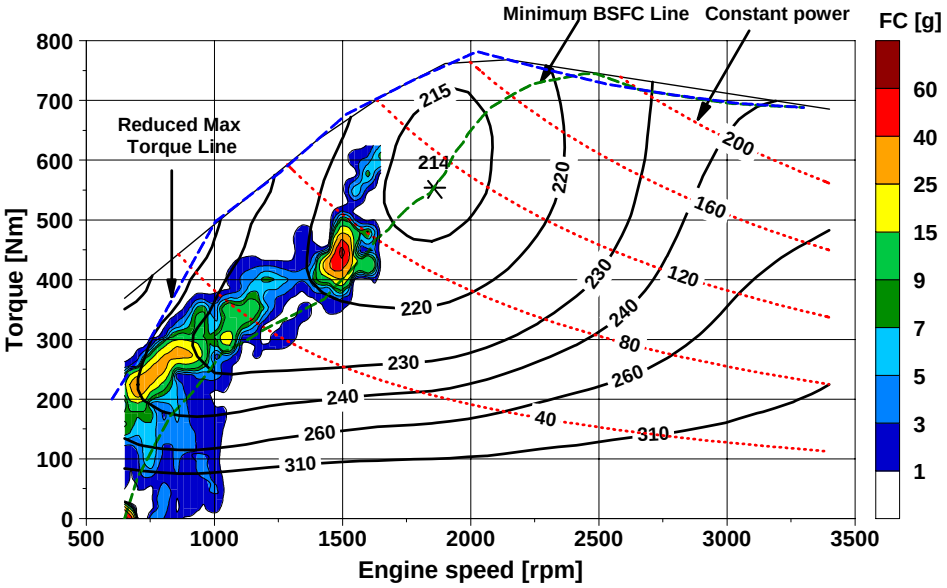

Figure 4. 7. Integrated fuel consumption in SHH DDP during FUDS (β = 25)

In the case of the SHH system, the engine is connected only to the P/M$_{gen}$ and the engine power is only used to pump the hydraulic fluid to the accumulator. Therefore, the combined efficiency of the engine and P/M$_{gen}$ is used to analyze DDP results. The combined BSFC can be calculated as the ratio of the fuel input to the engine to the P/M$_{gen}$ flow power as Equation (4.13). As a result, BSFC$_{combined}$ is the BSFC divided by the total efficiency of the P/M$_{gen}$ in Equation (2.12).

$$\mathrm{BSFC}_{combined} = \frac{fuel\ consumption}{P_{flow}} = \frac{fuel\ consumption}{P_{shaft} \cdot \eta_{total,gen}} = \mathrm{BSFC} \cdot \eta_{total,gen}^{-1} \qquad (4.13)$$

BSFC$_{combined}$ is the function of the pressure difference between the accumulator and reservoir (ΔP_{fluid}) because the total efficiency of the P/M$_{gen}$ is the function of ΔP_{fluid}. BSFC$_{combined}$ maps are shown according to five different pressure differences as shown in Figure 4. 8. For the same engine torque, the displacement factor decrease as the ΔP_{fluid} increases. Thus, BSFC$_{combined}$ at the same engine speed and torque is aggravated as the

ΔP_{fluid} increases. This clearly explains why the high ΔP_{fluid}, which is roughly proportional to the SOC, is avoided and the SOC frequently goes down to low SOC in Figure 4. 4(a).

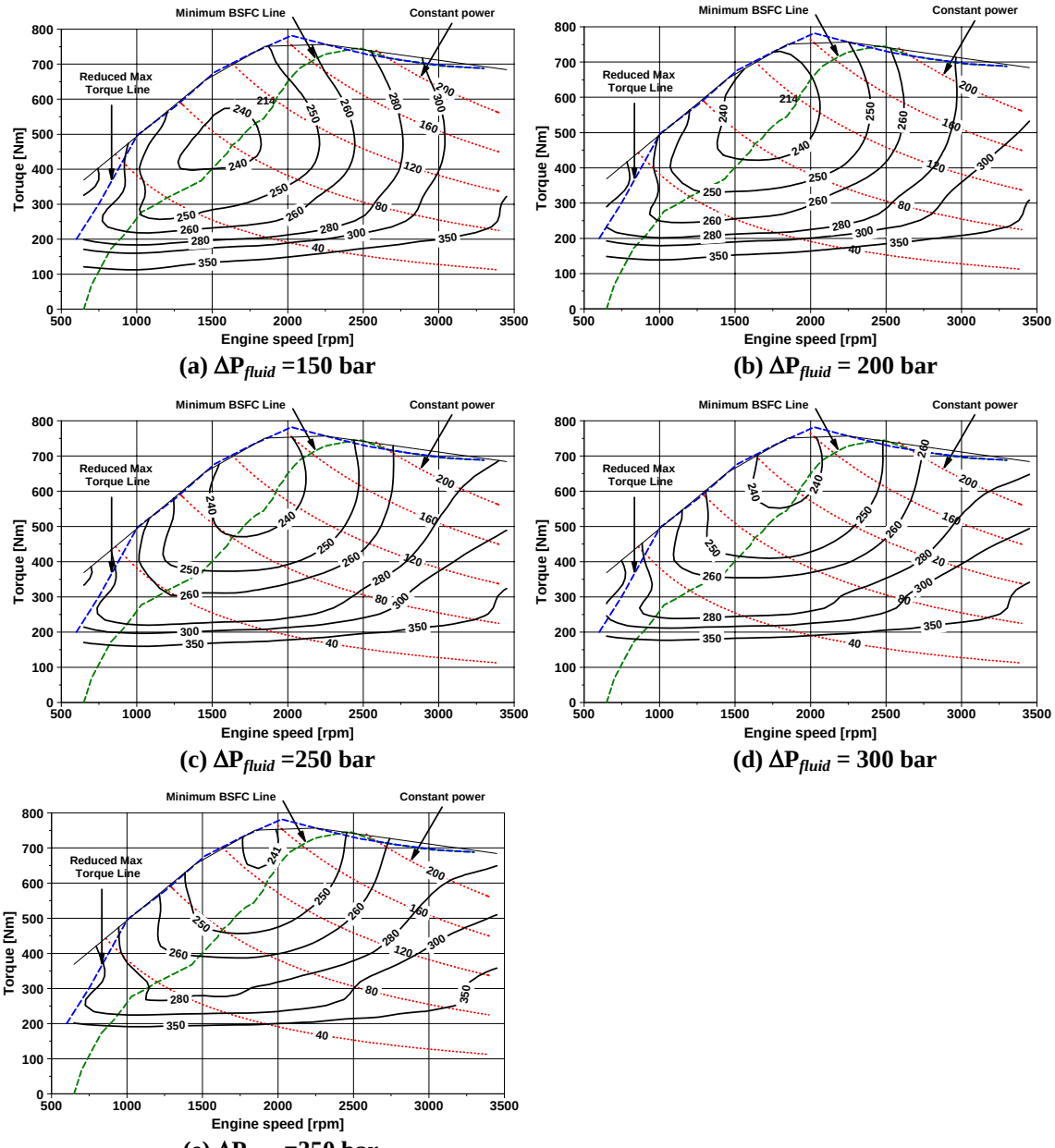

(a) ΔP_{fluid} =150 bar

(b) ΔP_{fluid} = 200 bar

(c) ΔP_{fluid} =250 bar

(d) ΔP_{fluid} = 300 bar

(e) ΔP_{fluid} =350 bar

Figure 4. 8. $BSFC_{combined}$ maps according to the hydraulic pressure difference, ΔP_{fluid}

The band of minimum $BSFC_{combined}$ lines is located in the higher load area in comparison with the minimum BSFC line in Figure 4. 9. Surprisingly, the integrated fuel consumption area of the SHH DDP results coincides with the band of the minimum $BSFC_{combined}$ lines.

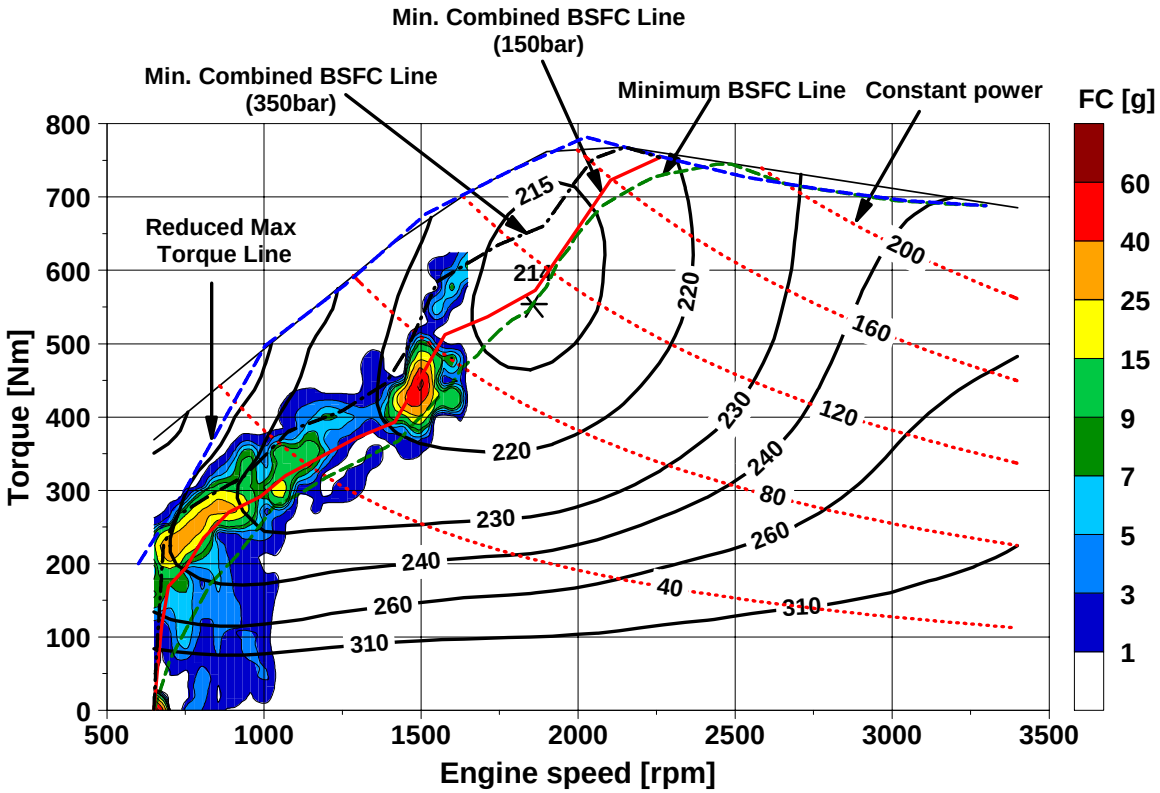

Figure 4. 9. Minimum BSFC$_{combined}$ line band and the integrated fuel consumption of DP ($\beta = 25$)

Extracting implementable rules from the DDP results is not easy and time-consuming process in order to include as many conditions as possible in the actual SHH application. Instead, applying the minimum BSFC$_{combined}$ band concept by reflecting the benchmark engine-operation range to the modulated SOC control is relatively viable. Minimum BSFC$_{combined}$ lines according to different ΔP_{fluid}s are saved in the look-up table. The engine speed demand and torque demand can be calculated for a given ΔP_{fluid} and engine power demand from the modulated SOC control. As a result, the fuel economy with the minimum BSFC$_{combined}$ band is 16.5 mpg, which is a 0.6% increase compared to the original minimum BSFC line approach. The total increase is not significant because the engine operation line is still close to the original minimum BSFC line (see Figure 4. 10) and engine control strategies are the same.

In addition, it is interesting that the engine operation line is close to the minimum BSFC$_{combined}$ line of 350 bar when the power demand is small and the engine operation line is close to the minimum BSFC$_{combined}$ line of 150 bar when the engine power demand is high. It is because the small engine power is usually used at the start and stop of the

vehicle when the SOC usually is high and the large engine power is usually used at the vehicle cruising condition when the SOC becomes close to the target SOC.

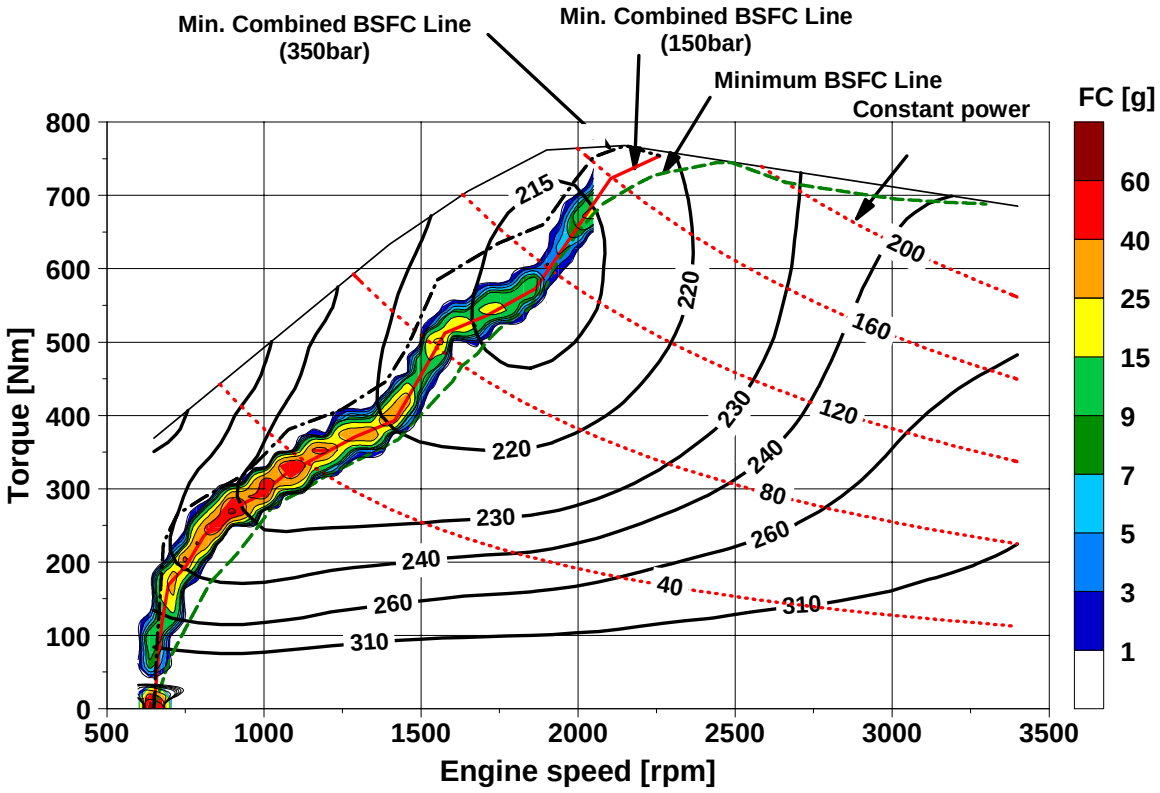

Figure 4. 10. Integrated fuel consumption of modulated SOC control with minimum BSFC$_{combined}$ band during FUDS

As a result, the DDP technique finds the way to improve the fuel economy demand by charging, load leveling and operating the engine in the transient manner when the engine power demand is small. However, these are possible because of the preview feature of the DDP. Instead of finding a sub-optimal rule-based power management learned from the benchmark power management, the implementable semi-optimal power management from the SDP technique is introduced in next section.

4.4. Series Hydraulic Hybrid Power Management Optimization with Stochastic Dynamic Programming

As for the SHH system, the studies of implementable optimal power management controls with the stochastic dynamic programming (SDP) technique are none. The result of the SDP technique gives full-state feedback controller from multiple inputs and provides the engine power demand, which can be implemented to real-time applications. As the semi-optimization power management, SDP solves the infinite horizon problem of

the time-invariant system and generates the control policy based on the probability distribution generated from pre-selected samples.

4.4.1. Stochastic Dynamic Programming Algorithm

The transition probability function is generated from the stationary Markov chain model in which the stochastic behavior of the expected vehicle power demand can be extracted from multiple driving schedules [80]. For a specific hybrid vehicle system and given driving schedules, the vehicle power demand can be calculated from the wheel torque and wheel speed. From the already-known vehicle power demand and wheel speed range, a stationary Markov chain is used to generate the expected vehicle power demand, P_{dem}^{j}, which depends on the current vehicle power demand P_{dem}^{i} and wheel speed ω_i [79].

The vehicle power demand, P_{dem}, is discretized as

$$P_{dem} \in \left\{ P_{dem}^{1}, P_{dem}^{2}, ..., P_{dem}^{N_p} \right\} \tag{4.14}$$

The wheel speed, ω, is discretized as

$$\omega_{wh} \in \left\{ \omega_{wh}^{1}, \omega_{wh}^{2}, ..., \omega_{wh}^{N_\omega} \right\} \tag{4.15}$$

Then, the transition probability becomes

$$p_{il,j} = \Pr\left\{ P_{dem} = P_{dem}^{j} \mid P_{dem} = P_{dem}^{i}, \omega_{wh} = \omega_{wh}^{l} \right\}, \quad i, j = 1, 2, ..., N_p, l = 1, 2, ..., N_\omega \tag{4.16}$$

If the actual vehicle power demand, P_{dem}, and wheel speed, ω, do not exactly match discrete values, they are interpolated to the nearest values in discretized sets in Equation (4.14) and (4.15). However, the training data for the Markov probability function are only limited numbers of driving schedules, so the probabilities of some unseen state transitions exist. Therefore, the smoothing approach is applied for the reasonable probability distribution [75]. This smoothing approach also improves the convergence of the SDP control generation.

Assuming that the number of stages is infinite and the system is stationary, the control input policy, π, is stationary. As a result, the SDP algorithm can be represented as follows [70].

Expected total cost minimization is given below.

$$J_\pi(x_0) = \lim_{N\to\infty} \underset{\substack{w_k \\ k=0,1,...}}{E} \left\{ \sum_{k=0}^{N-1} \gamma^k g_k(x_k, \pi(x_k)) \right\}, \quad u = \pi(x), \quad 0 < \gamma < 1 \tag{4.17}$$

where g_k is the instantaneous cost incurred at time k and γ is the discount factor.

In the state vector $x = (SOC, \omega_{wh}, P_{dem})$, SOC has to be discretized.

$$SOC \in \left\{ SOC^1, SOC^2, ..., SOC^{Nsoc} \right\} \tag{4.18}$$

In addition, the control input u, that is P_{eng} in this problem, is also discretized.

$$P_{eng} \in \left\{ P_{eng}^1, P_{eng}^2, ..., P_{eng}^{Nu} \right\} \tag{4.19}$$

Assuming that the initial arbitrary stationary policy π is given, SDP performs a "policy evaluation", which computes $J_\pi(x)$ as the solution of the linear system of equations

$$J_\pi^{s+1}\left(x^i\right) = g\left(x^i, \pi\left(x^i\right)\right) + E\left\{\gamma J_\pi^s\left(x^{'}\right)\right\} \quad \textit{for every } i \tag{4.20}$$

where s is the iteration number, and $x^{'}$ is a new state, such as $x^{'} = f\left(x^i, \pi\left(x^i\right), w\right)$.

If the first two states of the new state $x^{'}$, SOC and ω_{wh}, do not fall on the exact grid points, the linear interpolation of the cost function along the first two dimensions is carried out.

Only a fixed number of iterations are done to accelerate the convergence and reduce the computation time [72].

Then, SDP performs a "policy improvement", which computes a new policy μ^{k+1} as

$$\pi^{'}\left(x^i\right) = \arg\min_{u\in U\left(x^i\right)} \left[g\left(x^i, u\right) + \underset{w}{E}\left(\gamma J_\pi\left(x^{'}\right)\right) \right], \quad \forall x^i \tag{4.21}$$

where J_π is the approximate cost function obtained from the policy evaluation step. The algorithm stops when $J_\pi(x)$ converges below pre-designated tolerance.

Smoothing the resultant control policy is found to be important for specific problems to reduce the unrealistic rapid change of the control, causing states to be unstable since solving the SDP problem is a purely mathematical procedure regardless of physical aspects of the plant, and the control policy is based on the discrete state vectors.

4.4.2. Generation of Stochastic Markov Chain

As a first step of SDP, the stochastic Markov chain modeling from samples of the vehicle power demand is carried out by pre-selected training sets, driving schedules. From the viewpoint of the light duty truck application, five driving schedules (FUDS, UDDSHDV, WVUSUB, WVUCITY and HWFET), which do not include too high speed and too frequent start-and-stop, are selected for the Markov chain modeling. The characteristics of chosen driving schedules are represented in Table 4. 5 and actual vehicle speed profiles are shown in Figure 4. 11 [64].

Table 4. 5. Characteristics of driving schedules

	NYCC*	WVUCITY	UDDSHDV	SC03*	FUDS	WVUSUB	WVUINTER*	HWFET
Time [sec]	598	1408	1060	600	1372	1665	1640	765
Distance [mile]	1.18	3.3	5.55	3.58	7.45	7.44	15.51	10.26
Max speed [mph]	27.7	35.8	58	54.8	56.7	44.8	60.7	59.9
Mean speed[mph]	7.09	8.4	18.8	21.4	19.6	16.1	34.0	48.2
Max accel [m/s^2]	2.7	1.1	2	2.3	1.5	1.3	1.4	1.4
Max decal [m/s^2]	2.6	-3.2	-2.1	-2.6	-1.5	-2.2	-1.9	-1.5
Mean accel [m/s^2]	0.6	0.3	0.5	0.5	0.5	0.3	0.2	0.2
Mean decal [m/s^2]	-0.6	-0.4	-0.6	-0.6	-0.6	-0.4	-0.2	-0.2
Idle time [sec]	210	427	353	117	259	420	153	6
Idle/total time[%]	35.1	30.3	33.3	19.5	18.9	25.2	9.3	0.8
no. of stop	18	14	14	6	17	9	9	1

***not used for generating Markov chain but only used for the test of SDP control**

As the first step, wheel speed data are extracted from the given driving schedules and vehicle power demands are extracted from wheel power data in the actual simulation. The wheel speed and vehicle power demand are discretized as shown in Table 4. 6.

Table 4. 6. Wheel speed and vehicle power demand discretization in SHH SDP

	Range	Grid number
Wheel speed [rad/s]	0 : 65	15 grids
Vehicle power demand [kW]	-110 : 110	20 grids

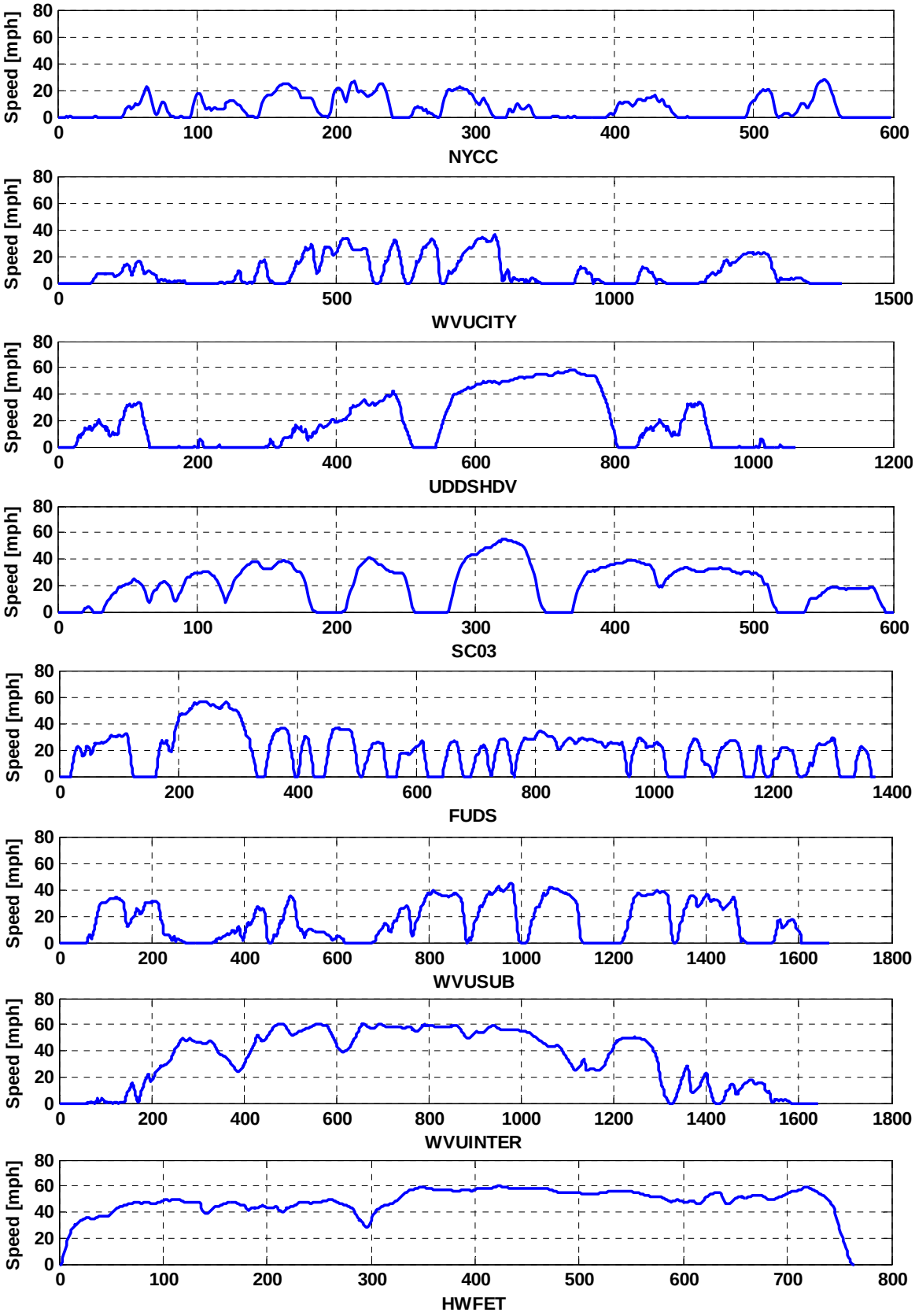

Figure 4. 11. Vehicle speed profiles of driving schedules for the SDP training and test

The transition probability graphs show a highly correlated relation between the current and the next vehicle power demand lying along the diagonal of the plane of current and next vehicle power demands in Figure 4. 12.

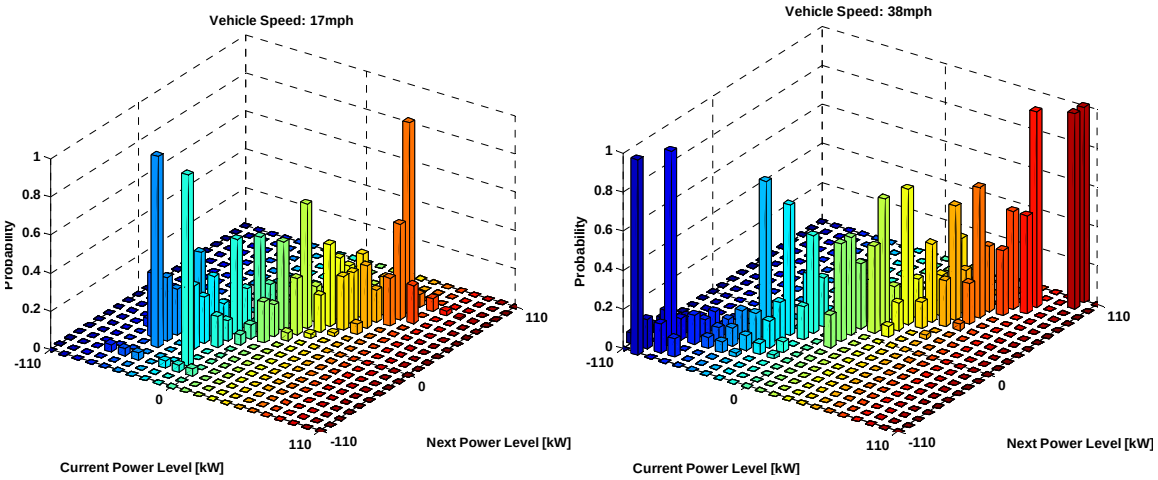

(a) Before smoothening

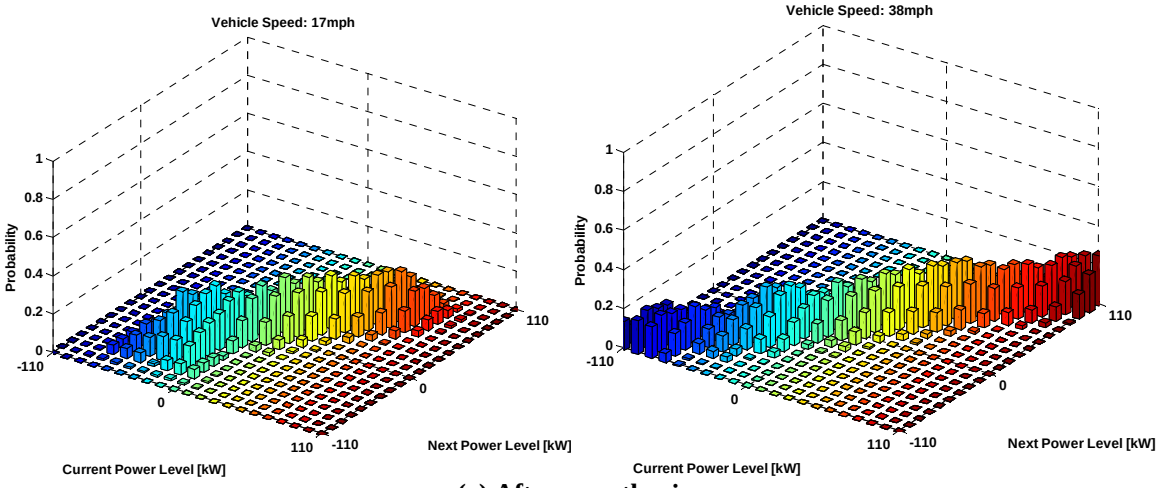

(a) After smoothening

Figure 4. 12. Markov transition probability function before- and after- smoothening

Even though five driving schedules are used to generate the transition probability function, still there exist vacancies in the vehicle power demands (see Figure 4. 12(a)) and this incomplete transition probability function aggravates the convergence of control policy and causes the resultant SDP controller to be unstable. As a countermeasure, smoothening of the transition probability function is carried out (see Figure 4. 12(b)).

4.4.3. SHH SDP Setup

The power relations among the power devices are still valid in the SHH SDP model as shown in Equation (3.2) ~ Equation (3.4). The vehicle power demand is directly

transferred to the P/M_{prop} and the engine power is calculated from the full state feedback controller generated by the SDP technique. However, the engine power demand does not include the engine speed and torque information, i.e., the low-level engine control is not defined by the SDP technique. Thus, the engine speed and torque control can be designed according to the control objective for a given engine power demand. In this study, the engine speed and torque are controlled to follow the minimum BSFC line in the SHH SDP model to achieve the fuel economy objective, even though it does not guarantee the systematic optimization. The same engine speed and torque control strategy is also applied to the actual simulation that implements the SDP controller. The P/M_{gen} speed is the same as the engine speed and the P/M_{gen} torque is the output of the engine speed controller whose output is the P/M_{gen} command, i.e., displacement factor.

The state variables, control output and grid discretization are represented in Table 4. 7. The engine power is the function of the vehicle power demand, SOC and wheel speed, so that the resultant SDP controller has the form of three dimensional look-up table. The grid size is selected to be small enough to reflect the system dynamics, but at the same time, to be large enough to guarantee the fast convergence and not to delay the actual SDP control application.

Table 4. 7. State and control variables and grid discretization in SHH SDP

State	Vehicle power demand	-110 :110	20 grids
	SOC	0 : 0.04 : 1	25 grids
	Wheel speed	0:65	15 grids
control	Engine power	0:240	20 grids

To reduce the computation time, the high fidelity SHH model is simplified such that the basic system dynamics of the high fidelity model match that of the simplified model. Firstly, the fast dynamics that are much faster than 1 Hz are neglected. Thus, engine torque generation in the engine model is changed to a static look-up table. Secondly, accumulator gas dynamics model which has the gas pressure and temperature as independent variables are changed to a polytropic state equation model, where the gas volume is only the function of the gas pressure, instead of the high-fidelity real-gas dynamic model. The coefficients of the polytropic process are acquired from the curve

fitting of the cycle simulation result of the high fidelity HMMWV VESIM. Thirdly, the high-fidelity vehicle model is changed to the simple road-load vehicle model. The rolling resistance coefficients of the simple vehicle model are calibrated to show almost the same vehicle power demands, so the fuel economy is close to that of high fidelity vehicle model with less than 1% difference. In addition to the simplification of the SHH model, the vehicle power demand is vectorized in the policy evaluation step and the engine power demand is vectorized in the policy improvement step.

Physical constraints of the optimization process are represented at Equation (4.22) ~ Equation (4.24) and if constraints are violated, infinite penalty is given to the cost function. The SOC should be between zero and one and the engine speed and P/M_{prop} torque should be inside of the given specifications. In contrast with the case of HEVs, the charging and discharging limits are not added because of high power density of hydraulic accumulator.

$$0 \le SOC(k) \le 1 \tag{4.22}$$

$$\omega_{eng\_\min} \le \omega_{eng}(k) \le \omega_{eng\_\max} \tag{4.23}$$

$$T_{P/M_{prop}\,min} \le T_{P/M_{prop}}(k) \le T_{P/M_{prop}\,max} \tag{4.24}$$

The reliable drivability is considered by adding a square distance from the minimum SOC (SOC_{min}) only when the SOC goes below the SOC_{min} in the cost function of the SHH SDP setup as shown in Equation (4.25).

$$g_k = \begin{cases} fuel\ consumption(k) + \alpha\left(SOC_{min} - SOC(k)\right)^2 & if\ \ SOC(k) < SOC_{min} \\ fuel\ consumption(k) & if\ \ SOC(k) > SOC_{min} \end{cases} \tag{4.25}$$

Even though the hydraulic accumulator does not have an operation limit in the SOC, there exists a SOC_{min} to be maintained during the normal driving condition, and works as an energy buffer when an unexpected large vehicle power demand occurs in the actual vehicle application, such as the SOC_{target} in the modulated SOC control.

4.4.4. SHH SDP Result

The tuning of α affects the performance of the SDP controller in maintaining the hydraulic energy buffer and affects the drivability in Figure 4. 13. The larger α guarantees the reliable driving by keeping the SOC from dropping below SOC_{min}. The

fuel economy is almost the same when α changes from 100 to 800 but the lowest SOC changes from 0.11 to 0.16 during 190~220 second region. Therefore, tuning of α is indispensable for the reliable SHH SDP application and the baseline α is selected as 800.

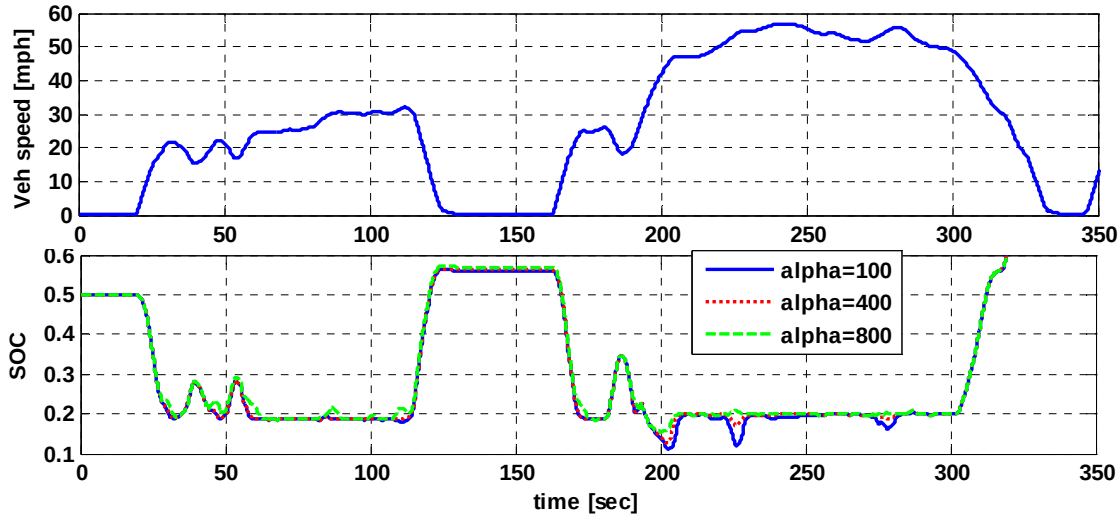

Figure 4. 13. Effect of α on SOC prediction in SHH SDP (SOC_{min} = 0.2)

As another tuning factor, SOC_{min} works as the level of the hydraulic energy buffer as shown in Figure 4. 14. Because the accumulator size is large enough to capture the regenerative braking energy completely up to the SOC_{min} of 0.3, the fuel economy is almost the same below the SOC_{min} of 0.3 and fuel economy decreased about 2% in the case of SOC_{min} of 0.4. As a result, the SOC_{min} of 0.2 is selected as the baseline SOC_{min} improving fuel economy without degrading the driveability.

The three dimensional representation of the final SDP controller according to the wheel speed is shown in Figure 4. 15. Instead of using a power split ratio, using the direct engine power output removes the possibility of the infinite engine power demand and smooth transition when the vehicle power demand is close to zero and changes the sign, respectively. Interestingly, the engine power demand proves to be a week function of the wheel speed except in the braking case in the SHH SDP control.

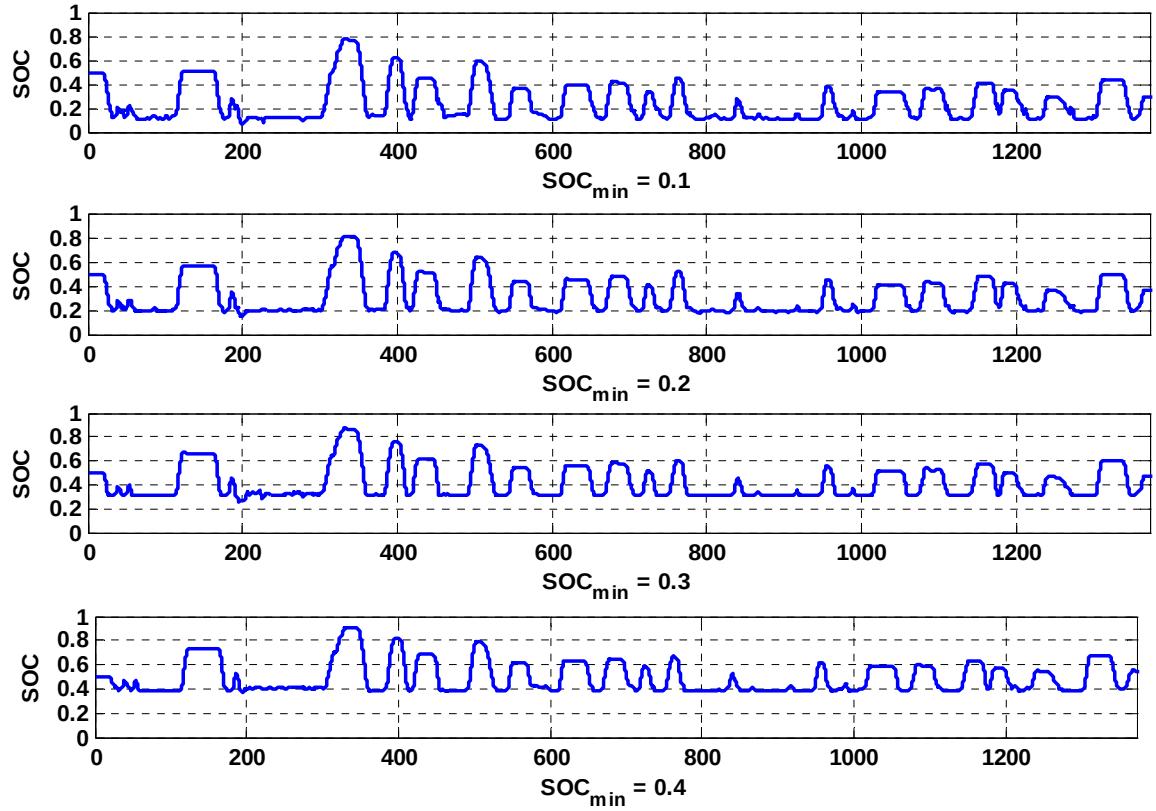

Figure 4. 14. Effect of SOC_{min} on SOC prediction in SHH SDP (α = 800)

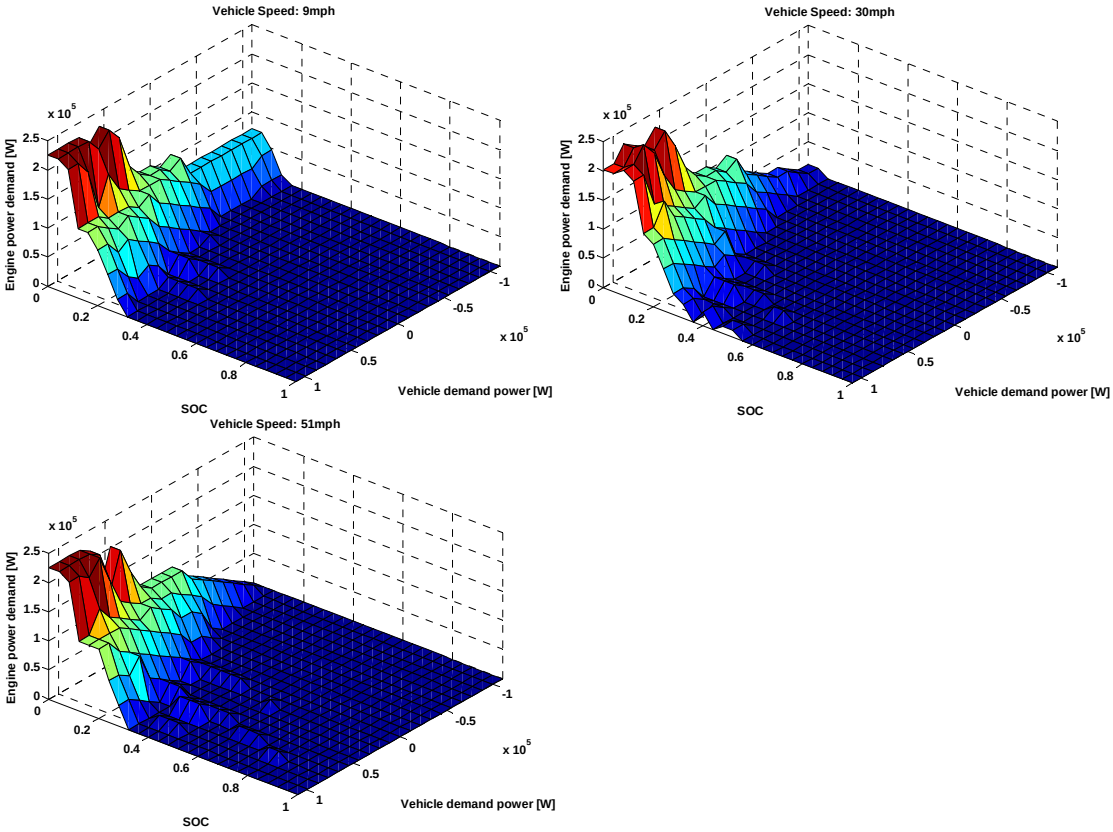

Figure 4. 15. Engine power demand in the optimal SHH SDP controller

The system behavior shows the rate of the engine power demand is significantly high in Figure 4. 16.

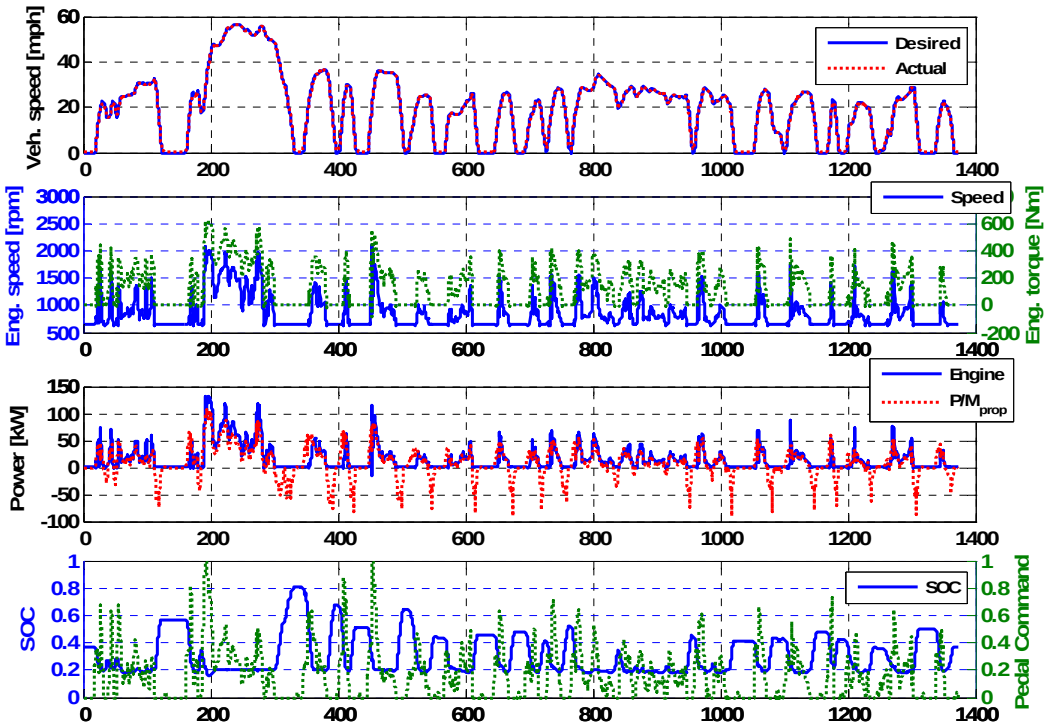

(a) System behavior during FUDS

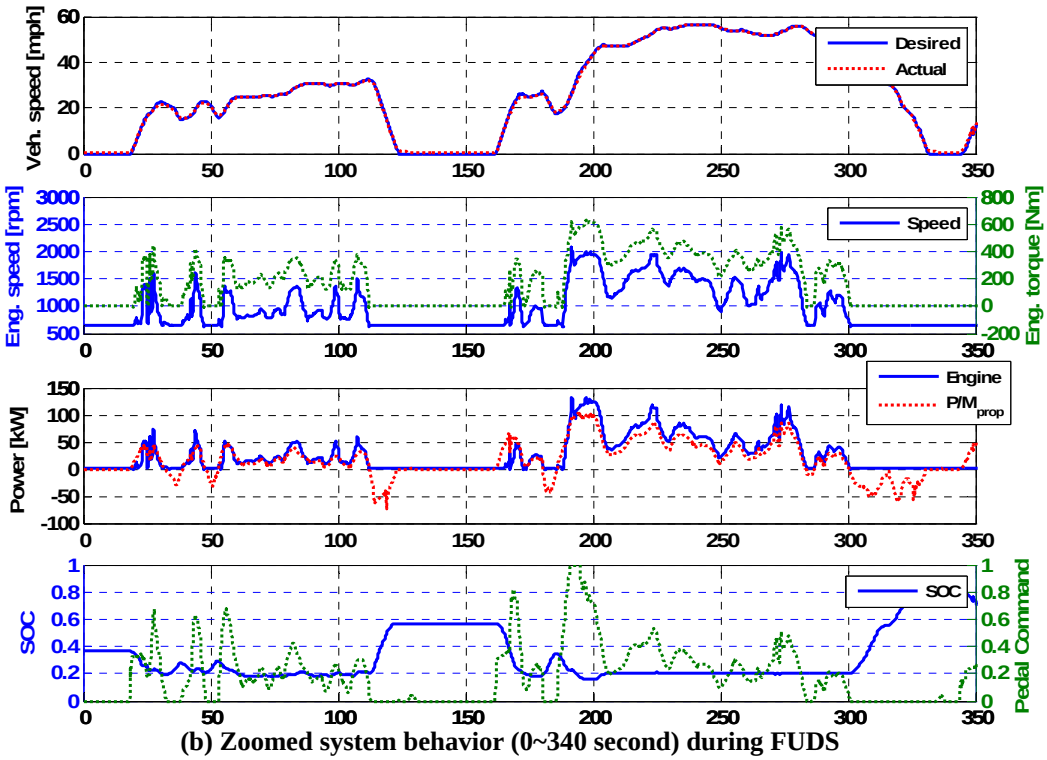

(b) Zoomed system behavior (0~340 second) during FUDS

Figure 4. 16. System behavior with SHH SDP during FUDS

With this high rate of engine power, the engine and P/M_{gen} can use the high load area and improve the system efficiency. However, the engine speed becomes more transient. This highly transient engine power demand can cause the speed control problem and increase the transient exhaust emissions in the real SHH vehicle application. The effect of the transient engine power is validated by the EIL tests in Chapter 8.

The engine power vs. vehicle power demand with the SDP control during FUDS is shown in Figure 4. 17. Considering the engine power should be much larger than the vehicle power demand because of the significant energy conversion loss in the SHH system, it seems that the hydrostatic drive and hydraulic-only drive occupies most of the total driving schedule and the hydraulic-assist drive is used for the transition between the hydrostatic drive and hydraulic-only drive.

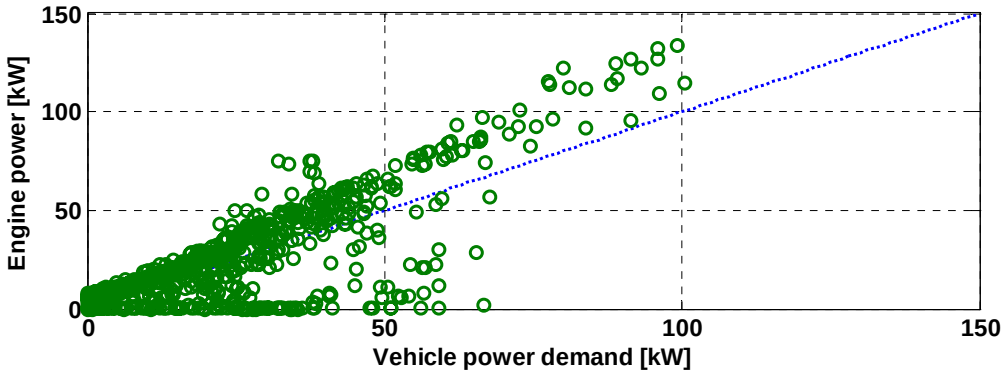

(a) Engine power vs. vehicle power demand

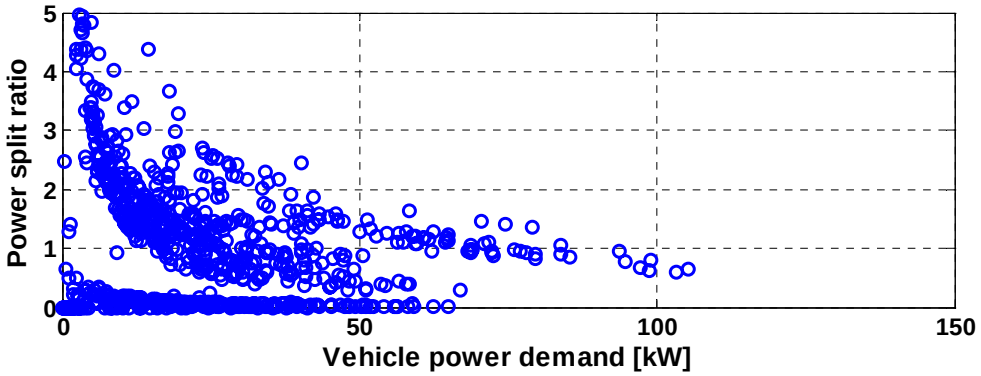

(b) Power-split ratio vs. vehicle power demand

Figure 4. 17. Engine power vs. vehicle power demand with SHH SDP during FUDS

Finally, the SHH SDP control is applied for various cycles and compared with modulated SOC control results (see Table 4. 8). The SDP control shows slightly better fuel economy for all driving schedules with 1~3% of the fuel economy improvement than the modulated SOC control case, including the cycles that are not used for the SDP

controller training. In other word, the modulated SOC control is proven to perform closely to the optimized power management case.

Table 4. 8. Fuel economy comparison between SDP and modulated SOC control without idle-stop

Cycle (* not used for training SDP)	Modulated SOC control	SDP	Fuel economy improvement [%]
NYCC*	12.6	12.7	0.8
WVUCITY	13.7	13.9	1.5
UDDSHDV	14.3	14.5	1.4
SC03*	15.8	16.2	2.5
FUDS	16.4	16.8	2.4
WVUSUB	16.1	16.5	2.5
WVUINTER*	14.4	14.5	0.7
HWFET	14.4	14.6	1.4

CHAPTER 5

ENGINE-IN-THE-LOOP CAPABILITY FOR A SERIES HYDRAULIC HYBRID SYSTEM

The EIL test validates simulation results and gives the insight on transient emissions of the hybrid system that depend on the power management in the system level and specific hybrid system characteristics. In the previous chapter, the engine model uses the quasi-steady BSFC and emission maps with a first-order time delay to compensate the turbo-lag of the diesel engine. However, transient effects on exhaust emissions are known to be large [40] and the simple map-based engine model will be inadequate to predict actual exhaust emissions only by applying the first-order time delay.

The accurate predictions of transient emissions are still challenging even with highly complicated CFD models and chemical kinetics models [116], [117]. In addition, computation loads of such sophisticated simulations are too high for the high fidelity engine models to be used for driving schedule simulations and optimization processes. As a result, the direct application of a real engine into the simulation is the most viable alternative for accurately assessing the impact of the powertrain design and control on exhaust emissions [105]. In the EIL setup, transient effects can be captured by replacing the engine model with the real engine in the test cell.

Generally, the hybridization of a vehicle propulsion system leads to frequent engine power fluctuations to improve the system efficiency by the supervisory control because fuel-economy oriented power managements usually use the high load region of the power devices, e.g., engine, P/M and M/G. For example, the high rate of engine power demand will increase hydrocarbon emissions and particulate matters (PM) particularly in diesel engine operations. In addition, valve deposit and premature engine failure related to the inadequate lubrication may happen with transient engine operations. Thus, the exhaust emission control becomes demanding in the case of hybrid vehicle applications [49].

The largest advantage of the EIL test is that it can measure actual exhaust emissions and fuel consumption resulting from engine system operation with real actuators, while ensuring transient conditions that correspond to driving conditions for a given vehicle configuration. The convenient changes of devices and power managements without an actual vehicle and an expensive chassis-dynamometer test system are possible through changes in the simulated driveline. As a result, the numerous error sources from the real vehicle test, e.g., noise, can be removed, and more repeatable and relatively inexpensive tests can be accomplished. In addition, the possibility of a real engine scaling can extend advantages of the EIL test by scaling different sizes of engines with a real engine.

Previous studies on applying the EIL setup to SHH system is almost none and this study may the first try to implement the real engine in the SHH simulation. In this study, the Engine-in-the-Loop setup for the series HHV system is developed to validate simulation results and the test results are analyzed to grasp transient effects on fuel consumption and exhaust emissions according to the thermostatic and modulated SOC control. To realize the SHH system with the current conventional vehicle EIL setup, there are challenges to overcome beyond the general EIL setup problems. Primary challenge stems from the fact that there is no mechanical coupling between the engine and the wheels in the real system, instead the engine is coupled to a highly dynamic hydraulic pump, and that makes stability issues critical. Next, the coupling between the power generation sub-system and the (virtual) storage has to be addressed, since the load-absorbing device in the test cell is electric (AC Dynamometer), while the real system includes a hydraulic pump

5.1. Experimental Setup

The engine used in this study is a 6.0 L V-8 direct-injection diesel engine manufactured by the International Truck and Engine Corporation. Primary engine specifications are given in Table 3.1. This engine uses advanced technologies to provide a high power density and meet emission regulation [40]. The engine is coupled to the fast response dynamometer system especially suited for the transient engine test. The specifications of the dynamometer are represented in Table 5. 1.

The electronic engine control unit (ECU) controls the fuel-injection system, for example, the start of injection, injection pressure, injection duration and pilot injection.

The exhaust gas recirculation (EGR) is used to reduce NO_x emissions and the variable geometry turbocharger (VGT) is implemented to reduce turbo-lag and increase the engine performance at the low- and high- engine speed together by controlling the turbine vein size. Monitoring and controlling the engine is carried out by the powertrain control module (PCM) through ETAS INCA software. Using this software, all of the engine parameters, e.g., injection, EGR and VGT settings and controls, can be monitored and calibrated. In addition, INCA software is linked to the PUMA dynamometer operating system via a communication link that operates on ASAM (Association for Standardization of Automation and Measuring Systems) protocol, so the input and output of engine parameters can be shown and stored in the PUMA dynamometer operating system in real time. Crank angle-based data is obtained by an AVL Indimaster Advanced 671 indicating system. With the resolution of 0.1^o crank angle degree (CAD), the cylinder pressure and various crank angle-based phenomena can be measured and analyzed.

Table 5. 1. Transient Dynamometer specifications

Manufacturer	AVL
Name	ELIN series 100 APA Asynchronous Dynamometer
Speed range	± 8000 rpm
Torque range	-1273 to +1400 Nm
Power (Absorbing/Motoring)	330/300 kW
Rotational Inertia	2.91 kgm2
Torque Response	5 ms
Torque Reversal	10 ms (-100% to 100%)
Operating System	AVL PUMA OPEN
Input/Output System	AVL Fast Front End Module (FFEM)

AVL Combustion Emissions Bench II (CEB-II) is used to sample, condition, and measure exhaust gas. Carbon monoxide (CO), carbon dioxide (CO_2), oxygen (O_2), total hydrocarbons (THC), and oxides of nitrogen (NO_x) in the exhaust gas are measured, and CO_2 levels in the intake manifold is also measured to calculate EGR rates. These

analyzers do not have the response time necessary to capture fully the emissions formed during transient engine operations. They distort emission dynamics and generally overestimate transient widths and underestimate transient peak values. Nevertheless, even though these steady-state devices do not accurately follow the instantaneous emission prediction, they give accurate integrated emission responses [36], [50].

The mass flow of NO_x is calculated from the NO_x concentration output from the NO_x analyzer in Equation (5.1). The air mass flow and fuel mass flow are measured by a laminar air flow meter and coriolis fuel flow meter, respectively.

$$\dot{m}_{NO_x} = \frac{ppm_{NO_x}}{10000} \cdot \frac{MW_{NO_x}}{MW_{exhaust}} \cdot \left(\dot{m}_{air} + \dot{m}_{fuel} \right) \tag{5.1}$$

where $\dot{m}_{NO_x}$ is the mass flow of NO_x, $\dot{m}_{air}$ is the mass flow of air, $\dot{m}_{fuel}$ is the mass flow of fuel, MW_{NO_x} is the molar mass of NO_x, and $MW_{exhaust}$ is the molar mass of the exhaust gas.

Differential mobility spectrometer (DMS) 500 manufactured by Cambustion, Limited, is used to measure the fast response particulate mass flow. This instrument measures the number of particles and their spectral weighting in the 5 nm to 1000 nm size range with the time response of 200 ms. The instrument provides aerosol size spectral data by using a corona discharge to place a prescribed charge on each particle. The charged particles are then introduced into a strong electrical field inside a classifier column as shown in Figure 5. 1. This electrical field deflects the particles away from the electrode through a sheath flow toward electrometer detectors. Particles with lower aerodynamic drag-to-charge ratios will deflect more quickly and are attracted towards electrode rings closer to the beginning of the classifier column, and vice versa. The classification of small particles in this manner is effective because the electrostatic force is very high relative to any others, e.g., inertia. As the particles land on the grounded rings, they give up their charge and these outputs from the electrometers are processed in real time to provide spectral data and other desired parameters [40], [51].

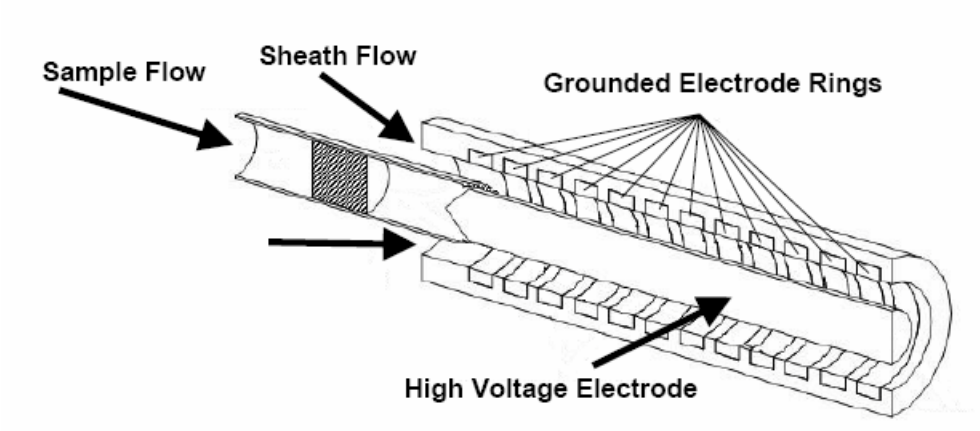

Figure 5. 1. DMS 500 classifier column

Converting aerosol spectral size data into particulate mass data is not straight-forward because agglomerates formed during the diesel combustion are non-spherical and therefore their mass does not correlate with the cube of the particle diameter. In addition, constituents of particles change as their diameters vary and consequently there is no direct correlation between the particle density and diameter. To convert the particle spectral density to mass, a relationship has been suggested by the manufacturer that is based on published results obtained from SMPS (Scanning Mobility Particle Sizer) and an APM (Aerosol Particle Mass) Spectrometer [52]. The density of the particles within each discrete size range is assumed constant and the mass of particles within each size range is determined by Equation (5.2)

$$Particle\,Mass = 6.95\times10^{-3}\cdot D_P^{2.34}\cdot Number\ of\ Particles \tag{5.2}$$

where leading coefficient accounts for the pseudo-density which affected by particle constituents and the unit change and D_P is the particle diameter.

The non-spherical nature of each particle shape is accounted for by the diameter exponent less than 3. After the particle mass is calculated for each bin, the total particle mass is calculated by integrating the particle mass over all the diameters in each bin and dividing the particle mass by the number of bins per decade in Equation (5.3) [40].

$$Total\ Mass = \frac{\sum_{Bins} Mass}{Bins\,/\,Decade}\ [\mathrm{kg/m^3}] \tag{5.3}$$

To validate the accuracy of the mass concentration output of the DMS 500, the steady-state measurement is compared with the data from the smoke meter. The AVL 415S

Variable Sampling Smoke Meter is used to obtain soot emissions on a mass-per-volume basis, and the following correlation is given by [53] as Equation (5.4).

$$Soot\,Concentration = \frac{1}{0.405} \cdot 4.95 \cdot FSN \cdot e^{0.38 \cdot FSN} \ [\mathrm{mg/m^3}] \qquad (5.4)$$

where FSN is AVL smoke meter number.

The correlation of the soot concentration between the DMS 500 and AVL smoke meter is tested in the test cell. The data obtained over a variety of speed and load points with two instruments are shown in Figure 5. 2. An agreement is found to be acceptable between these two methods below smoke numbers of around 1.5, which corresponds to the concentration level of 32.4 [mg/m^3] [40].

The higher reading in the DMS 500 can be attributed to the fact that the smoke meter measures only soot emissions and cannot account for the soluble organic fraction (SOF) in the exhaust. Since the DMS measures both soot and SOF, its readings are expected to be higher than the smoke meter's [40]. Considering that measuring methods completely differ for both systems, it seems that the results are close and the DMS 500 can be used to quantify the transient particle mass concentration.

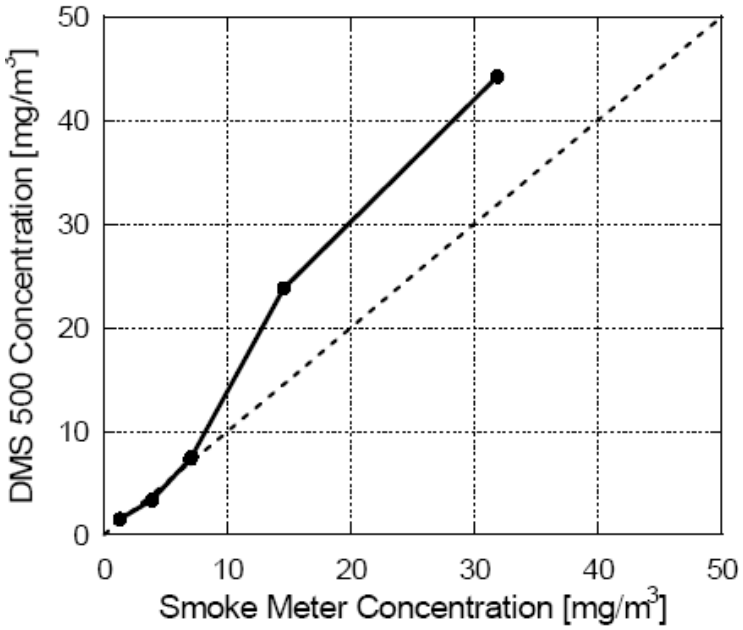

Figure 5. 2. Soot concentration comparison between DMS 500 and AVL smoke meter [40]

5.2. Engine-in-the-Loop Integration Challenges

The initial EIL setup challenges are integration issues concerning operating safely and achieving the full functionality of test equipments and models [35], [105].

First, the connection causality defines which signal should be an input and decides which signal should be an output between the dynamometer system and simulation. Traditionally, engine-dynamometer test setups have controlled engine torque and measured engine speed with a torque sensor [54], [55] in the steady state. However, controlling the engine torque is very difficult because of the noisy torque sensor signal in transient conditions leading to the unstable engine control even after carefully tuning dynamometer controller gains. That is because controlling the torque involves the engine acceleration control with the dynamometer, so the torque signal is a higher order comparison with the engine speed signal. Thus, a high-bandwidth actuator is needed for the torque control. In this study, the EIL setup's connection causality is reversed by replacing the torque input with the engine speed input to the dynamometer system and the dynamometer system output becomes the torque signal. Therefore, the setup's bandwidth increases to the desired range (15~25 Hz) alleviating the stability problem [36].

Second, measured signals are susceptible to the noise and communication time delay. These two problems are solved through the introduction of low-pass filtering to eliminate the sensor noise and lead filtering to counterbalance the phase lags introduced by the communication time delays [37], [38].

Third, the original virtual driver is unable to follow the rapid fluctuations of the reference vehicle speed in FUDS. According to the emission test standard for the light-duty vehicle from EPA [39], the vehicle test fails when the continuous vehicle speed deviation from the reference speed is more than 2 mph for one second. In this study, ensuring the desired dynamic performance of the driver model is achieved by adding the low-pass filter to reduce measurement noises and 1-, 2-, 3- second previews with proportional preview gains as shown in Figure 5. 3 [35].

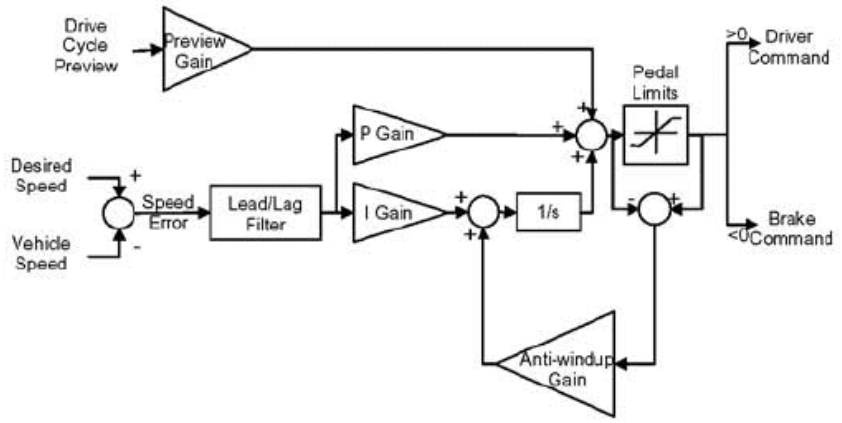

Figure 5. 3. Preview driver model in the EIL setup

In addition to the general challenges described above, there exists challenges originate from the SHH system itself. Firstly, the engine speed controller in the simulation block cannot be used any longer because of the unstable engine speed control in the EIL test with the original SHH system model. With the reversed causality, the dynamometer controller controls the actual engine speed and P/M_{gen} controller controls the engine speed in the simulation with the engine dynamics model that is composed of only the engine torque, load torque (P/M_{gen} torque) and engine and P/M_{gen} inertia. As a result, there exist two engine speed controllers in the simulation and dynamometer system and the synchronization of engine speed and torque control are uncontrollable because the dynamometer's speed controller and P/M_{gen} controller crashes to control the small inertia engine-P/M system. To increase the bandwidth of the engine speed controller, the original EIL setup for the SHH system is modified as shown in as shown in Figure 5. 4. In the modified EIL setup, the engine dynamics block is removed from the simulation and the desired engine speed is directly sent to the dynamometer system with using only the dynamometer controller for the engine speed control.

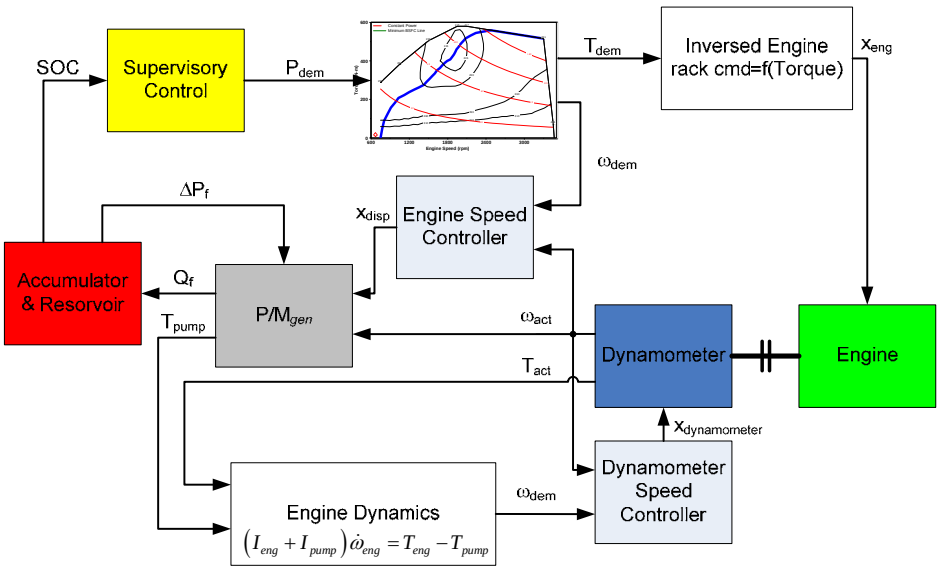

(a) Original SHH EIL setup

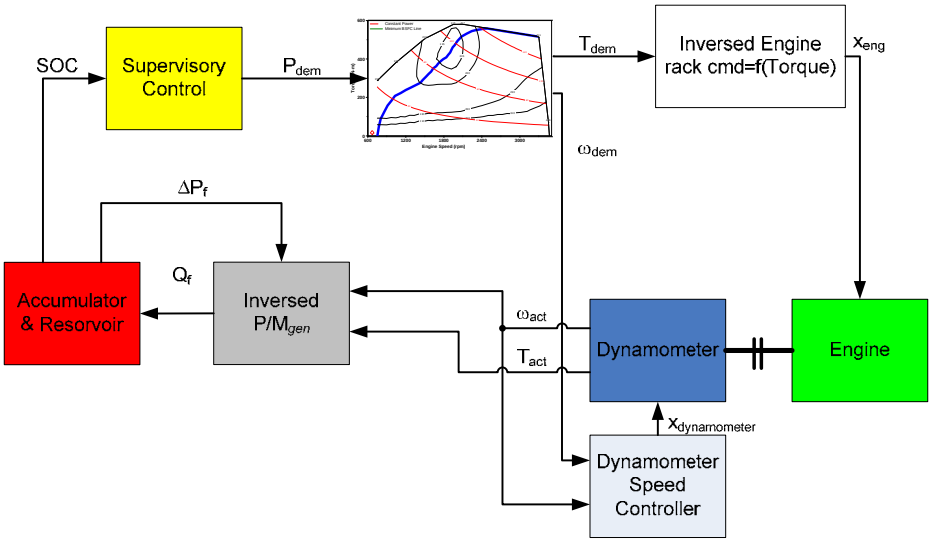

(b) Modified SHH EIL setup

Figure 5. 4. Diagram of the SHH Engine-in-the-Loop setup before and after the modification

Secondly, the fluid flow from the P/M$_{gen}$ cannot be calculated without the displacement factor of the P/M$_{gen}$ because the engine-speed controller block, which is used to calculate the displacement factor in the simulation, is removed. To overcome this problem, an inverse P/M$_{gen}$ model is developed to find the displacement factor from the dynamometer torque output assuming the dynamometer torque is same to torque of the P/M$_{gen}$. The displacement factor can be inversely calculated from the measured P/M$_{gen}$ torque (dynamometer torque) signal from Equation (2.9) and Equation (2.10).

From the torque efficiency equation, a cubic equation whose solution contains a displacement factor is derived in Equation (5.6). This special cubic equation has the general form of $ax^3 + bx + c = 0$, and has the coefficients as shown in Equation(5.7).

$$\eta_{T,pump} = \frac{T_i}{T_a} = \frac{|x|\Delta pD}{T_a} = \frac{1}{1 + \frac{C_v S}{|x|} + \frac{C_f}{|x|} + C_h x^2 \sigma^2} \tag{5.5}$$

$$T_a = \Delta pD|x| + C_v S\Delta pD + C_f \Delta pD + C_h \sigma^2 \Delta pD|x|^3 \tag{5.6}$$

$$a = C_h \sigma^2 \Delta pD, \quad b = \Delta pD, \quad c = C_v S\Delta pD + C_f \Delta pD - T_a \tag{5.7}$$

The solutions of the general form of $ax^3 + bx + c = 0$ are represented in Appendix A.5. In the case of the pump operation, T_a can be assumed always negative. Because a, b and c are all positive, x_1 is always real and x_2 and x_3 are always complex conjugates. Therefore, the displacement factor in the case of the pumping is x_1 and x_1 is proven a correct displacement factor by comparing x_1 with the actual displacement factor from the P/M$_{gen}$ model in the simulation.

In case of the motor operation, substituting T_i with Equation (2.6) in Equation (2.10) leads to Equation (5.8) and Equation (5.9). Equation (5.9) has also the form of the cubic equation, $ax^3 + bx + c = 0$, and the coefficients are as shown in Equation (5.10)

$$\eta_{T,motor} = \frac{T_a}{T_i} = \frac{T_a}{|x|\Delta pD} = 1 - \frac{C_v S}{|x|} - \frac{C_f}{|x|} - C_h x^2 \sigma^2 \tag{5.8}$$

$$T_a = \Delta pD|x| - C_v S\Delta pD - C_f \Delta pD - C_h \sigma^2 \Delta pD|x|^3 \tag{5.9}$$

$$a = C_h x^3 \sigma^2 \Delta pD, \quad b = -\Delta pD, \quad c = T_a + C_v S\Delta pD + C_f \Delta pD \tag{5.10}$$

In the case of the motor operation, x_3 is proven the correct displacement factor by comparing x_3 with the actual displacement factor from the P/M$_{gen}$ model in the simulation. As a result, the fluid flow from the P/M$_{gen}$ can be calculated if the P/M$_{gen}$ torque is known. Thus, the dynamometer torque is multiplied by -1 and interpreted as a P/M$_{gen}$ torque assuming the P/M$_{gen}$ is always used for the pumping only. In the current SHH EIL test setup, the dynamometer mostly works as a pump without idle-stop-and-start function.

Thirdly, even though the dynamometer is regarded as a P/M_{gen} assuming dynamometer torque is same to the P/M_{gen} torque in the SHH EIL setup, the dynamometer's inertia is too large in comparison with the P/M_{gen}'s inertia. As a result, the engine behavior cannot be the same as the actual SHH system. However, this transient dynamometer system provides the inertia compensation function that can remove almost up to 70% of dynamometer inertia with the model inside the dynamometer system. This is critical function for the success of the EIL test for the SHH system. By using inertia compensation function, the engine speed and torque measurements from the dynamometer are pretty close to those of pure simulation results in Figure 5. 16 and Figure 5. 17. In the current EIL setup, the dynamometer inertia is 3.084 and it is compensated down to be 0.9252 kgm^2. The engine inertia is 0.55 kgm^2 and hydraulic P/M inertia is assumed to be around 0.058 kgm^2.

5.3. Engine-in-the-Loop Test Result

The EIL test verifies SHH simulation results during FUDS and HWFET in the case of the V8 and downsized V6 engines. The FUDS cycle test results show the capability of improving fuel economy with frequent vehicle-stops with intermittent acceleration cases and the HWFET cycle test shows how the system efficiency of the SHH system can improve fuel economy without regenerative braking. Assuming the engine downsizing is just from a V8 to V6, the engine downsizing in the EIL test is simply accomplished by multiplying the engine-cylinder number ratio, 6/8, to the measured outputs, e.g., torque, fuel consumption, and exhaust emissions from the test cell.

The fuel economy is measured without idle-stop in the EIL test. Even though the actual engine-stop and -start during the driving schedule is not applied to the current EIL setup, the fuel economy with idle-stop can be post-processed assuming the engine starting condition, starting fuel consumption, and starting exhaust emissions. In this study, firstly, the starting fuel consumption, NO_x and soot emissions are measured in the preliminary test. By dividing the starting fuel amount by idle fuel consumption, the minimum idle-stop time is calculated as around 7~8 seconds. Considering starting NO_x and soot emissions, 10 seconds is assumed the threshold time for the engine stop-and-start criterion. Thus, if the engine power demand is zero over 10 seconds, that period is

assumed the engine-stop and the starting fuel, NO_x and soot amounts are added respectively to the total measurements after the idle measurements are removed.

The dramatic difference of engine behaviors between the simulation and EIL test occur in the case of thermostatic SOC control because of the severely transient characteristics. In the EIL test, the step input of engine power demand overshoots the engine speed corresponding to the threshold power and undershoots the engine torque to negative when the engine power demand becomes zero with the step function. As a result, the engine speed and torque control becomes unstable. As a countermeasure, the rate limits of the engine power demand should be applied for the safety of the engine and dynamometer system. The engine power-rate limits are found to be 40kW/s for the power-up and 20kW/s for the power-down with the trial-and-error method.

The pure simulation does not have to apply the engine power-rate limit, even though the engine speed and torque overshoot because they are not so severe with simple engine dynamics and without signal delay. The necessity of putting engine power-rate limit in the actual thermostatic SOC control can only be discovered through the actual engine application such as the EIL test. Adding the engine power-rate limits affects fuel economy and emissions inevitably and the results are shown in the next section.

5.3.1. FUDS Test

The fuel economy, NO_x and soot emissions during FUDS are represented for various SHH systems with and without idle-stop in Table 5. 2 and in bar graph in Figure 5. 5. Relative comparisons with conventional vehicle case are shown in Figure 5. 6.

The optimized series hydraulic HMMWV model with a V6 engine shows the fuel economy improvement of 57% without idle-stop and 70% with idle-stop in the case of modulated SOC control over the conventional vehicle case. Even if the thermostatic SOC control scheme shows almost the same fuel economy as the modulated SOC control case in the simulation (see Table 3. 9), the thermostatic control shows about 6% lower fuel economy than the modulated SOC control case without idle-stop. Even with engine-stop capability, the modulated SOC control scheme case shows 2% higher fuel economy than the thermostatic SOC control case. In other words, the thermostatic SOC control should adopt the idle-stop capability to have a competitive fuel economy in comparison with modulated SOC control case.

Table 5. 2. EIL test results for the conventional vehicle and various SHH systems

(without / with idle-stop)	Convent-ional	Baseline SHH, V8	Optimized SHH, V8	Optimized SHH, V6	Thermostatic Control, V6
Fuel economy [mpg]	11.2	16.0 / 17.7 (43 / 58 %↑)	17.0 / 18.8 (51 / 68 %↑)	17.6 / 19.4 (57 / 72 %↑)	17.0 / 19.1 (51 / 70%↑)
NO_x [g/km]	2.82	2.69 / 2.35 (5 / 17%↓)	2.55 / 2.22 (10 / 21%↓)	2.47 / 2.17 (12 / 23%↓)	2.53 / 2.13 (10 / 24%↓)
Soot [g/km]	0.0865	0.0282 / 0.0275 (67 / 68%↓)	0.0225 / 0.0198 (74 / 77%↓)	0.0231 / 0.0226 (73 / 74%↓)	0.0361 / 0.0339 (58 / 61%↓)

NO_x emissions reduce in the SHH system in comparison with conventional vehicle but the reduction rate is much less than the fuel economy improvement because the engine uses the fuel-efficient area, where generally the $BSNO_x$ is also high, in the engine map. NO_x emission is not sensitive to the engine size because small engine uses more fuel-efficient area with the same engine power demand than the V8 engine case. As a result, NO_x decreases about 10% without engine stop and 20% with idle-stop capability in most of SHH system including the thermostatic control case. Soot emissions decreases dramatically in the case of the modulated SOC control with relatively smooth engine operation. Especially, soot emission is known to be very sensitive to the transient operation and especially, diesel engine is vulnerable with turbo-lag [40]. As a result, the modulated SOC control shows best performance in reducing the soot emissions for the SHH system with the diesel engine application. As expected, the soot emission reduction is smaller in the case of the thermostatic control because of the highly transient engine operation even though the engine power-rate limiting is applied.

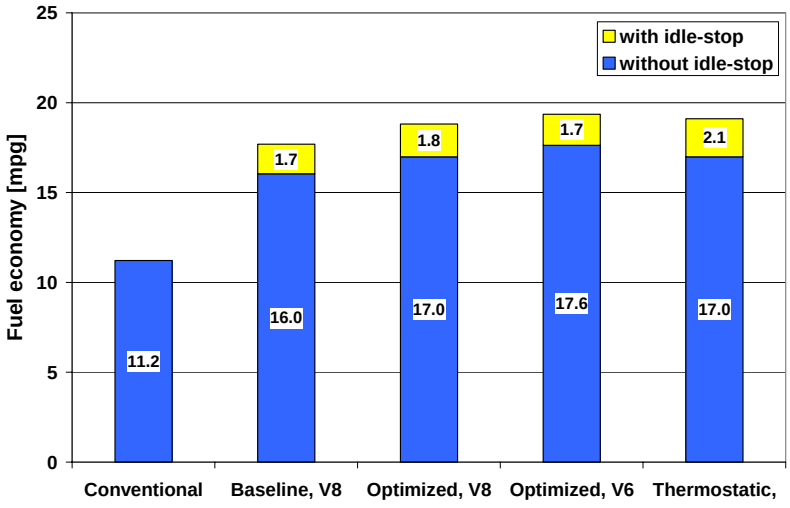

(a) Fuel economy

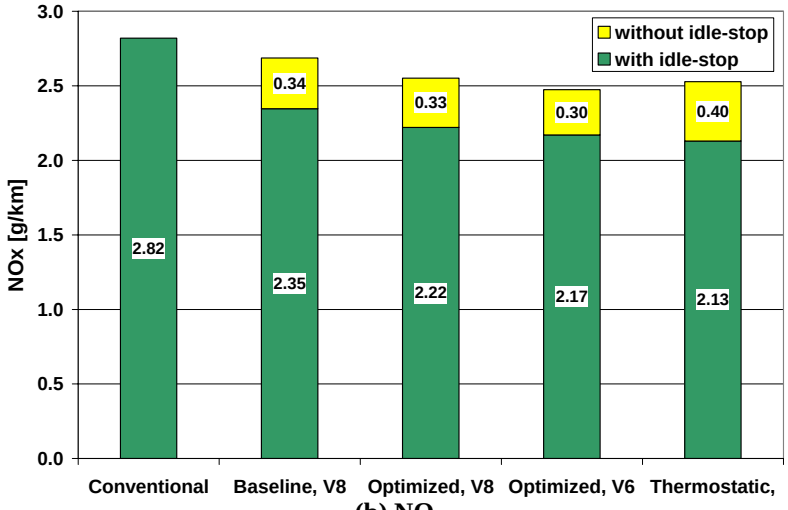

(b) NO_x

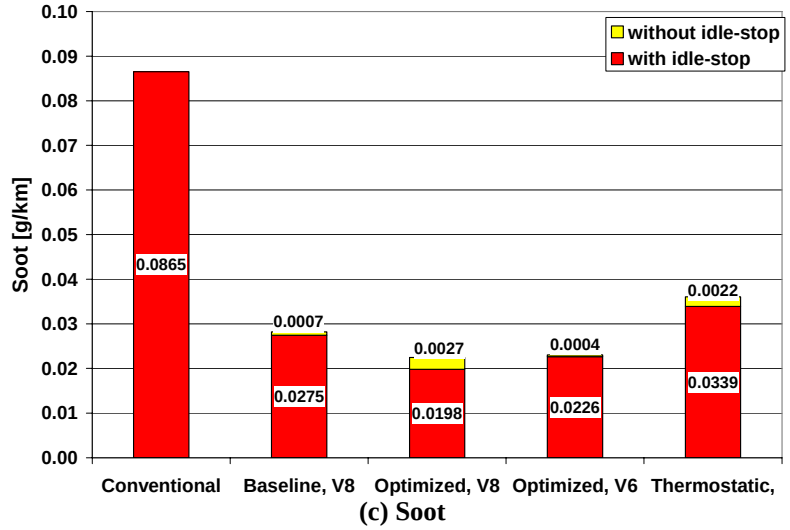

(c) Soot

Figure 5. 5. Fuel economy, NO_x and soot values for each vehicle system

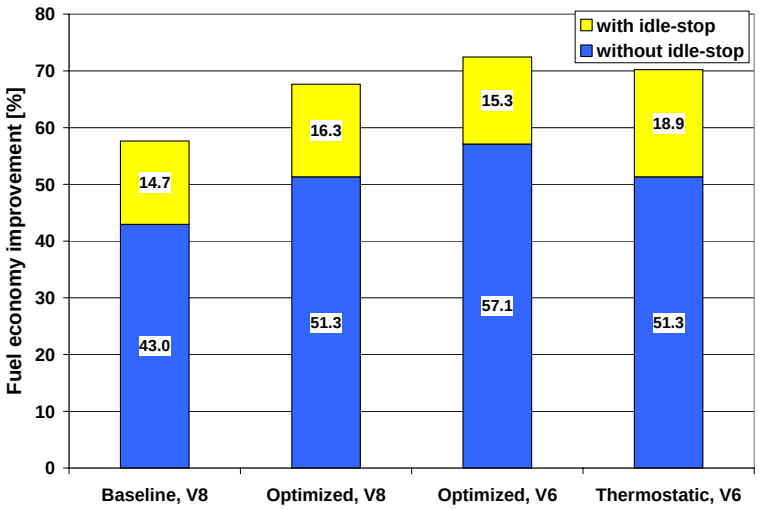

(a) Fuel economy

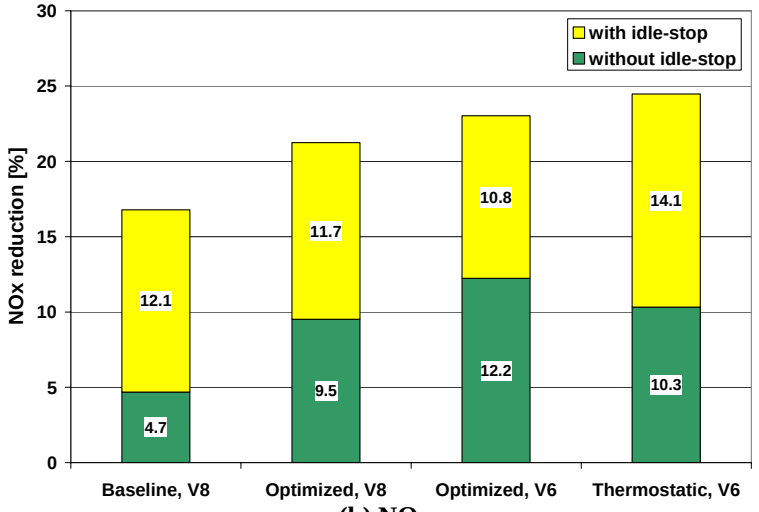

(b) NO_x

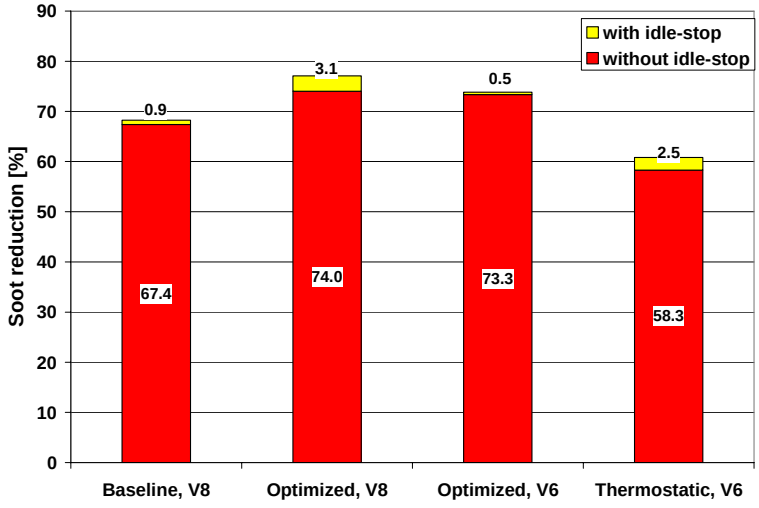

(c) Soot

Figure 5. 6. Fuel economy improvement and NOx and soot reduction

Interestingly, NO_x and soot emissions are almost the same level when the engine is downsized because the engine operation becomes more transient to produce same power with downsized engine, i.e., the downsized engine cases use the higher speed and higher load area than the original engine cases.

In contrast to the case of NO_x, the idle-stop capability does not decrease the soot so much, because the soot amount from the engine starting is not negligible. The modulated SOC control reduces about 75% of the soot emissions and the thermostatic control case reduces about 60% of soot emissions in comparison with the conventional vehicle case.

In the EIL test, the fuel consumption of the conventional vehicle is scattered at the low load and high engine speed area, where the fuel efficiency is relatively low, below the minimum BSFC line (see Figure 5. 7). In addition, with the automatic torque converter, idle fuel consumption is significant with the positive torque at the idle speed.

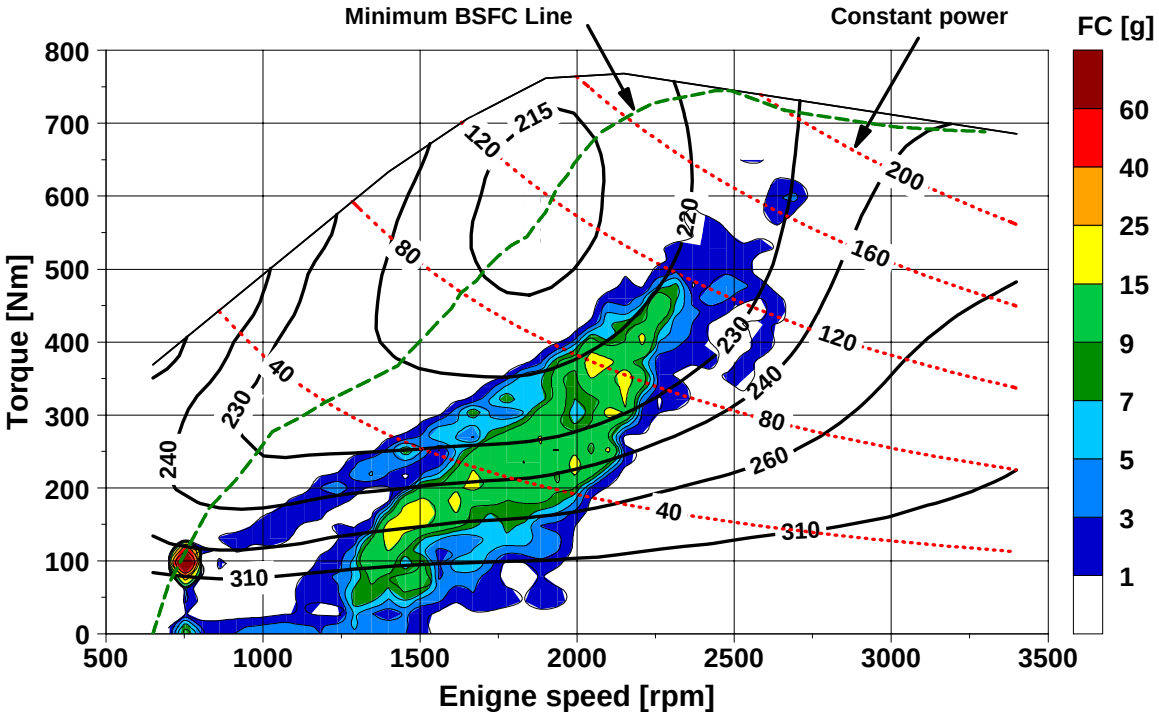

Figure 5. 7. Integrated fuel consumption conventional vehicle during FUDS

The fuel consumption in the SHH system is concentrated on the minimum BSFC line by moving the engine operation points to the low speed and high load area where the fuel efficiency is better for the same engine power (see Figure 5. 8). In contrast to the case of the pure simulation, the synchronization of the engine speed and torque is difficult with system delays and the real engine dynamics in the EIL test, so the engine operation

becomes more transient in comparison with the pure simulation case. As a result, the engine operation points scatter over the broader area in comparison with the pure simulation in Figure 3. 25

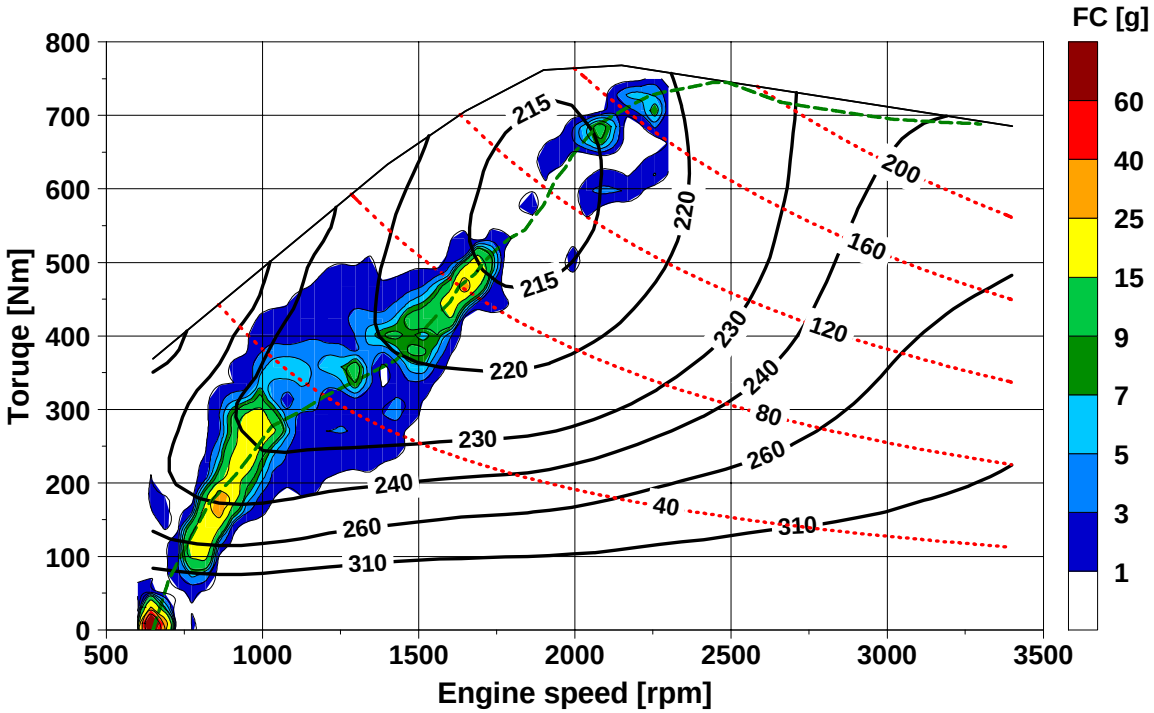

Figure 5. 8. Integrated fuel consumption of SHH with modulated SOC control

Clearly, the downsized V6 engine cases use more "sweet spot" area on the steady-engine map than the V8 engine case during FUDS in Figure 5. 9. However, the drawback of engine downsizing is witnessed in the EIL test when the engine power demand reached higher than "sweet spot" power where the engine efficiency becomes lower. Especially, a severely transient system behavior is observed in the thermostatic SOC control, which produces scattered engine operation points around the engine map even with the power rate limits (see Figure 5. 10). In addition, the synchronization of engine speed and torque control on the minimum BSFC line becomes difficult because of the transient engine operation. Therefore, the system durability and driver's comfort can be issues in the case of the thermostatic SOC control.

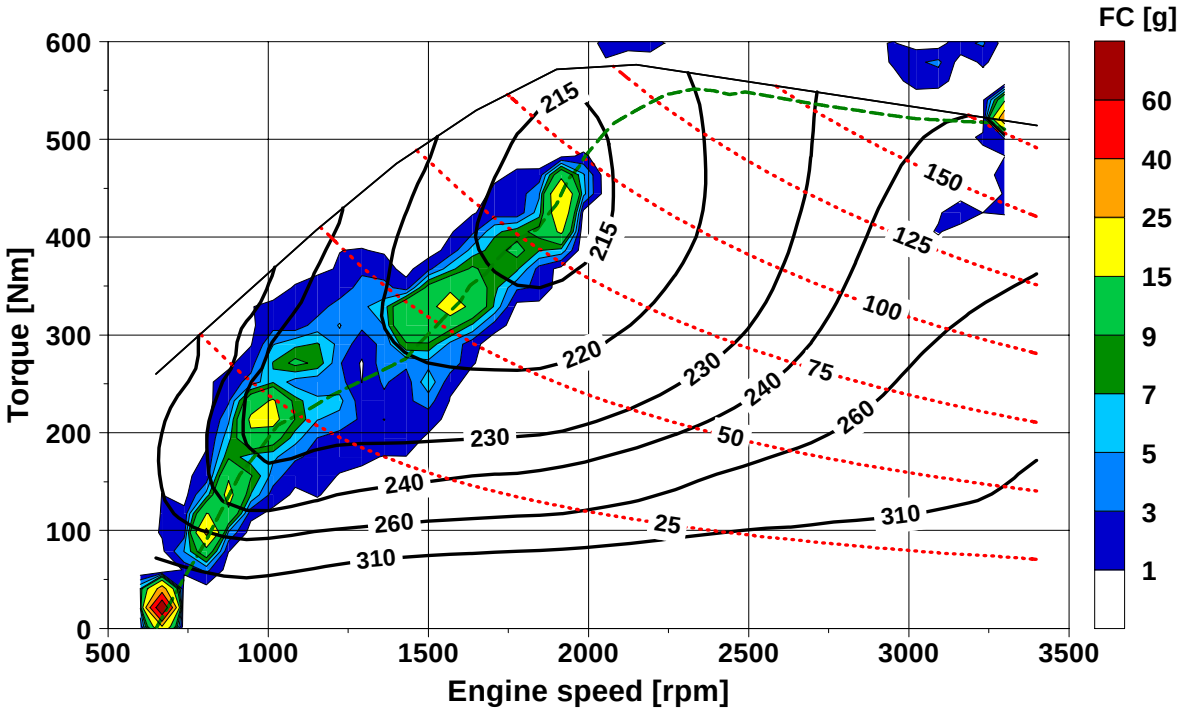

Figure 5. 9. Integrated fuel consumption of SHH V6, modulated SOC control

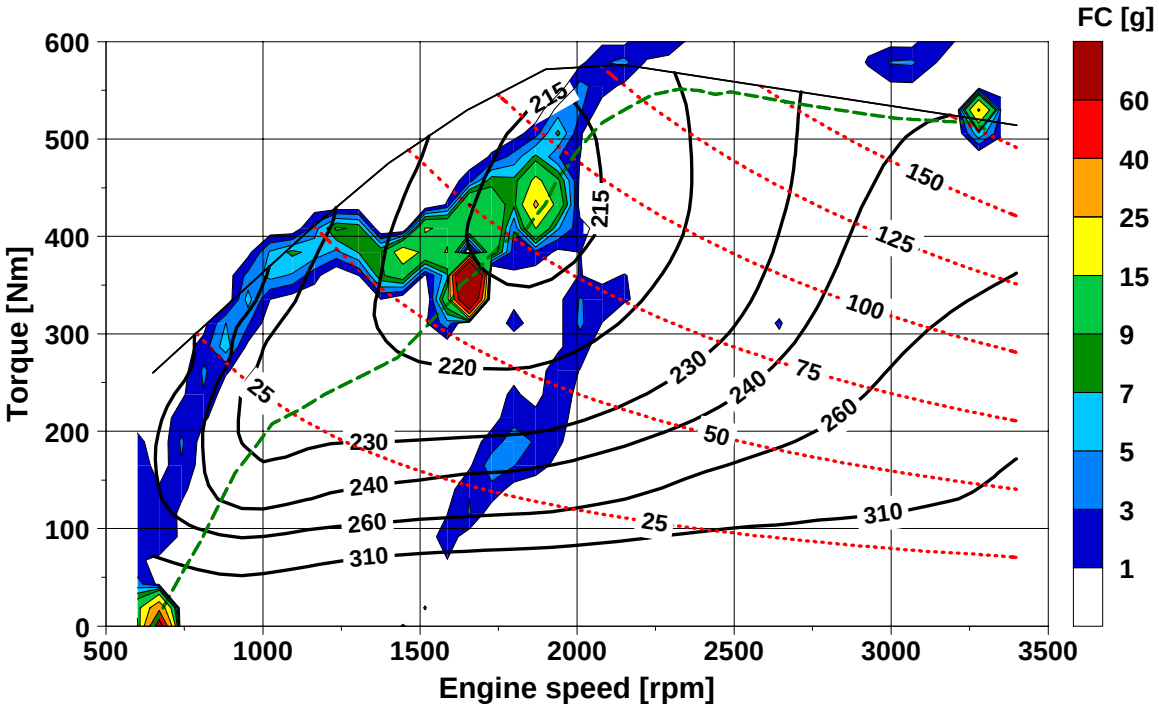

Figure 5. 10. Integrated fuel consumption of SHH V6 with thermostatic SOC control

The smoke is arbitrarily assumed visual when the soot concentration is above 2.0 of the Bosch Smoke Number (BSN). According to this assumption, the soot concentration of about $77\,mg/m^3$ corresponds to the critical value for the visual signature. The

visibility test is carried out by the DMS soot concentration measurement as shown in Figure 5. 11.

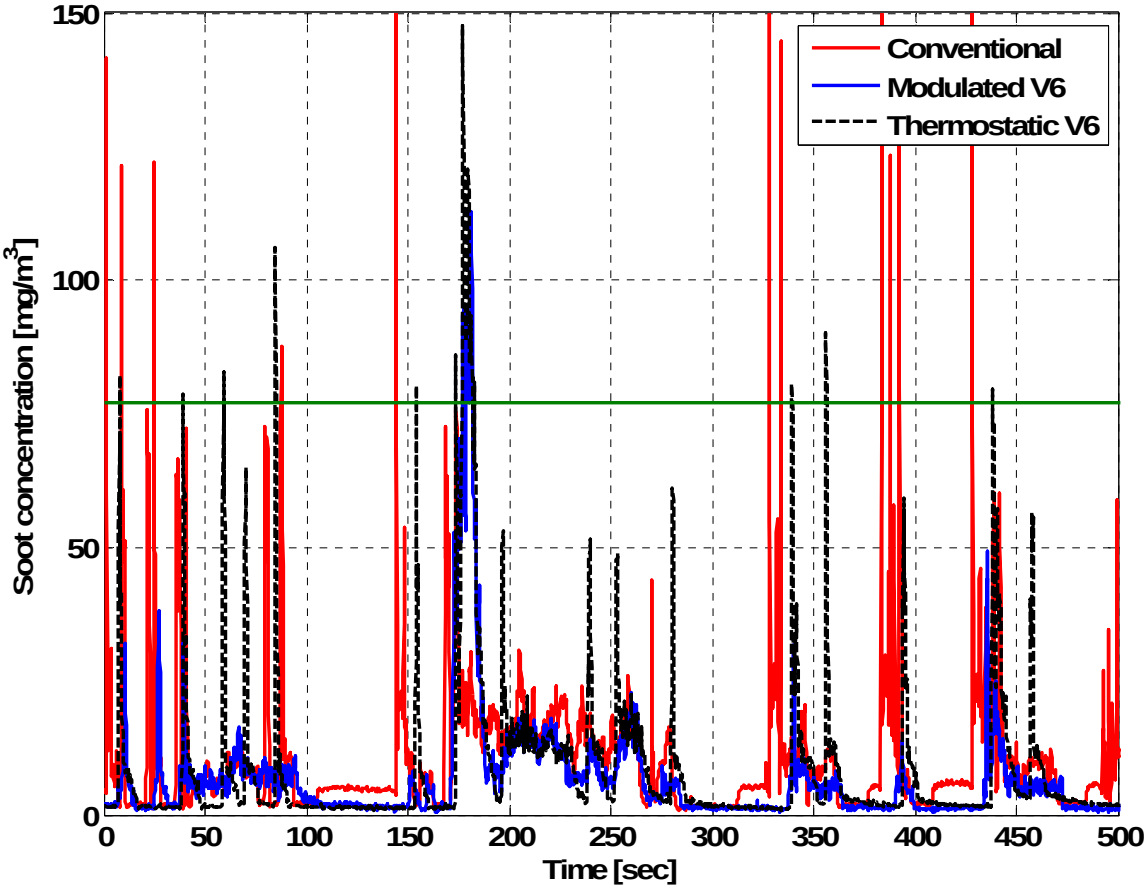

Figure 5. 11. Soot concentration measurement during FUDS

The modulated SOC control scheme shows the best performance by suppressing most of visual signatures with smooth engine power control (see Table 5. 3). Even though the thermostatic SOC control reduces the severely transient engine operations by using the power-rate limiting, the visual signature occurs so frequently as the conventional vehicle case.

Table 5. 3. The number of times over the visibility limit

	Number of times
Conventional	25
SHH V6, thermostatic control	23
SHH V6, modulated control	1

5.3.2. HWFET Test

With rare chances of regenerative braking, the fuel economy of the parallel hybrid system is almost the same as that of the conventional vehicle. Thus, the higher fuel economy in highway cycle is only possible by increasing the system. In contrast to the parallel hybrid system, the series hybrid system can show better fuel economy during the highway-driving schedule than the conventional vehicles by the engine operation on the fuel-efficient area and the high-energy conversion efficiency of hydraulic hybrid devices. EIL tests validate that the SHH super-HMMWV with downsized V6 engine case has about 11% of the fuel-economy improvement over the conventional vehicles (see Table 5. 4). Thus, it can be said that most fuel-economy gains come from the high SHH system efficiency, e.g., the engine operation on the minimum BSFC line, high hydraulic device efficiency and sequential 4x4 operation.

Table 5. 4. Fuel economy gains of SHH during HWFET

(without / with idle-stop)	Fuel economy [mpg]
Conventional V8	13.9
SHH, V8, modulated control	15.1 / 15.2 (8.6 / 9.4 % ↑)
SHH, V6, modulated control	15.4 / 15.5 (10.8 / 11.5 %↑)

To test advantages of series hybrid system in the highway driving, EIL tests are carried out for the conventional and SHH system with HWFET in Figure 5. 12. Conventional vehicles clearly use high-speed and high-load areas in comparison with FUDS cases (see Figure 5. 7) but still engine operation area is lower than the minimum BSFC line. In the case of the SHH system, high engine power demands with more steady and less transient engine operations than the cases of FUDS are clear in Figure 5. 13 and Figure 5. 14. As the case of FUDS, the SHH V6 engine case has more chances to be close to the “sweet spot” than the SHH V8 engine case. However, at some high vehicle power demands, V6 case uses higher power over “sweet spot”, so the fuel economy gains decrease. As a result, the fuel economy gains are similar in both V8 and V6 cases.

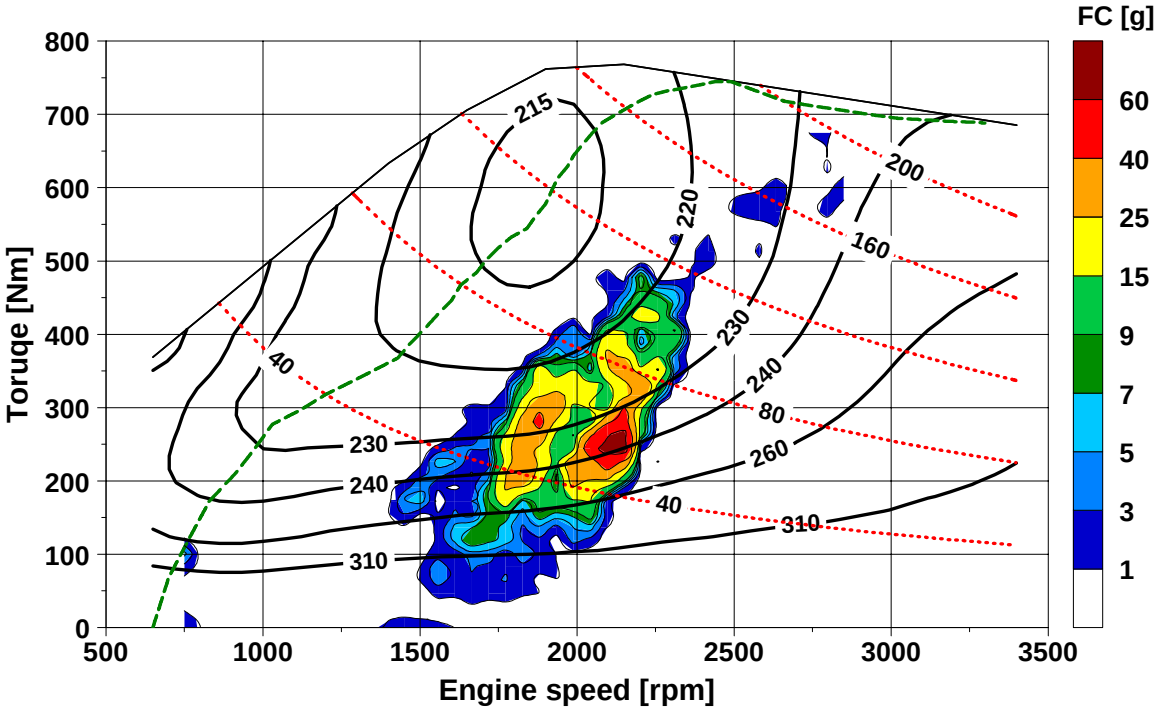

Figure 5. 12. Integrated fuel consumption of conventional vehicle during HWFET

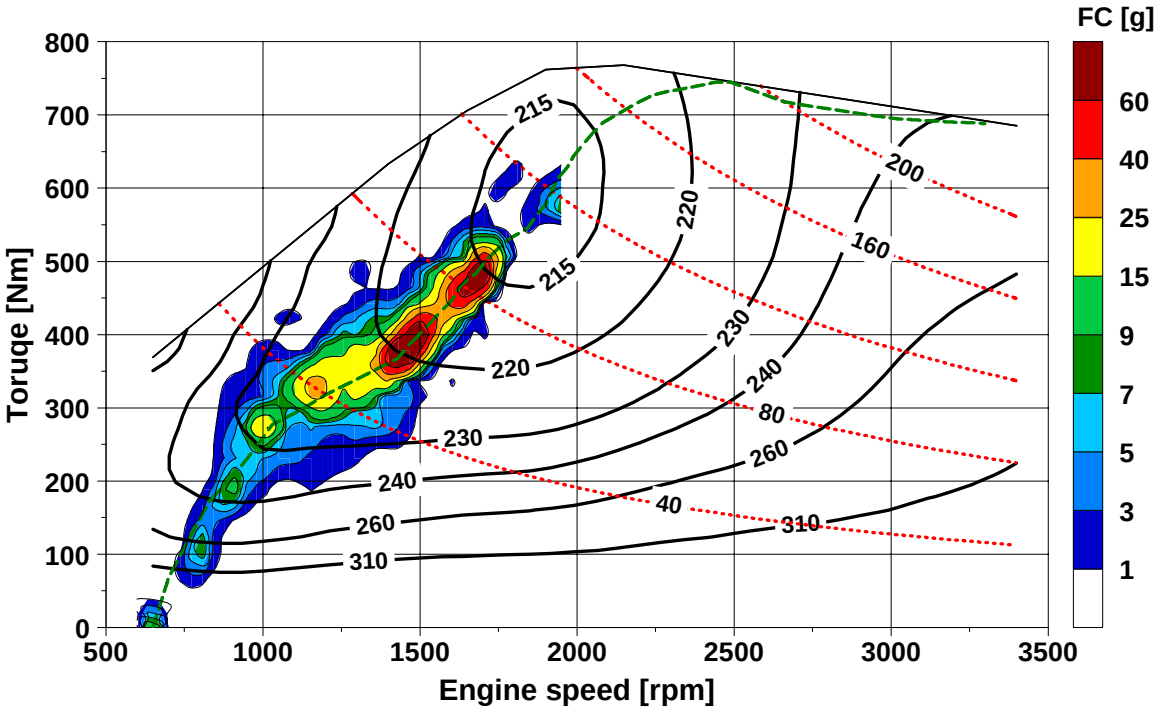

Figure 5. 13. Integrated fuel consumption of SHH V8 with modulated SOC control during HWFET

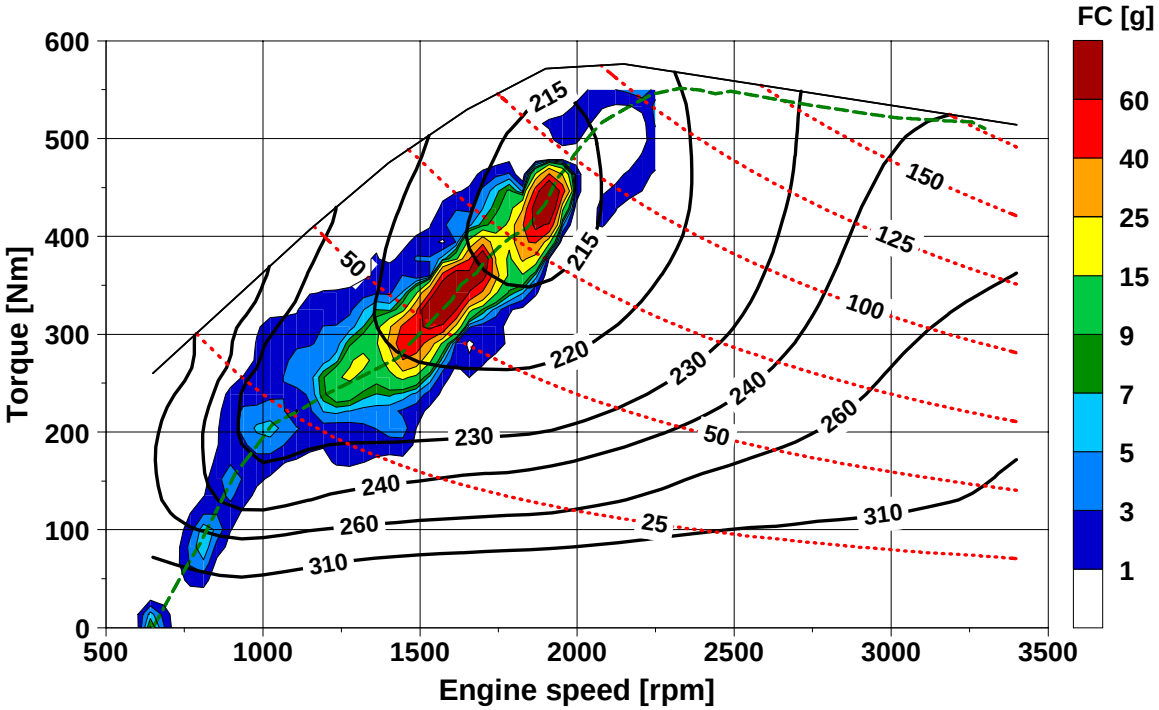

Figure 5. 14. Integrated fuel consumption of SHH V6 with modulated SOC control during HWFET

5.3.3. Comparison of EIL and Simulation

The comparison between the simulation and EIL test results shows that the fuel consumption and NO_x emission trends are predicted well in the simulation with quasi-steady assumption but soot emissions are much higher with the real engine in the EIL test during FUDS as shown in Table 5. 5 and Figure 5. 15.

Table 5. 5. Comparison of EIL test and simulation without idle-stop

	Fuel economy (EIL-sim)/sim [%]	NO_x (EIL-sim)/sim [%]	Soot (EIL-sim)/sim [%]
Baseline, V8	-5.1	-9.2	74.1
Optimized, V8	-3.5	-10.5	46.0
Optimized, V6	-5.2	-3.7	28.1
Thermostatic, V6	-6.2	-4.2	100.3

The simulation underestimated about 5 % of fuel economy for the SHH system cases and the gaps between EIL test and simulation results increase as the engine operation becomes more transient. As for NO_x emissions, simulation underestimated about 4~11 % lower.

In the case of soot emission, the SHH simulation with modulated SOC control underestimates soot about 30~50 % in comparison with the EIL test results. This discrepancy between the simulation and EIL test results increase as the engine operation becomes more transient. Therefore, in the thermostatic control case, the EIL test result is 100% higher than the simulation prediction. This proves that the transient effect dominates the formation of soot emissions in the real engine operation so the simulation with quasi-static engine model cannot be used to predict exhaust soot emission.

Even though the relatively simple engine model in the pure simulation is good enough for the optimization process and the study of characteristics of hybrid system, the actual engine application in the EIL test shows that the transient effect is significant in the real world and brings many control issues.

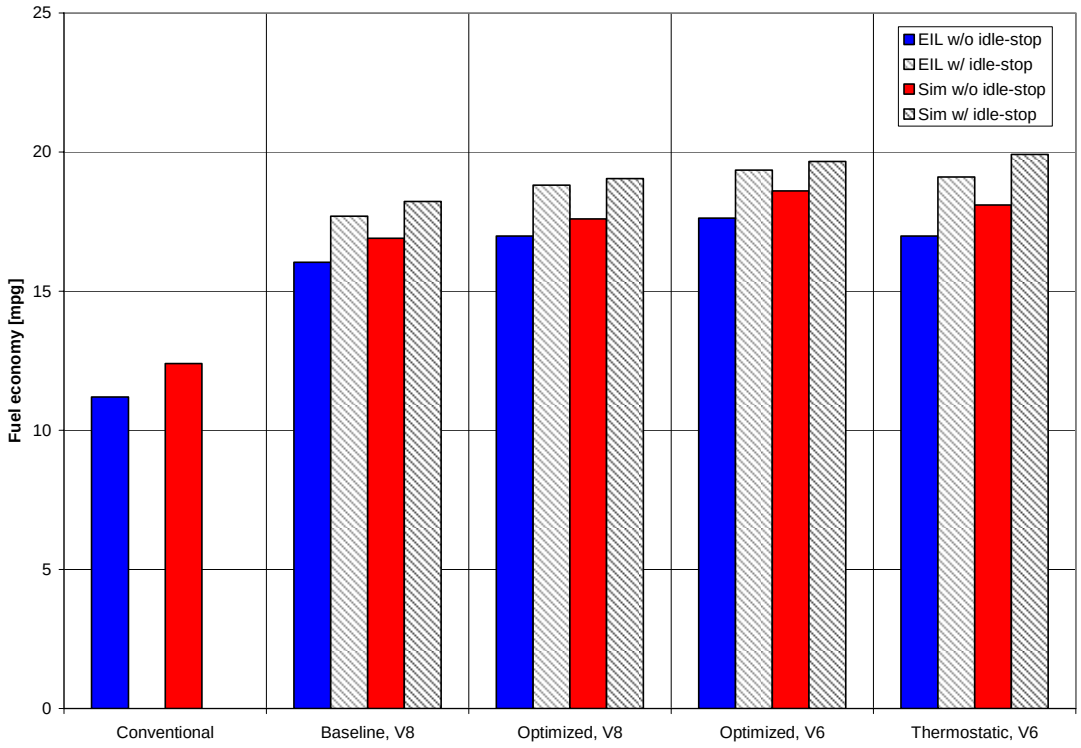

(a) Fuel economy

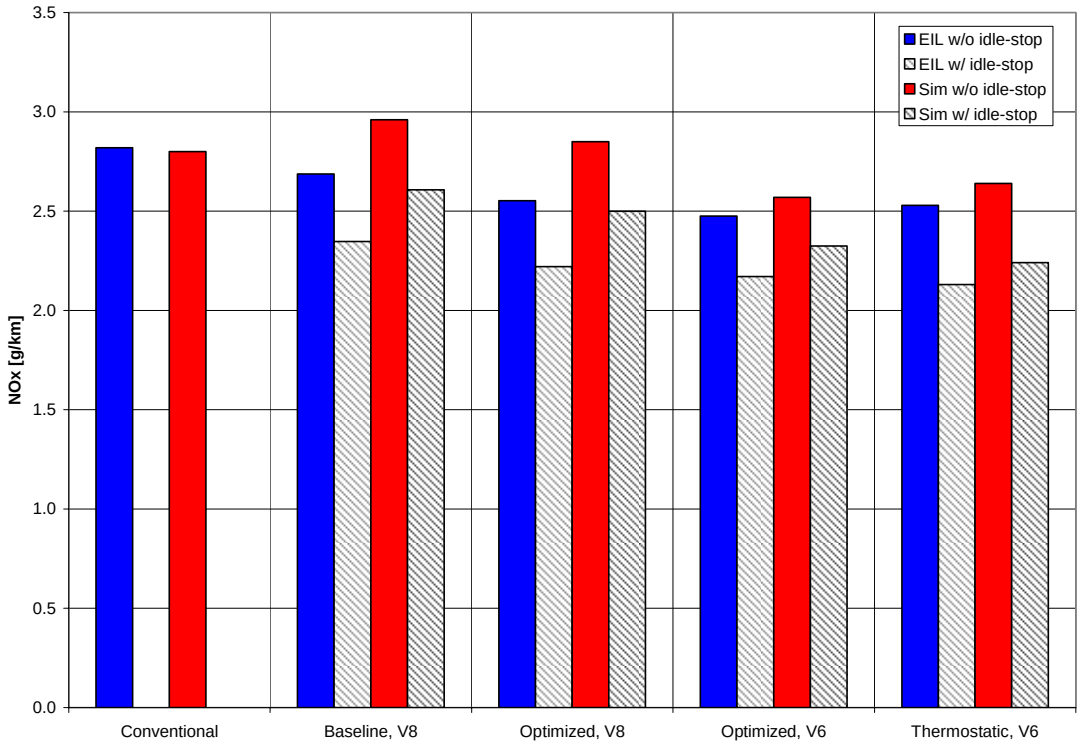

(b) NO_x

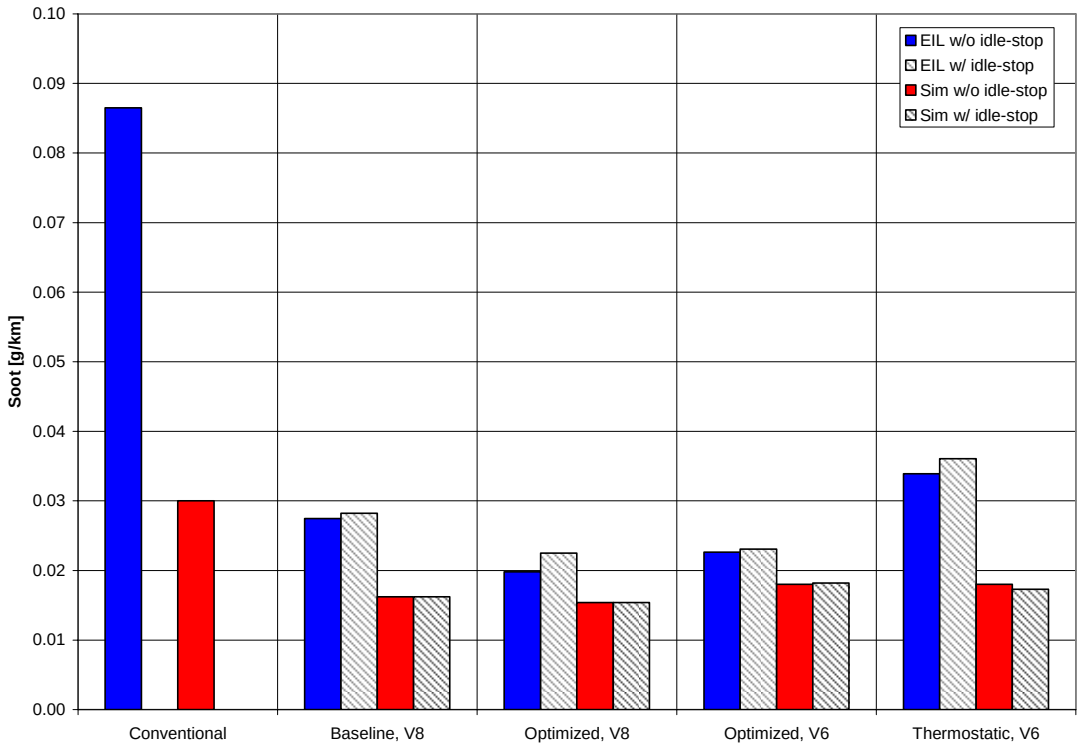

(c) Soot

Figure 5. 15. Comparison between the EIL and simulation results

The system behavior predictions of the simulation and EIL test during FUDS are compared for modulated SOC control with downsized V6 engine in Figure 5. 16. In the modulated SOC control, the simulation and EIL result are remarkably close except for the soot emissions. This closeness shows that the modulated SOC control restrains the transient engine operations and the simulation using the static engine map can predict actual engine behavior closely.

In addition, the similarity of the SOC prediction proves that the causality-inversed P/M_{gen} model, assuming the dynamometer as P/M_{gen}, works well in the EIL test. In other words, dynamometer's engine-speed controller controls engine speed as well as the engine speed controller does in the simulation. The fuel consumption and NO_x emissions predictions are close to each other in the simulation and EIL test results. However, the simulation underestimates the soot so much that it is not suitable to use the simulation that is based on the quasi-static engine model to predict soot emissions.

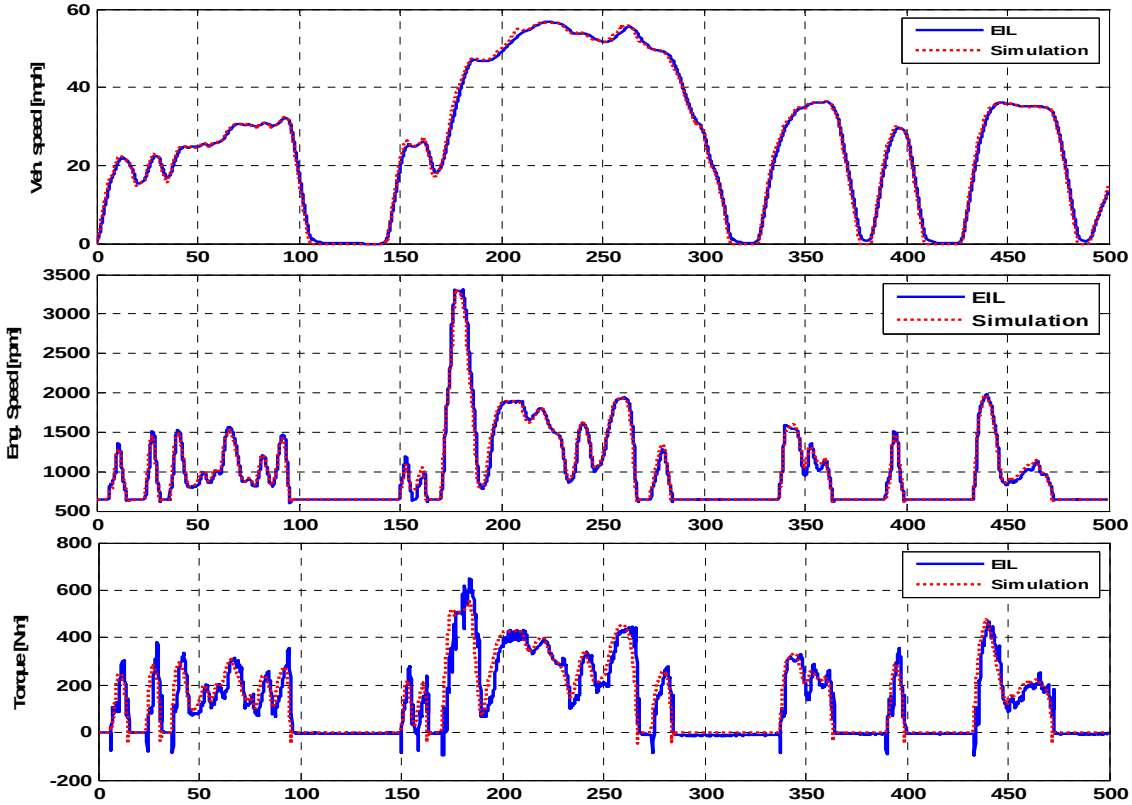

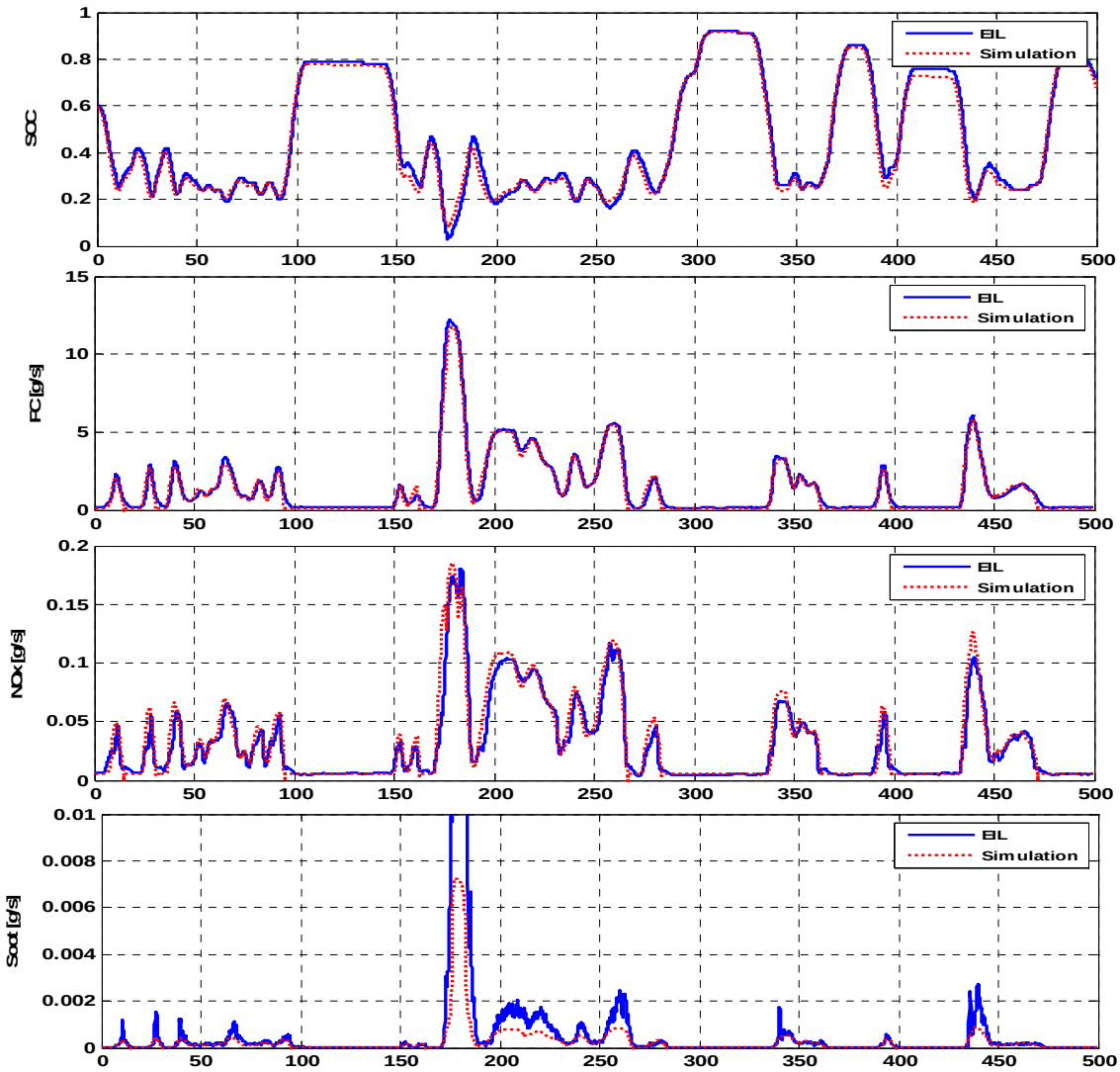

Figure 5. 16. Comparison between simulation and EIL results of the modulated SOC control

The system behavior predictions of the simulation and EIL test results during FUDS are compared for the thermostatic SOC control with downsized V6 engine case in Figure 5. 17. Contrary to the closeness between the simulation and EIL test in the modulated SOC control case, the engine-power measurement of the real engine does not synchronize with the simulation in the case of the thermostatic SOC control. The overshooting of engine speed in the EIL test makes a slightly higher SOC prediction even with a power-rate limit. Thus, the prediction of the engine power demand in the EIL test, calculated from the higher SOC, delays the next engine power demand in comparison with the prediction of the simulation's engine power. This indicates that the simple engine-dynamics model in the simulation falls short of predicting the actual engine dynamics in

thermostatic SOC control case. That is why the EIL test is needed to validate of the simulation result, especially when the system operation is expected to be highly transient.

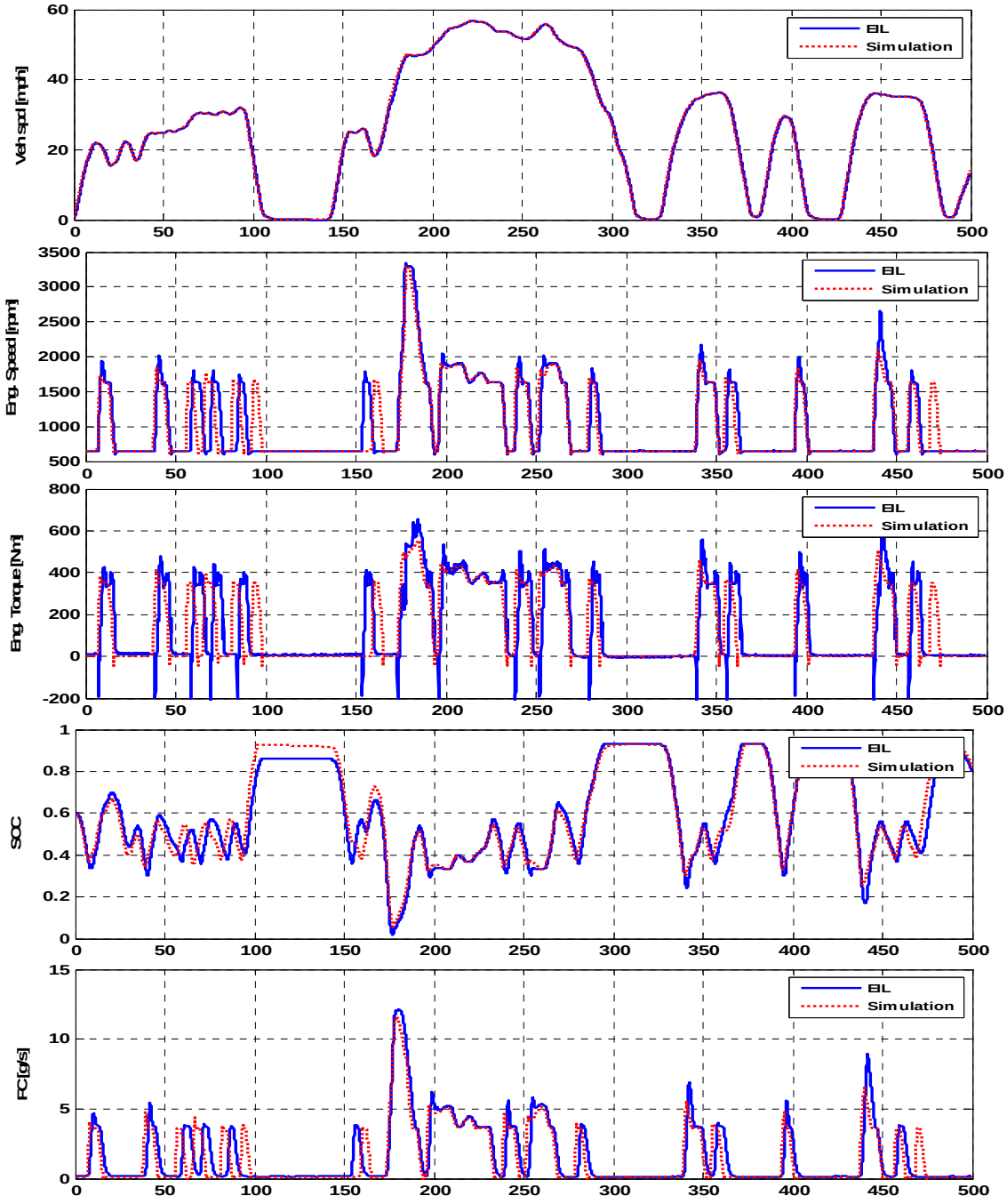

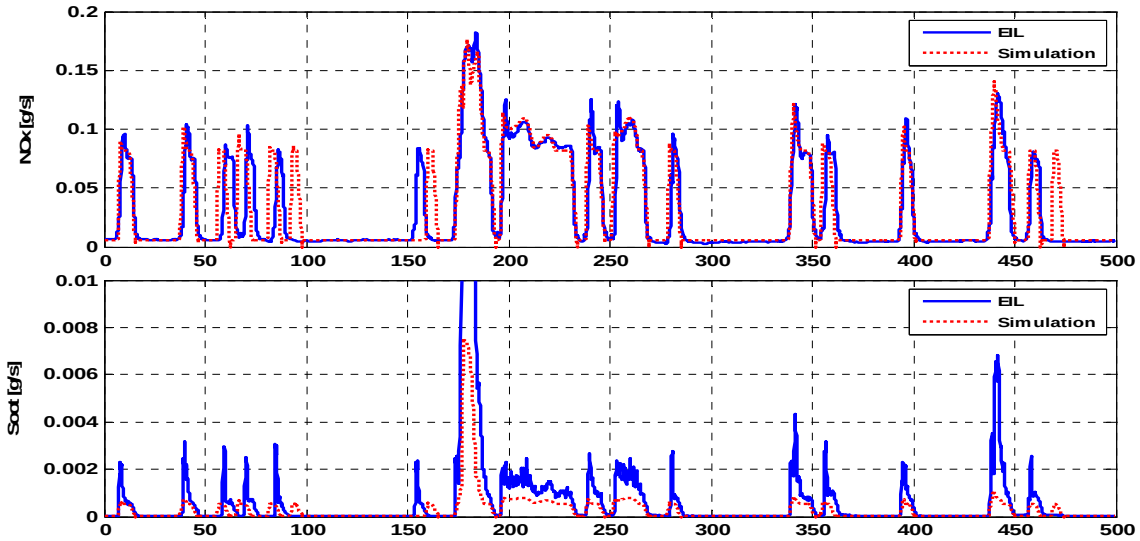

Figure 5. 17. Comparison between simulation and EIL results of the thermostatic control

CHAPTER 6

MODELING AND POWER MANAGEMENT OPTIMIZATION OF A PARALLEL HYDRAULIC HYBRID SYSTEM

The parallel hybrid system can carry over most of powertrain parts from the conventional vehicle. Because initial changes from the conventional vehicle are relatively small, parallel hybrid system can be more easily implemented than the series or power-split hybrid configuration. Most parallel hybrid vehicles can be propelled only with the engine power so parallel hybrid vehicles are more reliable than series or power-split vehicles which always need the assists from secondary power devices for normal vehicle operations. As a result, the parallel hybrid system can have the additional performance gains and improve fuel economy by the efficient operations of the engine and secondary power device combination. However, when the engine is on, its power is mechanically transferred to the wheels; therefore the flexibility in controlling the engine operation is limited.

Extensive studies of power management have been carried out on the parallel HEV system. Because the parallel hybrid system carries over most of the conventional vehicle parts and stand-alone propulsion is possible with the engine was easier to analyze and build prototype so, early hybrid studies concentrated on the parallel hybrid system.

Rahman et al. [99] showed two parallel HEV control concepts: the “thermostat” and the “power-split”. They compared three parallel HEV architectures: pre-transmission, post-transmission, and continuously variable transmission (CVT). In the thermostat control, the engine operates with a wide-open throttle between pre-designed lower- and higher SOC values. The excessive engine power over vehicle power demand is used for charging. In the power-split control, the electric drive operates only when the engine runs inefficiently or extra power is needed for the acceleration.

Kolmanovsky et al. [93] showed how to improve rule-based power management by optimally selecting thresholds of engine speed and SOC for motor engagement and

engine torque threshold, which is a function of engine speed in a parallel HEV. Lin et al. [43] presented a parallel HEV model for a truck with initial rule-based power management and then applied an improved rule-based power management, which was based on control characteristics observed from the optimal control trajectory calculated from the DDP technique. A similar process was carried out with the cost function of not only fuel economy but also including emissions. The improved rule-based power management was extracted from DDP result as the power-split ratio between the engine and the vehicle power demand [44]. The gearshift logic is also extracted from engine and gearshift control inputs, respectively. Fuel economy improvement of the semi-optimized rule-based power management in comparison with the initial rule-based power management was validated by a real vehicle test [101].

Paganelli et al. [78], [91] , Kleimaier et al. [90] and Sciarretta et al [84] suggested ECMS for parallel HEVs as implementable optimal power managements. The ECMS calculates the extra fuel consumption that will be required for recharging the battery in the future. Therefore, the electric energy consumed is converted to an average fuel consumption of the engine. Musardo et al. [82] presented an adaptive ECMS (A-ECMS) that periodically updates the control parameters (e.g., equivalence factors) according to the road conditions with past- and predicted-vehicle speed and GPS data so that SOC is sustained at a pre-designated level, and the fuel consumption can be minimized. Johnson et al. [92] included emissions in the cost function of a real-time control strategy (RTCS) using the replacement energy concept, such as an ECMS. They showed that the instantaneous optimization strategy could be expanded to not only for improving the fuel economy, but also for emissions reduction while sustaining the SOC.

Earlier studies on the PHH system have been analytical modeling and parametric design studies to show the potential of PHH systems [13], [14], [15], [16] and most of them used similar strategies with HEVs based on the engineering intuition. With the parallel hydraulic hybrid (PHH) system, Buchwald et al. [7] evaluated three different strategies on city buses and one of them is on-off control with the half of the maximum engine power. Tollefson et al. [8] predicted fuel economy of PHH systems with 3- and 4-speed transmissions and shows three different accumulator pressure effects for three driving schedules. Kapellen et al. [13] presented PHH heavy refuse-collection truck

simulations and showed significant fuel economy improvement using on-off power managements.

Wu et al. [11], [104] developed a DDP technique to find the optimal power management of light-duty trucks and applied a benchmark power management that resulted in an improved rule-based power management for a PHH system. Filipi et al. [12] showed a methodology to optimize the design and power management for the medium-duty PHH vehicle. They applied a DDP technique to extract the improved rule-based power management, and analyze the fuel economy gains in the process of the design and power management optimization.

Previous study already found the rule-based power management by analyzing deterministic dynamic programming results for the PHH system. In this study, the deterministic dynamic programming technique is also applied to find out the fuel economy benchmark of the optimized design with the given vehicle. The stochastic dynamic programming technique is then pursued for the PHH system and the comparison is carried out between the rule-based control and SDP control. . The SDP has been investigated as a methodology for developing a directly implementable control of an electric parallel system in a pioneering work by Liu et al. [122], but the hydraulic hybrid configuration with low energy capacity storage presents a new challenge.

6.1. Parallel Hydraulic Hybrid Vehicle Modeling

A simplified parallel hydraulic hybrid (PHH) system is shown in Figure 6. 1. The engine is connected to the torque converter and the clutch is not used between the engine and torque converter to keep the conventional vehicle configuration as much as possible. A P/M_{prop} is connected to the driveshaft after the automatic transmission for the most efficient regenerative braking through a 2-speed gearbox. When the vehicle speed is low, the low gear is used to assist the engine during the launching or acceleration of the vehicle. When the vehicle speed is high, the high gear is used to reduce the P/M_{prop} speed below the maximum speed of the P/M_{prop}, which is assumed as 4000rpm in this study. The high- and low-pressure accumulators are used as energy storage devices.

As a baseline vehicle, the same HMMWV and engine model in Chapter 3 is used as a vehicle platform. The engine and vehicle specifications, used in the modeling, are presented in Appendix A.1.

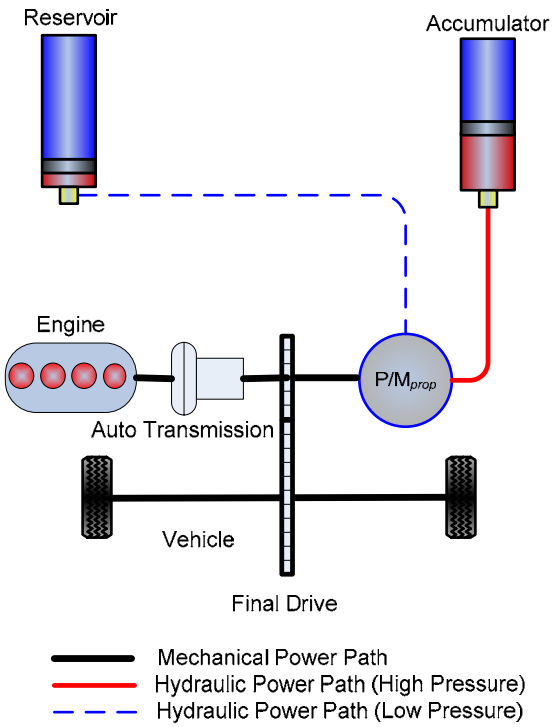

Figure 6. 1. PHH system configuration

The complete forward-looking PHH vehicle model is integrated in the MATLAB/Simulink environment (see Figure 6. 2). From the vehicle speed demand and the feedback signal of the actual vehicle speed, the driver model generates the vehicle power demand, the power-management block determines the engine- and P/M$_{prop}$-power demands according to system conditions, e.g., the engine, accumulator and vehicle condition.

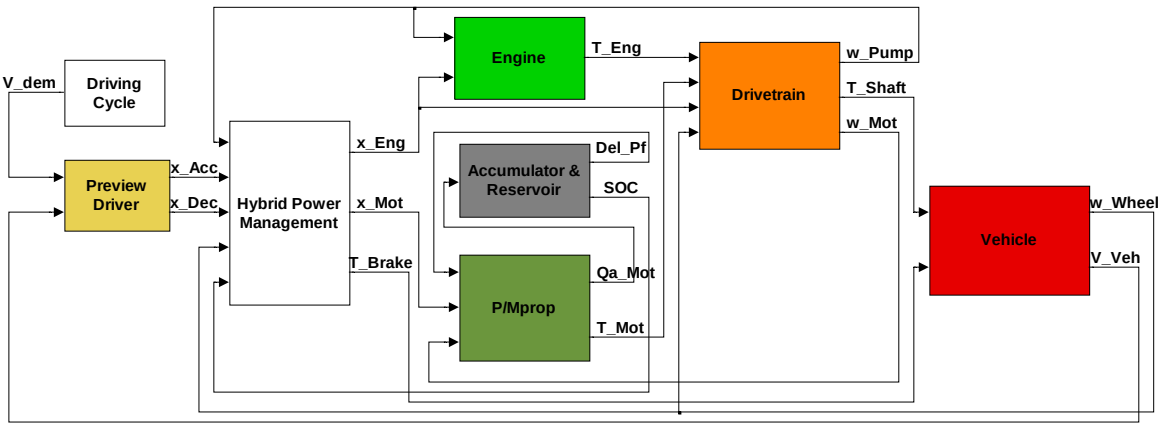

Figure 6. 2. Integrated forward looking PHH vehicle simulation in SIMULINK

The drivetrain block includes a conventional torque converter model and transmission model. The accumulator and reservoir blocks calculate the SOC from the

thermodynamic equations of the energy conservation. The same engine and driver models are used as described in Chapter 3 and FUDS and HWFET cycle is used for the simulation.

6.2. Parallel Hydraulic Hybrid Power Management

Extensive studies of power management have been carried out on the parallel HEV system. Because the parallel hybrid system carries over most of the conventional vehicle parts and stand-alone propulsion is possible with the engine was easier to analyze and build prototype so, early hybrid studies concentrated on the parallel hybrid system.

The baseline power management for the PHH system simulation is a semi-optimized power management suggested by Wu et al [11]. Wu et al. used the deterministic dynamic programming (DDP) technique to find an optimal power management trajectory during FUDS and extract an implementable semi-optimized rule-based power management. They claimed that DDP uses the engine and P/M_{prop} exclusively on the contrary to common rules used by HEVs [33] as follows; the engine operation is divided by three regions on the BSFC engine map, such as the motor-only drive, engine-only drive and hydraulic assist drive regions. So according to the vehicle power demand, the engine is designed to operate on the fuel-efficient area. In the background, engine charges the battery between the narrow low- and high-threshold SOCs in the thermostatic manner.

In contrast to the HEV case, hydraulic accumulators do not need the narrow SOC window concept and can use the whole SOC range from 0 to 1. As a preliminary study, this power management is tested with the current PHH model and the result shows that charging with engine always lowers fuel economy and increasing the motor-only area always shows better fuel economy. As a result, it is found that the extreme case that the charging engine power is set as zero and the motor-only power limit is set as the maximum engine power is same to the semi-optimal rule-based control that is suggested by Wu et al. [11]. By using the engine power and hydraulic power exclusively, the total system efficiency increases. In this semi-optimized rule-based control, the vehicle launching is done only by the P/M_{prop} until the SOC goes down to zero and the charging of the accumulator is only done by next regenerative braking. This semi-optimized rule-based power management can be represented below.

$$
\begin{aligned}
&\textit{if } SOC > 0 \textit{ then} \\
&\quad P_{P/M_{prop}} = min(P_{veh}, P_{P/M_{prop\_max}}) \\
&\quad P_{eng} = P_{veh} - P_{P/M_{prop}} \\
&\textit{else} \\
&\quad P_{eng} = P_{veh} \\
&\quad P_{P/M_{prop}} = 0
\end{aligned}
$$

This simple but efficient rule reflects the characteristics of the PHH system and main features of DDP results. In addition, this rule-based control can be easily implemented in the actual simulation.

6.3. Parallel Hydraulic Hybrid Design Optimization

The approach used for the PHH system design is applying the multi-start design optimization technique with the rule-based power management in the same way as described in Chapter 3 and in Filipi et al. [12]. The optimized design is used as a baseline PHH platform for the power management optimization.

6.3.1. PHH Design Optimization Setup and Result

In the PHH design optimization, the engine, powertrain and vehicle models are the same as those of the conventional HMMWV model as described in Chapter 3. The fuel economy is the objective of the design optimization and design constraints are listed below. The constraints are based on the performance of the conventional HMMWV model with the upgraded high-power engine and standard HMMWV operation performances. The FUDS is used as a baseline driving schedule.

Objective: maximize fuel economy

Constraints:

0-50 mph acceleration time (initial SOC: 1.0) $\leq$ 10.8 second (of conventional vehicle)

Maximum speed $\geq$ 65 mph

Maximum grade $\geq$ 60% slope

Cruising grade (@ 50mph) $\geq$ 2% slope

Cruising grade (@ 40mph) $\geq$ 3% slope

Test-fail condition: continuous deviation of more than 2 mph from the reference speed over 1 second

The optimization process follows the same as described in Chapter 3.4.1. The optimization procedure is shown in Figure 4. 1. The boundaries of design variable are shown in Table 6. 1. These boundaries are based on the values from the series hydraulic HMMWV optimization in Chapter 3.

Table 6. 1. Design variables and boundaries of the design optimization in PHH

	Lower	Upper
Accumulator volume [Liter]	35	140
P/M_{prop} size [cc/rev]	90	270
Final-gear ratio	1.0	3.0

Five multi-start points are selected after cycle simulations with randomly chosen 100 points selected by a DOE and the design optimization result from multi-start points is shown in Table 6. 2. Most of the optimizations converge near 16.2 or 16.3 mpg of fuel economy even though they started from different points in the design space.

Table 6. 2. Multi-start points and optimization result in PHH

No	Accumulator Volume [Liter]	P/M_{prop} Size [cc/rev]	P/M_{prop} Gear ratio	0-50 mph Time [sec]	FE [mpg] w/o idle-stop	FE [mpg] w/ idle-stop
#1	102	189	1.69	7.8	16.3	19.1
Optimized	102	189	1.86	7.8	16.3	19.1
#2	100	178	2.1	8	16.2	19.1
Optimized	**89**	**170**	**1.86**	**7.8**	**16.3**	**19.2**
#3	85	186	1.89	8.0	16.3	19.2
Optimized	103	258	1.41	7.7	16.3	19.2
#4	95	259	1.08	7.8	16.2	18.9
Optimized	101	270	1.33	7.7	16.3	19.2
#5	91	134	2.27	7.9	16.2	19.0
Optimized	103	211	1.69	7.8	16.3	19.2

Even though PHH system has large gain in 0-50 mph acceleration over the conventional vehicle, when the SOC depletes as the cruise condition, the performance is same to the conventional vehicle. Thus, engine downsizing is mostly avoided in the case of the PHH system. With similar fuel economy and vehicle performance, the

optimization point from #2 is selected as baseline because it has smallest accumulator size.

The PHH system behavior is shown in Figure 6. 3. The exclusive operation between the engine and P/M_{prop} is clear and the rate of engine power, when engine kicks in, is high. The SOC is goes down to zero after the vehicle launch and charged only by the next regenerative braking. Even though this rule-based power management works for the simulation, the engine-power increasing rate is too stiff to compensate the vehicle power demand as soon as the P/M_{prop} power becomes zero when the SOC becomes zero in Figure 6. 3(b). This rule-based power management may cause emission problems and aggravate driver's comfort. These issues are validated with a real engine by the EIL setup in Chapter 8.

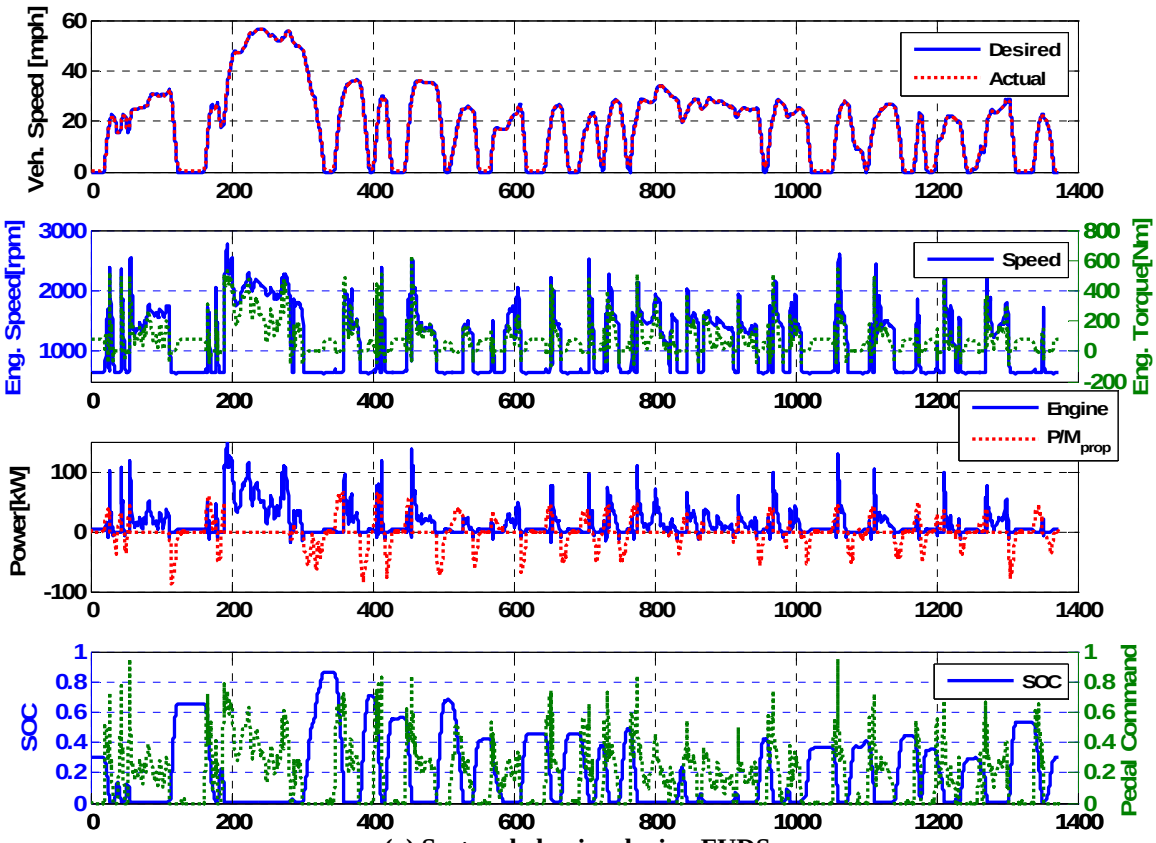

(a) System behavior during FUDS

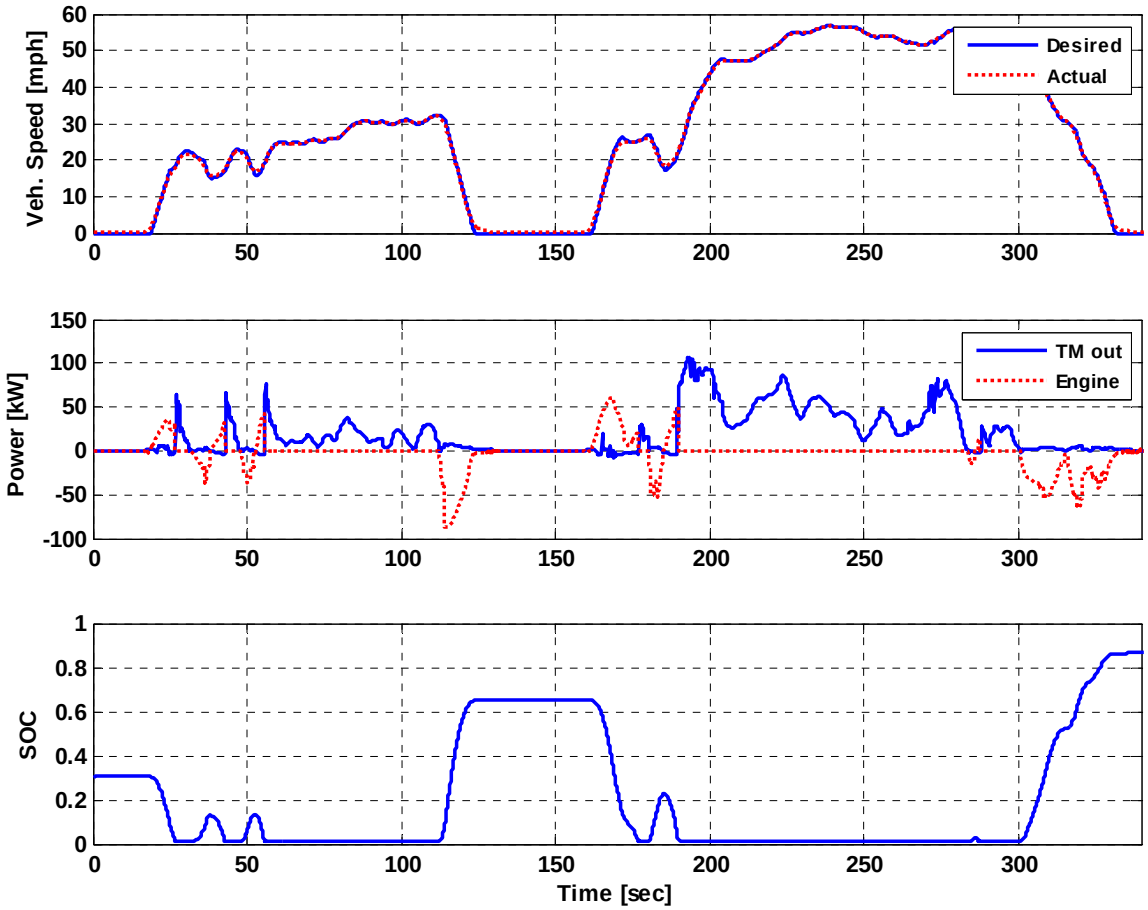

(b) System behavior zoomed at 0~340 second during FUDS

Figure 6. 3. PHH system behavior in FUDS

It is clear that the semi-optimized power management uses the engine power and the hydraulic power exclusively as shown in Figure 6. 4. The vehicle power demand is mostly provided by the transmission output power from the engine or by the hydraulic power from the P/M_{prop}. However, the hydraulic-assist drive is observed when the engine power is between the 1:1 line and zero power line. When the vehicle power demand is higher than P/M_{prop}'s maximum power, the engine power assists the vehicle propulsion even though the SOC is not zero.

The integrated fuel consumption during FUDS is shown on the engine map in Figure 6. 5. In comparison with the conventional vehicle case, the engine operation range is mostly the same but the fuel consumption amount decreases due to the hydraulic-only drive with the stored hydraulic energy especially when the vehicle starts.

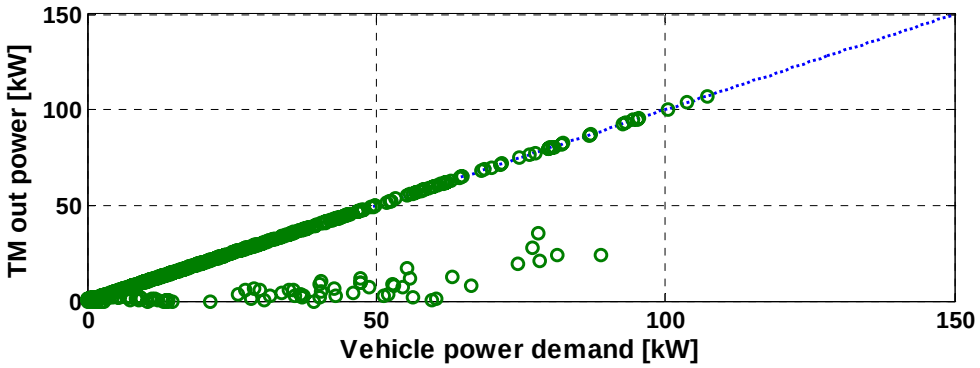

(a) TM out power vs. vehicle power demand

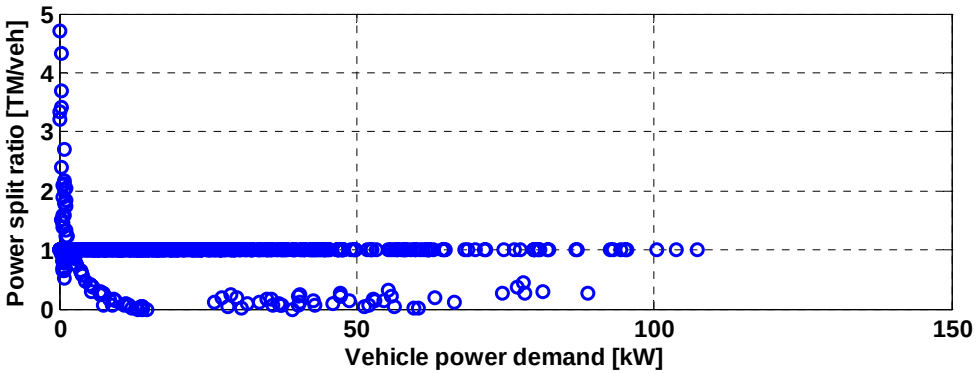

(b) Power-split ratio vs. vehicle power demand

Figure 6. 4. Engine power vs. vehicle power demand during FUDS

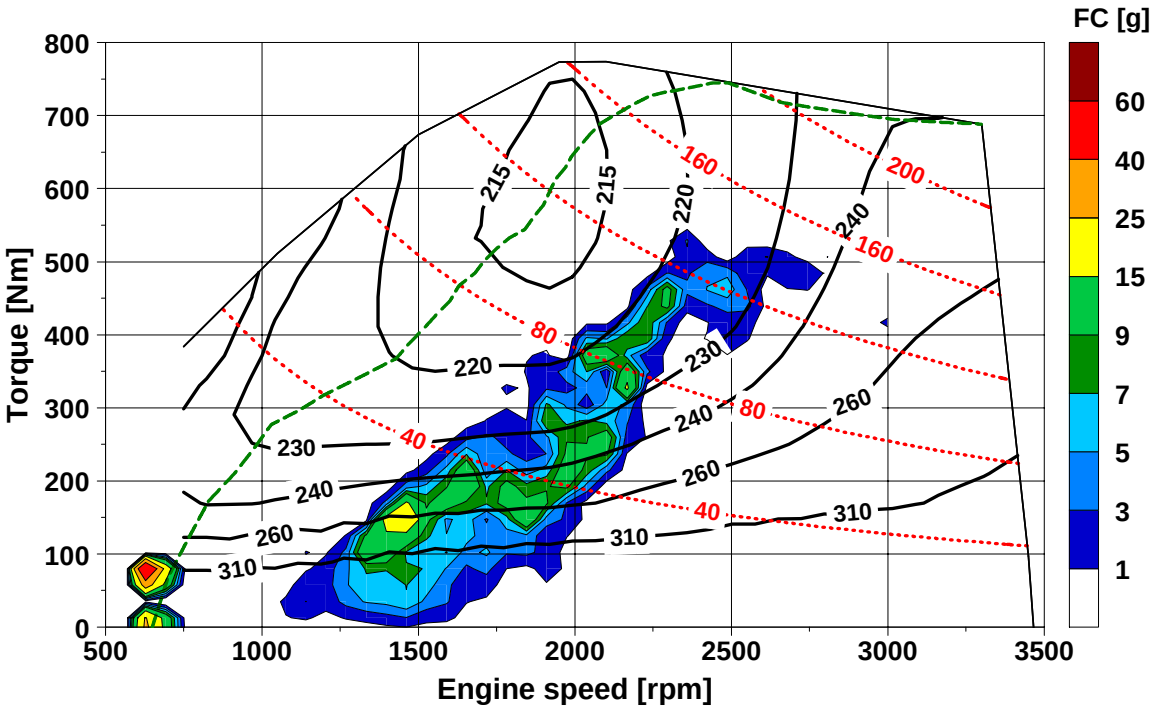

Figure 6. 5. Integrated fuel consumption on the engine map

The overall energy flow and energy conversion efficiencies across hybrid system devices during FUDS are represented in Table 6. 3. The accumulator efficiency is as high as 96% and the P/M efficiency is almost 90% during FUDS. P/M_{prop} efficiencies are slightly higher than the sequential 4x4 operation case in the SHH system because of using high-displacement factors with exclusive engine and P/M_{prop} operations.

Table 6. 3. Overall energy flow and conversion efficiency of each hydraulic device

	Energy in [kJ]	Energy out [kJ]	efficiency [%]
Engine (with/without idle) (Diesel LHV : 42.8 MJ/kg)	62316/ 52971	18690	30.0 / 35.2
Accumulator*	7775	7442	95.7
Reservoir*	364	349	95.8
P/M_{prop} pumping	7078	6436	90.0
P/M_{prop} motoring	8250	7427	90.0

*** Bypassed energy after the accumulator pressure reaches the maximum is not counted**

The break down of fuel economy gains shows that the idle fuel consumption has a large portion in the PHH system because of using the torque converter in Figure 6. 6. 43 % of fuel economy gain is possible with the idle-stop and start capability. If idle-stop is not applied, most of fuel economy gains come from regenerative braking in the PHH system.

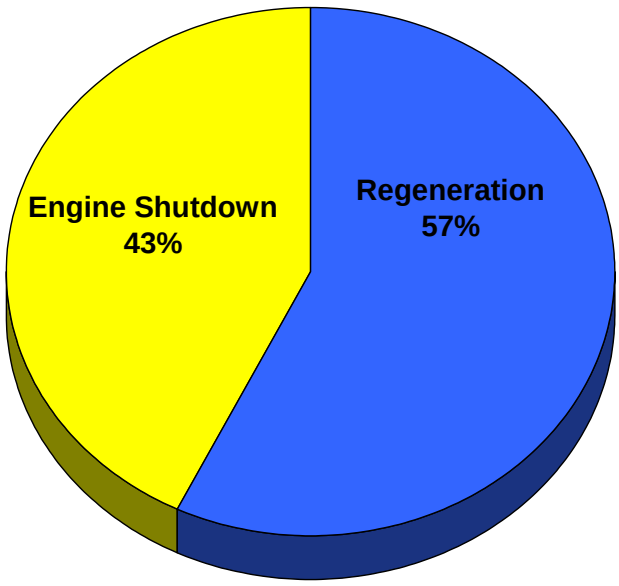

Figure 6. 6. Breakdown of fuel economy gains in PHH

6.3.2. PHH Super-HMMWV Performance

The PHH super-HMMWV's 0~50 mph acceleration test result is shown in Figure 6. 7. For this test, the driver's pedal position changes to the maximum by a step function when the vehicle starts. The acceleration during the start is excellent with the torque converter and assist from the P/M_{prop}. However, due to the small energy density, the accumulator energy depletes in less than 8 seconds.

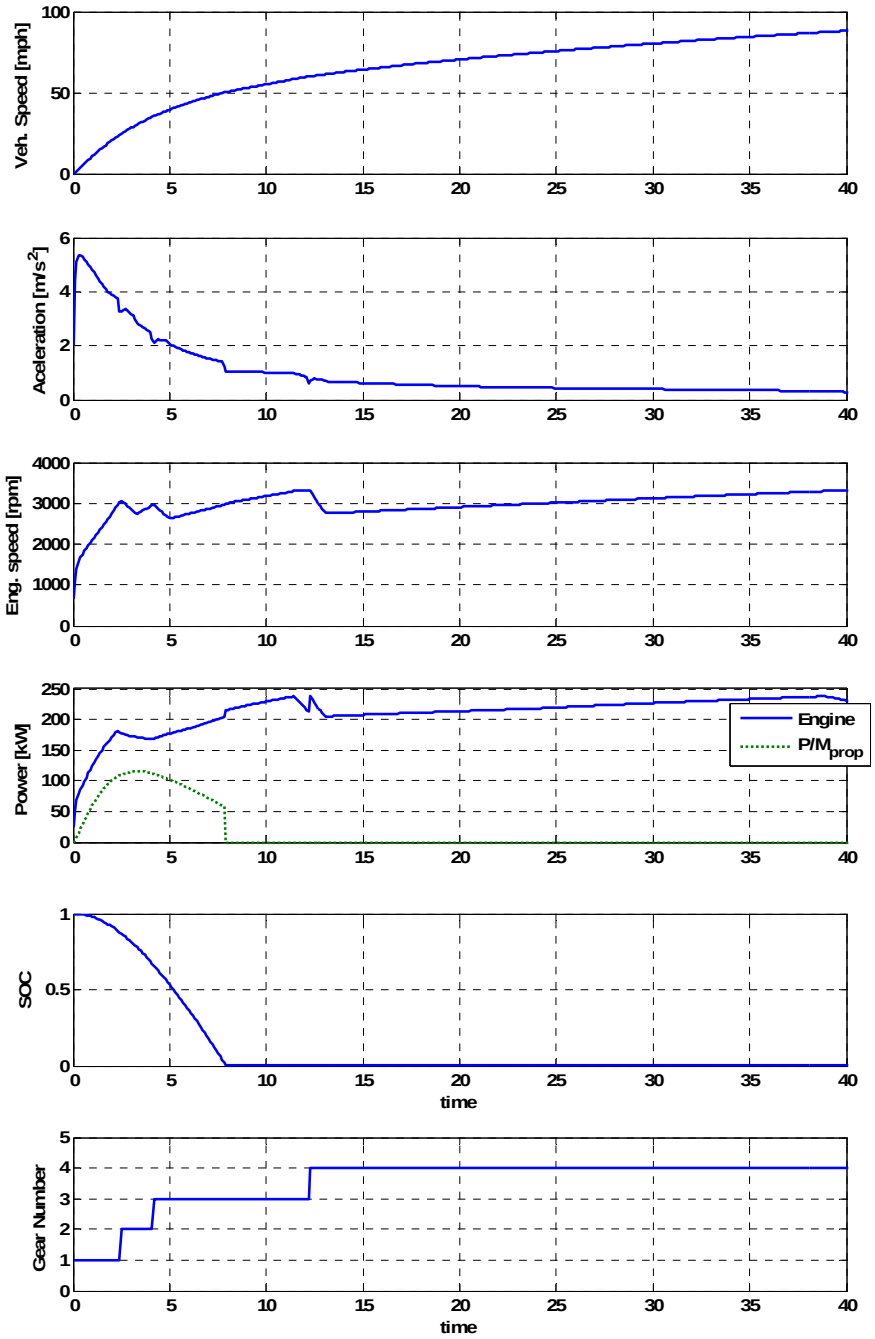

Figure 6. 7. 0-50mph acceleration test result of PHH HMMWV

6.4. Parallel Hydraulic Hybrid Power Management Optimization with Deterministic Dynamic Programming

The supervisory powertrain control refers to the power management among multiple power devices, e.g., engine, generator/motor and hydraulic P/M, in the hybrid propulsion system. The lower-level powertrain control manages each power device control from the given power demand. The power-management optimization is the optimization of the control strategy about the distribution of the vehicle power demand to each power device at the system level. With increase degrees of freedom in the control of power devices of the hybrid system, the engineering intuition or traditional trial and error methods is almost impossible to find an optimal control strategy in the supervisory control.

As a global supervisory control optimization algorithm, the deterministic dynamic programming (DDP) technique is introduced in Chapter 4 and the same algorithm is applied for the PHH. As for the PHH system, the studies of using the DDP technique have been introduced by Wu et al. [11] and Filipi et al. [12]. In their modeling of the PHH system, they used a clutch between the engine and transmission and disconnected the engine and transmission when the engine power demand is zero. In this study, the torque converter model is included in the DDP modeling without changing the conventional vehicle system. The result of the DDP technique shows the benchmark prediction of each power device operation such as the speed and torque of the engine or P/M_{prop} during FUDS. In addition, the fuel economy from the DDP technique is the theoretical potential with the given design of the PHH system.

6.4.1. PHH DDP Setup

The optimized hardware design of the PHH system in the previous section is used as the baseline platform for the DDP setup. To setup DDP, states and controls are to be determined first. The vehicle power demand is extracted from the wheel power of high fidelity PHH VESIM data and used as the pre-determined disturbance.

From the complex actual state variables and control inputs in the PHH system, two state variables and two control inputs are selected to represent the PHH system and the discretization of states and controls is shown in Table 6. 4. The DDP technique is so expensive calculation in terms of the computation time and memory occupation. The number of states and controls, grid size and time step are critical to decide whether the DDP can be setup and solved with the limited computation capability. The grid sizes for

the states and control inputs are selected after pre-DDP grid sensitivity tests. The state and control grid sizes should be selected to be small enough to represent the system dynamics. If the grid size is too large in comparison with the dynamics of the system, the state does not change as the control changes and stays at the same value. However, because DDP needs intensive computation, the grid size should not be too small.

Table 6. 4. State and control variables and grid discretization in PHH DDP

State	SOC	0 : 0.02 : 1	50 grids
	Gear stage	1, 2, 3, 4	4 grids
Control	Engine command	0 : 0.02 : 1	50 grids
	Gear shift	-1 : 0 : 1	3 grids

The time step is also related to the price of the intensive computation of DDP. It is observed that if the time step is too small, the state does not change with different control inputs. Thus, the time step should be determined large enough but small enough to represent the system dynamics. The time step is also pre-tested with various values and determined as one second.

To make the computation faster, the simplification of the high fidelity PHH vehicle model is carried out such that it can shows the basic system dynamics and reasonably similar results with the high fidelity model. Firstly, the fast dynamics that much faster than 1 Hz, e.g., engine torque generation, are changed to the static look-up table. Secondly, the accumulator gas dynamics is changed to the polytropic state equation model, where the gas volume is only the function of the gas pressure, instead of the high fidelity real-gas dynamic model. The coefficients of the polytropic process are acquired from curve fitting the cycle simulation result of the high fidelity HMMWV simulation. Thirdly, the high-fidelity vehicle model is changed to the simple road-load vehicle model. The rolling resistance coefficients of the simple vehicle model are calibrated to show almost the same vehicle power demands, so the fuel economy is close to that of high fidelity vehicle model with less than 1% difference.

The DDP technique is generally divided into three phases, such as the forward transition cost table generation, backward minimum cost sweep at each node and forward optimal solution search. In addition to the simplification for the fast calculation, the

vectorization approach is used to reduce the calculation time dramatically in generating the forward transition cost table. The SOC is vectorized, so 50 grids of the SOC are calculated at one calculation step. The Simulink model is used to represent the PHH system with the torque converter model inside. Even though, the state and control variables changes every one second time step, the internal time step of the Simulink model is as small as that of the high fidelity model.

The engine speed is calculated from the wheel speed and the gear stage and P/M_{prop} torque are calculated from the P/M_{prop} power and wheel speed. The P/M_{prop} power is decided by Equation (6.1) at every time step.

$$P/M_{prop} \text{ power=Vehicle power demand - } TM_{out} \text{ power} \tag{6.1}$$

Physical constraints are given below and if the constraints are violated, an infinite penalty is given to the cost function.

$$0 \le SOC(k) \le 1 \tag{6.2}$$

$$\omega_{eng\_\min} \le \omega_{eng}(k) \le \omega_{eng\_\max} \tag{6.3}$$

$$T_{P/M_{prop}\,min} \le T_{P/M_{prop}}(k) \le T_{P/M_{prop}\,max} \tag{6.4}$$

Unlike the HEV case, the accumulator's charge and discharge limits are not included because of the high-power density of the accumulator. In addition, the SOC can be from 0 to 1 in the hydraulic accumulator in contrast to the narrow available SOC window of a battery.

The cost function, $g(k)$, is calculated given below.

$$g(k) = fuel\,consumption(k) + \beta\left(gear(k+1) - gear(k)\right)^2 \tag{6.5}$$

The idle-stop capability is not applied in DDP setup, so the idle fuel consumption is included in the cost function. In addition to the pure fuel consumption, the penalty for the frequent gearshift is introduced by multiplying the shift reduction factor, β, to the square of gear stage changes assuming frequent gearshifts are not realistic in the perspective of the system durability and driver's comfort [44]. For various values of weight, β, the DDP technique is applied in the following section.

The final SOC needs to be equal to the initial SOC to simulate the charge sustaining capability. The penalty of the SOC deviation is squared distance from the initial SOC in Equation (6.6) and added to the cost function in the final step.

$$g_N\left(x_N\right) = \alpha\left(SOC - SOC(0)\right)^2 \tag{6.6}$$

where α is the weighting factor for the charging sustaining.

Finally, the total cost to be minimized is represented in Equation (6.7).

$$\begin{aligned}\min \sum_0^N g_k = \min \sum_0^{N-1} \Big(& \textit{fuel consumption}(k) + \beta\left(gear(k+1) - gear(k)\right)^2 \Big) \\ & + \alpha\left(SOC\left(N\right) - SOC\left(0\right)\right)^2\end{aligned} \tag{6.7}$$

6.4.2. PHH DDP Result

The DDP technique is applied to the PHH system including the gearshift reduction factor, β, which can be seen to affect the fuel economy as shown in Table 7. 6. As β increases, the gearshift is suppressed as expected, and the fuel economy decrease. The fuel economy benefit of optimal control trajectory is around 5 % when $\beta = 0.125$ in comparison with the case of the comparable gear shift frequency of the conventional vehicle.

Table 6. 5. Effect of β on fuel economy

β	Fuel economy [mpg]	% to rule-based control
0	19.6	120
0.065	17.2	106
0.125	17.1	105
0.1875	16.6	102
0.25	16.5	101

The effect of β to the gearshift profile during the FUDS is shown in Figure 6. 8. In the case of $\beta = 0$, gearshift is too frequent and is not realistic because of the durability and driver's comfort problems. The cases when $\beta \geq 0.125$ seem to have reasonable gearshift and to be similar with the case of the conventional vehicle. In the future study, the reasonable gearshift holding time limit may replace this simple addition of the gearshift penalty.

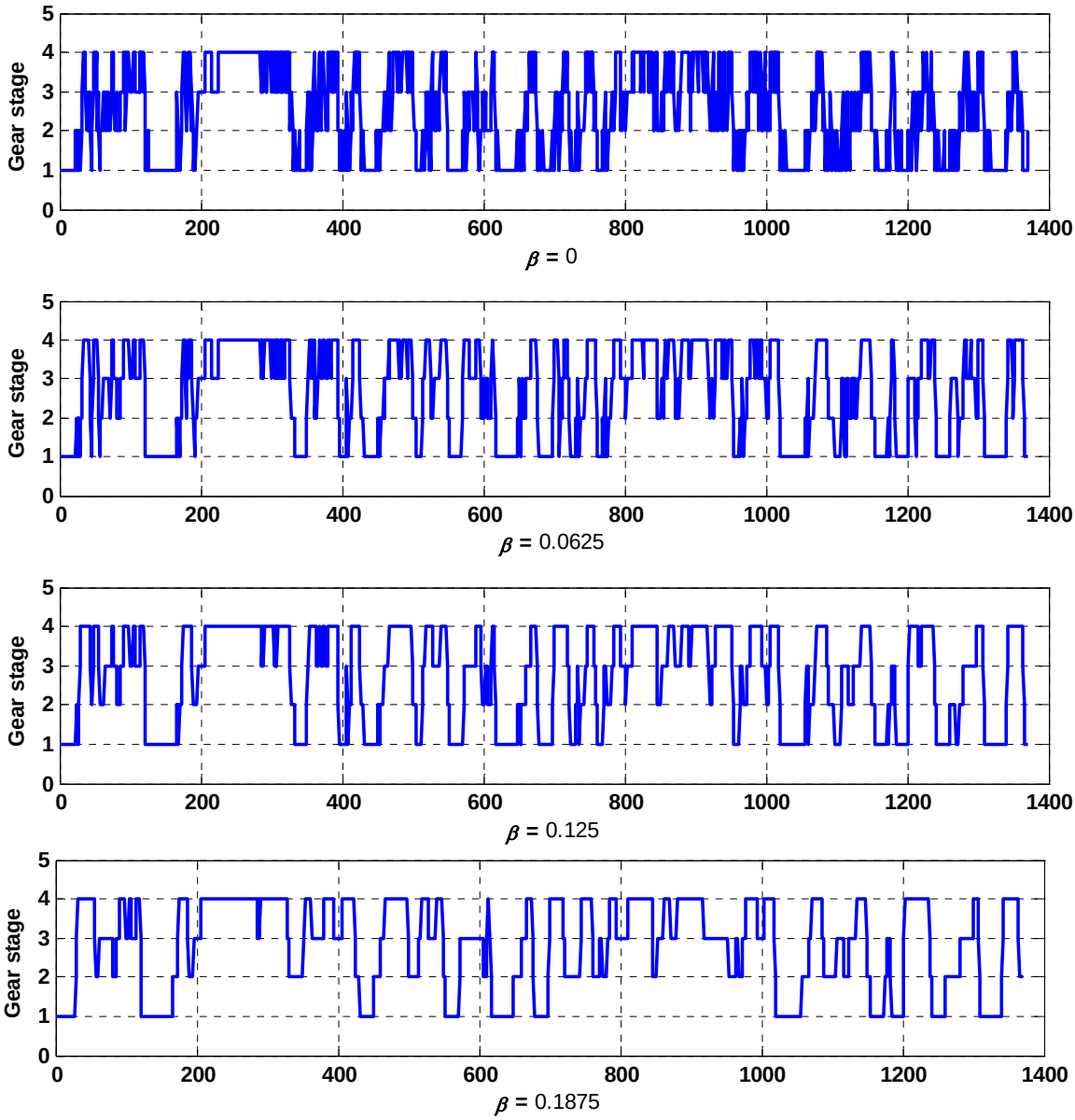

Figure 6. 8. Effect of β on gear shift in PHH DDP during FUDS

The PHH DDP results are shown in Figure 6. 9, with β equals to 0.125. The vehicle follows the FUDS and the SOC goes down to zero by fully utilizing accumulator energy as shown in Figure 6. 9 (a). Most of vehicle starts are done by the P/M_{prop} consuming the stored energy. Interestingly, the engine charges the accumulator during 60~65 second and 80~85 second ranges keeping engine power high for the better fuel efficiency even with the low energy conversion efficiency when the vehicle power demand is low in Figure 6. 9 (b).

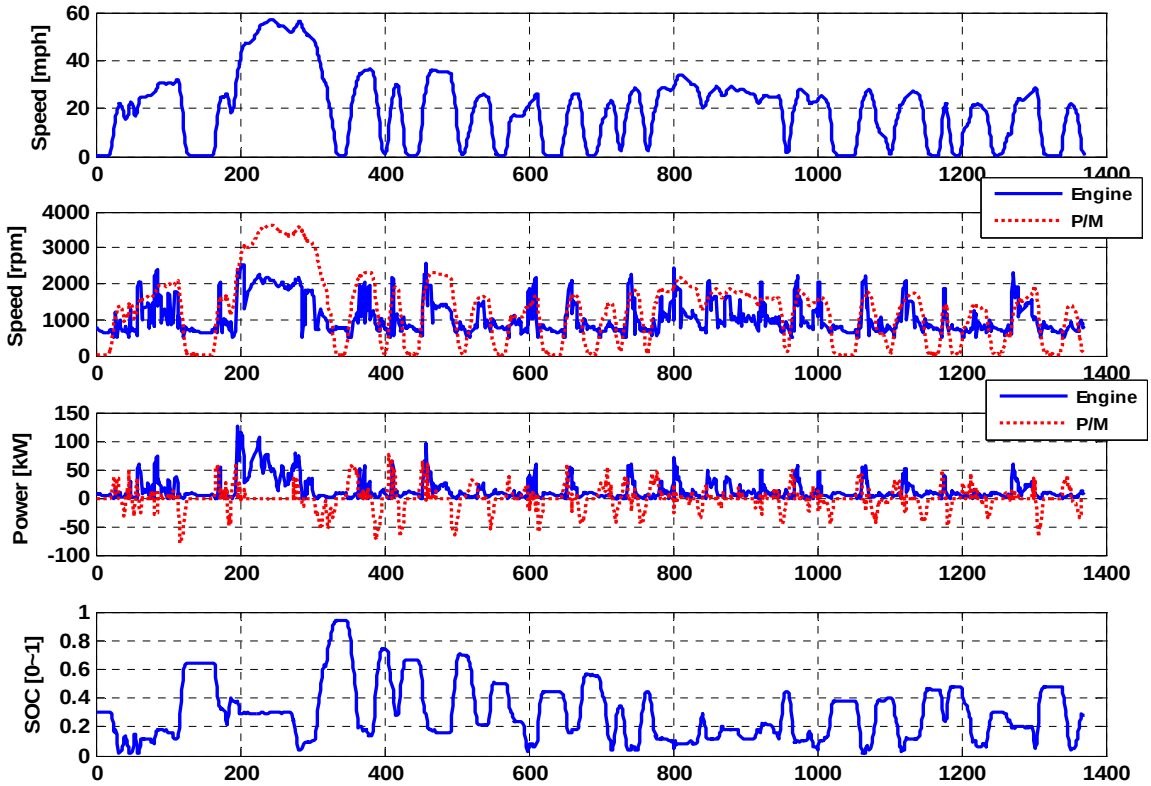

(a) PHH DDP result during FUDS (β=0.125)

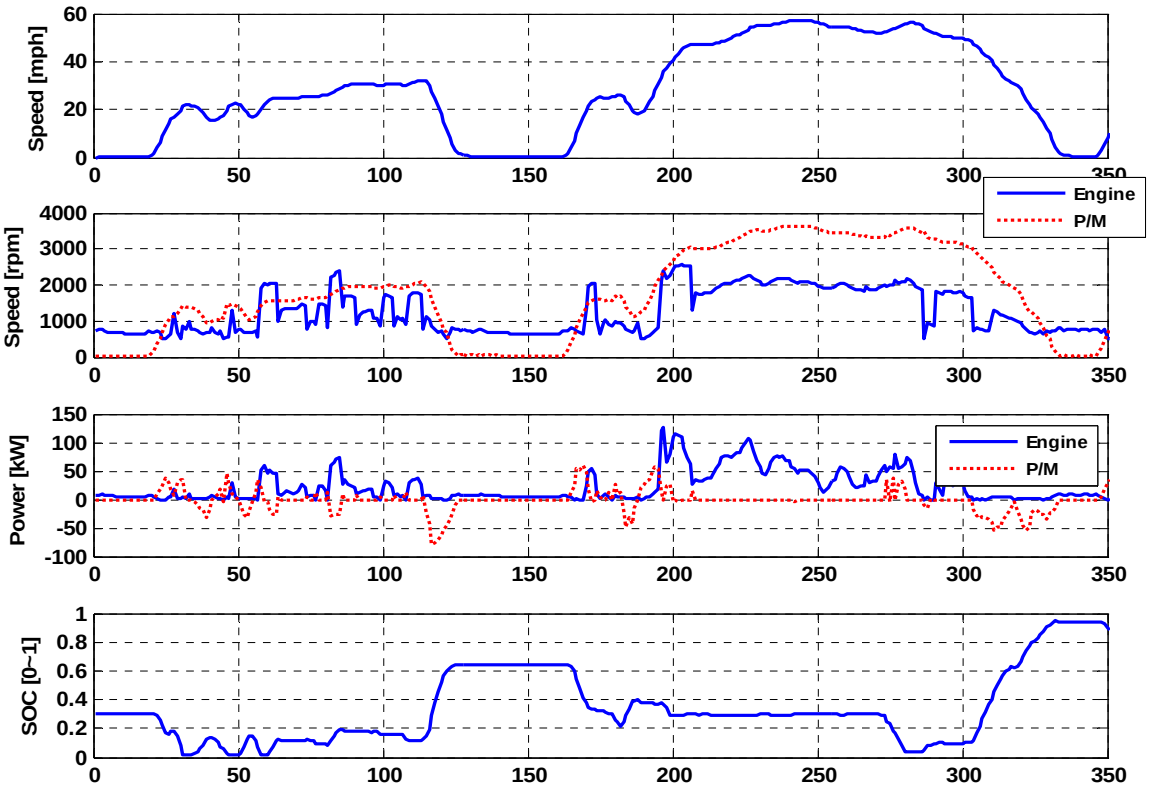

(b) PHH DDP result from 0 to 350 seconds during FUDS (β=0.125)

Figure 6. 9. PHH DDP result during FUDS (β=0.125)

The hydraulic-assist drive is carried out consuming the SOC with preventing the engine power from being too high during the 270~280 second range. However, this optimal decision of charging, consuming or maintaining the SOC at arbitrary SOC levels is only possible with trade-off between the current cost and expected future cost at each time step by the preview feature – backward solution search – of the DDP.

The engine power versus vehicle power demand during FUDS is shown in Figure 6. 10. Even though, the exclusive usages of the engine and P/M_{prop} account for the most of vehicle propulsion, when the vehicle demand is 10~40 kW, the engine charging is observed at 30~80 kW range as shown in Figure 6. 10(a). In addition, the P/M_{prop} assists the engine in the broad range of the vehicle power demand in Figure 6. 10(b).

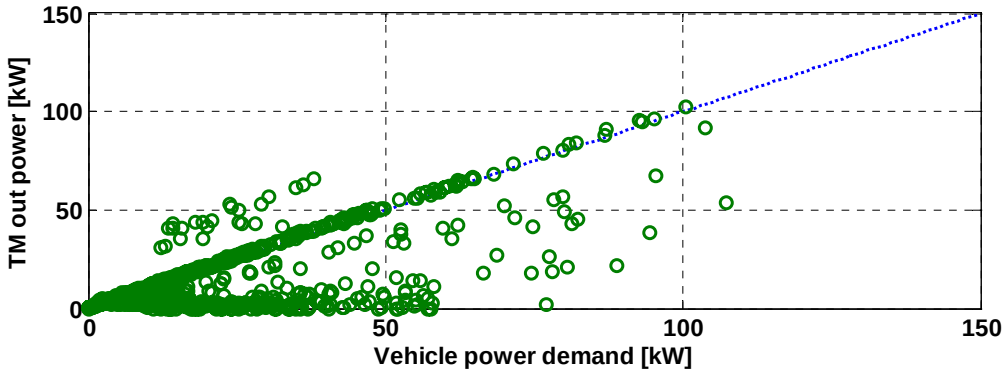

(a) TM-output power vs. vehicle power demand

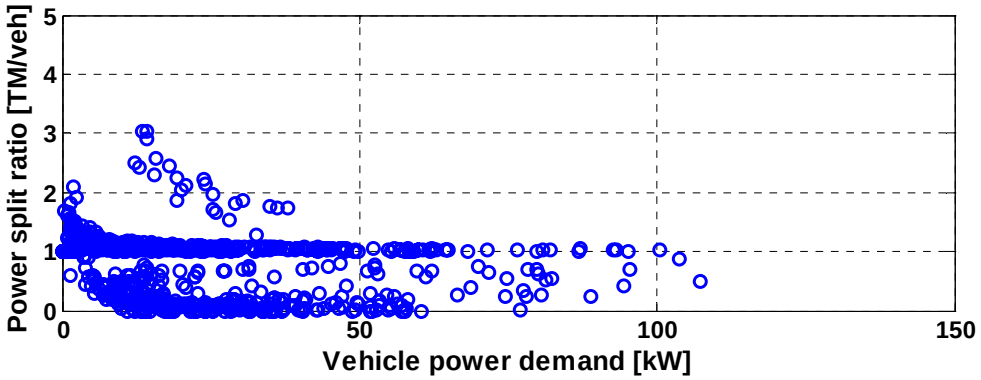

(b) Power-split ratio vs. vehicle power demand

Figure 6. 10. Engine power vs. vehicle power demand during FUDS (β = 0.125)

The integrated fuel consumption is shown in Figure 6. 11. In comparison with the rule-based control case, the highest fuel consumption area moves from the 260g/kWh BSFC range to the 240g/kWh BSFC range on the BSFC map in the DDP results. In the

systematic perspective, the DDP results improve the systematic efficiency by moving the engine operation points to the higher power area of the engine map.

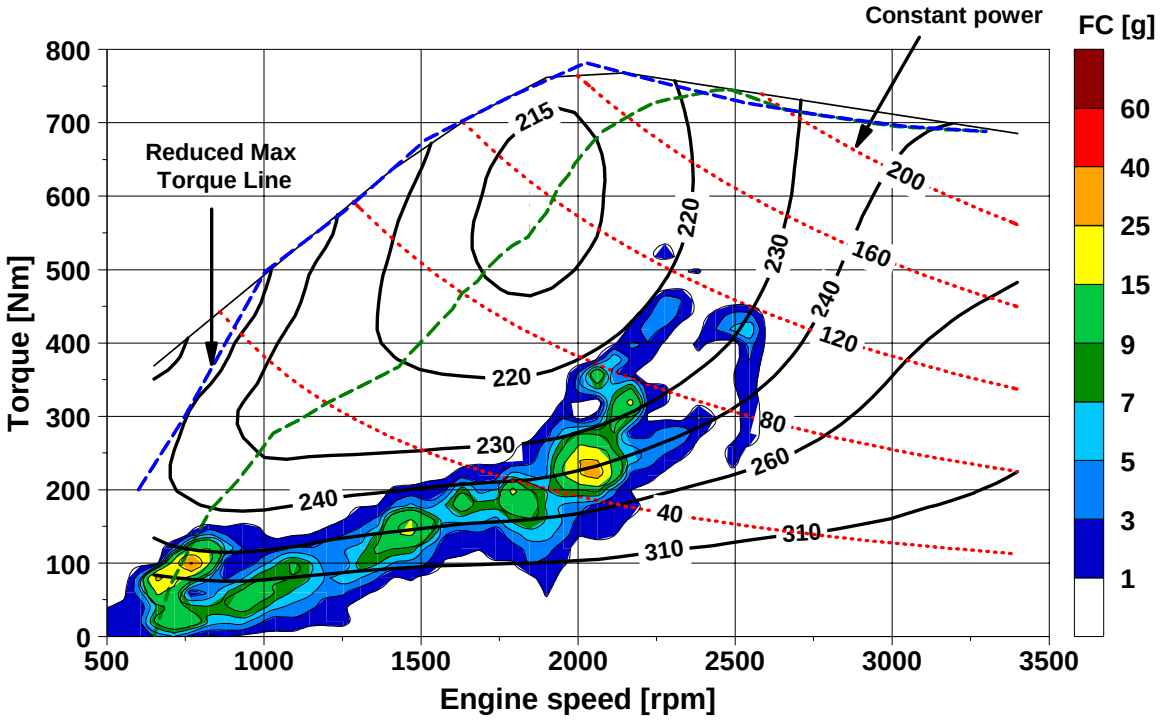

Figure 6. 11. Integrated fuel consumption of PHH DDP during FUDS (β = 25)

6.5. Parallel Hydraulic Hybrid Power Management Optimization with Stochastic Dynamic Programming

As for the parallel hybrid system, the studies of implementable optimal power management controls using the stochastic dynamic programming (SDP) technique has be done for HEVs [36], [79], but the SDP studies are none for the PHH system. Because of the low energy density and no limit in using full SOC range, the result of the PHH SDP control may have different shapes from those of HEV SDP control. The result of SDP technique gives full-state feedback controller from multiple inputs and provides the engine power demand, which can be implemented to real-time applications. As a semi-optimized power management, SDP solves the infinite horizon problem of the time-invariant system and generates the control policy based on the probability distribution learned from pre-selected samples.

The algorithm of SDP technique is introduced in Chapter 4 and the same concept is applied to the PHH system. In addition, the generation of Markov chain is the same as that of SHH with the same vehicle model. The same driving schedules are selected for

sampling and the vehicle power demand is extracted from the high fidelity PHH VESIM. The resultant Markov transition table is slightly different from that of SHH system but the trend is almost the same as shown in Figure 4. 12.

6.5.1. PHH SDP Setup

The state and control variables with the grid discretization are represented in Table 6. 6. Assuming the engine power is the function of the vehicle power demand, SOC and wheel speed, the resultant SDP controller has the form of three-dimensional look-up table. The grid size is selected to be small enough to reflect the system dynamics, but at the same time large enough to guarantee the fast convergence and not to delay the actual SDP control application.

Table 6. 6. State and control variables and grid discretization in PHH SDP

State	Vehicle power demand	-115 :110	20 grids
	SOC	0 : 0.04 : 1	25 grids
	Wheel speed	0:65	15 grids
control	Engine power	0:240	20 grids

The SOC and P/M_{prop} torque is calculated based on the P/M_{prop} power, and P/M_{prop} power is decided by Equation (6.8) at every time step.

$$P/M_{prop}\ \text{power} = \text{Vehicle power demand} - TM_{out}\ \text{power} \tag{6.8}$$

The infinite penalty is applied to the cost function during the optimization process when the constraints in Equation (6.9)~(6.11) are violated. The SOC should be between 0 to 1, and the engine speed and P/M_{prop} torque should be inside of the given specifications. In contrast to the case of HEVs, the charging and discharging limits are not added because of the high power density of the hydraulic accumulator.

$$0 \le SOC(k) \le 1 \tag{6.9}$$

$$\omega_{eng\_\min} \le \omega_{eng}(k) \le \omega_{eng\_\max} \tag{6.10}$$

$$T_{P/M_{prop}\,min} \le T_{P/M_{prop}}(k) \le T_{P/M_{prop}\,max} \tag{6.11}$$

The cost function g_k is only function of the fuel consumption in the PHH system. On the contrary to the SHH and PSHH cases, the vehicle propulsion is possible only with the

engine power. As a result, the penalty of deviation from the pre-fixed reference SOC is not necessary.

$$g_k = \textit{fuel consumption}(k) \tag{6.12}$$

6.5.2. PHH SDP Result

The result of SDP has the form of look-up table with three input states, SOC, wheel speed, vehicle power demand and one control output, engine power demand. Thus, the engine power is the output of SDP controller as Equation (6.13) and the P/M_{gen} power is decided by Equation (6.14).

$$\text{Engine power} = \textit{function of}\ \text{SDP controller}(\text{SOC}, \omega_{wheel}, P_{veh\_dem}) \tag{6.13}$$

$$P/M_{prop}\ \text{Power} = \text{Vehicle power demand} - TM_{out}\ \text{power} \tag{6.14}$$

The three dimensional representation of the final SDP controller according to the vehicle speed is shown in Figure 6. 12.

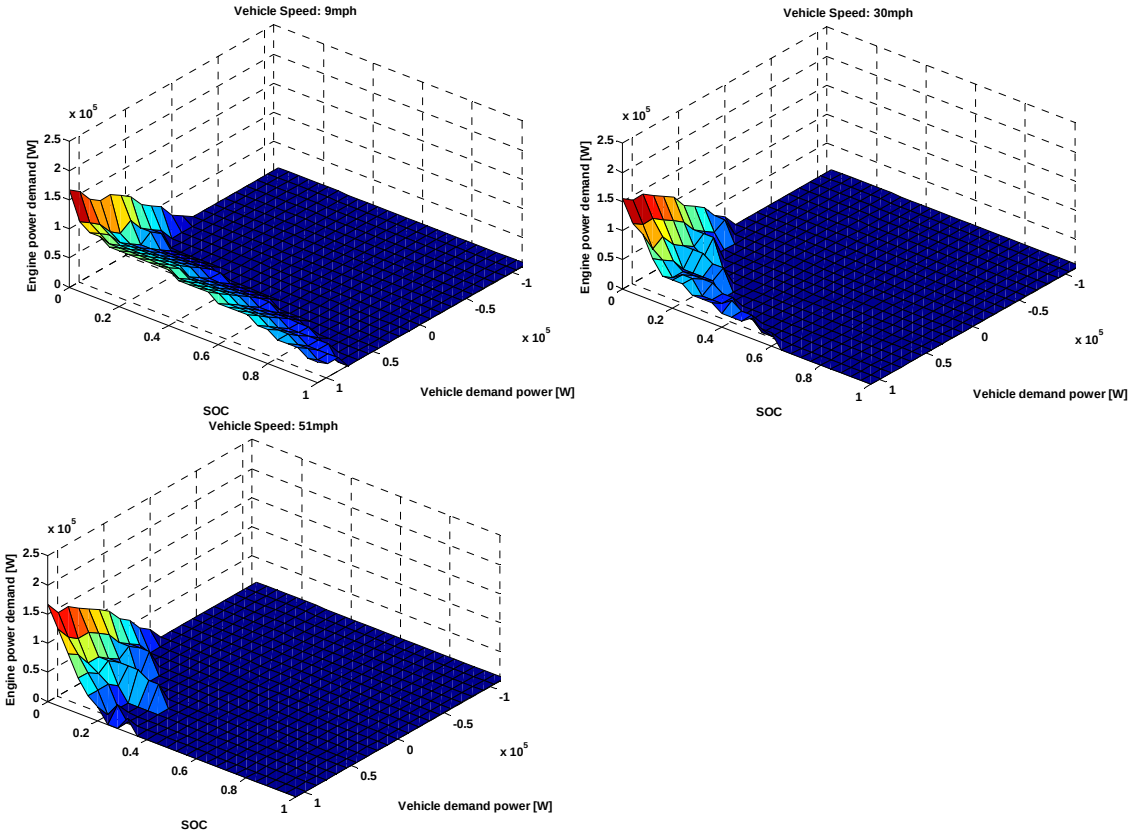

Figure 6. 12. Engine power demand in optimal PHH SDP controller

Instead of using the power split ratio, the direct use of the engine power demand removes the possibility of the infinite engine power demand and smooth transition when

the vehicle power demand is close to zero and changes the sign, respectively. Interestingly, it seems that the engine power demand decreases as the SOC increase to prevent engine charging and make a room for the regenerative braking energy because the amount of regenerative braking also increases when the vehicle speed increases. The system behavior with SDP control during FUDS is shown in Figure 6. 13. P/M_{prop} always starts the vehicle and the engine kicks in when the SOC become close to zero by preventing the SOC from being zero. Interestingly, the SDP controller depletes the SOC close to zero but not exact zero. Even though maintaining the SOC slight over zero is the proof that SDP algorithm works well but very small amount of charging and discharging happens controlling the SOC when SOC becomes close to zero. This SOC control by SDP controller may lower the fuel economy in comparison with the semi-optimized rule-based control case that does not have the feedback control of the SOC.

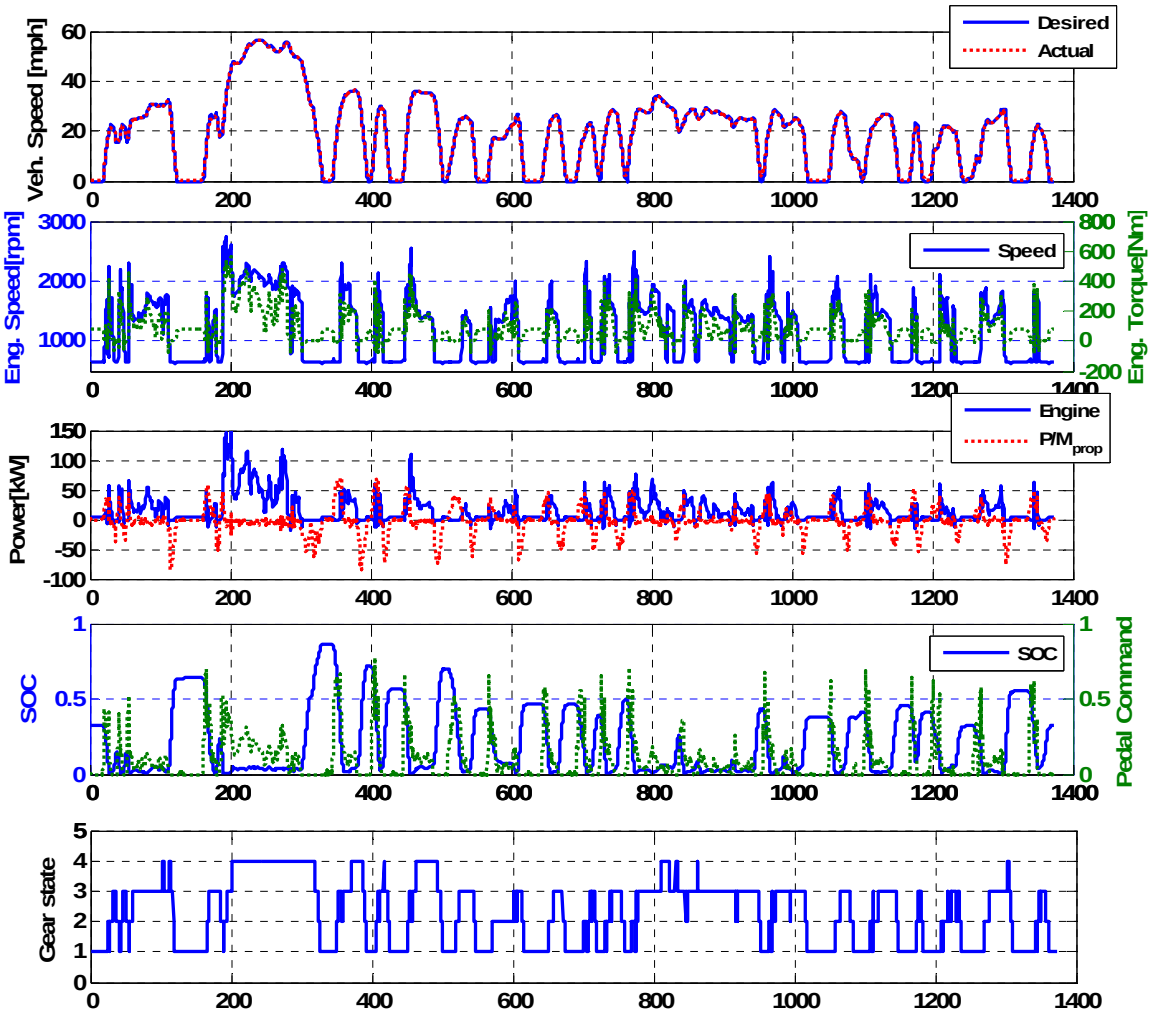

(a) System behavior during FUDS

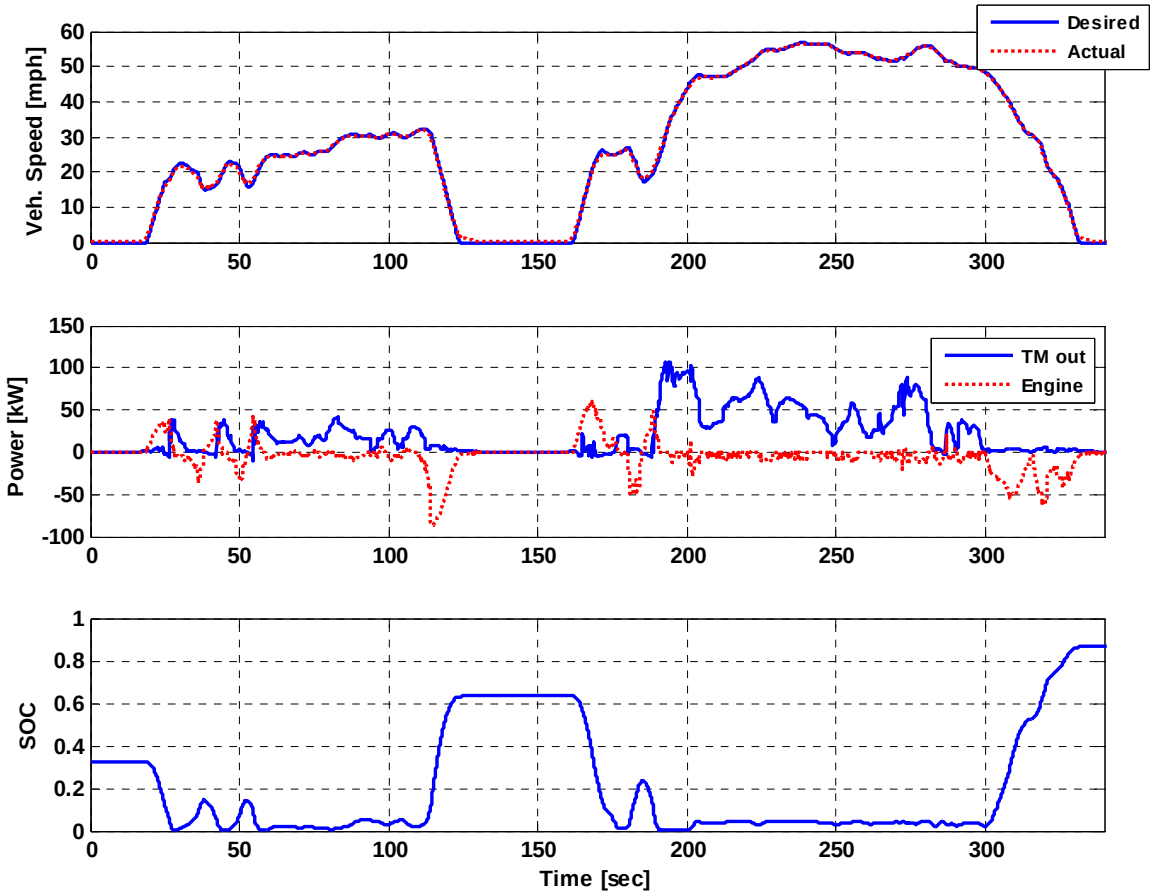

(b) System behavior zoomed at 0~340 second during FUDS

Figure 6. 13. System behavior with PHH SDP during FUDS

The engine power versus vehicle power demand with the SDP control during FUDS is shown in Figure 6. 14. In comparison with DDP results, SDP control does not charge at specific ranges of the engine power in Figure 6. 14 (a) but there are points where the transmission output powers are slightly higher and lower than the 1:1 power line and this implies that the small amount of charging and assisting with the engine power. There also exist significant hydraulic-assist points that show the transition between the engine-only drive and hydraulic-only drive in Figure 6. 14 (b). These hydraulic-assist drive points contribute to smooth engine operations and reduce transient engine operations when the engine kicks in.

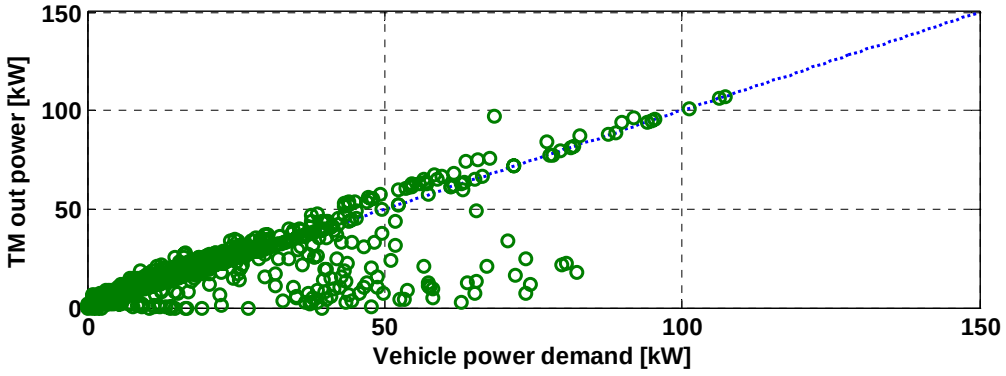

(a) TM out vs. vehicle power demand

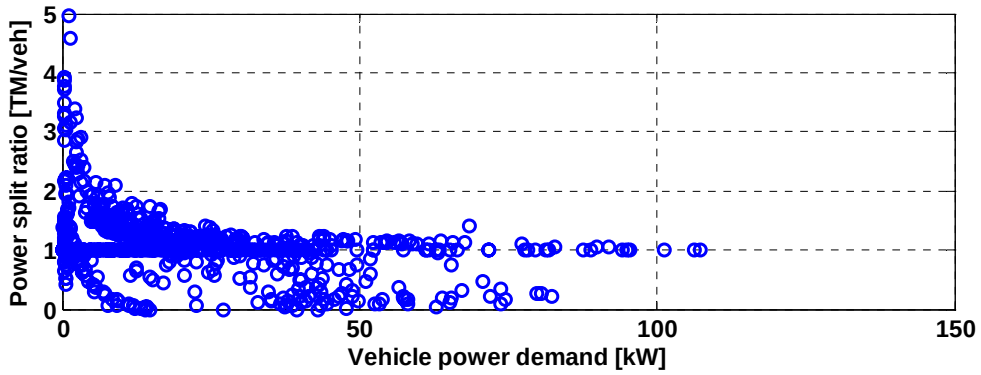

(b) Power-split ratio vs. vehicle power demand

Figure 6. 14. Engine power vs. vehicle power demand with PHH SDP during FUDS

The PHH SDP control is tested for various cycles (see Table 6. 7). The SDP control shows mostly 3~7% lower fuel economy than the fuel economy of the semi-optimized rule-based control for all driving schedules including the cycles that are not used for the SDP controller training, i.e., Markov chain modeling.

In the rule-based control, engine power is not the function of state inputs, e.g., SOC, wheel speed and vehicle power demand. Engine power is calculated by subtracting the maximum P/M power from the vehicle power demand only when maximum P/M power is smaller than the vehicle power demand. On the contrary, the SDP control calculates the engine power demand with the full state-feedback. As a result, charging and discharging is inevitable to control the SOC when the SOC is close to zero. As a result, the oscillatory charging and discharging, when the SOC is close to zero, lowers the system efficiency.

Table 6. 7. Fuel economy comparison between the SDP control and rule-based control without idle-stop

Cycle (* not used for training SDP)	Rule-based control	SDP	Fuel economy improvement [%]
NYCC*	11.4	11.1	-2.6
WVUCITY	12.7	12.1	-4.7
UDDSHDV	13.9	13.0	-6.5
SC03*	15.6	14.7	-5.8
FUDS	16.3	15.2	-6.7
WVUSUB	15.8	14.8	-6.3
WVUINTER*	14.6	13.6	-6.8
HWFET	14.8	13.8	-6.8

CHAPTER 7

MODELING AND POWER MANAGEMENT OPTIMIZATION OF A POWER-SPLIT HYDRAULIC HYBRID SYSTEM

The power-split hybrid system has features of both series and parallel hybrid systems. For example, the engine speed can be controlled independently of the wheel as the series system and the part of the engine torque is directly transferred to the wheel as the parallel system. If this system is carefully designed and controlled, the power-split hybrid system can take advantage of both the series and parallel hybrid systems and remove weak points of both systems. In the power-split system, generally two P/Ms (or M/Gs) and an engine are connected to the power-split device that is generally a planetary gear train.

The engine power is divided by the power-split device, and the divided engine power is delivered to the other two nodes of the planetary gear train where a P/M_{gen} (or M/G_{gen}) and the driveshaft of a vehicle are connected to [5]. While the power-split is the main staple of the passenger car applications (e.g. Toyota Prius), the application of this concept to hydraulic hybrids and trucks has not been demonstrated yet. Particular challenges that may create very significant obstacles are a limited speed-range of the hydraulic pump motor and a much lower energy density of the accumulator when compared to a battery.

The engine speed can be independently controlled by manipulating the speed of the P/M_{gen} (or M/G_{gen}) and the P/M_{gen} (or M/G_{gen}) generates the energy with the part of the engine power like the series hybrid system. The other part of engine power is transferred to the wheel through the mechanical path. Therefore, the power-split hybrid system can use the high mechanical efficiency like the parallel hybrid system.

Because of the potential of maximizing the system efficiency through the power-split system, the number of automakers applying the power-split hybrid systems into their line-ups increases. For example, Toyota hybrid system (THS) uses a single mode power-split system and Ford hybrid system (FHS) and GM-Allison hybrid system (AHS) are

known to use a dual mode power-split system that is made of two planetary-gear trains or three. However, novel implementations of more planetary gear trains are possible.

However, the increased degrees of freedom in the power-split hybrid system considerably increase the number of design parameters and complicate controls of three power devices, e.g., engine, generator (or P/M_{gen}) and motor (or P/M_{prop}), become challenging.

Gelb et al. [56] introduced and analyzed the modern power-split device with an electromechanical transmission concept for hybrid vehicle powertrains. The Prius, the first-mass produced power-split propulsion HEV, was introduced by Toyota Motor Co. in the late '90s [57] and patented by Harada et al. [58]. The initial-stage Prius (2000 model year) was tested and analyzed by Duoba et al. [62], [63], and the test data were used for modeling in Advisor [64] and PSAT [65]. Liu et al. [66] modeled the power-split system of the Prius and presented the power-management optimization of the power-split system [83]. However, most of researches concentrated on the power-split HEV system and studies on the hydraulic hybrid power-split system are rare [3] despite the hydraulic hybrid system is able to use the higher power density and efficiency of the hydraulic accumulator and P/M over their electric counter parts, e.g., the battery and generator/motor.

The studies on the PSHH system are very rare. Hewko et al. [103] presented a parallel, series and power-split hydraulic hybrid passenger-car simulation result and suggested that the parallel hybrid system is the most fuel-efficient hybrid system. However, their study did not show any detail of the system modeling, design process and power management. In addition, the hydraulic P/M efficiency that they simulated was very low in comparison with current propulsion-oriented P/M. Beachley et al. [97] reported the evaluation of a power-split hydraulic hybrid system but did not include any concrete modeling and power management strategy.

In contrast to HEV, the low maximum speed of the hydraulic P/M and the low energy density of the hydraulic accumulator pose special challenges in the case of the PSHH configuration. In this study, by modeling the speed reduction mechanism and applying the modulated SOC control to keep a constant energy buffer level during the normal driving condition and to smooth the transient engine behavior, which typically results

from the low energy density of the hydraulic accumulator, the modeling of the PSHH system is carried out. The deterministic dynamic programming is firstly applied in the PSHH system and the globally optimized control shows the benchmark control and the potential of the fuel economy improvement. The stochastic dynamic programming technique is also firstly applied in the PSHH system and an implementable sub-optimal supervisory control policy is provided for the fuel economy improvement.

7.1. Power-Split Hydraulic Hybrid Vehicle Modeling

In the power-split hydraulic hybrid (PSHH) system, the engine, P/M_{gen}, and P/M_{prop} are connected through the power-split device, a planetary gear train. High- and low-pressure accumulators are used as energy storage devices. As a baseline vehicle, the same HMMWV model introduced in Chapter 3 is used as a simulation platform. Generally, this light-duty vehicle is less sensitive to the noise, packaging, and increased mass, to which the passenger-car will be very sensitive. The engine and vehicle specifications are presented in Appendix A.1.

A complete forward-looking PSHH vehicle model is integrated in the MATLAB/Simulink environment (see Figure 7. 1). From the vehicle speed demand and the feedback signal of the actual vehicle speed, the driver model generates the vehicle power demand and the supervisory control determines the engine-, P/M_{gen}-, and P/M_{prop} power demands, respectively, from state variables, e.g., vehicle power demand, wheel speed and SOC.

The rotational speed of the planetary gear train and wheel torque is calculated from the planetary gear train model. The accumulator and reservoir models calculate the SOC from thermodynamic equations of the energy conservation introduced in Chapter 2. The same engine and driver models are used as described in Chapter 3 and FUDS and HWFET cycle is used for the simulation.

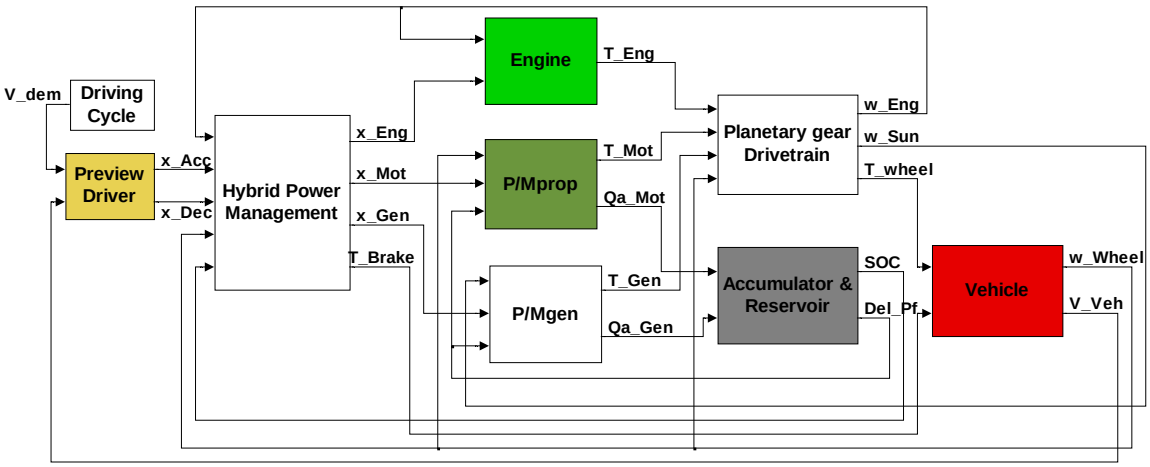

Figure 7. 1. Integrated forward looking PSHH vehicle simulation in SIMULINK

The essence of the power-split powertrain modeling is the modeling of the planetary gear system. Not only a single planetary gear train but also multiple combinations of planetary gear systems have been studied extensively and already patented by the automakers [59], [60], [61].

In this study, the single-mode power-split system is used as a baseline powertrain. In the baseline powertrain, the engine is connected to the carrier so that the engine power is split to the sun gear and the ring gear (see Figure 7. 2). According to the speeder and torquer concept, the speeder (P/M_{gen}) controls the engine speed with generating the flow energy and the torquer (P/M_{prop}) adds the propulsion power to the wheel [56]. The P/M_{gen}, connected to the sun gear, regulates the engine speed according to the pre-designed engine speed for a given engine power demand by pumping the fluid or motoring the engine. The P/M_{gen} can also be used to start the engine by the motoring function. The P/M_{prop}, connected to the ring gear, propels the vehicle or decelerates the vehicle by regenerative braking. In the baseline system modeling, the clutch model is not used between the engine and planetary gear train, and the ring gear is connected to the wheels through the final gear.

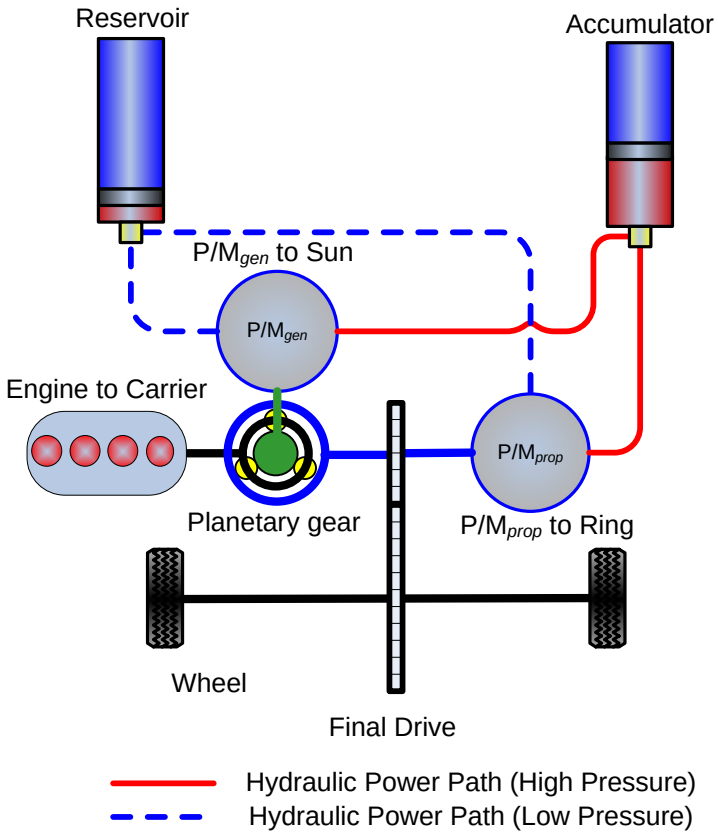

Figure 7. 2. PSHH system configuration

The modelings of dynamics of the planetary gear train with an engine and two generator/motors of the power-split HEV were done by Miller [5] and Liu et al. [66]. The rotational speed relationship of the planetary gear train is governed by the lever rule as shown in Figure 7. 3.

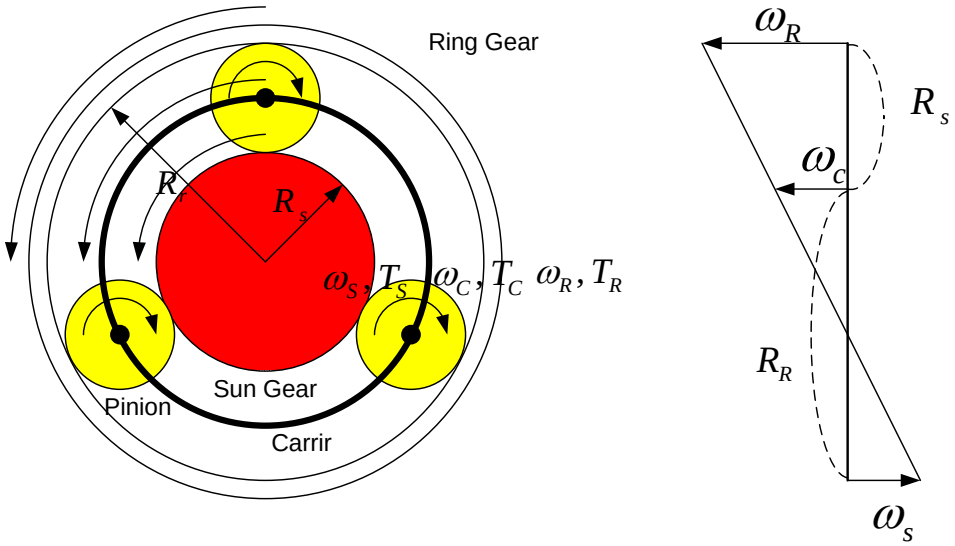

Figure 7. 3. Diagram of the planetary gear train and the lever rule

The counter clockwise rotation is assumed a positive direction for the rotational speed and torque. Thus, the pumping or motoring is decided by the sign of multiplication of torque and direction of rotation. The rotational speeds of the sun gear, ring gear and carrier are calculated from the gear tooth numbers or diameters of gears in Equation (7.1).

$$\omega_S R_S + \omega_R R_R = \omega_C (R_R + R_S) \tag{7.1}$$

where ω_S, ω_R and ω_c represent rotational speeds and R_S, R_R and R_C represent the radii of the sun gear, ring gear, and carrier, respectively. Even though the planetary gear train has three nodes, the degree of freedom becomes two because of the rotational speed relationship from the lever rule. Therefore, if the engine is connected to the carrier, and the ring gear is connected the wheel through the final gear, the speed ratio of the engine to the wheel can vary infinitely by controlling the sun gear speed. Thus, the planetary gear train is able to work as a CVT even though it does not multiply the torque as original CVTs do. From the law of conservation of energy, the Equation (7.2) needs to be satisfied assuming that there is no mechanical loss in the planetary gear train. Especially, in the steady state, Equation (7.3) is derived from the Euler's equations of motion.

$$T_S \omega_S + T_R \omega_R + T_C \omega_C = 0 \tag{7.2}$$

$$T_S + T_R + T_C = 0 \tag{7.3}$$

where T_S, T_R and T_C represent the torques acting on the sun gear, ring gear and carrier respectively. Thus, the engine torque, acting on carrier, is split and act on the ring and the sun gear according to Equation (7.4) and (7.5).

$$T_R = -\frac{R_R}{R_R + R_S} T_C \tag{7.4}$$

$$T_S = -\frac{R_S}{R_R + R_S} T_C \tag{7.5}$$

The powertrain dynamics is derived from the free-body diagram shown in Figure 7. 4. The left direction is assumed positive for the rotational speed and torque from the sign convention.

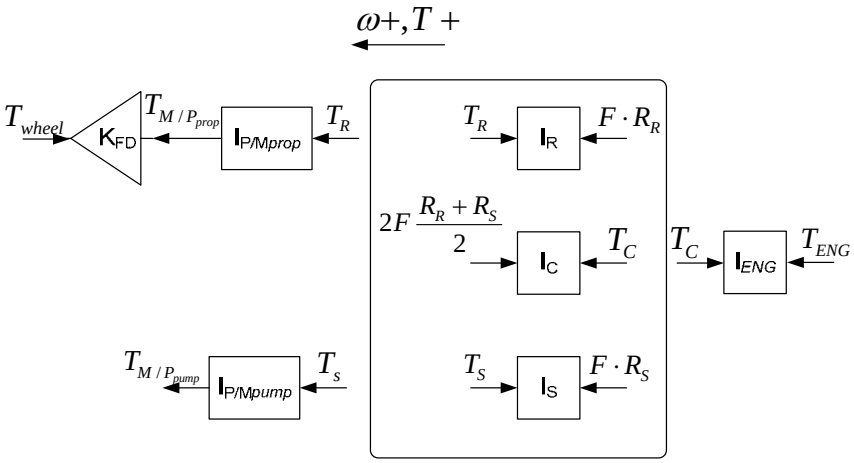

Figure 7. 4. Free body diagram of the power-split powertrain

The internal force, F , which acts through the pinion gear, and torques, which act on the planetary gear train, are governed by the Euler's equations of motion in Equations (7.6) ~ (7.8). The Coulomb's force is assumed negligible to simplify the modeling.

$$I_R\dot{\omega}_R = F \cdot R_R - T_R \tag{7.6}$$

$$I_C\dot{\omega}_C = T_C - F \cdot R_R - F \cdot R_S \tag{7.7}$$

$$I_S\dot{\omega}_S = F \cdot R_S - T_S \tag{7.8}$$

where I_R , I_C and I_S represent inertias and $\dot{\omega}_R, \dot{\omega}_C$ and $\dot{\omega}_S$ represent the angular accelerations of the ring gear, carrier gear and sun gear, respectively.

The equations of dynamics among the engine, P/M$_{gen}$, and P/M$_{prop}$ are shown in Equations (7.9)~(7.11).

$$I_{P/M_{gen}}\dot{\omega}_{P/M_{gen}} = T_S + T_{P/M_{gen}} \tag{7.9}$$

$$I_e\dot{\omega}_e = T_e - T_C \tag{7.10}$$

$$T_{wheel} = \left(T_{P/M_{prop}} + T_R - I_{P/M_{prop}}\dot{\omega}_R\right)K_{FD} = \left(T_{P/M_{prop}} + F \cdot R_R - \left(I_{P/M_{prop}} + I_R\right)\dot{\omega}_R\right)K_{FD} \tag{7.11}$$

where T_{wheel} is the wheel axis torque, and K_{FD} is the final gear ratio. $T_{P/M_{pump}}$, $T_{P/M_{prop}}$ and T_e are torques and $I_{P/M_{pump}}$, $I_{P/M_{prop}}$ and I_e are inertias of P/M$_{gen}$, P/M$_{prop}$ and the engine, respectively. The pinion gear is assumed a pure force transmitter between the sun and ring gear because the pinion gear is so small that the inertia can be negligible. The mechanical efficiency of the planetary gear train is not considered and it may slightly

overestimate the vehicle performance and fuel economy. In the simulation, only mechanical efficiency of final drive, η_{FD}, is multiplied to $T_{P/M_{prop}}$ and $F \cdot R_R$ respectively. The HMMWV vehicle model explained in Chapter 3 can be used by connecting the T_{wheel} output of the powertrain model with the vehicle model after solving Equation (7.12).

$$\begin{pmatrix} I_S + I_{P/M_{gen}} & 0 & 0 & -S \\ 0 & I_C + I_{eng} & 0 & R+S \\ 0 & 0 & 1 & -RK\eta_{FD} \\ -\frac{S}{R} & \frac{R+S}{R} & 0 & 0 \end{pmatrix} \begin{pmatrix} \dot{\omega}_{gen} \\ \dot{\omega}_{eng} \\ T_{wheel} \\ F \end{pmatrix} = \begin{pmatrix} T_{gen} \\ T_{eng} \\ T_{P/M_{prop}} K\eta_{FD} - \left(I_R + I_{P/M_{prop}}\right)\dot{\omega}_{ring} K \\ \dot{\omega}_{ring} \end{pmatrix} \quad (7.12)$$

In the case of using simple road load model, a point mass vehicle model based on Newton's second law can be derived without tire dynamics and lateral force as shown in Equation (7.13).

$$M_{veh}\frac{R_{tire}^2}{K} = T_{wheel} - T_f - M_{veh} g f_r R_{tire} - 0.5\rho A C_d \left(\frac{\omega_R}{K}\right)^2 R_{tire}^3 \quad (7.13)$$

From Equation (7.1), (7.6)~(7.13), the drivetrain dynamics in the power-split system is simplified in the matrix form by removing T_C, T_S, T_R, T_{wheel} [83]. The rotational speed of the each power device can be calculated by Equation (7.14).

$$\begin{pmatrix} I_S + I_{P/M_{gen}} & 0 & 0 & -S \\ 0 & I_C + I_{eng} & 0 & R+S \\ 0 & 0 & \left(\frac{R_{tire}}{K}\right)^2 M_{veh} + I_{P/M_{prop}} + I_R & -R\eta_{FD} \\ S & -(R+S) & R & 0 \end{pmatrix} \begin{pmatrix} \dot{\omega}_{P/M_{gen}} \\ \dot{\omega}_{eng} \\ \dot{\omega}_{P/M_{prop}} \\ F \end{pmatrix} = \begin{pmatrix} T_{P/M_{gen}} \\ T_{eng} \\ \left(T_{P/M_{prop}} K\eta_{FD} - T_f - M_{veh} g f_r R_{tire} - 0.5\rho A C_d \left(\frac{\omega_R}{K}\right)^2 R_{tire}^3\right)/K \\ 0 \end{pmatrix} \quad (7.14)$$

7.1.1. Speed Reduction in PSHH System

Even if the power-split hybrid system has both the benefits of the series and parallel hybrid systems, it has drawbacks of higher production costs and complicated control problems. The hydraulic hybrid option adds two general challenges, such as the low maximum speed of the P/M and the low energy density of the accumulator.

The relatively low maximum speed of the hydraulic P/M is an issue in the PSHH system because the high speed of the P/M is required for some typical driving conditions (see Figure 7. 5). The explanation of the each condition is given below.

1: Vehicle stops – the engine stops or is idling.

2: Vehicle starts and accelerates at the low speed range with a mild acceleration – the engine stops or is idling and only the P/M_{prop} drives the vehicle.

3: Vehicle starts with the severe acceleration – the P/M_{gen} speed becomes high as the engine speed increases.

4: Vehicle speed increases in the normal condition – The P/M_{prop} speed increases and the P/M_{gen} speed decreases and can be negative.

5: Vehicle accelerates at the high speed – The engine speed increases and the P/M_{gen} speed becomes very high

Therefore, the P/M_{gen} speed can be very high in the condition 3 and 5 and the P/M_{prop} speed can be very high in the condition 4.

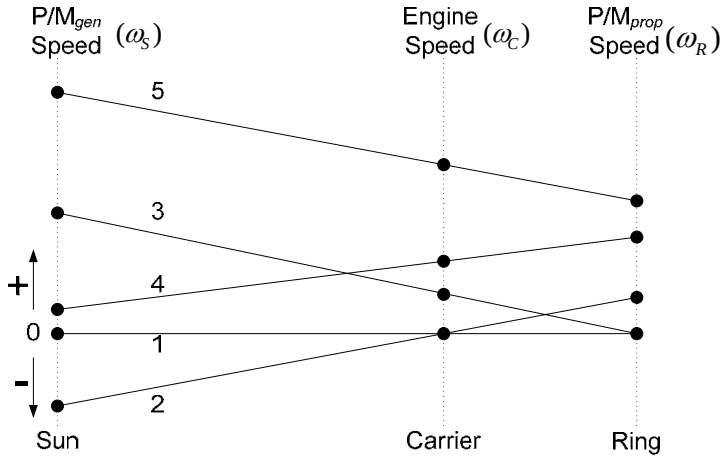

Figure 7. 5. Planetary gear speed diagram at various driving conditions

The rotational speeds of the sun and ring gears at extreme conditions are represented by the lever rule in Figure 7. 6 and calculated for the variable combinations of the ring gear to sun gear speed ratio, K (= R_R / R_S), as shown in Table 7. 1. The carrier is directly connected to the engine, and the maximum speeds of the engine and hydraulic P/M are assumed 3300 and 4000 rpm respectively. C and R represent the carrier and ring gear.

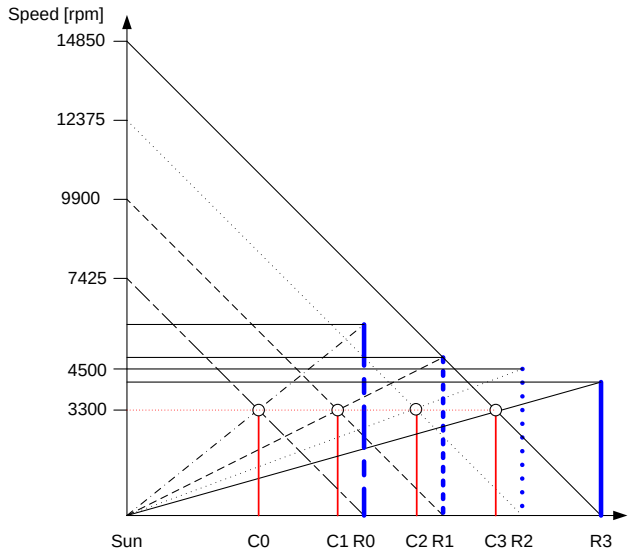

Figure 7. 6. Sun, ring, and carrier speed relationship according to the lever rule

The sun gear speed can reach from 7425 rpm to 14850 rpm, and the ring gear speed can be from 4243 rpm to 5940 rpm according to the various gear ratios assuming the engine is at the rated condition. The maximum sun gear speed and ring gear speed show a trade-off relation, so the lower maximum sun gear speed leads to the higher maximum ring gear speed and vice versa. In addition, the maximum ring gear speed corresponds to the maximum vehicle speed, so the maximum ring gear speed is fixed at the initial design stage. The maximum speeds in a simple power-split arrangement are much higher than the reasonable limits for hydraulic pump/motors (typically ~4000 rpm).

Table 7. 1. Sun gear and ring gear speed relation (carrier speed @ 3300 rpm)

Vertex location	Sun gear to carrier speed ratio (R/S+1)	Sun gear speed [rpm]	Ring gear speed [rpm]
C0,R0	2.25:1	7425	5940
C1,R1	3:1	9900	4950
C2,R2	3.75:1	12375	4500
C3,R3	4.5:1	14850	4243

To keep the P/M_{gen} speed lower than its maximum speed, an additional planetary gear needs be added as a speed reducer between the P/M_{gen} and the sun gear [69], [74]. The P/M_{gen} is connected to the carrier of the additional planetary gear, the ring gear is grounded to the housing, and the sun gear of the additional planetary gear is connected to

the sun gear of the main planetary gear. The speed-reduction ratio of the secondary planetary gear is 1:1 + *K*. For example, if the diameter ratio of the additional planetary gear's ring gear and sun gear is 2:1, the maximum sun gear speed can be up to 12000 rpm with the P/M_{gen} at 4000 rpm. However, this speed reduction causes the P/M_{gen} torque, transferred to the main planetary gear, to be reduced by the speed reduction ratio, so the P/M_{gen} size need to be increased in proportion to the speed reduction ratio. As a result, the system efficiency decreases.

The P/M_{prop} speed reduction depends on the vehicle's maximum speed, final gear ratio and tire diameter. In the case of HMMWV, the maximum vehicle speed is not as important as the wheel torque at the low vehicle speed. Therefore, an additional two-speed planetary gearbox is added between the P/M_{prop} and drive shaft. In two-speed planetary gearbox, the sun gear of the additional planetary gear is connected to the P/M_{prop}, and the carrier of the additional planetary gear is connected to the drive shaft. Therefore, if the vehicle speed is low, the ring gear is grounded to the housing and the torque is multiplied by the (1+*K*):1. Thus, the P/M_{prop} torque is multiplied by the gear ratio and the small size P/M_{prop} can accelerate the vehicle easily with increasing the system efficiency. If the wheel speed is high, the ring gear of the addition planetary gear is locked with the carrier making 1:1 gear ratio reducing the P/M_{prop} speed.

This 2-stage-planetary gearbox can be realized by applying a band clutch on the ring gear and a multi-disk clutch between the ring gear and carrier [17]. The optimal shift speed is selected through the design optimization process in the following section. The clutch dynamics are not considered in this study so the gearshift occurs without time delay and the vehicle speed does not changes during the gearshift. Neglecting clutch dynamics may show slightly optimistic vehicle performance and fuel economy. The conceptual diagram and actual configuration of the PSHH super-HMMWV with three-planetary gear system are shown in Figure 7. 7.

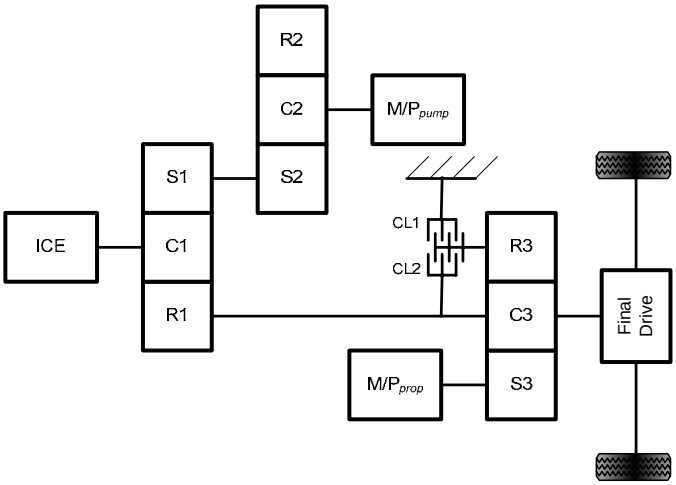

(a) Conceptual power-split system diagram with three planetary gears

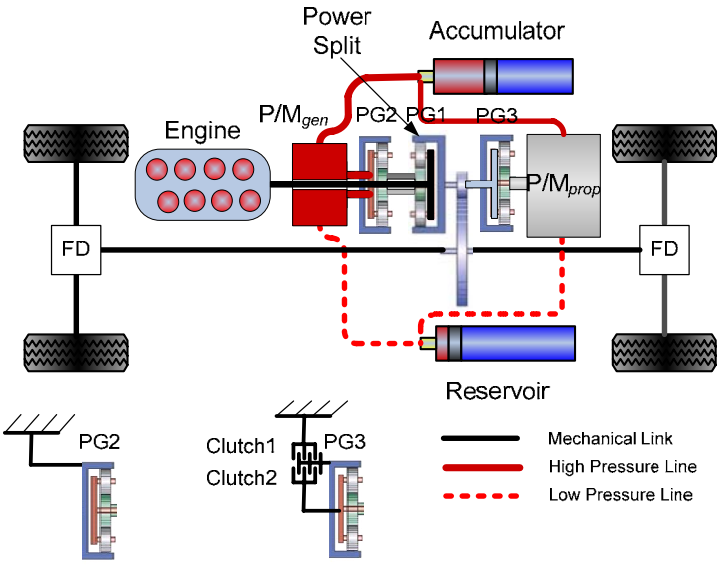

(b) Actual power-split system diagram with three planetary gears

Figure 7. 7. PSHH super-HMMWV system

The effects of two additional planetary gears during the severe vehicle launch test are shown in Figure 7. 15. The maximum sun gear speed is around 10000 rpm as expected and the P/M$_{gen}$ speed is maintained below the maximum speed of 4000 rpm. The P/M$_{prop}$ torque is multiplied when the vehicle speed is low and the P/M$_{prop}$ speed remains below the maximum speed of 4000 rpm when the vehicle speed reaches the maximum speed constraint.

7.1.2. PSHH Power Management

In the power-split hybrid system, part of the engine power is used to generate the energy as the series hybrid system, and the rest is directly transferred to the wheel as the

parallel hybrid system. Thus, well-organized power management can take advantage of both the series and parallel hybrid systems to improve fuel economy. The studies on power management on the power-split hybrid system have been mostly concentrated on HEVs [5].

Gelb et al. [56] introduced an electro-mechanical-transmission (EMT) concept for a power-split HEV system, using the speeder-torquer concept for the generator and traction motor control. In speeder-torquer concept, the speeder controls the engine speed to be constant (pseudo-CVT mode), and the torquer mainly assists the engine torque to propel the vehicle. Gelb et al. suggested two modes for the hybrid system operation, e.g., power-split and direct driving (parallel hybrid) modes. They also proposed five operational regions of the EMT powertrain that became the general basis of the modern power-split hybrid's power management (see **Error! Reference source not found.**).

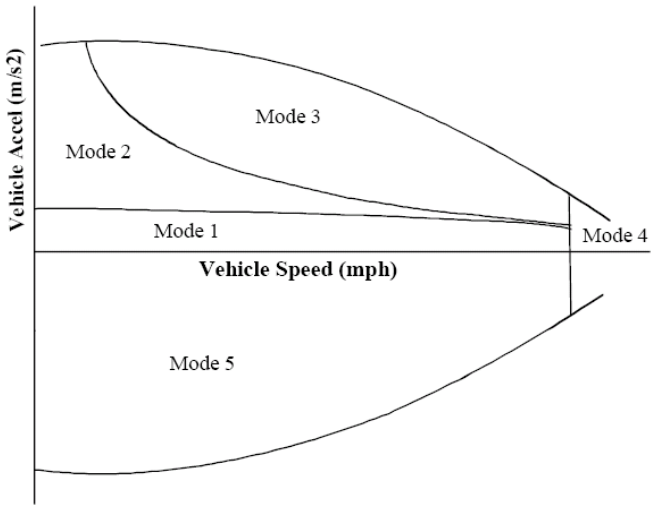

Figure 7. 8. Example of power-split HEV power management [56]

Mode 1: Low acceleration events when an internal combustion engine (ICE) power exceeds the road load. Excess engine power is used to charge the battery by using M/G1 and M/G2 in their generating mode. If the engine power matches road load but has insufficient torque, the "torquer" M/G acts as a motor to deliver additional torque to wheels by discharging the battery.

Mode 2: Low speed launching and light cruise. The "speeder" M/G remains in generator mode and delivers engine power to the "torquer" via the electric path. Excessive electric power may be used to charge the battery

Mode 3: High acceleration of the vehicle. Road-load torque exceeds the available engine torque. The battery (ESS) contributes additional boost power to both the motor "torquer" and generator "speeder".

Mode 4: High cruising speeds. "Speeder" is locked up and the engine is throttled up. "Torquer" operates in motoring or generating mode as needed.

Mode 5: Deceleration of the vehicle. Both M/Gs operate in generating mode to recuperate vehicle kinetic energy to the battery.

Rizoulis et al. [74] derived a mathematical model based on dynamics of a power-split HEV. They suggested the concept of the generator's speed reduction and the use of five vehicle-operation modes that were introduced by Gelb et al. [56]. They tested city driving schedule and the acceleration test was performed with the simulation model using pre-designed, pedal-position vector inputs.

Liu et al. [66] developed and analyzed the dynamic model of the Toyota hybrid system (THS) [67] deriving dynamic equations of the planetary gear train. They integrated a complete forward-looking dynamic model with a rule-based power management, and they validated their control during a driving schedule simulation. Basic power-split HEV power management is composed of low- and high-power lines dividing the motor-only drive, engine-only drive and power-assist drive from the battery. The SOC is maintained with the pre-designed charging power between the low and high SOCs. This power management seems to be close to the rule-based PHH power management introduced in Chapter 6 but the difference is that the engine always generates electric energy through electric path (or hydraulic) when the engine is running except the idle condition, so even engine-only mode uses the electric motor in the power-split system.

Han et al. [73] designed a power-split HEV and introduced several optimal power management algorithms. Firstly, they showed a static optimization result with battery-power concept using sequential quadratic programming (SQP) for a given vehicle speed, desired torque, and battery SOC. Secondly, they determined the optimal power distribution and vehicle operating-mode transitions using a DDP algorithm combined with the SQP algorithm during a city cycle simulation. However, they did not show the detailed behavior of the power devices and their characteristics. Liu et al. [83] showed a power-split dynamic model of the THS and applied DDP technique to find a globally

optimal benchmark of the power management. The DDP result was used to improve the ECMS.

After preliminary tests in PSHH system, the traditional power managements used for the power-split HEV show that the charging by the engine lowers fuel economy and increasing motor-only area improves fuel economy. In addition, the step changes of the engine power from the motor-only drive to the engine-only drive overshoot the engine speed and the control becomes unstable. Unlike parallel system, the inertia of the engine and hydraulic P/M is small, so exclusive usages of the engine power and hydraulic power bring instability problems. In addition, the thermostatic control running in the background makes frequent engine on-off's in comparison with HEV case because of the low energy density of the hydraulic accumulator. In contrast to PHH case, the SOC should be maintained over zero for P/M_{gen} to control engine speed properly the same as SHH case. As a result, the modulate SOC control is applied to PSHH system as an alternative power management because the modulated SOC control can maintain the SOC over zero reliably and restrain the engine charging. The accumulator is charged mostly from the regenerative braking energy by the P/M_{prop}.

The accumulator power can assist the engine power in the case of the high vehicle power demand with the stored accumulator energy at the constant level, SOC_{target}, and the SOC_{target} works as a buffer improving drivability. The assist of the hydraulic energy at the SOC_{target} is especially useful for the diesel engine operation, because of the turbo-lag during the severe acceleration.

The modulated SOC control scheme uses a PI feedback controller to maintain the SOC_{target} as shown in Equation (7.15). The control input signal is ΔSOC, which is $SOC_{\text{target}} - SOC$, and the controller output is the normalized engine power level between zero and one. The engine power demand is calculated by multiplying the maximum engine power by the normalized engine power level.

$$P_{eng,demand} = P_{eng,max} \times \left[K_p \left(SOC_{target} - SOC_{current} \right) + K_i \int \left(SOC_{target} - SOC_{current} \right) dt \right] \quad (7.15)$$

where $P_{eng,demand}$ is the engine power demand, $P_{eng,max}$ is the rated engine power, SOC_{ref} is the target SOC, K_p is a proportional gain and K_i is an integral gain. The controller performance is tuned by the proportional gain and integration gain but finding

suitable gains is not an easy task. The proper proportional gain and integral gain are selected from the EIL test with the baseline PSHH mode because the EIL test condition is more demanding than the pure simulation with a relatively simple engine model. These final gains show quite robustness that changes of hydraulic device sizes do not affect much on the controller performance. Therefore, final gains can be used for the design optimization process that changes system parameters at the each run of the cycle simulation.

The SOC_{target} needs to be high enough to guarantee the vehicle mobility. However, it also needs to be low enough to absorb the regenerative braking energy as much as possible for a given accumulator size and duty cycle. Accordingly, the design value of the target SOC highly depends on the accumulator size and the driving schedule, i.e., the energy buffer size and regenerative braking potential. The vehicle power demand is the sum of the engine power and accumulator power in Equation (7.16). Because the accumulator power is composed of the P/M_{gen} and P/M_{prop} powers in Equation (7.17), the vehicle power demand is the sum of engine, P/M_{gen}, and P/M_{prop} powers. Except for the engine power, the P/M_{gen} and P/M_{prop} powers can be negative or positive according to the pumping or motoring mode, respectively. After calculating the engine power demand from the modulated SOC control, the P/M_{prop} power demand is calculated in Equation (7.18).

$$\text{Vehicle power demand} = \text{Engine power} + \text{Accumulator power} \tag{7.16}$$

$$\text{Accumulator power} = P/M_{gen}\ \text{Power} + P/M_{prop}\ \text{Power} \tag{7.17}$$

$$P/M_{prop}\ \text{power} = \text{Vehicle power demand} - \text{Engine power} - P/M_{gen}\ \text{power} \tag{7.18}$$

The actual control block of the engine power demand in MATLAB/Simulink environment is shown in Figure 7. 9.

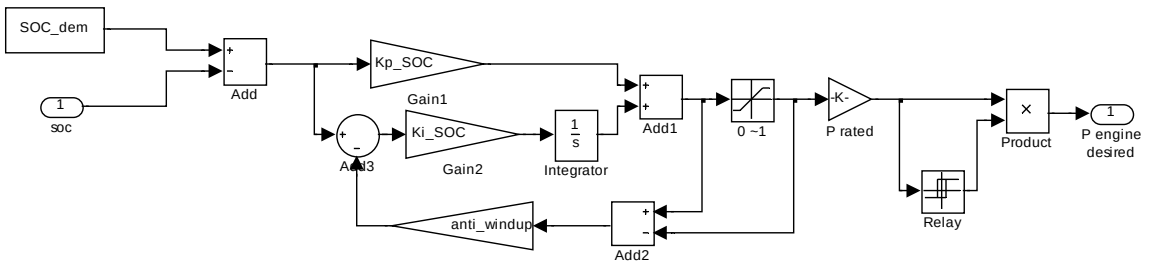

Figure 7. 9. Modulated SOC control in Simulink

The engine can be idle or idle-stop when the engine power demand is zero. To prevent the oscillation of the engine power demand near zero, a relay function is added at the end of the controller.

The modulated SOC control in the PSHH system is observed to have four different driving modes as shown in Figure 7. 10. Firstly, when the SOC is high enough, only hydraulic energy is used to drive the vehicle. Usually, the accumulator is charged after the braking, so this mode always happens when the vehicle starts. The engine power and P/M_{gen} power are zero and the P/M_{prop} only propels the vehicle consuming the stored energy in Figure 7. 10 (a).

Secondly, as the SOC is close to the SOC_{target}, the engine starts to provide the part of the vehicle power demand in Figure 7. 10 (b). The start of this mode is tuned by the controller gain in Figure 7. 9. As the gains increase, the hydraulic-assist mode starts earlier. The part of the engine power is transferred to the P/M_{prop} through hydraulic path bypassing the accumulator and the other part of the engine power is directly transferred to the wheel. This mode is the transition from the hydraulic-only drive to the engine-only drive.

Thirdly, when the SOC becomes the SOC_{target}, only the engine power is used to drive the vehicle in Figure 7. 10(c). The part of the engine power is transfer to the wheel directly and the rest is transfer to the P/M_{prop} through electric path. The energy stored at SOC_{target} is used as a buffer when the driver needs sudden accelerations compensating the system delay, e.g., turbo-lag.

Fourthly, if the driver needs more power than the maximum engine power, the hydraulic energy at the SOC_{target} is used until it reaches the pre-designed SOC_{min} that the power management has set to prevent the cavitation inside the hydraulic path in Figure 7. 10(d). Instead of using the shut-off valve, the power management reduces the vehicle power demand to maintain the SOC_{min}.

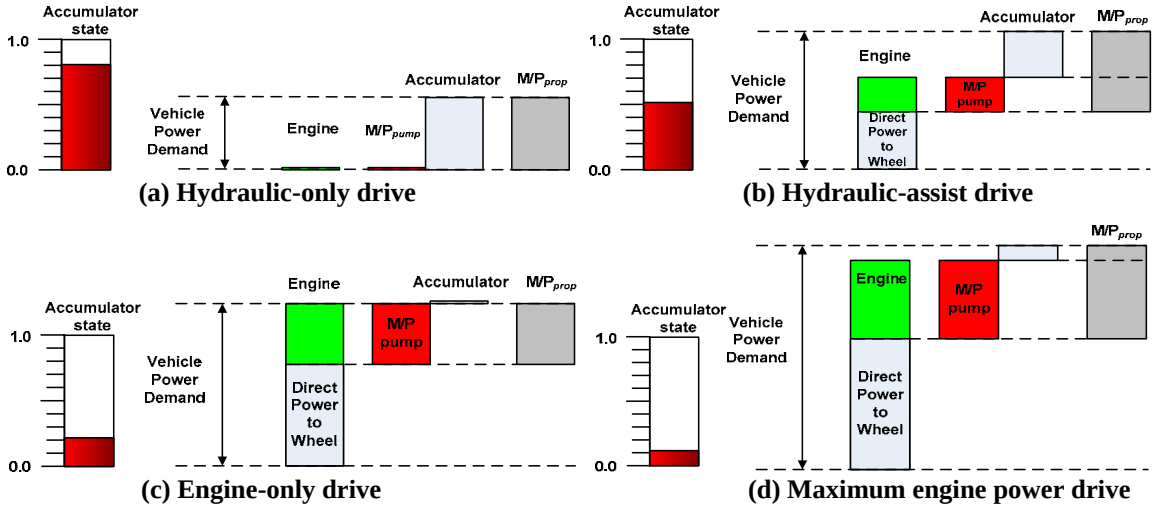

(a) Hydraulic-only drive (b) Hydraulic-assist drive

(c) Engine-only drive (d) Maximum engine power drive

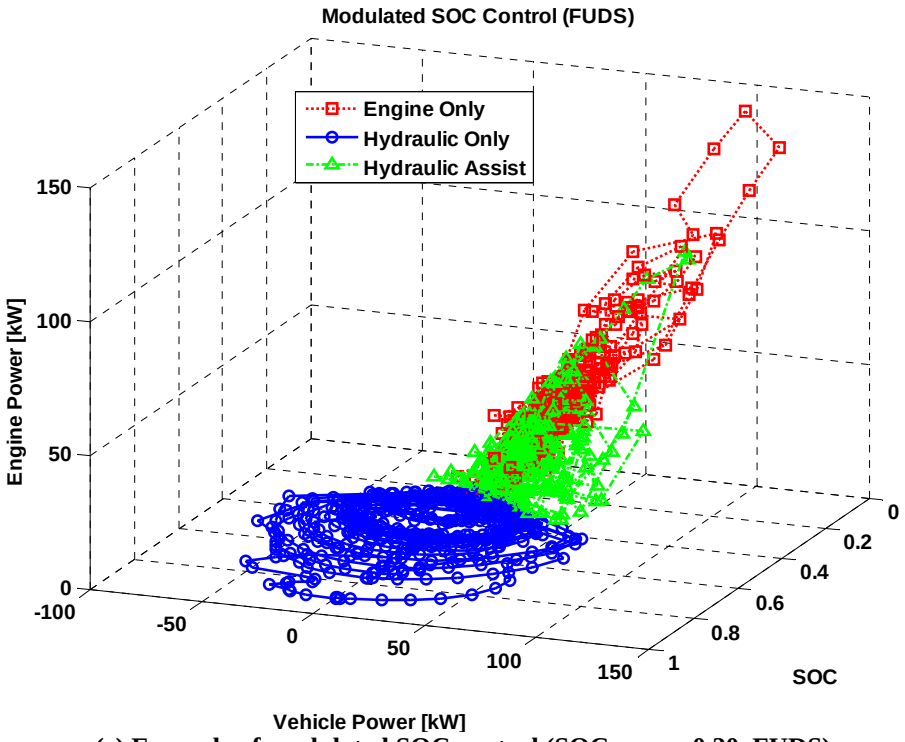

(e) Example of modulated SOC control (SOC $_{target}$ = 0.20, FUDS)

Figure 7. 10. Modulated SOC control in the PSHH system

As a result, the cavitation and durability issues can be avoided. When the SOC reaches the SOC_{min}, the engine power maintains the rated condition at the hydrostatic equilibrium. The example of the modulated SOC control during FUDS clearly shows how the modulated SOC control scheme works according to the vehicle power demand and SOC in Figure 7. 10(e).

The example of the modulated SOC control is shown in Figure 7. 11. The modulated SOC control scheme controls the engine power demand smoothly because the accumulator works as an energy buffer. Therefore, the modulated SOC control can reduce transient exhaust emissions and improve the driver's comfort in the actual vehicle application. In the modulated SOC scheme, the controller gains must be selected to be reliable not to deplete the SOC even at the most severe acceleration point in the given driving schedule and not to oscillate the engine power.

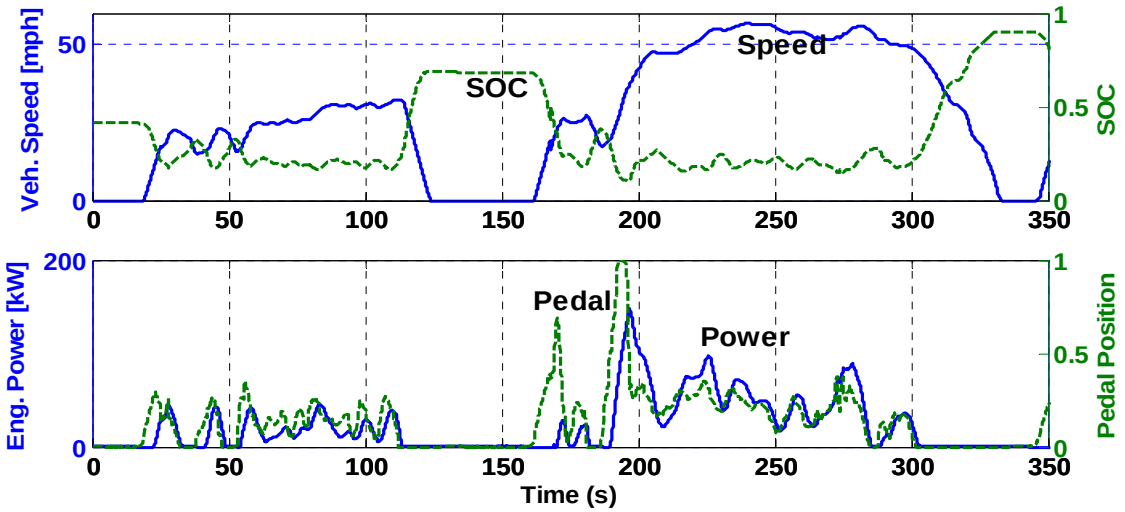

Figure 7. 11. Engine power prediction and PSHH system behavior of the modulated SOC control

7.1.3. Engine Speed and Torque Control

In the power-split hybrid system, the engine speed and torque can be independently controlled as series hybrid systems from the given engine power demand. In Figure 7. 7, the P/M_{prop} is connected to the wheel through the final gear so the engine speed can be controlled by controlling the P/M_{gen} speed that is calculated by the lever rule. Thus, it is assumed that the P/M_{gen} works as a speeder and P/M_{prop} works as a torquer in this study. Thus, the desired engine speed and torque are pre-designed corresponding to the engine power demand from the supervisory control according to the specific objective, e.g., best fuel efficiency. In this study, the objective of the engine speed and torque control is fuel economy improvement, so the engine speed and torque are controlled along the pre-calculated minimum BSFC line in Figure A. 1(a). However, the optimization of only the engine operation does not guarantee the system level optimization.

As a result, the engine speed is controlled by the P/M_{gen} torque and the engine torque is controlled by the engine rack signal that determines the fuel delivery to the engine.

The engine speed deviation from the reference speed is input to the feedback engine-speed controller in Equation (7.19) and the controller output is normalized between -1 to 1 and given to the P/M_{gen} as a displacement factor. The anti-windup scheme is used to remove the integration error saturation.

$$x_{P/M_{gen}} = K_p\left(\omega_{eng,ref} - \omega_{eng,current}\right) + K_i\int\left(\omega_{eng,ref} - \omega_{eng\_current}\right)dt \tag{7.19}$$

where $\omega_{eng,ref}$ is the engine speed demand, $\omega_{eng,current}$ is the measured engine speed, K_p is a proportional gain, and K_i is an integration gain.

The engine torque control is much harder than the speed control because the torque control is controlling the acceleration implicitly, so the torque signal is a higher order signal than the speed signal. As a result, the feedback control of the engine torque is not easy even with the simplified engine model and needs the torque measurement that is expensive and noisy in real vehicle applications. Therefore, the open-loop torque control is applied with pre-measured engine rack values corresponding to the pre-set torque values for given engine power demands. The main assumption of the open loop control is as follows. Firstly, the speed control is fast and reliable. Secondly, the calibrated rack position for the given torque is repetitive. Thirdly, the transient effect in the torque build-up, e.g., turbo-lag, is not significant. As a result, the actual engine speed can synchronize the torque output as the pre-set point on the engine map. This open loop torque control works better when the engine power demand is controlled smoothly. These engine speed and torque control strategy is proven to work by successful EIL validation tests presented in Chapter 8.

7.2. Power-Split Hydraulic Hybrid Design Optimization

The PSHH vehicle design studies are rare because the power-split designs are mostly patented and the auto manufactures have been developing their own system confidentially. Niasar et al. [88] presented the design methodology of the power-split HEV but their design methodology is not based on the dynamic modeling but based on the power matching for the performance. The approach used for the PSHH super-HMMWV design is applying the multi-start design optimization technique with the modulated SOC control. The optimized design is used as a baseline PSHH platform for the power management optimization.

7.2.1. PSHH Design Optimization Setup and Result

The engine and vehicle models are the same as the conventional super-HMMWV presented at Chapter 3. The fuel economy is the objective of the design optimization, and the design constraints are listed below. The design constraints are mostly based on the performance of the conventional super-HMMWV model with the upgraded high-power engine and standard HMMWV operations. The FUDS is used as a baseline driving schedule.

Objective: maximize fuel economy

Constraints:

0-50 mph acceleration time (initial SOC: 1.0) $\leq$ 10.8 second

Maximum speed $\geq$ 65 mph

Maximum grade $\geq$ 60% slope

Cruising grade (@ 50mph) $\geq$ 2% slope

Cruising grade (@ 40mph) $\geq$ 3% slope

Test-fail condition: continuous deviation of more than 2 mph from the reference speed over 1 second

The optimization process follows the same as described in Chapter 3.4.1. The optimization procedure is shown in Figure 4. 1. The boundaries of design variables are shown in Table 7. 2. These boundaries are based on the values from the SHH super-HMMWV optimization in Chapter 3.

Five multi-start points are selected after cycle simulations with randomly chosen 100 points selected by a DOE and the design optimization result from multi-start points is shown in Table 7. 3. The optimized fuel economy values converge near 19.2 and 19.3 even though the individual design variables shows large differences in some cases which means they are local maxima.

Table 7. 2. Design variables and boundaries of the design optimization in PSHH

	Lower	Upper
Accumulator volume [Liter]	50	150
Target SOC	0.1	0.5
P/M_{prop} size [cc/rev]	90	270
P/M_{gen} size [cc/rev]	150	450
P/M_{prop} -shift speed [rpm]	1000	3000
Final-gear ratio	2.5	6.5

Finally, the optimized point from #3 is selected as the baseline design parameter for the PSHH system and will be used for the power management optimization. The optimization process roughly improves fuel economy by 6% from the best fuel economy of the multi-start points. The PSHH system behavior is shown in Figure 7. 12. While the vehicle follows the FUDS, the P/M_{gen} and P/M_{prop} speeds are within the maximum speed limit of 4000rpm and the SOC is maintained well over zero.

Table 7. 3. Multi-start points and optimization result in PSHH

No	Accumulator Volume [Liter]	SOC_{target}	P/M_{prop} Size [cc/rev]	P/M_{gen} Size [cc/rev]	Shift Speed [rpm]	Final Gear ratio	0-50 mph Time [sec]	FE [mpg] w/o idle-stop	FE [mpg] w/ idle-stop
#1	121	0.22	252	203	1061	5.40	7	18.9	21.3
Optimized	118	0.23	238	225	1086	5.16	7.4	19.2	21.7
#2	128	0.21	199	231	2961	4.82	7.6	18.8	21.1
Optimized	114	0.28	179	227	2698	4.99	7.9	19.3	21.7
#3	111	0.25	210	426	2557	4.50	8.0	18.9	21.2
Optimized	**98**	**0.20**	**230**	**333**	**2192**	**4.09**	**8.1**	**19.3**	**21.8**
#4	95	0.36	159	200	2899	5.31	7.9	19.1	21.4
Optimized	92	0.35	152	197	2802	5.35	8.1	19.2	21.6
#5	75	0.22	194	259	2495	5.09	7.8	19.2	21.6
Optimized	75	0.22	193	258	2479	5.09	7.8	19.2	21.6

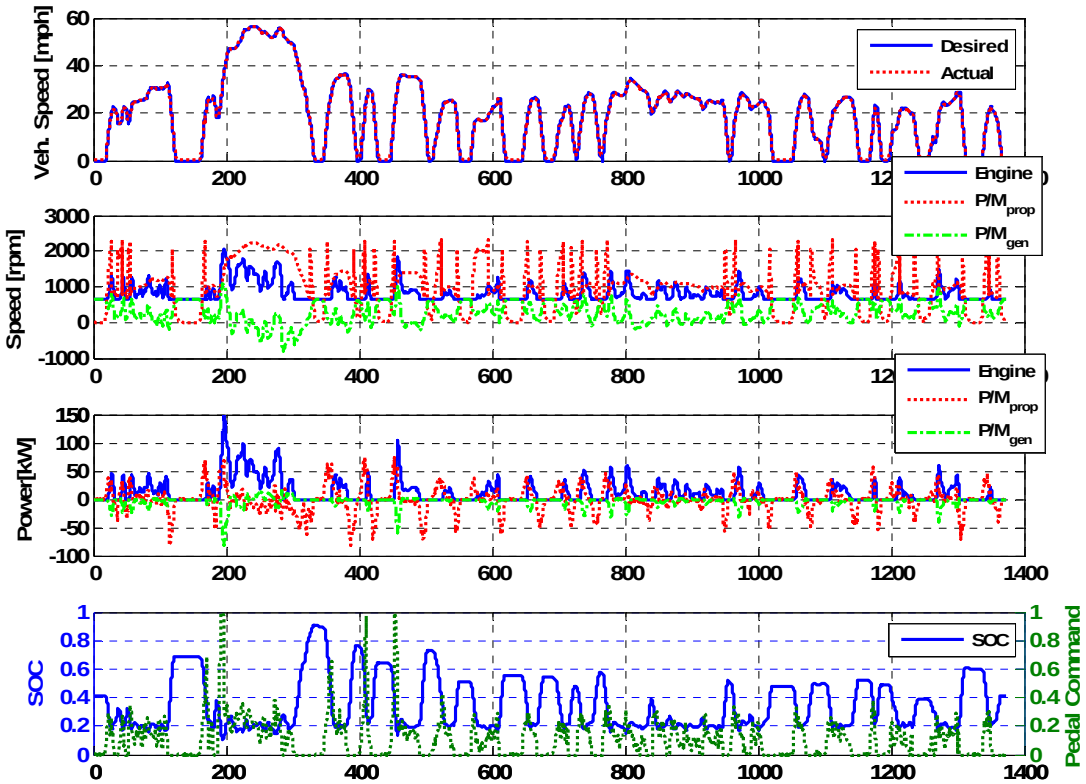

(a) System behavior during FUDS

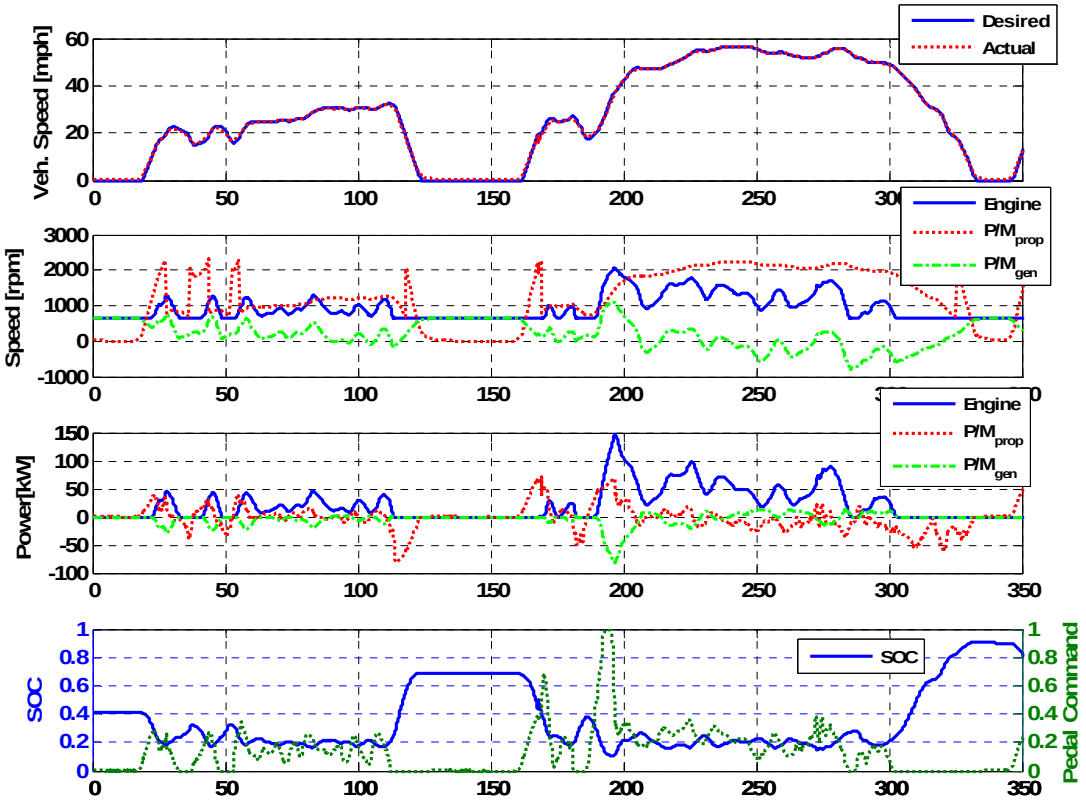

(b) Zoomed system behavior (0~340 second) during FUDS

Figure 7. 12. PSHH system behavior during FUDS

By the modulated SOC control, the vehicle starts with the hydraulic-power only and as the SOC close to SOC_{target}, the engine starts to assist the hydraulic power reducing the SOC decreasing rate. When the SOC is close to SOC_{target}, only engine power drives the vehicle through hydraulic and mechanical paths. The regenerative braking energy is only absorbed by the P/M_{prop} and the engine idles or stops with freewheeling of the P/M_{gen} when the engine power demand is zero. Interestingly, when the vehicle speed is high during 200~300 second region, the P/M_{prop} absorbs the part of the large engine torque to the wheel, designed by minimum BSFC line, such as the energy recirculation in power-split HEV case [102].

Figure 7. 13 shows the relations between the engine power demand and vehicle power demand by the modulated SOC control. When the SOC is close to SOC_{target} at the vehicle cruise condition, the engine power is slightly higher than the vehicle power demand because of the energy conversion and mechanical losses but the engine power maintains the engine-only drive without the assist of the hydraulic energy. The hydraulic-only drive occurs when the engine power is zero and vehicle power demand is positive.

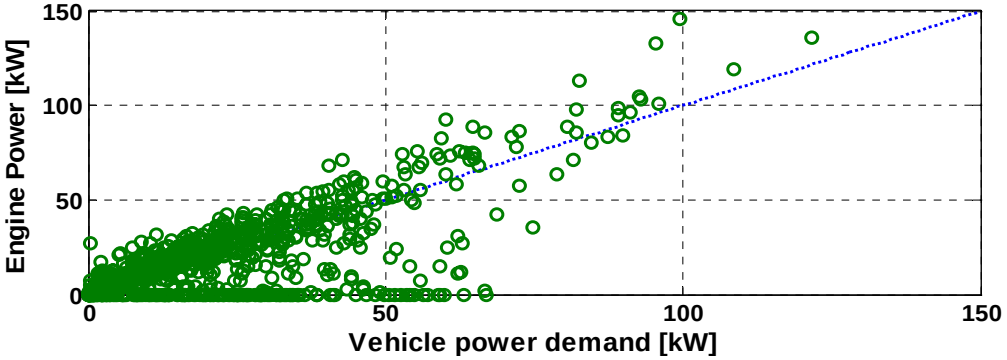

(a) Engine power vs. vehicle power demand

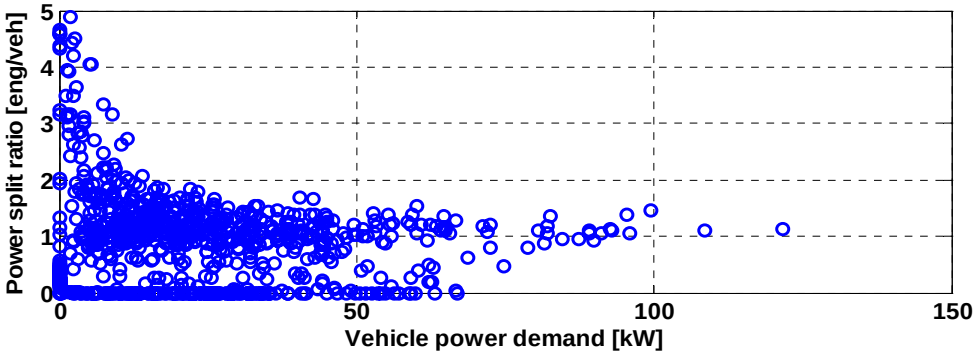

(b) Power-split ratio vs. vehicle power demand

Figure 7. 13. Engine power vs. vehicle power demand during FUDS

The hydraulic-power assists the engine when the engine power is between the 1:1 power line and zero power line. The hydraulic-power assist is the transition between the hydraulic-only drive and engine-only drive according to the SOC control. It is clear that the inefficient direct engine charging is prevented in the modulated SOC control.

The integrated fuel consumption during FUDS is shown on the engine map in Figure 7. 14. For a given engine power, the engine speed and torque are well controlled to be located on the minimum BSFC line and the fuel consumed mostly on the minimum BSFC line. For FUDS, the engine size seems to be large because only the half of the maximum engine power is used during FUDS. If the engine size is reduced, the sweet spot in the engine map will be more frequently used and the potential of improving fuel economy will increase. Just like the series system, the engine can provide the maximum power at any vehicle condition, so the engine downsizing is viable.

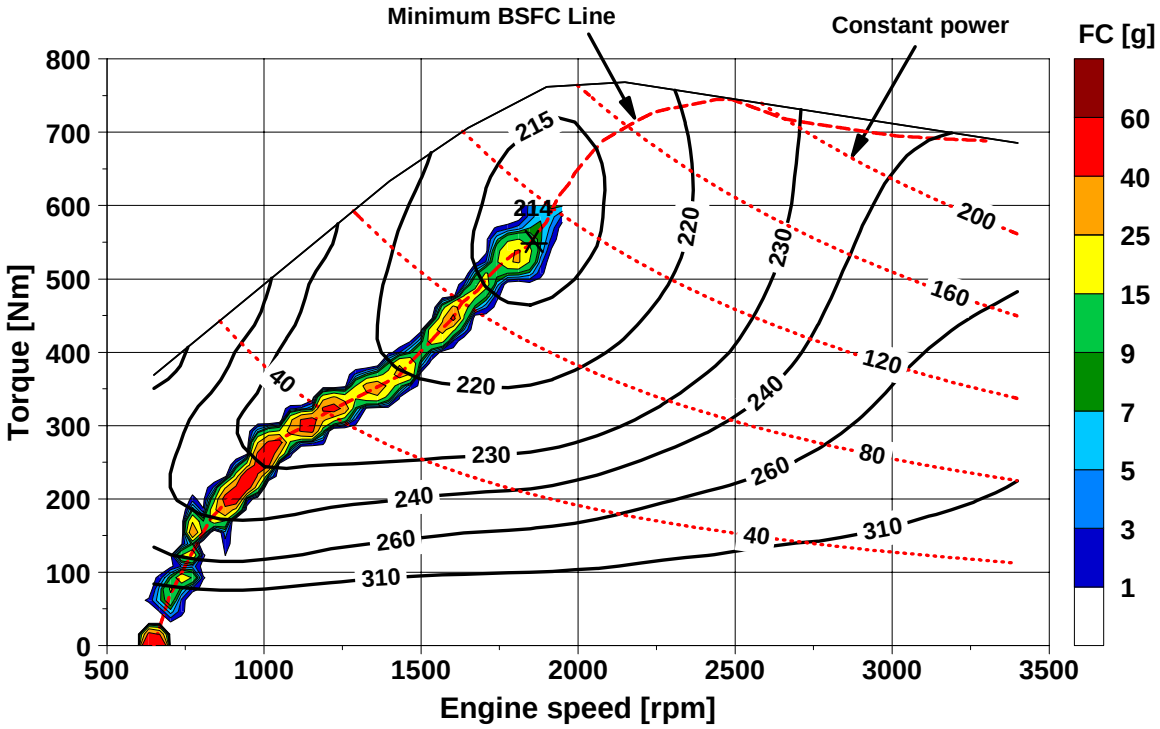

Figure 7. 14. Integrated fuel consumption of PSHH with the modulated SOC control

The design optimization predicts that fuel economy improves about 55% without idle-stop and over 74% fuel economy improvement with idle-stop capability in FUDS. Not only FUDS but highway cycle (HWFET) fuel economy improves over 16 % because of efficient engine operations and the high mechanical efficiency in transferring the part of the engine power directly to the wheel.

7.2.2. PSHH Super-HMMWV Performance

The PSHH super-HMMWV's 0~50 mph acceleration test result is shown in Figure 7. 15. For this test, the engine power demand becomes the maximum by a step function bypassing the power management demand that is calculated from SOC. The engine power reaches its maximum very fast because it can be independent of the wheel speed by controlling P/M_{gen} speed. The SOC increases just after the gear shift because the P/M_{prop} speed decrease and the discharging rate from the P/M_{prop} decreases with same pumping rate from the P/M_{prop} with the maximum engine power. The vehicle reaches the hydraulic equilibrium condition after around 18 second.

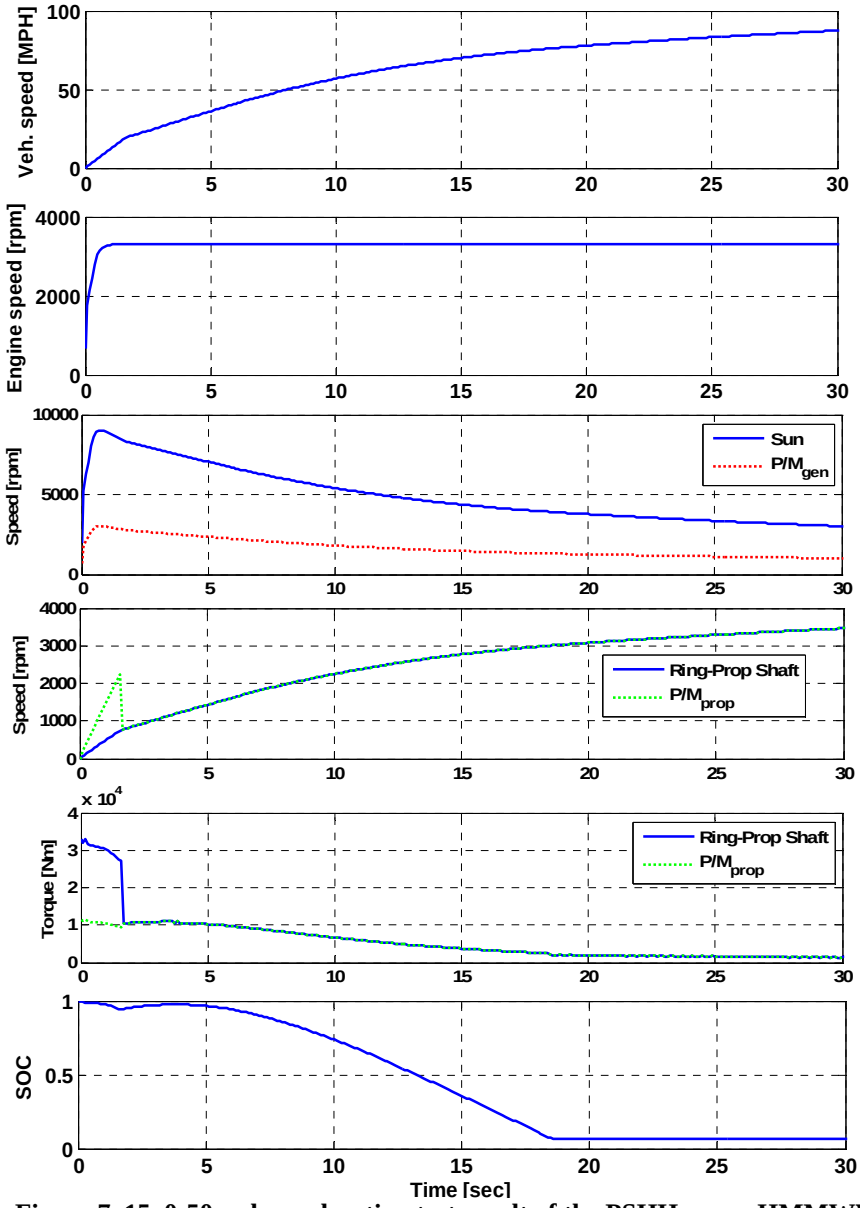

Figure 7. 15. 0-50mph acceleration test result of the PSHH super-HMMWV

The overall energy flow across the hybrid system devices and energy conversion efficiencies during FUDS are shown in Table 7. 4. The accumulator efficiency is as high as 96% and the P/M efficiencies are almost 90% during the FUDS. The P/M_{prop} efficiency is relatively low because the P/M_{prop} is designed as oversized for the performance concerns. The P/M_{gen} efficiency is relatively high, which means that the P/M_{gen} operates at the low speed and high load region due to the speed reduction mechanism.

Table 7. 4. Overall energy flows and conversion efficiencies of hydraulic hybrid devices

	Energy in [kJ]	Energy out [kJ]	Efficiency [%]
Engine (with/without idle) (Diesel LHV : 42.8 MJ/kg)	52571/ 46605	17089	32.5 / 36.7
Accumulator*	8970	8660	95.8
Reservoir*	366	351	95.8
P/M_{gen} pumping	4667	4069	87.2
P/M_{gen} motoring	599	497	83.0
P/M_{prop} pumping	9437	7765	82.3
P/M_{prop} motoring	10850	8920	82.2

*** Bypassed energy after the accumulator pressure reaches the maximum is not counted**

The break down of fuel economy gains shows that the idle fuel consumption occupies a significant portion in the PSHH system as shown in Figure 7. 16. 27 % of the fuel economy gain is possible with the idle-stop and start capability.

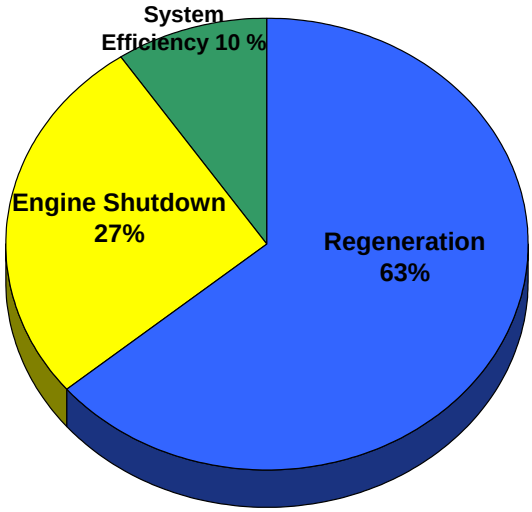

Figure 7. 16. Breakdown of fuel economy gains in PSHH

The system efficiency improvement that is derived from both the engine operation on the minimum BSFC line and using the power-split powertrain takes 10% of the fuel economy gain over the conventional vehicle's fuel economy.

7.3. Power-Split Hydraulic Hybrid HMMWV Power Management Optimization with Deterministic Dynamic Programming

The supervisory powertrain control refers to the power management among multiple power devices, e.g., engine, generator/motor and hydraulic P/M, in the hybrid propulsion system. The lower-level powertrain control manages each power device control from the given power demand. The power-management optimization is the optimization of the control strategy about the distribution of the vehicle power demand to each power device at the system level. With increase degrees of freedom in the control of the power devices of the hybrid system, the engineering intuition or traditional trial and error methods is almost impossible to find an optimal control strategy in the supervisory control.

As a global supervisory control optimization algorithm, the deterministic dynamic programming (DDP) technique is introduced in Chapter 4 and the same algorithm is applied for the PSHH. As for the PSHH system, the studies of using the DDP technique are almost none. The result of the DDP technique shows the benchmark prediction of the each power device operation such as the speed and torque of the engine and P/M. Therefore, the fuel economy result from the DDP technique is a theoretical potential with the given design of the PSHH system.

7.3.1. PSHH DDP Setup

The optimized hardware design of the PSHH in the previous section is used as a baseline platform for the DDP. To setup DDP, state variables and control inputs are to be determined first. The vehicle power demand is extracted from the wheel power data of the high fidelity PSHH VESIM and used as the pre-determined disturbance.

From complex actual states and controls in the PSHH system, two states and two controls are selected to represent the PSHH system in minimum states and controls and discretized as shown in Table 7. 5. DDP is so expensive in terms of the computation time and memory occupation. The number of states and controls, and grid sizes and time step are critical for DDP to be setup and solved successfully. The grid sizes for the states and controls are selected after pre-DDP grid sensitivity tests. The state and control grid sizes should be selected to be small enough to represent system dynamics. If the grid size is

too large in comparison with the dynamics of the system, the state does not change with the change of controls and stays at the same grid. However, because DDP needs intensive computation and large memory occupation, the grid size should not be too small.

The time step is also related to the price of the intensive computation of the DDP. It is observed that if the time step is too small, the state does not change with the change with different control inputs. Thus, the time step should be determined large enough but small enough to represent the system dynamics. The time step is also pre-tested with various values and determined as one second.

Table 7. 5. State and control variables and grid discretization in PSHH DDP

State	Engine speed	650 : 3300	40 grids
	SOC	0 : 0.025 : 1	40 grids
Control	Engine command	0 : 0.02 : 1	50 grids
	P/M_{gen} command	-1 : 0.025 : 1	80 grids

To make the computation faster, the simplification of the high fidelity PSHH vehicle model is done as long as the simplification shows reasonably similar results with the high fidelity model. Firstly, the dynamics that are much faster than 1 Hz, e.g., engine torque generation, are changed to the static look-up table. Secondly, the accumulator gas dynamics is changed to the polytropic state equation model, where the gas volume is only the function of the gas pressure, instead of the high fidelity real-gas dynamic model. The coefficients of the polytropic process are acquired from curve fitting the cycle simulation result of the high fidelity PSHH vehicle model simulation. Thirdly, the high-fidelity vehicle model is changed to the simple road-load vehicle model. The rolling resistance coefficients of the simple vehicle model are calibrated to show almost the same vehicle power demands, so the fuel economy is close to that of the high fidelity vehicle model with less than 1% difference.

The DDP technique is generally divided into three phases, such as the forward transition cost table generation, backward minimum cost sweep at each node and forward optimal solution search. In addition to the simplification for the fast calculation, the same vectorization and m-file approach introduced in Chapter 4 are used in generating the forward transition cost table.

Physical constraints are given below and if constraints are violated, an infinite penalty is given to the cost function.

$$0 \le SOC(k) \le 1 \tag{7.20}$$

$$\omega_{eng\_\min} \le \omega_{eng}(k) \le \omega_{eng\_\max} \tag{7.21}$$

$$T_{P/M_{prop}\,min} \le T_{P/M_{prop}}(k) \le T_{P/M_{prop}\,max} \tag{7.22}$$

Because the P/M_{gen} speed is lower than the maximum speed with the speed reduction mechanism even at the severe acceleration test, the P/M_{gen} speed limit is not added in constraints. Unlike the HEV case, the accumulator charge and discharge limits are not included because of the high-power density of the accumulator. In addition, the SOC can be from 0 to 1 in the hydraulic accumulator in contrast with the relatively narrow SOC window of the battery.

In addition to the physical constraints described above, the engine operation is restricted at the low engine speed and high torque area because of the noise and vibration problems that occur in the real vehicle application (see Figure 7. 21).

The cost function, $g(k)$, is setup is given below.

$$g(k) = fuel\,consumption(k) + \beta\left((\omega_{eng,k+1} - \omega_{eng,k})/\omega_{eng\,max}\right)^2 \tag{7.23}$$

In addition to the pure fuel consumption, the penalty for the unrealistic engine speed change is introduced by multiplying the engine-acceleration reduction factor, β, to the square of the normalized engine acceleration assuming the engine operation may become too transient without charging or discharging power constraints as in HEV cases [44]. In the future study, concrete transient operation limits from the perspective of transient emission restrictions or the driver comfort index may replace this simple addition of the arbitrary engine acceleration penalty. For various values of the weight, β, the DDP technique is applied in the following section. The idle-stop capability is not assumed, so the idle fuel consumption is included in the cost function.

Final SOC needs to be equal to the initial SOC to simulate the charge sustaining capability. The penalty of the SOC deviation is the squared distance from the initial SOC in Equation (4.11) and added to the cost function in the final step.

$$g_N\left(x_N\right)=\alpha\left(SOC-SOC(0)\right)^2 \tag{7.24}$$

where α is the weighting factor for charging sustaining.

Finally, the total cost to be minimized is represented in Equation (7.25).

$$\begin{aligned}\min\sum_0^N g_k = \min\sum_0^{N-1}\Big(& \textit{fuel consumption}(k)+\beta\left(\left(\omega_{eng,k+1}-\omega_{eng,k}\right)/\omega_{eng\ max}\right)^2\Big) \\ & +\alpha\left(SOC\left(N\right)-SOC\left(0\right)\right)^2\end{aligned} \tag{7.25}$$

7.3.2. PSHH DDP Result

The DDP technique is applied to PSHH system including the engine-acceleration reduction factor, β, which can be seen to affect the fuel economy as shown in Table 7. 6. As β increases, the engine speed acceleration is suppressed as expected but fuel economy decreases. Finally, fuel economy saturates when β is over 25 and the fuel economy gains of the optimal power management reduced to less than 10% in comparison with the modulated SOC control case in which the engine speed acceleration is relatively small.

Table 7. 6. Effect of β on the fuel economy

β	Fuel economy [mpg]	% to modulated SOC control
0	27.7	144
12.5	22.5	117
25	21.1	109
37.5	20.4	106
50	20.4	106

The effect of β to engine speed during the FUDS is shown in Figure 7. 17. When $\beta = 0$, the engine speed is highly transient and it seems to act as an extreme thermostatic SOC control. However, the extremely transient engine operation seems unrealistic in the actual SHH vehicle application. The cases when $\beta \geq 25$ seem to have reasonable engine operation in an engineering sense. Nevertheless, the study on proper maximum engine acceleration is rare and a proper engine acceleration limits or other criteria, e.g., power rate limit, if exists, can be used as a penalty in the future study.

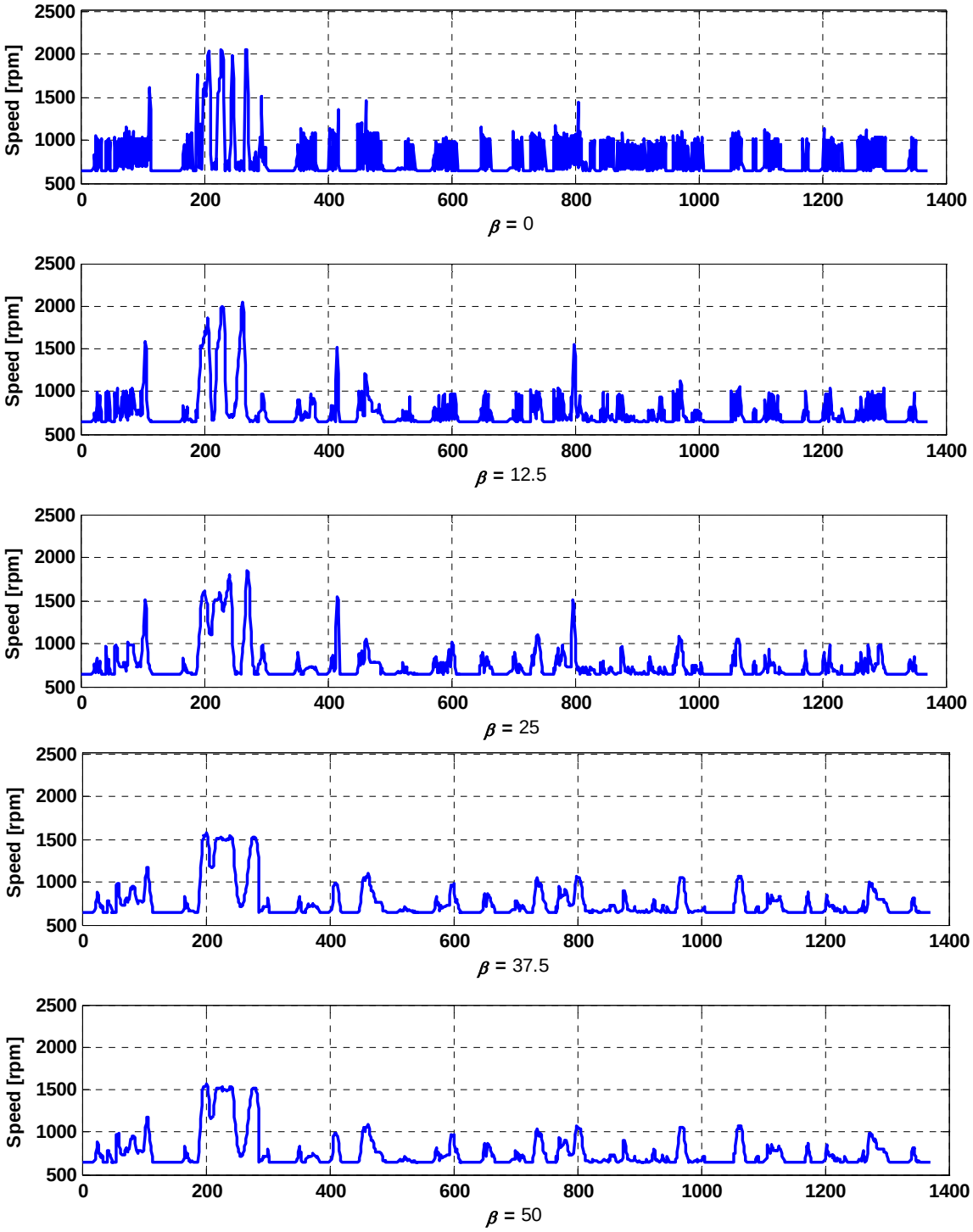

Figure 7. 17. Effect of β on engine speed in PSHH DDP during FUDS

The PSHH DDP result is shown in Figure 7. 18(a)~(d), when β equals to 25. The vehicle follows FUDS and the gear between P/M_{prop} and final gear is shifted according to the pre-designed shift speed. Interestingly, SOC goes below zero with fully utilizing the accumulator energy as shown in Figure 7. 18(a). By going down to zero SOC, the stored

energy can be fully used at each vehicle start and the accumulator has a room for the effective regenerative braking by maintaining the engine-only drive as much as possible at the low SOC. In addition, P/M_{gen} and P/M_{prop} use high displacement factors, so the system efficiency increases even though the high pressure is advantageous for P/M in Figure 2. 4. This trade-off relation may be reflected in the DDP solution. However, the vehicle propulsion operations at the low SOC can cause drivability problems in the real PSHH application so this benchmark power management may be possible because of the preview feature – backward solution search – of the DDP technique.

Clearly, DDP uses the accumulator power at the vehicle launch without the engine assist because the engine efficiency is low when the power demand is low in Figure 7. 18 (b). However, when the vehicle speed is high and the high power is needed at the second hill of the FUDS (around 160~340 seconds), the engine starts early and maintains the high power such as a load leveling in Figure 7. 18(b).

Even though the transient engine speed is suppressed by the engine acceleration reduction factor, β, the engine torque becomes very transient especially when the vehicle power demand is low during around the 20~125 second region in Figure 7. 18 (c). The engine power is used for charging the accumulator at 100~110, 240~250 and 260~275 second regions at the fuel-efficient high load area. The charged energy is used for the vehicle propulsion later.

With the SOC close to zero, the engine rack command and P/M_{gen} uses the high engine load exclusively. The engine rack command and pump rack command can be high values especially when the engine power demand is low. As a result, system efficiency improves but transient operations may cause excessive exhaust emissions and durability problems in the real PSHH application as shown in Figure 7. 18 (d). .

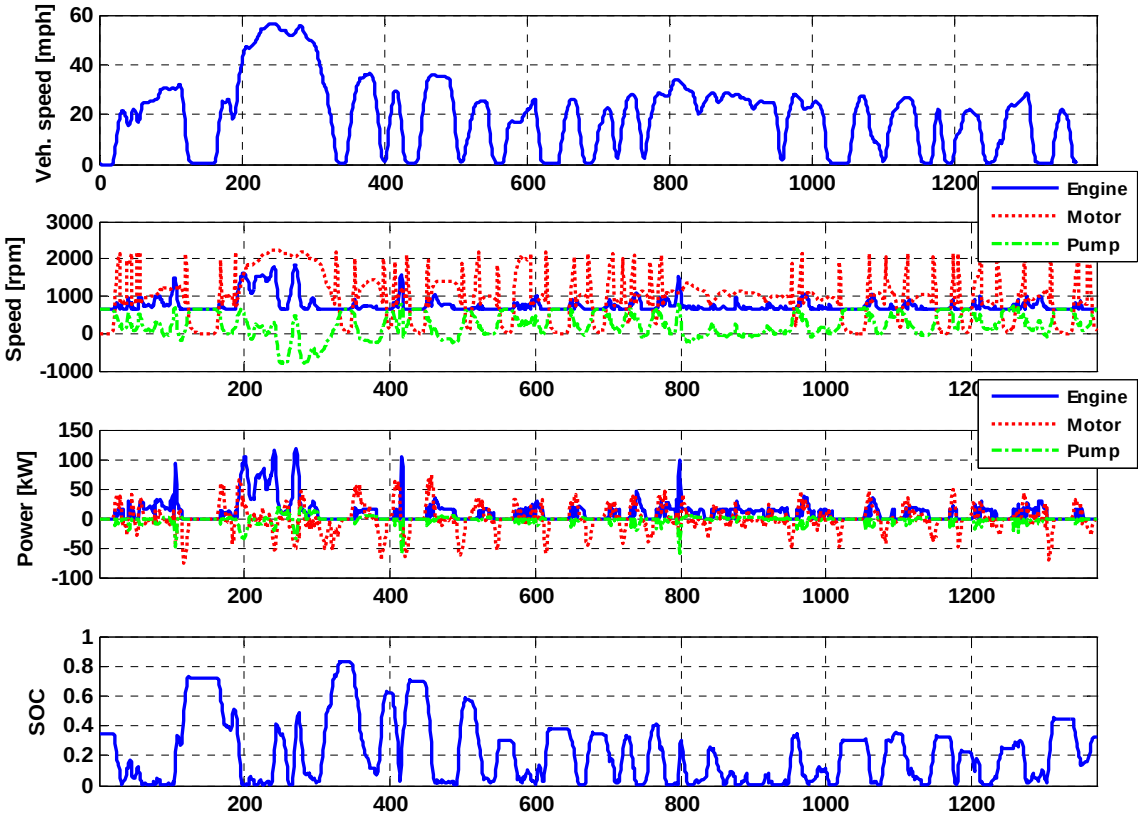

(a) PSHH DDP result during FUDS (β=25)

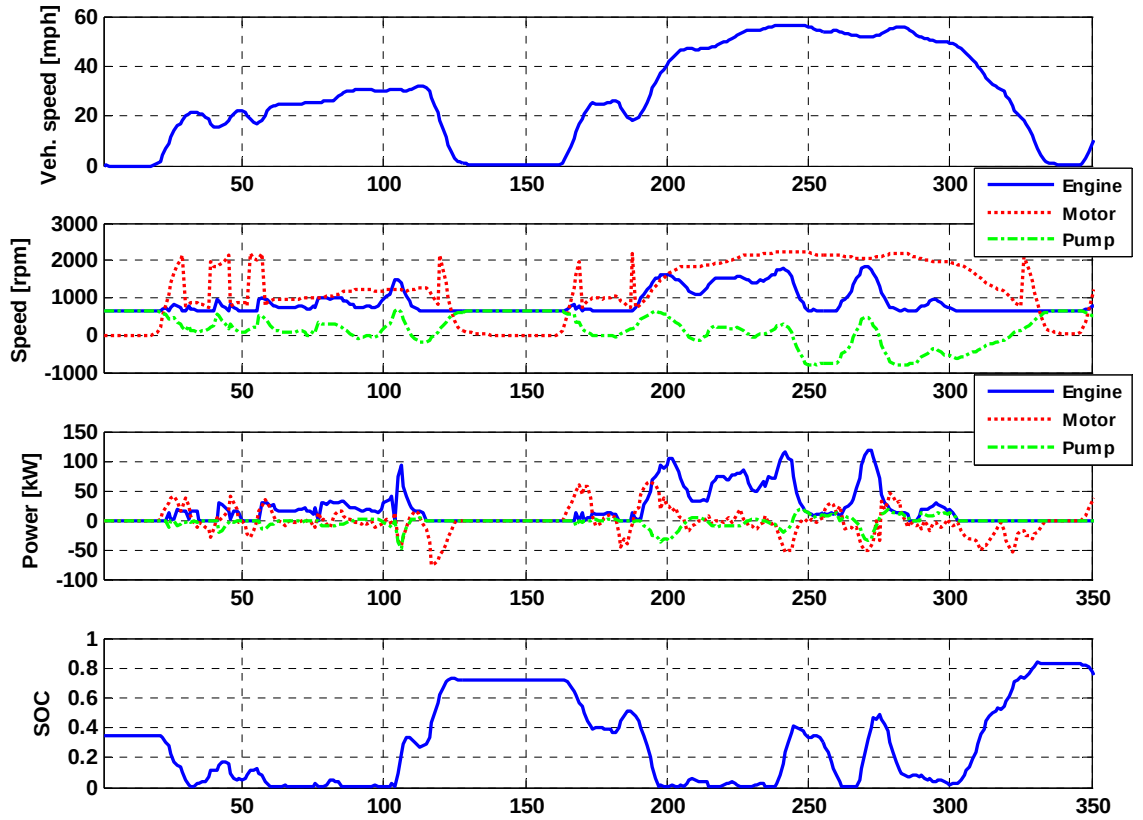

(b) PSHH DDP result from 0 to 350 seconds during FUDS (β = 25)

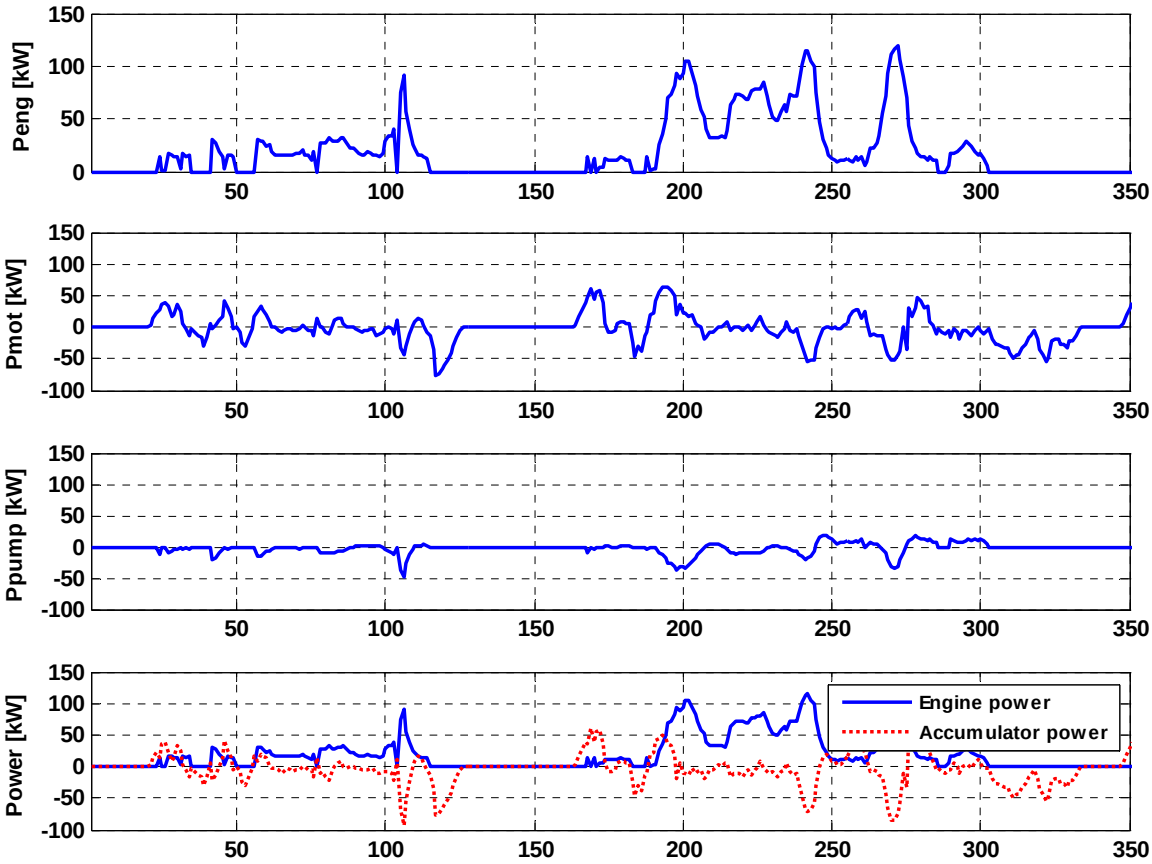

(c) Power-device power from 0 to 350seconds during FUDS (β = 25)

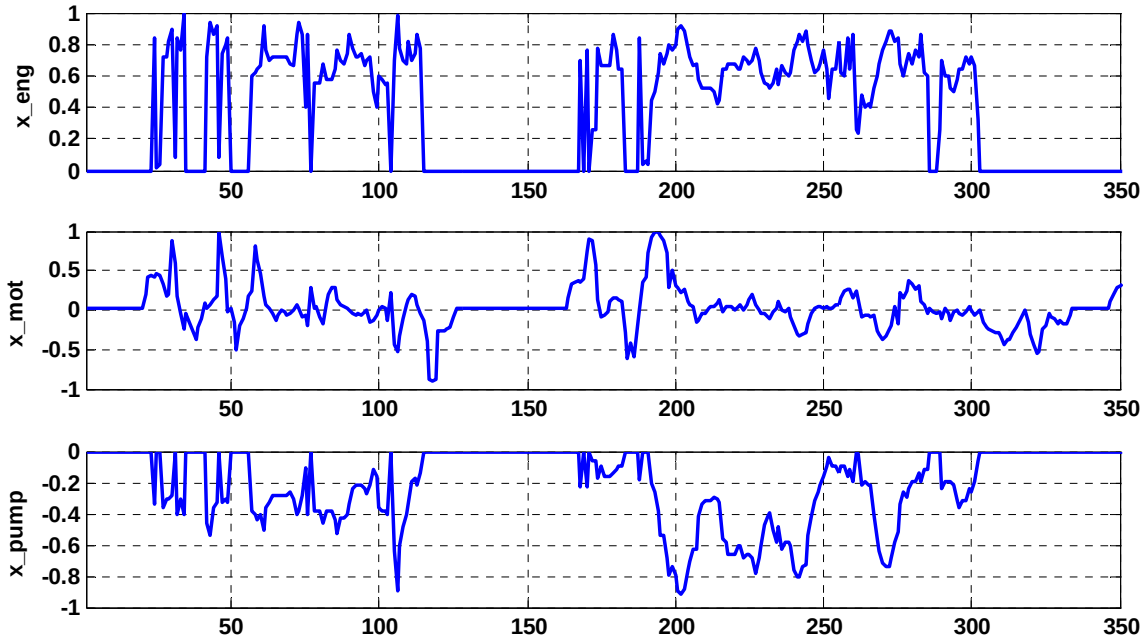

(d) Power-device control signal predictions during FUDS when β =25

Figure 7. 18. PSHH DDP result during FUDS (β = 25)

The parametric study of the minimum SOC effect is done by way of giving an infinite penalty when the SOC goes below the arbitrary pre-set SOC in Figure 7. 19, simulating the real PSHH application that has a hydraulic energy buffer to compensate for system delays and improve the drivability. The fuel economy does not change until the SOC_{min} is set to 0.2 and it decreases about 2 % when the SOC_{min} is set by 0.3. This result is reasonable because the accumulator size is pre-designed from the modulated SOC control with the target SOC of 0.2. As a result, the accumulator is large enough to hold the same regenerative braking energy without bypassing the compressed fluid at the maximum accumulator pressure until SOC_{min} is as high as 0.2. Therefore, the SOC_{min} below the SOC_{target} of the modulated SOC control does not affect the fuel economy result.

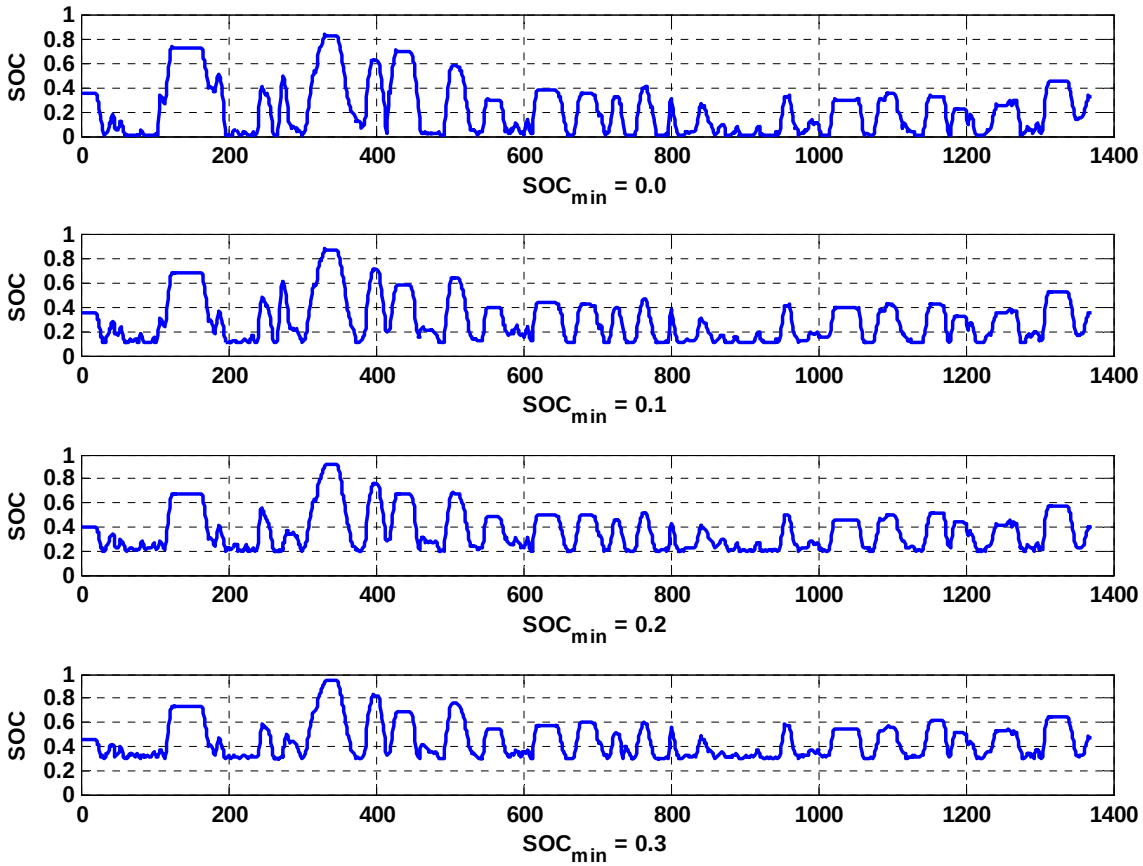

Figure 7. 19. Effect of SOC_{min} on the SOC prediction in PSHH DDP (β = 25)

The engine power versus vehicle power demand during FUDS is shown in Figure 7. 20. With stored hydraulic energy in the accumulator, the engine power can be zero realizing the hydraulic-only drive, even when the vehicle power demand is around 75 kW. The hydraulic-assist drive is also shown when the power split ratio is between 0.0 and 1.0

as a transition between hydraulic-only and engine-only drive. Because of the mechanical loss in the powertrain and energy conversion loss, power-split ratio becomes slightly over 1.0 even during the engine-only drive.

The engine power sometimes reaches as high as around 80~120 kW and seem to do load leveling when the vehicle power demand is around 15~50kW. As a result, the engine can use the efficient high load area by charging with trading off energy conversion losses. DDP finds the way to improve the fuel economy demand by charging the accumulator and highly transient engine operation when the engine power demand is small. However, finding a rule-based power management from this benchmark control seem to be difficult and time consuming, so the SDP power management optimization is applied to PSHH system to find semi-optimized implementable power management systematically in the next section.

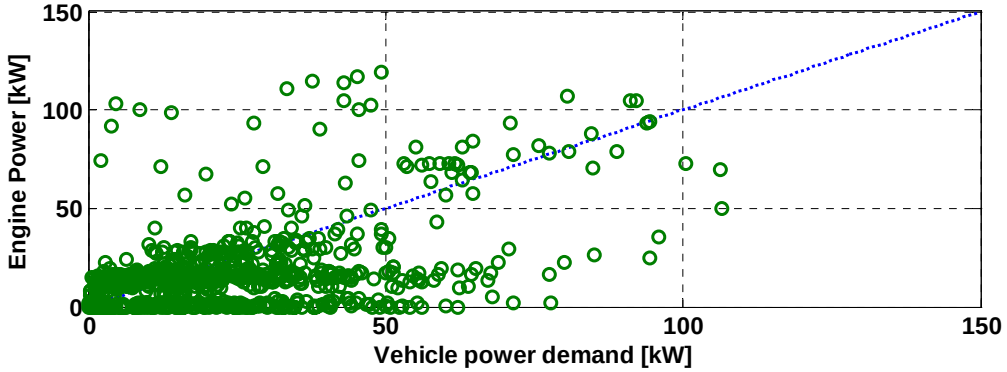

(a) Engine power vs. vehicle power demand

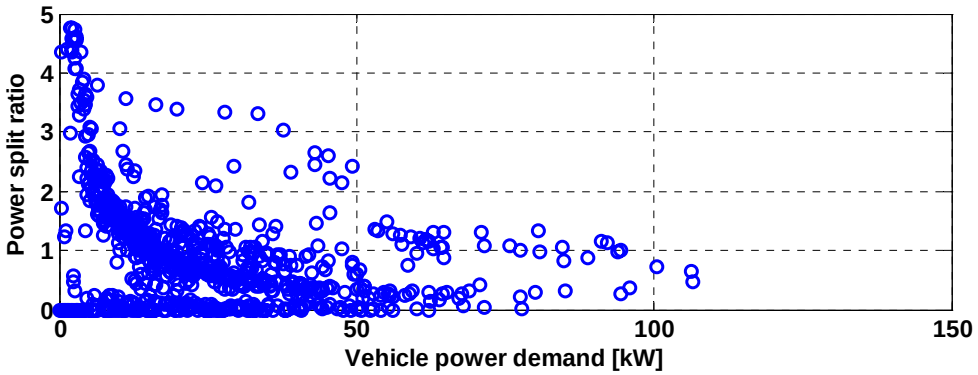

(b) Power-split ratio vs. vehicle power demand

Figure 7. 20. Engine power vs. vehicle power demand during FUDS (β=25)

The integrated fuel consumption is shown in Figure 7. 21. Interestingly, the fuel consumption is not on the minimum BSFC line contrary to the engineering intuition.

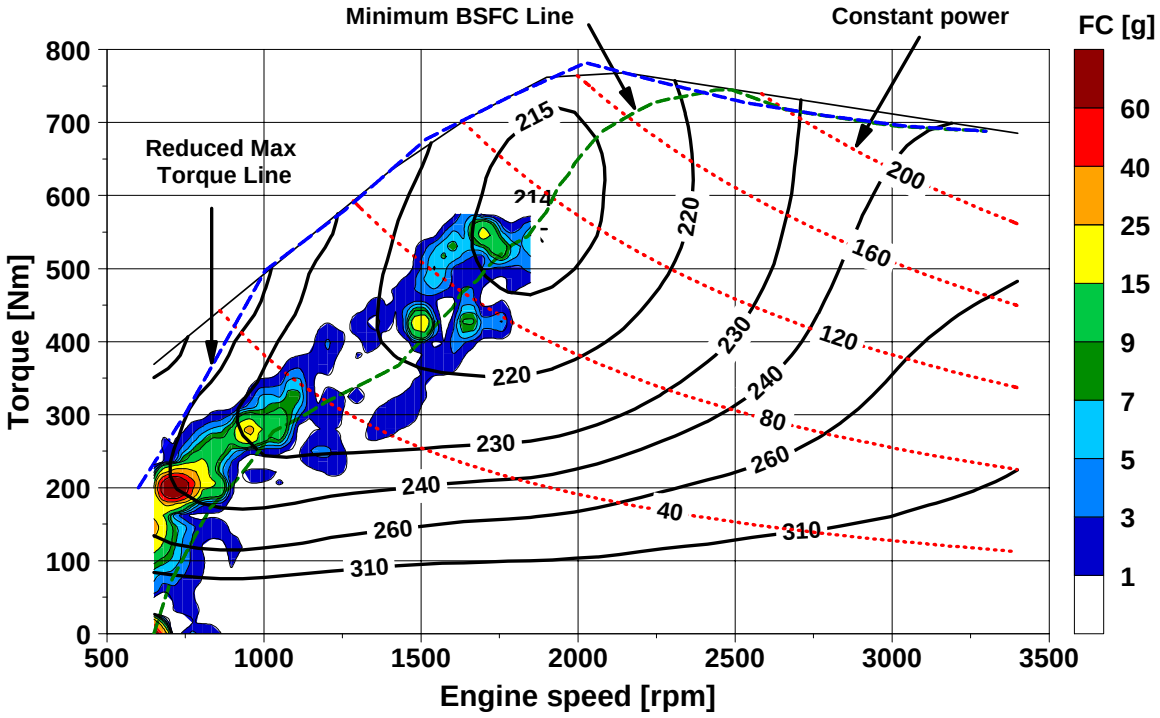

Figure 7. 21. Integrated fuel consumption of PSHH DDP during FUDS (β = 25)

In the systematic perspective, this fact implies that the DDP finds more efficient engine operation area in the system level that is relatively at the low speed and high load area of the engine map.

7.4. Power-Split Hydraulic Hybrid HMMWV Power Management Optimization with Stochastic Dynamic Programming

As for the PSHH system, the studies of implementable optimal power management controls with the SDP technique are almost none. The result of the SDP technique gives full-state feedback control policy from multiple inputs and provides the engine power demand that can be implemented to real-time applications. As a semi-optimized power management, SDP solves an infinite horizon problem with time-invariant system and generates the control policy based on the probability distribution generated from pre-selected samples.

The algorithm of the SDP technique is introduced in Chapter 4 and the same concept is applied to the PSHH. In addition, the generation of the Markov chain is the same as that of the SHH case with the same vehicle model. The same driving schedules are selected for sampling and the vehicle power demand is extracted from the high fidelity

PSHH VESIM. The resultant Markov transition table is slightly different from that of the SHH system but the trend is almost the same as shown in Figure 4. 12.

7.4.1. PSHH SDP Setup

The power relations among the power devices in Equation (7.16) and Equation (7.18) are also used in the PSHH SDP. The vehicle power demand is the sum of the engine, P/M_{gen} and the P/M_{prop} powers. The engine power is calculated from the SDP-full state feedback controller. The P/M_{gen} speed is calculated from the lever rule and the torque is calculated by the output of the engine speed controller whose output is the displacement factor with following the speeder and torquer concept. Thus, the P/M_{gen} power is calculated according to the engine speed demand in the SDP model. The engine speed and torque are assumed to follow the minimum BSFC line even though it does not guarantee the systematic optimization. After the engine power and P/M_{gen} power are calculated, the P/M_{prop} power is calculated from the vehicle power demand. The same power relation is also applied to the actual simulation that implements the SDP controller.

The state and control variables with grid discretization are represented in Table 7. 7. Assuming the engine power is the function of the vehicle power demand, SOC and wheel speed, the resultant SDP controller has the form of a three dimensional look-up table. Grid size is selected to be small enough to reflect the system dynamics but large enough to guarantee the fast convergence and not to delay the actual SDP control application.

Table 7. 7. State and control variables and grid discretization in PSHH SDP

State	Vehicle power demand	-115 :110	20 grids
	SOC	0 : 0.04 : 1	25 grids
	Wheel speed	0:65	15 grids
control	Engine power	0:240	20 grids

Physical constraints of the optimization process are represented as Equation (7.26) ~Equation (7.28). The SOC should be between 0 and 1 and the engine speed and P/M_{prop} torque should be inside given specifications. In contrast to the case of a HEV, the charging and discharging limits are not added because of the high power density of the hydraulic accumulator.

$$0 \le SOC(k) \le 1 \tag{7.26}$$

$$\omega_{eng\_\min} \le \omega_{eng}(k) \le \omega_{eng\_\max} \tag{7.27}$$

$$T_{P/M_{prop}\,min} \le T_{P/M_{prop}}(k) \le T_{P/M_{prop}\,max} \tag{7.28}$$

The Reliable drivability is considered by adding the square distance from minimum SOC (SOC_{min}) to the cost function only when the SOC goes below the SOC_{min} as shown in Equation (7.29).

$$g_k = \begin{cases} fuel\ consumption(k) + \alpha\left(SOC_{min} - SOC(k)\right)^2 & if\ \ SOC(k) < SOC_{min} \\ fuel\ consumption(k) & if\ \ SOC(k) > SOC_{min} \end{cases} \tag{7.29}$$

Even though the hydraulic accumulator does not have the operation limit in the SOC, there exists a SOC_{min} to be maintained during normal driving condition and works as a energy buffer when the unexpected high vehicle power demand in real PSHH applications.

7.4.2. PSHH SDP Result

The result of the SDP has the form of a look-up table with three inputs, SOC, wheel speed and vehicle power demand, and one output, engine power demand. The P/M_{gen} power is decided by controlling the engine speed and the P/M_{prop} power is decided by Equation (7.18). In contrast with other SDP VESIMs, the direct plugging of a PSHH SDP look-up table causes the engine power demand to be oscillatory. In PSHH system, the part of the engine power is directly transferred the wheel and the vehicle power demand is decided by the feedback controller in the driver model from the wheel speed and vehicle power demand is input to the SDP controller. Therefore, it seems that interactions between these controllers make the engine power demand oscillatory. As a countermeasure to reduce the high frequency vehicle power demand input to the SDP controller, a low-pass filter (2^{nd} order Butterworth filter with 1 rad/s pass-band edge frequency) is added between the vehicle power demand input and SDP controller. As a result, the engine power demand becomes smoother and the engine speed control becomes stable.

The tuning of α affects the performance of the SDP controller in maintaining the hydraulic energy buffer and affects the drivability. Larger α guarantees more reliable driving by keeping SOC from dropping below SOC_{min}. The fuel economy is almost the

same when α changes from 100 to 800 but the lowest SOC increase by 0.05 during the 190~220 second region in Figure 7. 22. Therefore, α is proven to be indispensable for the reliable PSHH SDP application and 800 is selected as a baseline value.

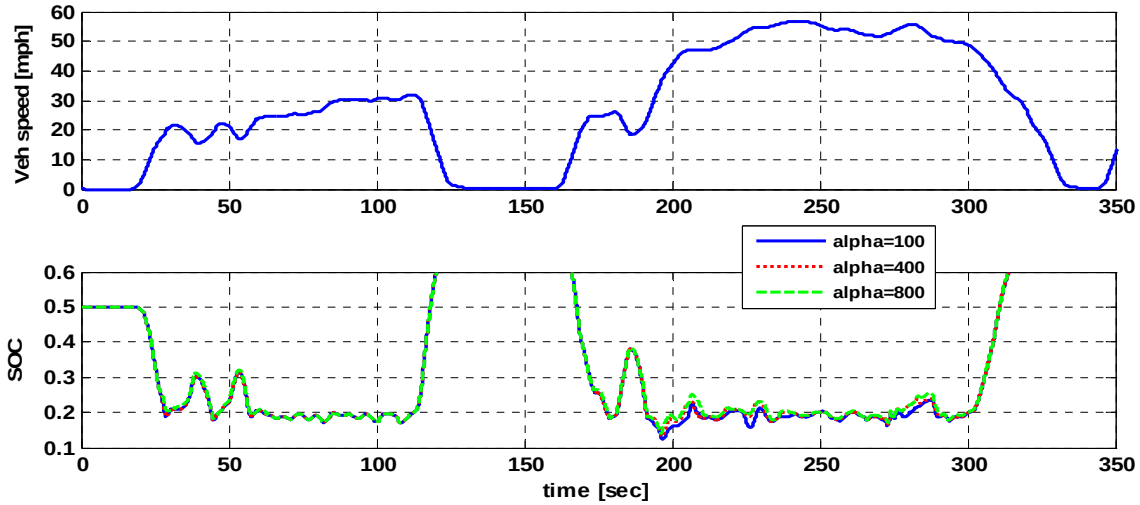

Figure 7. 22. Effect of α on the SOC prediction in PSHH SDP (SOC_{min} = 0.2)

As another tuning factor, SOC_{min} works as the level of the hydraulic energy buffer in Figure 7. 23.

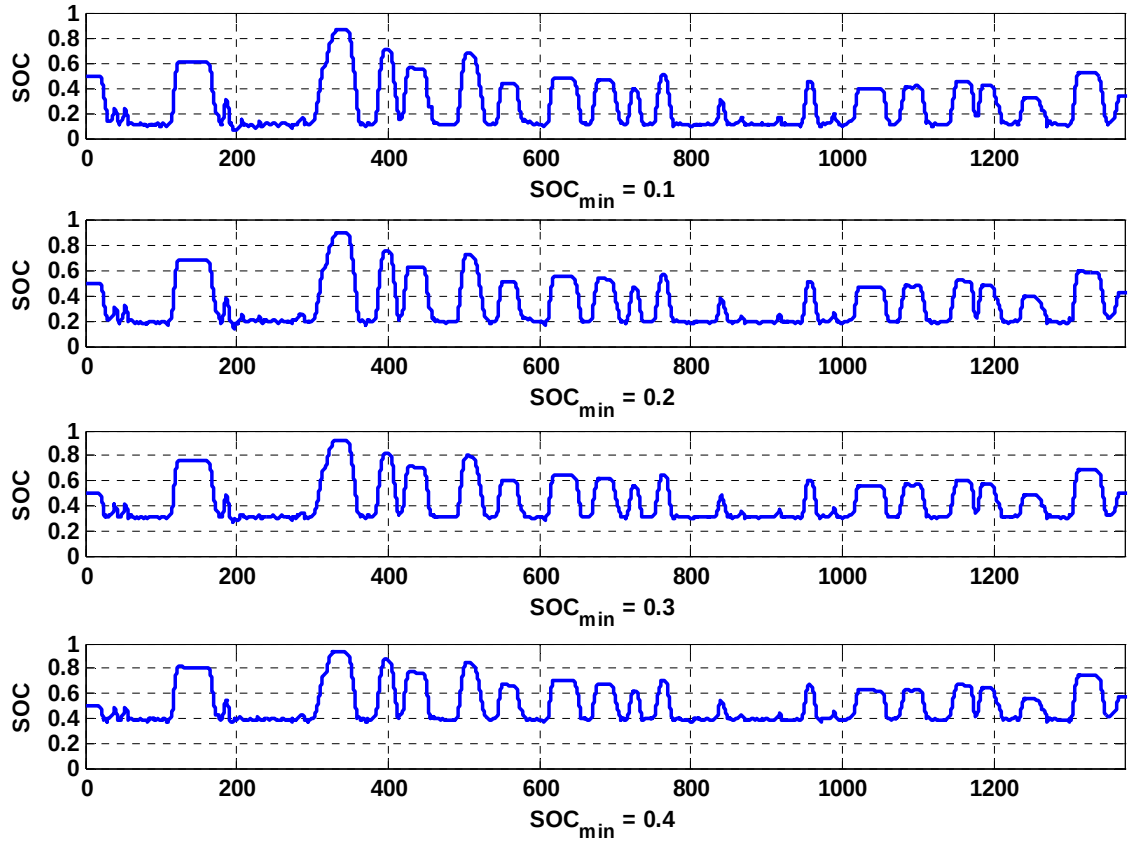

Figure 7. 23. Effect of SOC_{min} on the SOC prediction in PSHH SDP (α = 800)

Because the accumulator size is large enough to capture the regenerative braking energy completely up to the SOC_{min} of 0.2, the fuel economy is almost the same below the SOC_{min} of 0.2 and fuel economy decreases about 2% in the case of SOC_{min} of 0.3. As a result, SOC_{min} of 0.2 is selected as the baseline SOC_{min} improving fuel economy without degrading the driveability. The three dimensional representation of the final SDP controller according to the wheel speed is shown in Figure 7. 24. Instead of using the power split ratio, using the direct engine power output removes the possibility of the infinite engine power demand and smooth transition when the vehicle power demand is close to zero or changes the sign, respectively. Interestingly, the engine power demand proves to be a week function of the wheel speed except in the braking case.

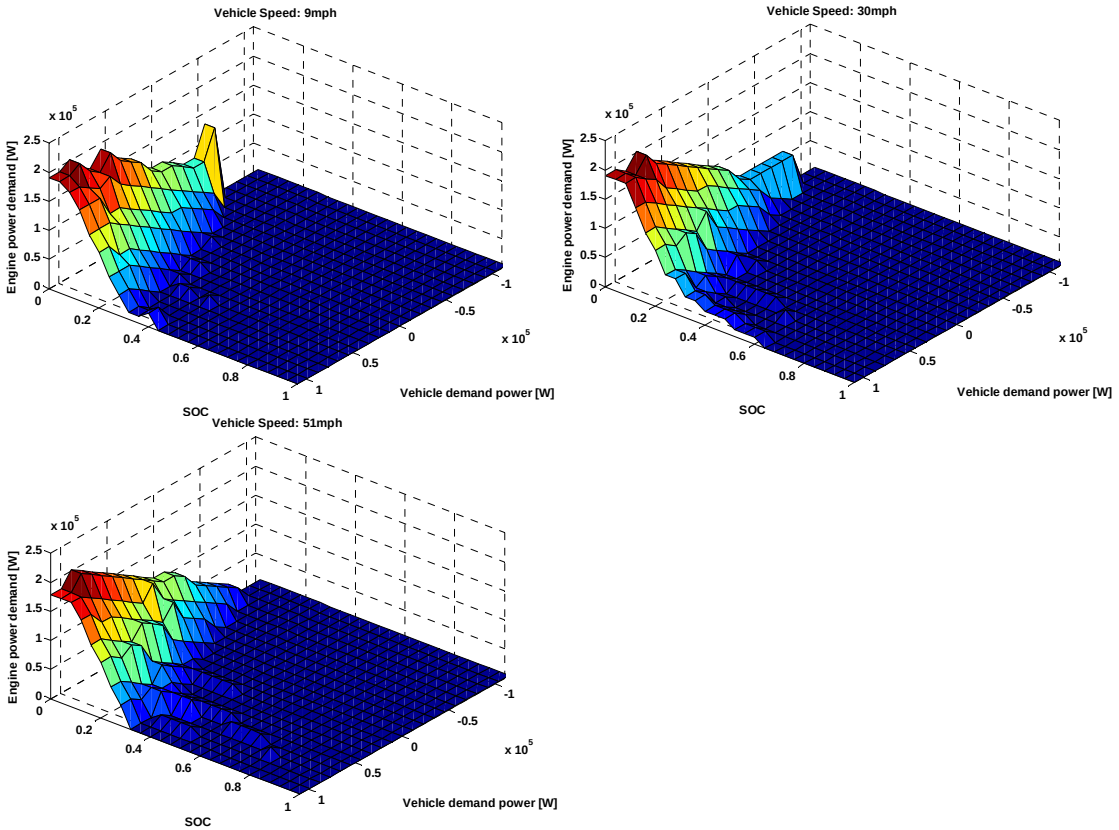

Figure 7. 24. Engine power demand in the optimal PSHH SDP controller

The system behavior and the engine power vs. vehicle power demand in the SDP control case during FUDS are shown in Figure 7. 25. The rate of the engine power demand is very high. With this high rate of the engine power, the engine and P/M_{gen} can use the high load area and improve the system efficiency. However, the engine speed becomes more transient.

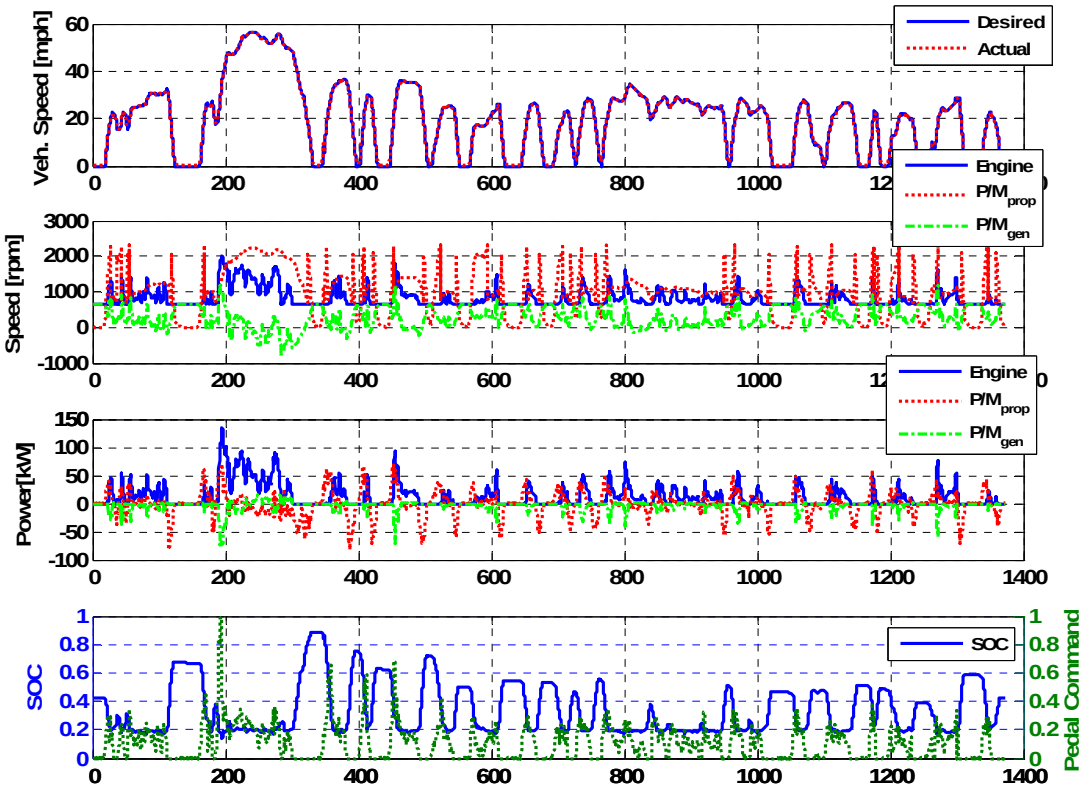

(a) System behavior during FUDS

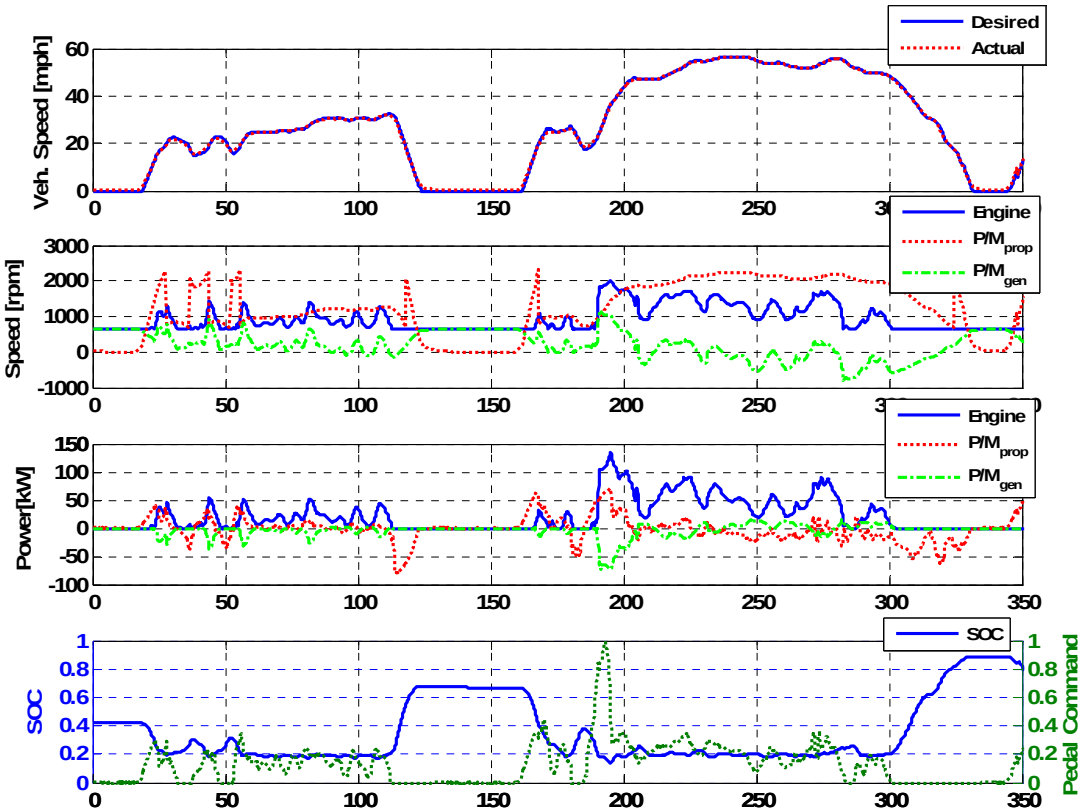

(b) Zoomed system behavior (0~340 second) during FUDS

Figure 7. 25. System behavior of PSHH SDP during FUDS

Therefore, this transient engine power demand can cause the speed control problem in the real PSHH vehicle application and increase the transient emissions. The effects of the SDP control in the PSHH system are validated with a real engine in the EIL test in Chapter 8.

The integrated fuel consumption in the simulation shows that the engine speed and torque is controlled well on the minimum BSFC map in Figure 7. 26.

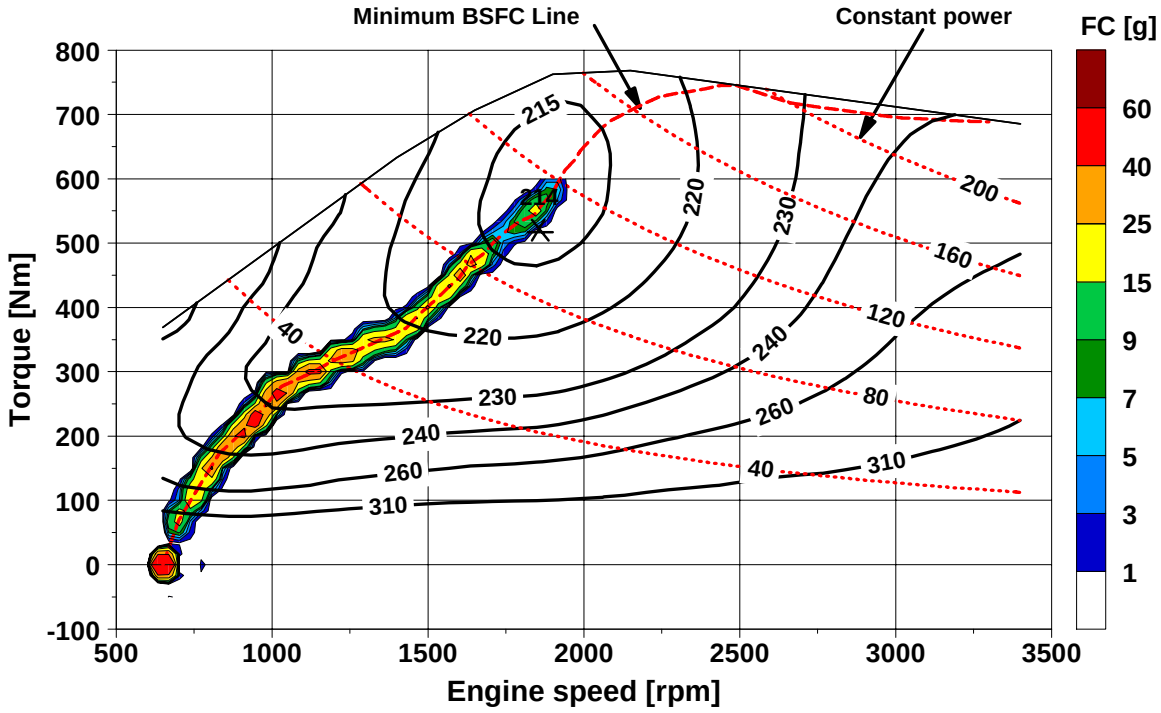

Figure 7. 26. Integrated fuel consumption of PSHH SDP during FUDS

Interestingly, SDP controller avoids the engine charging as modulated SOC control does in Figure 7. 27. Considering the engine power should be larger than the vehicle power demand because of the energy conversion loss and mechanical loss in the PSHH system, it seems that the engine-only drive and hydraulic-only drive occupies most of the total driving schedule and hydraulic-assist drive is used for the transition between the engine-only drive and hydraulic-only drive.

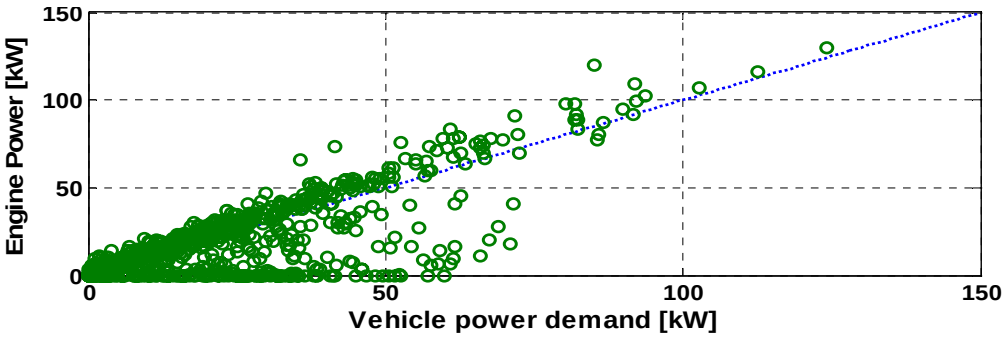

(a) Engine vs. vehicle power demand

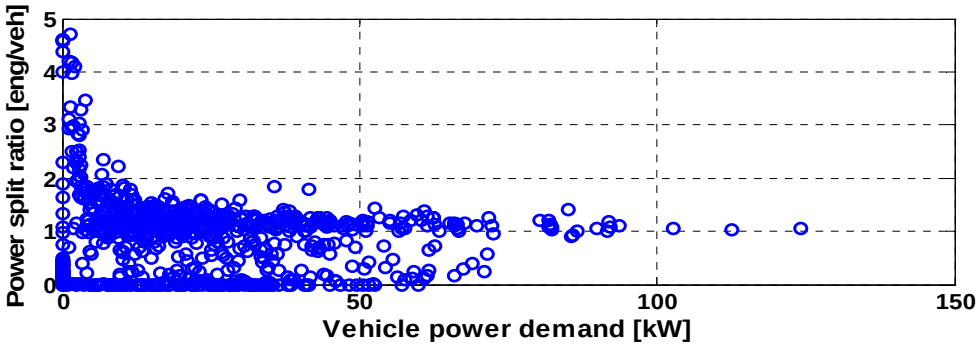

(b) Power-split ratio vs. vehicle power demand

Figure 7. 27. Engine power vs. vehicle power demand with PSHH SDP during FUDS

Finally, PSHH SDP is tested for various cycles as shown in Table 7. 8. The SDP gives almost the same fuel economy for all driving schedules including the cycles that are not used for the SDP controller training, i.e., Markov chain modeling. While the fuel further fuel economy improvements were not realized, the SDP direct state-feedback maps have a potential advantage of being more stable in practical implementations.

Table 7. 8. Fuel economy comparison between the SDP and modulated SOC control without idle-stop

Cycle (* not used for training SDP)	Modulated SOC control	SDP	Fuel economy improvement [%]
NYCC*	14.2	14.1	-0.6
WVUCITY	15.6	15.6	-0.2
UDDSHDV	16.4	16.4	0.0
SC03*	18.5	18.5	0.1
FUDS	19.3	19.4	0.3
WVUSUB	18.8	18.9	0.4
WVUINTER*	16.8	16.7	0.0
HWFET	16.9	16.9	-0.1

CHAPTER 8

VALIDATION WITH ENGINE-IN-THE-LOOP CAPABILITY

Aggressiveness of the driving schedules is known to affect the fuel economy significantly for a given propulsion system. Thus, defining the representative drive cycle is very critical for the initial vehicle system selection and influences the design and development of the vehicle system. In the case of the hybrid system, the fuel economy according to the driving schedule characteristics shows very different trends from the conventional vehicle case. However, there has not been a comprehensive study on the drive cycle effects on the fuel economy according to the hybrid configurations and instead most studies have been concentrated on the driving schedule effects on a pre-selected hybrid vehicle configuration. The fair comparison according to the degrees of hybridizations that is pursued here has the goal of including the choice of vehicle architecture into the hybrid design process. The synergetic experiments are pursued for validation of simulation predictions and assessment of the impact of design and power management on emissions.

In this study, the fair fuel economy comparison among three typical hydraulic hybrid configurations according to the aggressiveness of driving schedules is firstly performed by using the optimized designs and optimized power managements for each hydraulic hybrid system. The optimally designed parallel, series and power-split hydraulic hybrid systems satisfies the same performance constraints and the SDP control is used as a supervisory powertrain control for each system.

Supervisory power management controls in hybrid vehicle systems usually use the high load and high rate of power demands to improve the system efficiency with exclusive engine and secondary power device operations independently of driver's power demands. As a result, improved system efficiency or fuel economy through the high load and high rate of the power demand are accompanied by transient exhaust emissions. For example, the high rate of the engine power demand increases hydrocarbon emissions and

especially particulate matter (PM) in the case of diesel engines. While in principle there is a strong potential to reduce emission with hybridization, the high level of freedom in control and coupling of the engine to a highly dynamic device can make the emission control demanding [49]. The vehicle-engine simulation models in this study use the static engine map to predict the fuel consumption and exhaust emissions. Even though the engine model has a calibrated delay function compensating engine dynamics, e.g., turbo-lag, transient effects on exhaust emissions are known to be significant in real engine operations [40]. Accurate predictions of transient emissions are still challenging even with highly complicated CFD models including chemical kinetics models [116], [117]. In addition, computational loads of such sophisticated simulations are too high to be used for system assesses and power management evaluations during driving schedules. As a result, the direct application of a real engine into the virtual simulation becomes the most viable alternative option to predict accurately impacts of the powertrain design and power management control on exhaust emissions [105]. Thus, the Engine-in-the-Loop (EIL) setup can be a way to simulate system behaviors and transient emissions of real vehicle applications. The largest advantage of the EIL test is that it can measure actual emissions and fuel consumption with still keeping simulation advantages, e.g., convenient changes of devices and power management controls without an actual vehicle and an expensive chassis-dynamometer system. In addition, numerous error sources from real vehicle tests, e.g., noise, can be removed, and more repeatable and relatively inexpensive tests can be possible. In addition, the scaling of a real engine can extend advantages of the EIL test by simulating different sizes of a real engine. However, in contrast to the noiseless pure simulation environment, the EIL test should overcome the noise from the real engine and the dynamometer system controllers need to have the high enough bandwidth to control the engine speed and torque by reducing system delays. Measurement devices also need the fast response time to capture transient exhaust emissions.

In this study, with the same engine and EIL test setup introduced in Chapter 5, three typical hydraulic hybrid systems are firstly tested and compared with the real engine in the simulation loop. Challenges and countermeasures in developing the EIL setup are described for each hybrid system. As a result, effects of hybrid systems and power

managements on the transient fuel consumption and emissions are measured and analyzed with a real engine in the loop during FUDS.

8.1. Effects of Driving schedules and Hydraulic Hybrid Systems on Fuel Economy

The simulation results of the relationships among driving schedules and hybrid configurations are shown in Figure 8. 1 and Figure 8. 2. For fair comparisons, all hybrid systems designed are optimized with same vehicle performance constraints and optimized SDP controllers are used as power management controls.

First, the trend of the fuel economy in the conventional vehicle seems to increases as the average vehicle speed increases and the idle time and the number of vehicle-stops decrease according to cycle characteristics (see Table 4. 5).

In the case of without idle-stop in Figure 8. 1 (a), most hybrid systems show the best fuel economy at FUDS which has the highest number of the vehicle-stop and relatively large regenerative braking energy from the high average vehicle speed in comparison with other driving schedules that have similar number of vehicle-stops. As the total idle time increases or regenerative-braking chances decrease, the fuel economy values of hybrid vehicle systems decrease. In the case of the HWFET, fuel economy gains are only derived from the system efficiency of the each hybrid system, so the PSHH system shows the best fuel economy proving fuel-efficient engine operations and the direct transfer of the part of the engine power maximize the system efficiency. The fuel economy data of the parallel hydraulic hybrid system is even higher than that of the SHH system if 4x4 option is the simultaneous operation. As a result, the sequential 4x4 operation is indispensable for the fuel-economy oriented vehicle propulsion in the case of the SHH system.

In most of the driving schedules, PSHH system tops other hybrid systems except WVUCITY and NYCC, extreme city-driving schedules. In the case of these extreme city-driving schedules, SHH system with sequential 4x4 operation shows best fuel economy. It seems that it is because the propulsion and regenerative braking energy is most efficiently done by the sequential 4x4 operation due to the high efficiency using the high load with the smallest P/M_{prop}.

In the case of with idle-stop in Figure 8. 1 (b), the fuel economy gap between the SHH system with sequential operation and PSHH system increases because the idle-stop

time is longer in the case of the SHH system because SHH system absorbs more regenerative braking energy and has longer hydraulic-only drive.

The best fuel economy is shown for most of hybrid configurations at WVUSUB that has more idle time than FUDS. Worst fuel economy is shown for most of hybrid configurations at HWFET that has rare chances of the idle-stop. Interestingly, PHH system tops at WVUCITY and NYCC without the friction loss of the torque converter and shows better fuel economy than the SHH system with simultaneous 4x4 operation for most driving schedules. Except for the severe city driving schedules, e.g., WVUCITY and NYCC, PSHH system tops other hybrid configurations.

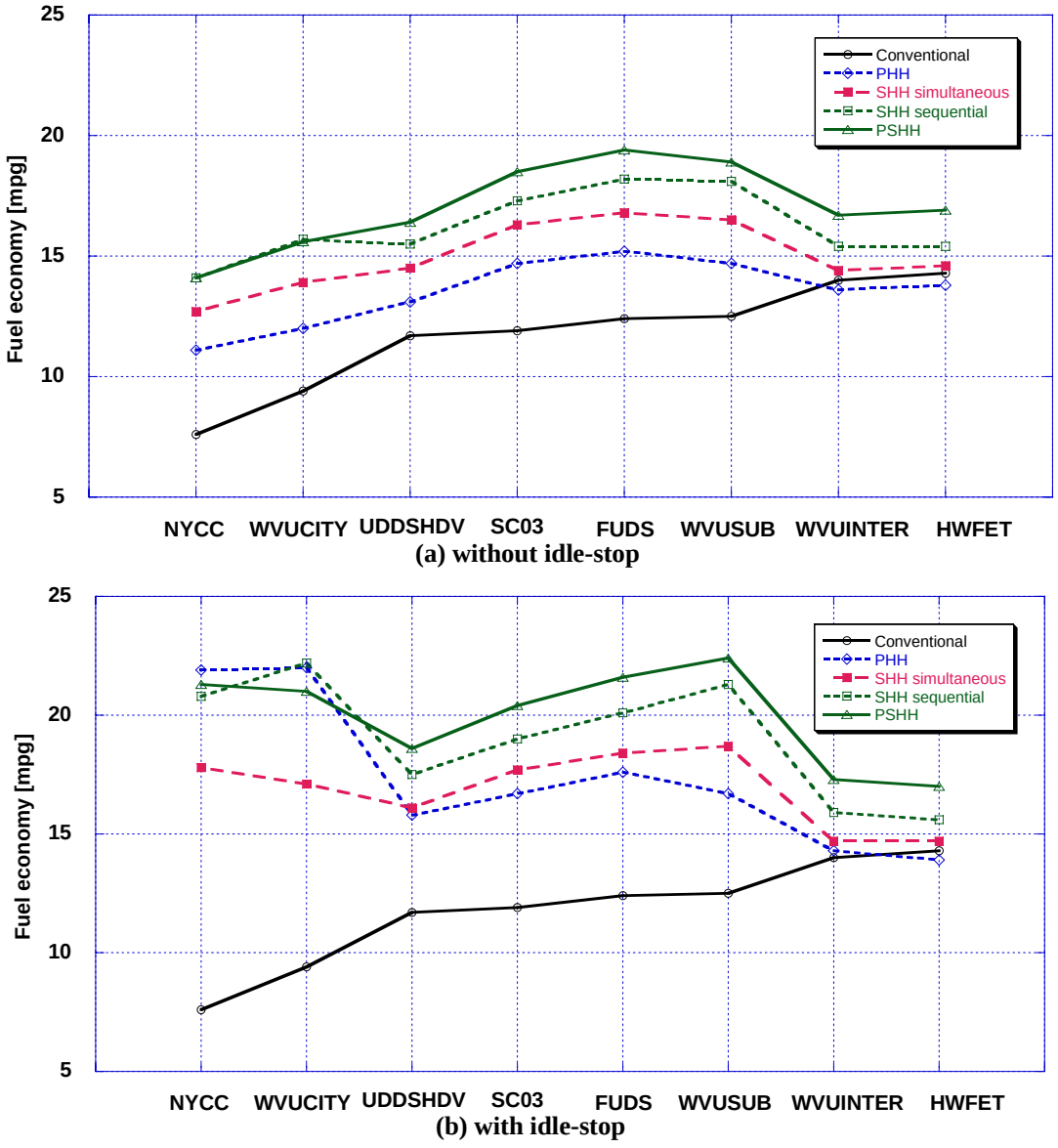

Figure 8. 1. Fuel economy according to driving schedules and hybrid configurations

Fuel economy improvements over the conventional vehicle case are shown according to driving schedules and hybrid systems without idle-stop in Figure 8. 2 (a). Fuel economy improvements increase as the driving schedules are close to city cycles which have the low average speed, many stops and long idle time because the absolute value of the fuel economy of the conventional vehicle is low. In these city-driving schedules, the engine uses the inefficient low load area in the conventional vehicle. In the case of the UDDSHDV, the fuel economy of the conventional vehicle is relatively high because it has the high-speed portion that uses the high engine load area, so most of the hybrid-system fuel economy improvements have a dip.

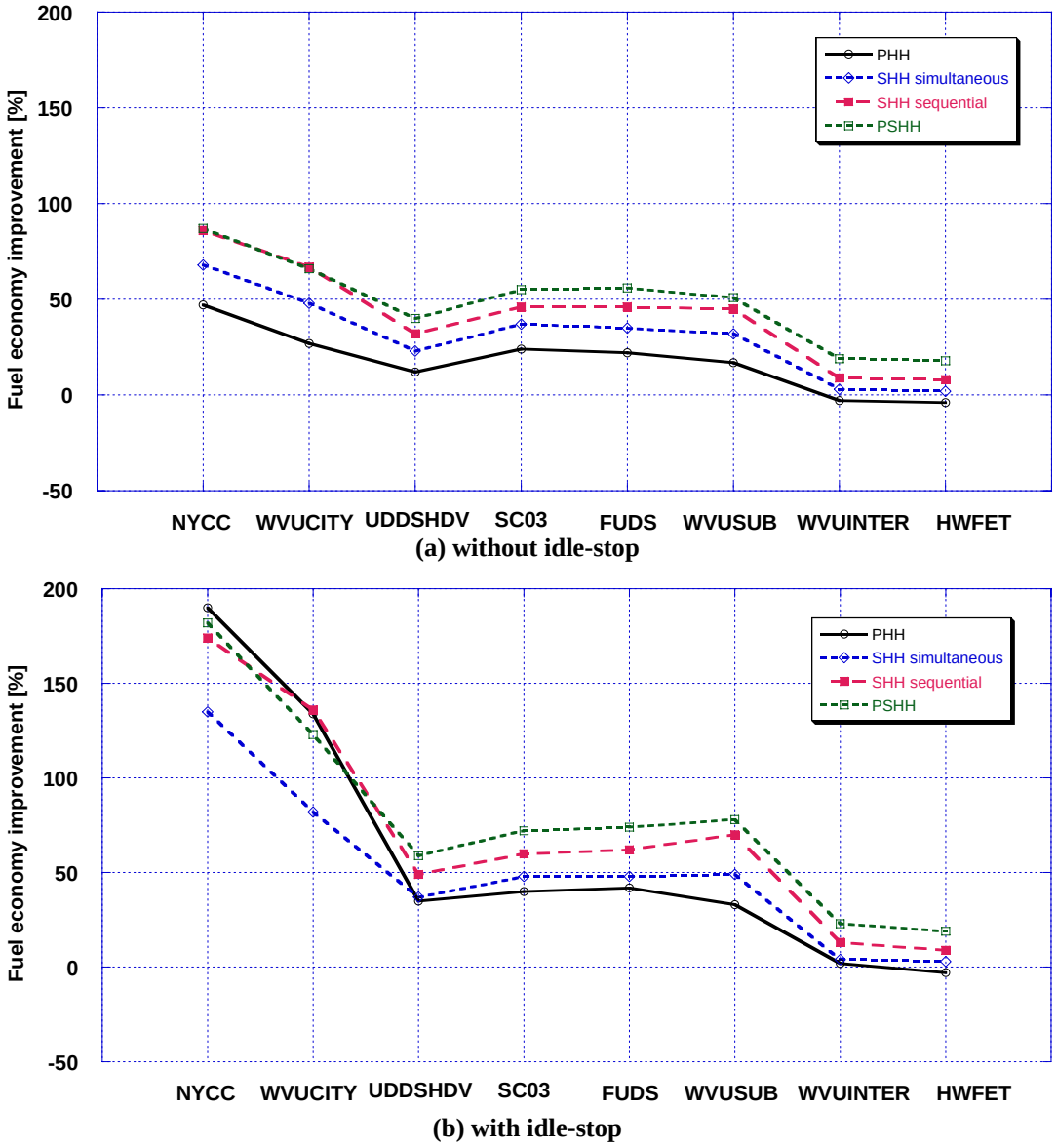

Figure 8. 2. Fuel economy improvement according to driving schedules and hybrid configurations

.In the case of with idle-stop, the fuel economy improvements dramatically increase at city cycles in Figure 8. 2 (b). Parallel configuration tops the fuel economy improvement at city cycles showing how significant the idle fuel consumption is in PHH system. The SHH system with simultaneous 4x4 operation shows the lowest fuel economy improvement with relatively short total idle-stop time.

8.2. Engine-in-the-Loop Test Result

As verifications of simulation results, all hybrid systems are tested by EIL tests with the fuel-economy oriented optimization of the design and power management. The driving schedule used for EIL tests is FUDS for all hybrid systems.

8.2.1. Conventional Vehicle Result

The conventional vehicle system, introduced in Chapter 3, is used for the EIL test. The engine speed output calculated from the drivetrain model and the engine rack signal derived from the driver's accel-pedal signal are provided to the dynamometer system.

The conventional vehicle test is carried out first for the baseline fuel economy and exhaust emission data (see Table 8. 1). The absolute values of fuel economy and emissions of a conventional vehicle are different from the values presented in Chapter 5 because the test conditions are different, e.g., air temperature, pressure, humidity and fuel property. However, relative comparison among data of different systems can be possible in this chapter because the test repeatability is validated by repeating baseline tests (see Table 8. 1.

Table 8. 1. EIL test result of the conventional vehicle

	Fuel economy [mpg]	NO_x [g/km]	Soot [g/km]
Mean (3 times)	11.0	3.35	0.147
Standard deviation	0.04	0.17	0.004

System behaviors are shown in comparison with pure simulation results in Figure 8. 3. Vehicle speeds are almost the same and the engine speed and torque measurement show sharp peaks in the EIL test but except peaks, pure simulation and EIL results are similar. As a result, the fuel consumption predictions are similar and differences are only sharp peaks between the EIL test and simulation.

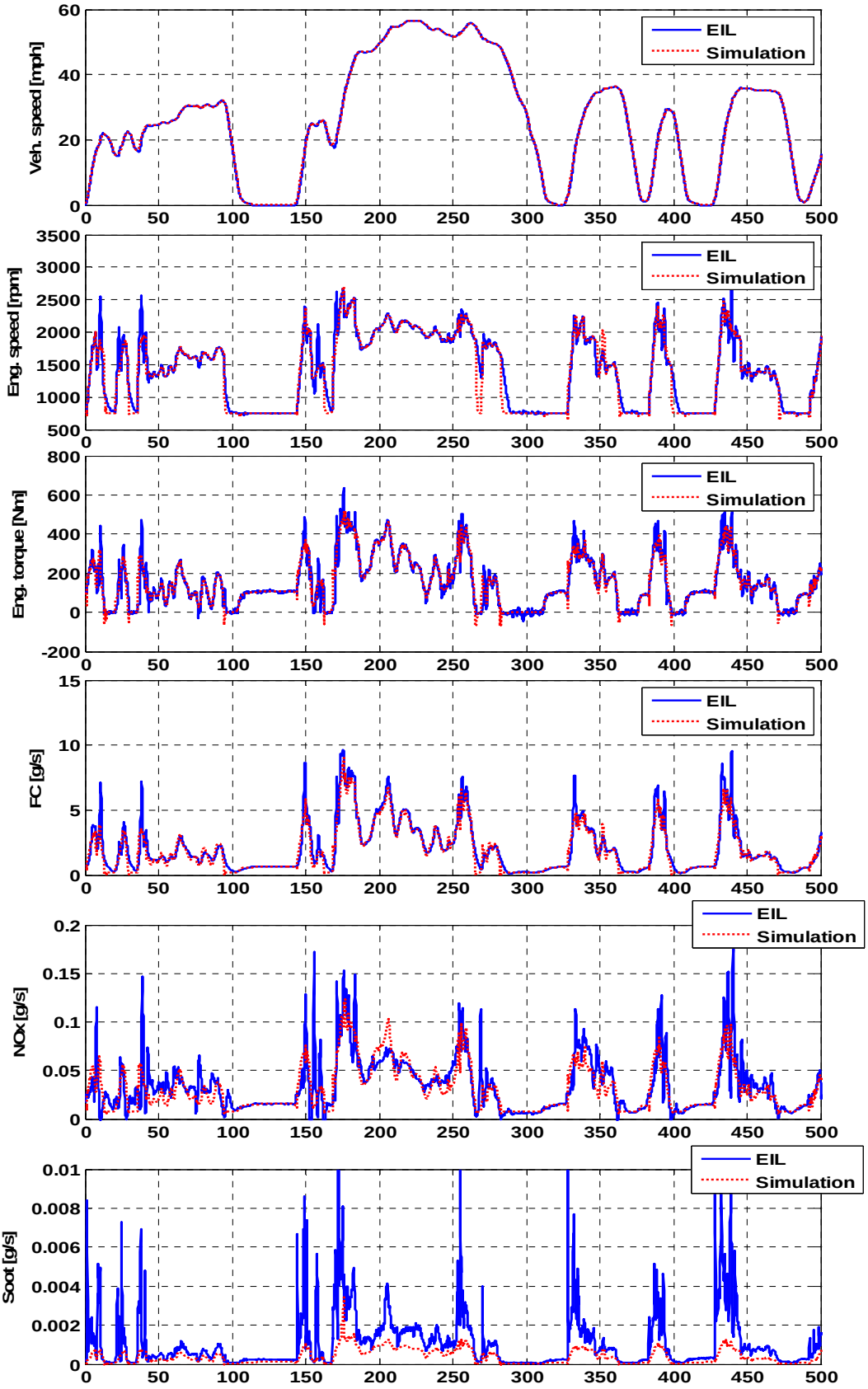

Figure 8. 3. Comparison between simulation and EIL test in the conventional vehicle

In the case of exhaust emissions, the simulation results only show rough trends of a real engine test results. Because the exhaust emission formation has different mechanisms from the fuel consumption, predictions with steady engine maps do not seem to be appropriate. Simulated NO_x data show relatively similar measurements with the integrative measurement of the AVL Combustion Emissions Bench II system [36], [50]. However, even with integrative NO_x measurements, peaks in the EIL test represent how transient the engine operations are.

Fast-response soot emission measurements show dramatic transient effects of the conventional vehicle's engine operations. As a result, deviations from simulation results are significant and show steep peaks at every beginning part of the engine tip-in. These results show how dominant transient effects are in the exhaust soot-emission generation and prove that the static soot map model is impossible to predict exhaust soot emissions of a real engine during cycle simulations.

Soot concentration measurements during FUDS are shown in Figure 8. 4. As described in Chapter 5, soot concentration of 77mg/m^3 is assumed as a visual limit corresponding to roughly Bosch number of 2.0. The high soot concentration appears at every tip-in condition and it is transient phenomenon. Exhaust soot concentration crosses over the visual limit in 37 times during FUDS.

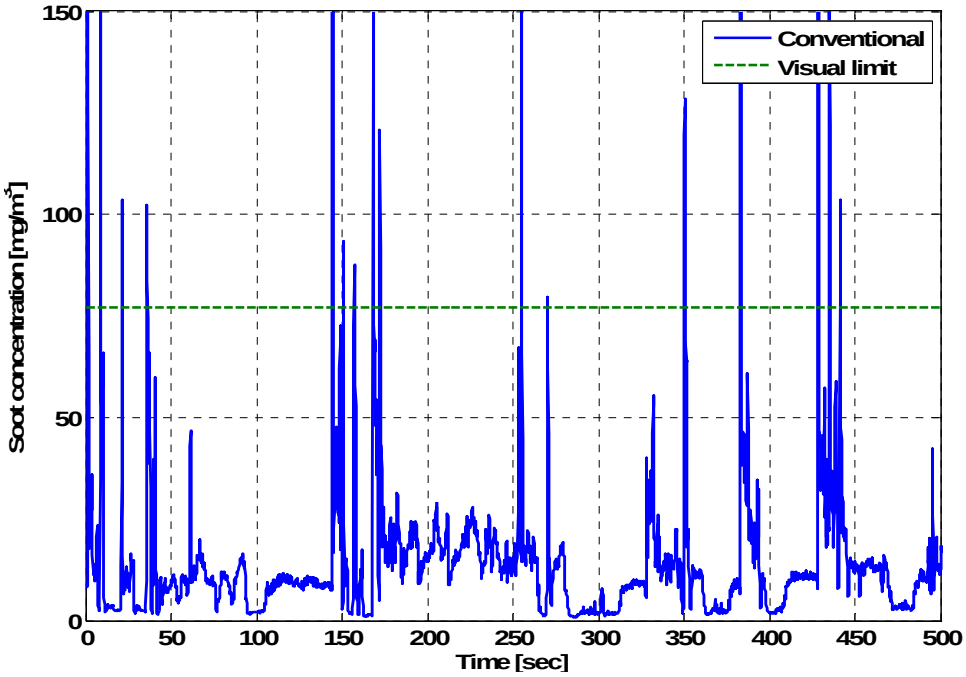

Figure 8. 4. Soot concentration measurement of the conventional vehicle in FUDS

The integrated fuel consumption of the real engine is shown in Figure 8. 5.

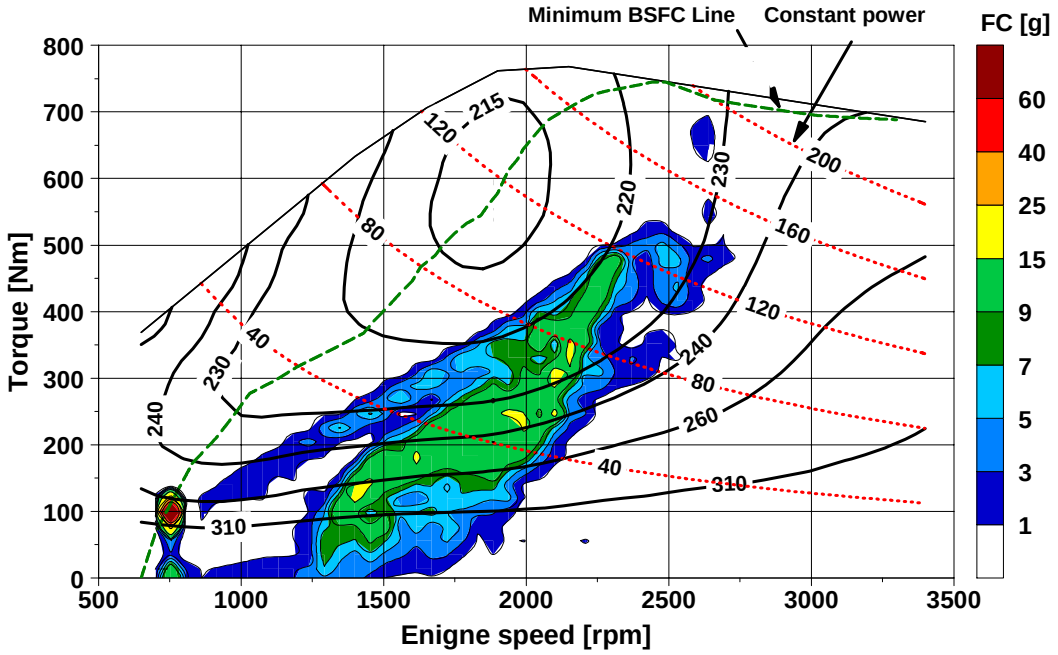

Figure 8. 5. Integrated fuel consumption of the conventional vehicle in the EIL test during FUDS

It can be seen that even though the absolute fuel consumption amount is not high, transient engine operations happen at the tip-in when the engine load increases from the idle to the high load and speed area. Most engine-operation points are distributed around the high speed and low torque area where the engine's fuel efficiency is relatively low. In addition, with torque converter, the fuel consumption at idle condition is significant in the conventional vehicle.

8.2.2. Parallel Hydraulic Hybrid System Result

The PHH vehicle system with optimized design and power managements, presented in Chapter 6, is used for the EIL test. The engine speed output from the drivetrain model and the engine rack signal calculated by the supervisory control are inputs to the dynamometer system. The PHH system model with fuel-economy oriented optimized design and power managements is the simulation part of the EIL setup. Even though the actual engine stop-and-start strategy is not applied in the current EIL setup, the fuel economy in the case of with idle-stop capability is post-processed without counting for the fuel consumption during the idle condition, when the engine power demand is zero. However, starting fuel consumption, NO_x and soot emissions are counted for the total

fuel consumption according to the pre-set engine starting condition as presented in Chapter 5.

The EIL test results are represented in Table 8. 2. The sub-optimal rule-based power management case shows slightly better fuel economy than SDP control and around 30 % of the fuel economy improved without idle-stop for both power managements. In the case of with idle-stop, the rule-base power management case has 50% of the fuel economy gain over conventional vehicle and SDP control case has 40% of the fuel economy improvement. The fuel economy gap between rule-based and SDP controls increases because the total idle time is much longer in the rule-based control case with extremely exclusive engine and hydraulic power usages. The fuel economy gap of pure simulation results between both power managements is 6.7 % in Chapter 6 but is reduced to only 3.5% in the EIL test because of critical transient effects.

In the rule-based control case, more than 20% of NO_x reduced but 40% of soot increased in comparison with the conventional vehicle case. In the most pure simulations, both exhaust emissions decrease as fuel consumption decrease in comparison with conventional vehicle case. These results mean that transient effects are so dominant that soot emissions increase significantly and NO_x decrease so much showing the clear trade-off relation. In the case of the SDP control, about 40% of soot decreases from conventional vehicle case with 7% decrease in NO_x. In simulations, the soot amount is around 0.0225 g/km for both power managements that is 25% lower than 0.031 g/km of the conventional case. As a result, it can be said that gaps between simulation and EIL test results increase, as the supervisory power management demands more transient operations among power devices.

Table 8. 2. EIL test result of PHH with modulated SOC control and SDP control

(without / with idle-stop)	Rule-based control	SDP
Fuel economy [mpg]	14.2 / 16.5 (29 / 50 %↑)	13.7 / 15.6 (27 / 42 %↑)
NO_x [g/km]	2.57 / 2.01 (23 / 40%↓)	3.10 / 2.60 (7 / 22%↓)
Soot [g/km]	0.207 / 0.185 (40 / 26%↑)	0.0877 / 0.0820 (40 / 44%↓)

The system-behavior predictions of the simulation and EIL test during FUDS are shown for the sub-optimal rule-based control case in Figure 8. 6. In the rule-based

control case, the key feature of the power management is extremely exclusive operations of the engine and hydraulic power. In addition, transient effects increase because of system delays including the turbo-lag of the real engine in the EIL setup. Therefore, the engine power data show higher peaks and the vehicle has problems in following the reference driving schedule at the point when the vehicle-driving power changes from the hydraulic to engine power because of the engine power delay. Differences in SOC predictions derive from the system delay in the EIL test and make the engine power predictions different between simulation and EIL test results. As for exhaust soot emissions, it is especially sensitive to transient engine operations and large spikes happen in the every engine tip-in condition.

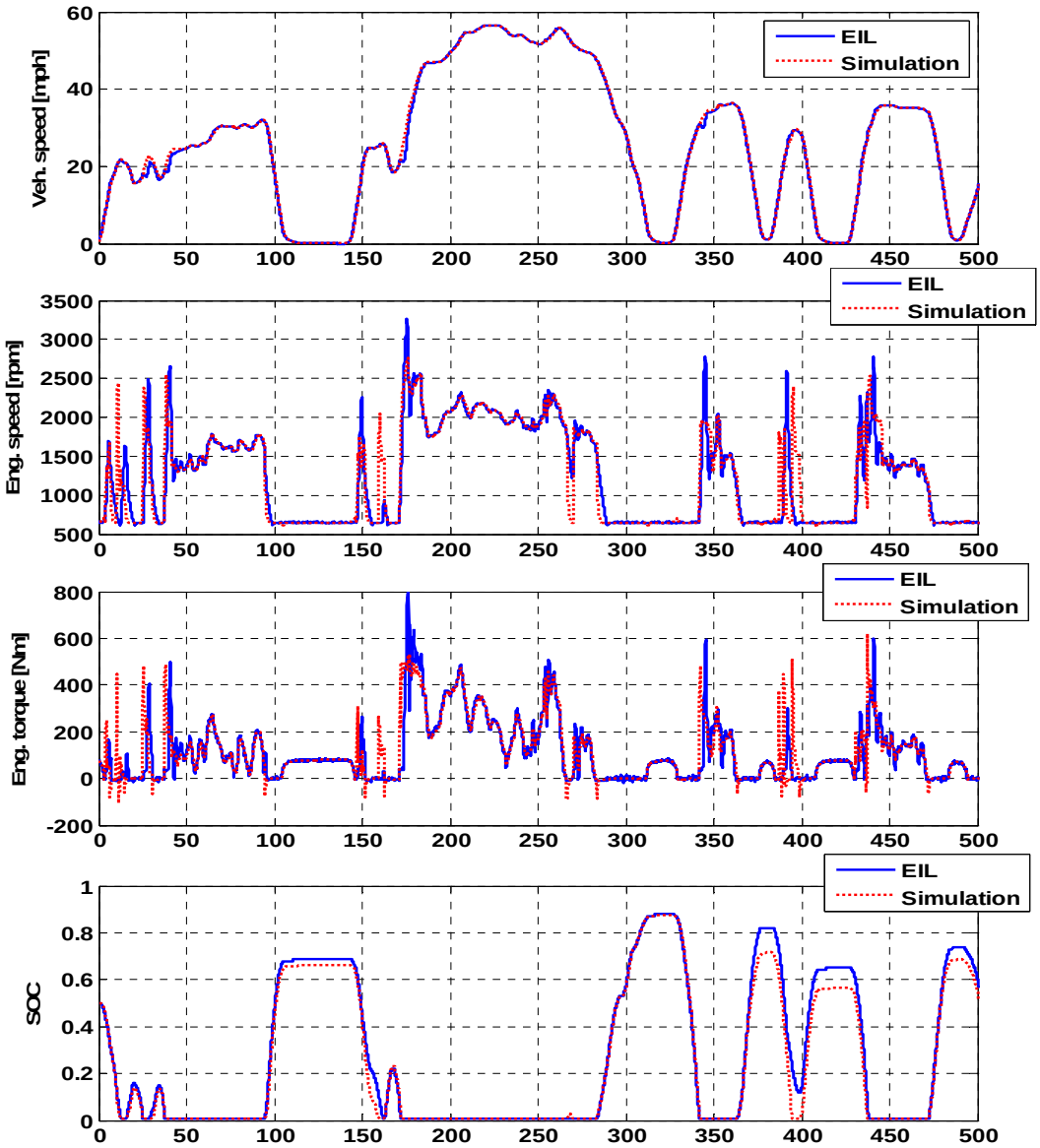

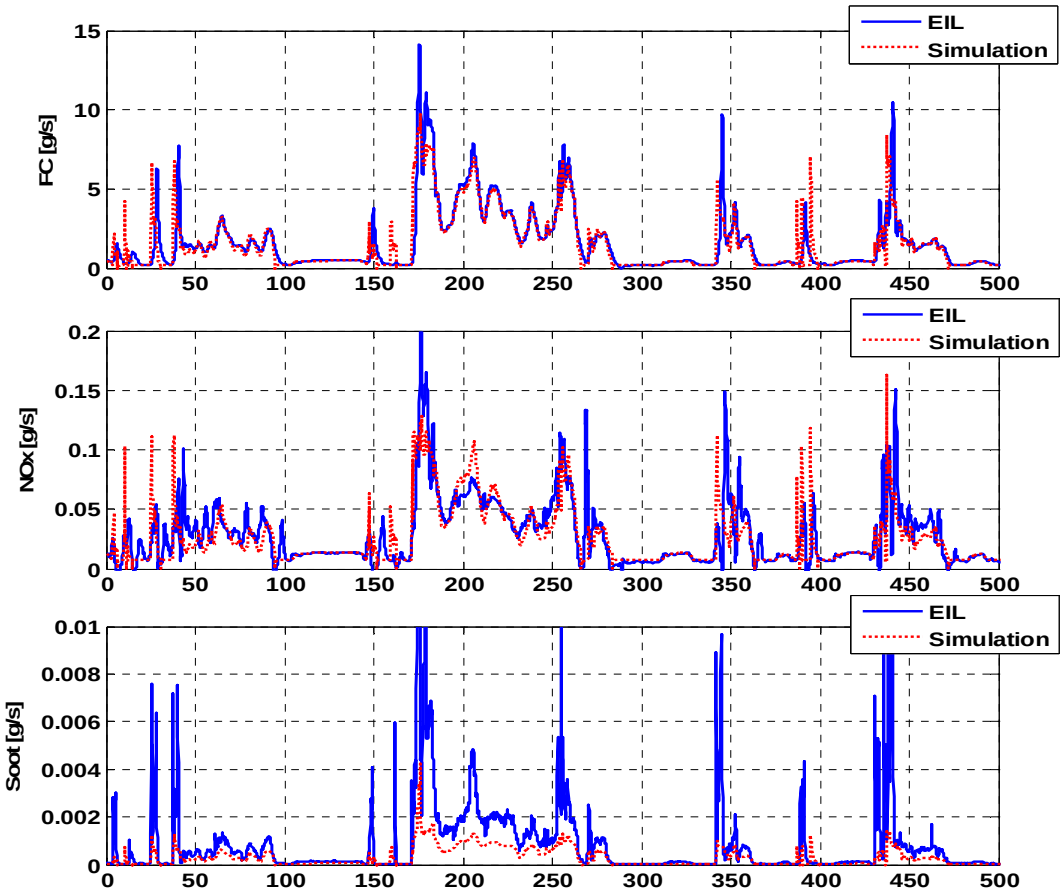

Figure 8. 6. Comparison between simulation and EIL test with rule-based control in PHH

The system-behavior predictions of the simulation and EIL test during FUDS are shown for SDP control in Figure 8. 7. In the case of the SDP control, the SOC is controlled slightly over zero and the engine power demand becomes smoother than that of the rule-base control case. Thus, vehicle follows driving schedule reliably with fewer and smaller excursions. The SDP control case shows slight loss in fuel economy but shows both NO_x and soot reduction in comparison with conventional vehicle case.

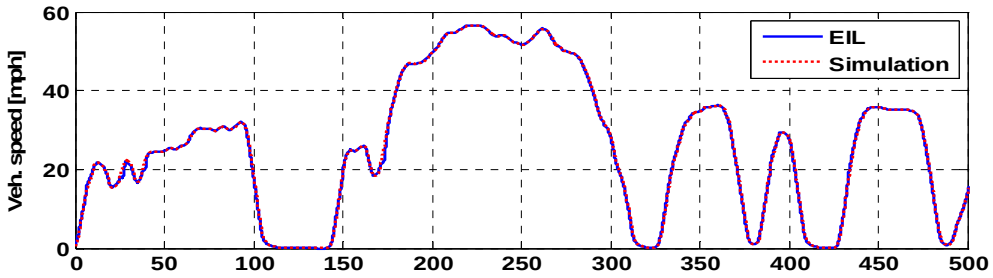

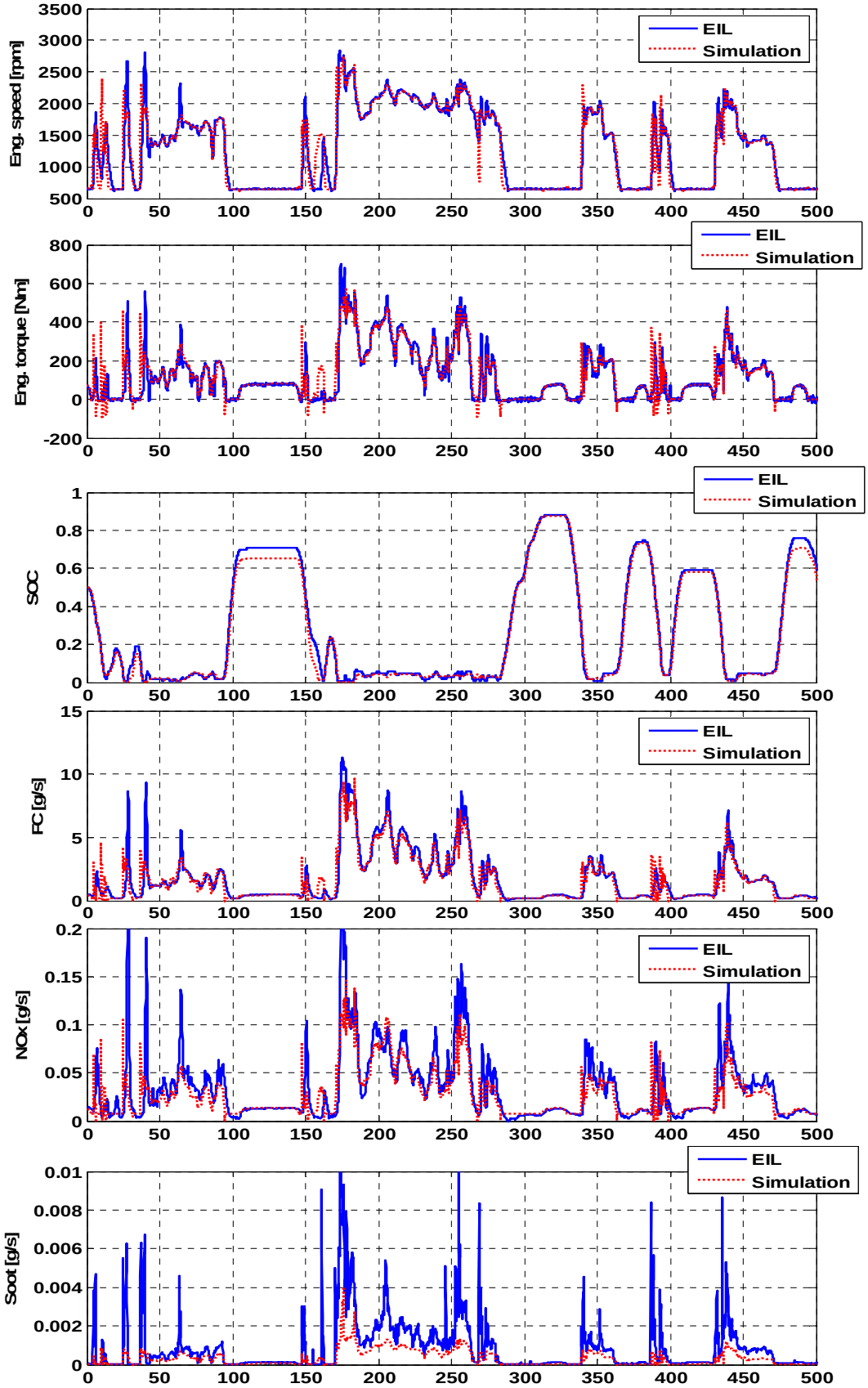

Figure 8. 7. Comparison between simulation and EIL test with SDP control in PHH

With extremely exclusive usages of the engine and hydraulic power, PHH system causes higher soot concentration when the engine kicks in and shows more visual signatures than the convention vehicle case in the case of the sub-optimal rule-based power management. In the case of the SDP control, the number of visual signatures during FUDS decreases and two more visual signatures than conventional vehicle case are predicted (see Table 8. 3). As a result, rule-based power management is proven unsuitable for the actual PHH vehicle application.

Table 8. 3. The number of times over visibility limit during FUDS in PHH

	Number of times
Rule-based control	48
SDP control	41

The soot concentrations are compared between rule-based and SDP power managements in Figure 8. 8. The soot concentration of the sub-optimal rule-based power management case has higher peaks with more frequent visual signatures than SDP case. In addition, the visual signatures last longer in the rule-based control.

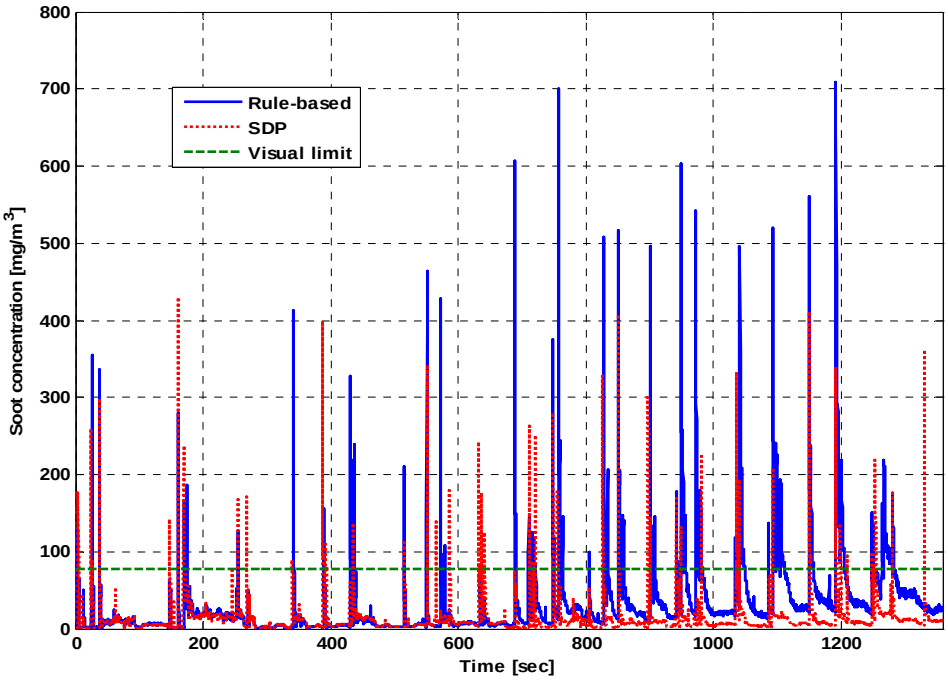

(a) during the total cycle

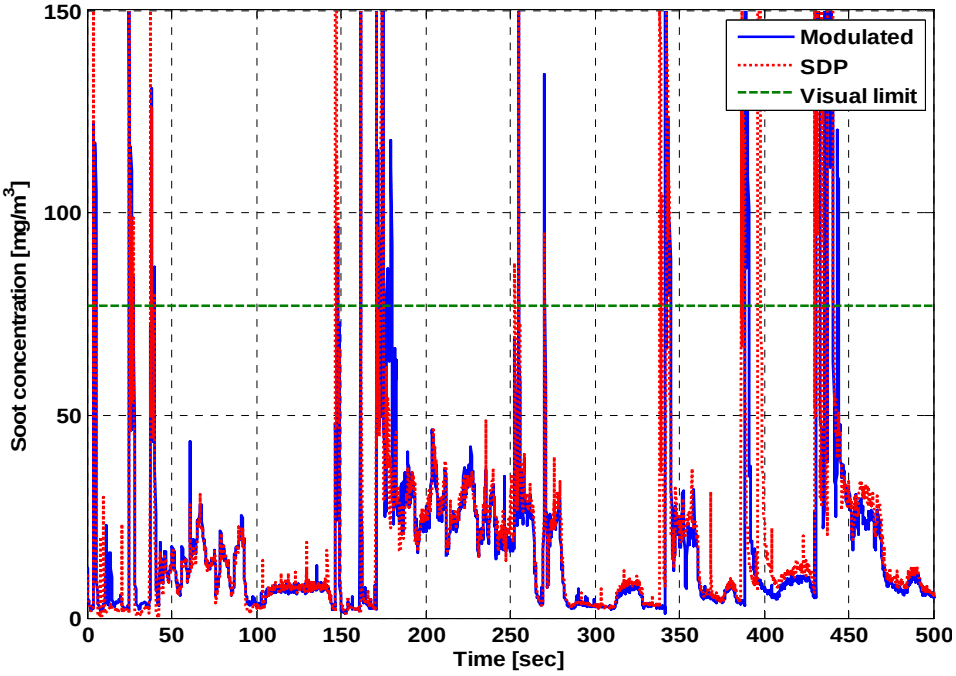

(b) zoomed at 0~500 seconds

Figure 8. 8. Soot concentration measurement during FUDS in PHH

The integrated fuel consumption of rule-based and SDP controls are shown in Figure 8. 9 and Figure 8. 10, respectively.

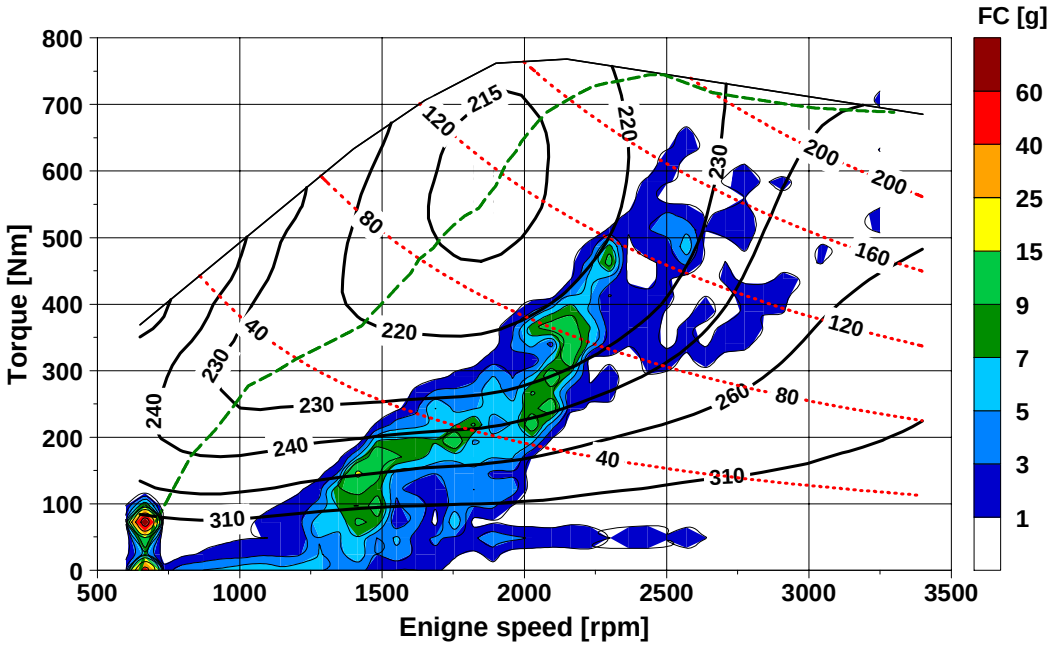

Figure 8. 9. Integrated fuel consumption of PHH with rule-based control in EIL test

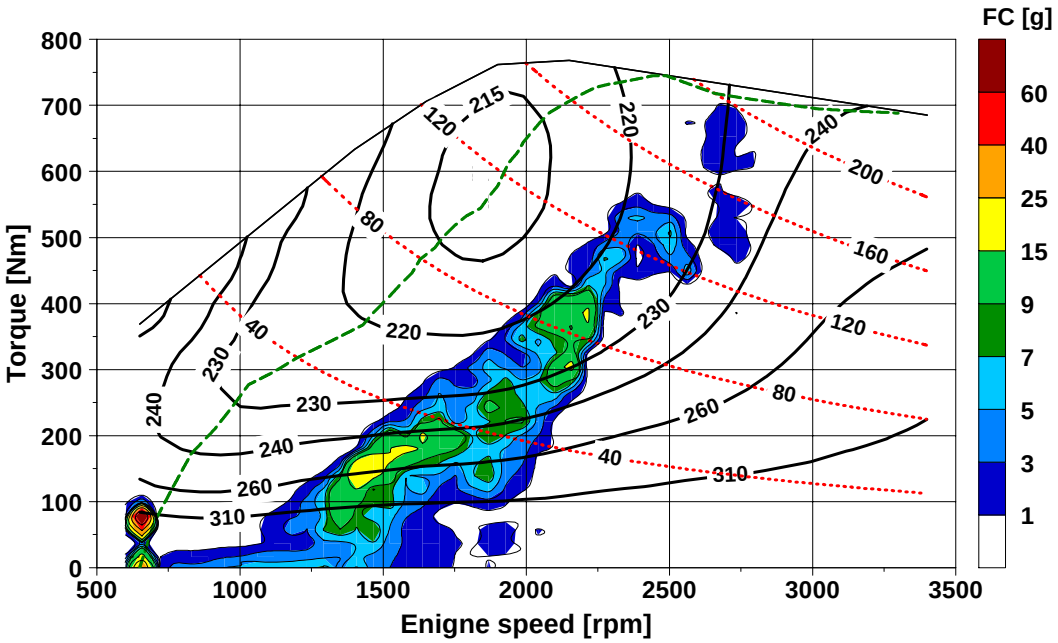

Figure 8. 10. Integrated fuel consumption of PHH with SDP control in EIL test

In comparison with the conventional vehicle's fuel consumption distribution, PHH systems use less fuel at low power area with the assist of the hydraulic power but visits high power area where BSFC becomes aggravated during transient operations. In the case of the SDP control, the engine visiting area is narrower than the rule-based control case and it is clear that the engine kick-in power is lower that the rule-based control case but the fuel consumption at the low engine power area is higher with the hydraulic assist drive. In addition, with torque converter, the fuel consumption at idle condition is as significant in PHH system as the conventional vehicle.

8.2.3. Series Hydraulic Hybrid System Result

The SHH system with optimized design and power managements, described in Chapter 4, is used for the EIL test. The EIL setup and challenges of the SHH system are presented in Chapter 5. As a supervisory power management, the modulated SOC control and SDP control are tested in the EIL test. The EIL test results are represented in Table 8. 4. The idle-stop and start capability is applied as the same way as the PHH system in the previous section. Both power managements show similar performance in fuel economy and exhaust emission reductions. In contrast to simulation results, the modulated control case shows slightly better fuel economy by relatively smooth engine

operations removing transient fuel consumption. In the case of emissions, the rule-based control case also shows slightly better emission reductions.

Table 8. 4. EIL test result of SHH with modulated SOC control and SDP control

(without / with idle-stop)	Modulated SOC control	SDP
Fuel economy [mpg]	15.0 / 16.4 (36 / 49 %↑)	14.7 / 16.1 (34 / 46 %↑)
NO_x [g/km]	2.97 / 2.61 (12 / 23%↓)	3.08 / 2.70 (9 / 20%↓)
Soot [g/km]	0.0595 / 0.0565 (59 / 61%↓)	0.0606 / 0.0571 (58 / 61%↓)

The system-behavior predictions of the simulation and EIL test results during FUDS are shown in Figure 8. 11 for the modulated SOC control case. In the case of the modulated SOC control, the simulation and EIL test results are remarkably close except for soot emissions. This closeness shows that the modulated SOC control restrains the transient engine operations so the simulation using the static engine map can predict actual engine behaviors so closely. The fuel consumption of EIL test results is similar with simulation results because it corresponds to the engine power demand that is similar with simulation data.

As for exhaust emissions, NO_x emission data of the EIL test are similar to the simulation results with the integrated emission responses described in Chapter 5. However, exhaust soot predictions based on the quasi-static engine test, even with relatively smooth engine operations, show significant differences between the simulation and EIL test results. This fact implies that even though engine operations are close to the simulation results, the soot emission mechanism highly depends on the transient engine operation.

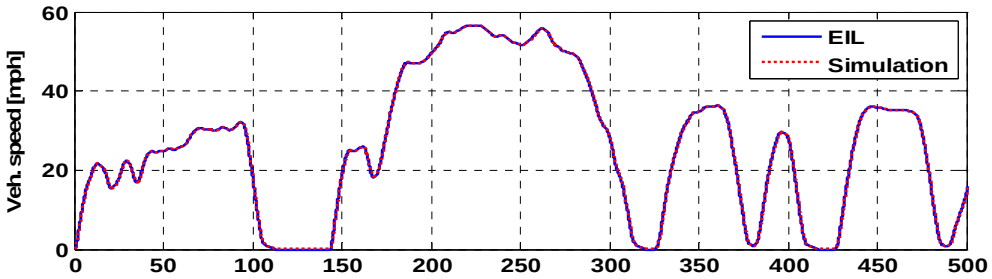

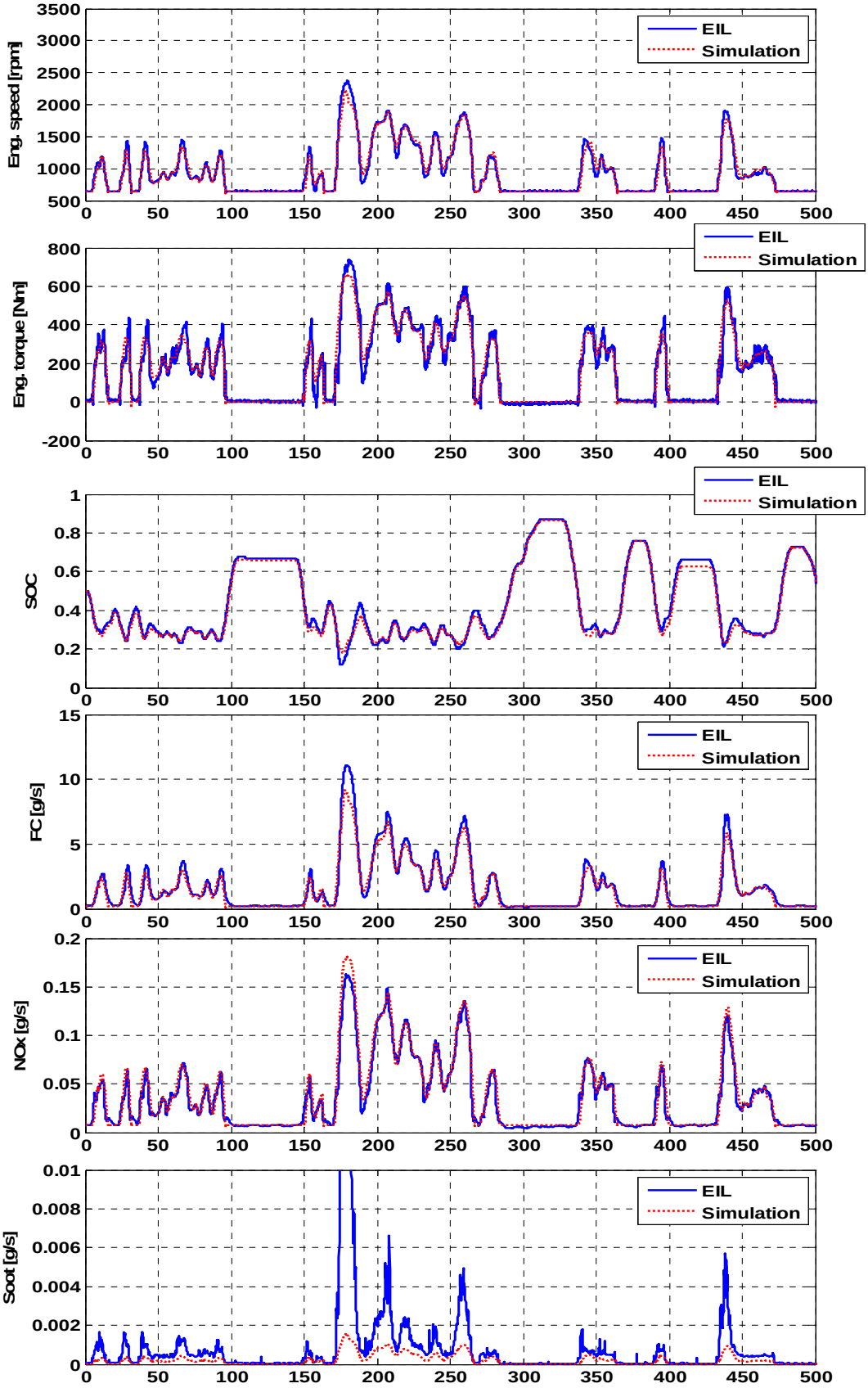

Figure 8. 11. Comparison between simulation and EIL test with modulated SOC control in SHH

Contrary to the closeness between the simulation and EIL test data in the modulated SOC control case, the engine-power measurement of the real engine does not synchronize well with the simulation result when SDP control is used as shown in Figure 8. 12. The overshooting of the engine power, derived from the system delay in the EIL test, makes differences in SOC predictions between EIL and simulation results because the engine power rate is higher in SDP control case than the modulated SOC control case. As a result, the fuel economy gains of the SDP control over the modulated SOC control in simulation results disappear with the real engine test in the EIL setup by the transient fuel consumption. That is why the EIL test is needed to validate simulation result especially when the system shows highly transient behaviors with the power management.

As for exhaust emissions, NO_x and soot emission data of the EIL test show high peaks when the engine kicks in with high rate power demand. Except the points of the engine-kick-in, NO_x emission data of the EIL test shows similar results with simulation data. However, exhaust soot predictions show significant differences between the simulation and EIL test results.

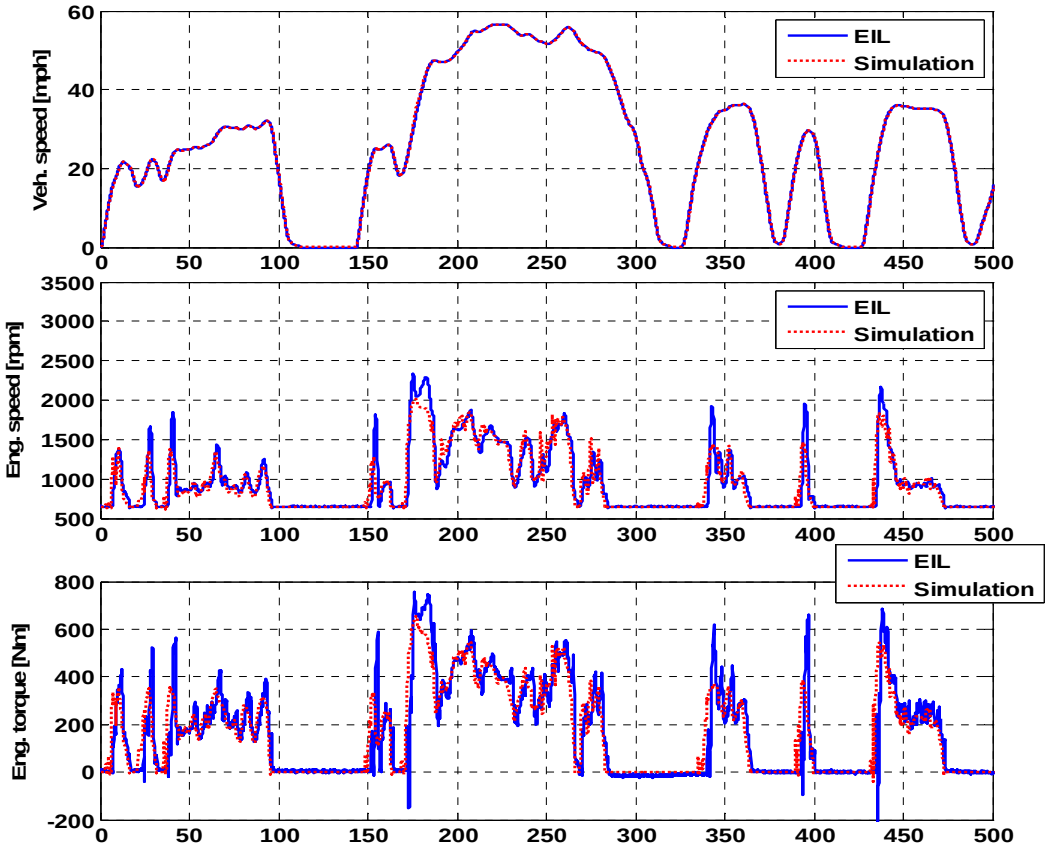

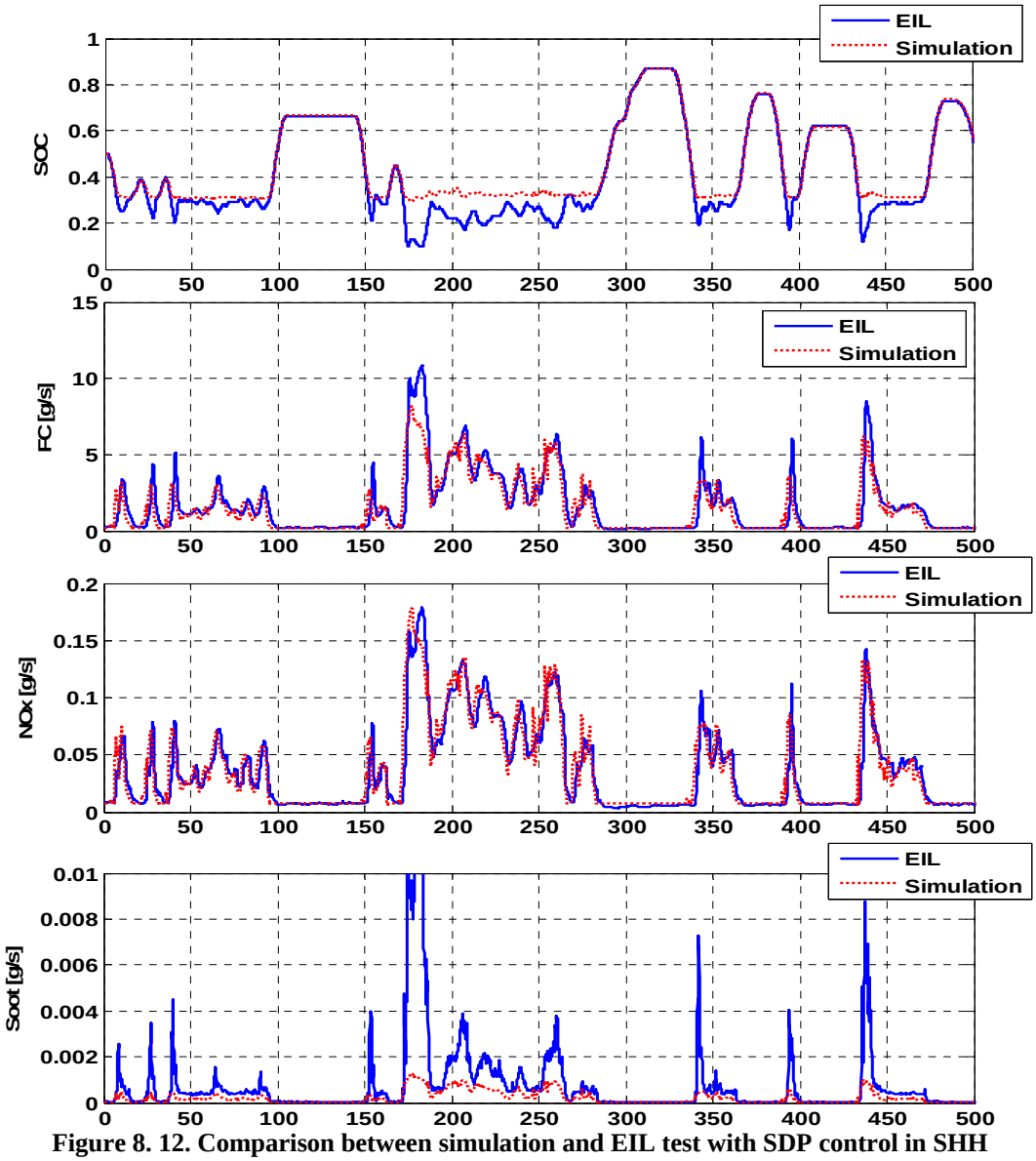

Figure 8. 12. Comparison between simulation and EIL test with SDP control in SHH

The modulated SOC control shows much better performance in suppressing the visual signature than SDP control by showing visual signatures only 2 times during FUDS (see Table 8. 5) even though SDP control also reduced visual signatures significantly.

The modulated SOC control suppresses visual signatures up to 95 % and SDP control reduces up to 75% by smooth engine power control than conventional vehicle system does.

Table 8. 5. The number of times over visibility limit during FUDS in SHH

	Number of times
Modulated SOC control	2
SDP control	9

The soot concentration is compared between the modulated SOC control and SDP control in Figure 8. 13. The soot concentration of the SDP control case has higher peaks than the modulated SOC control with more frequent visual signatures.

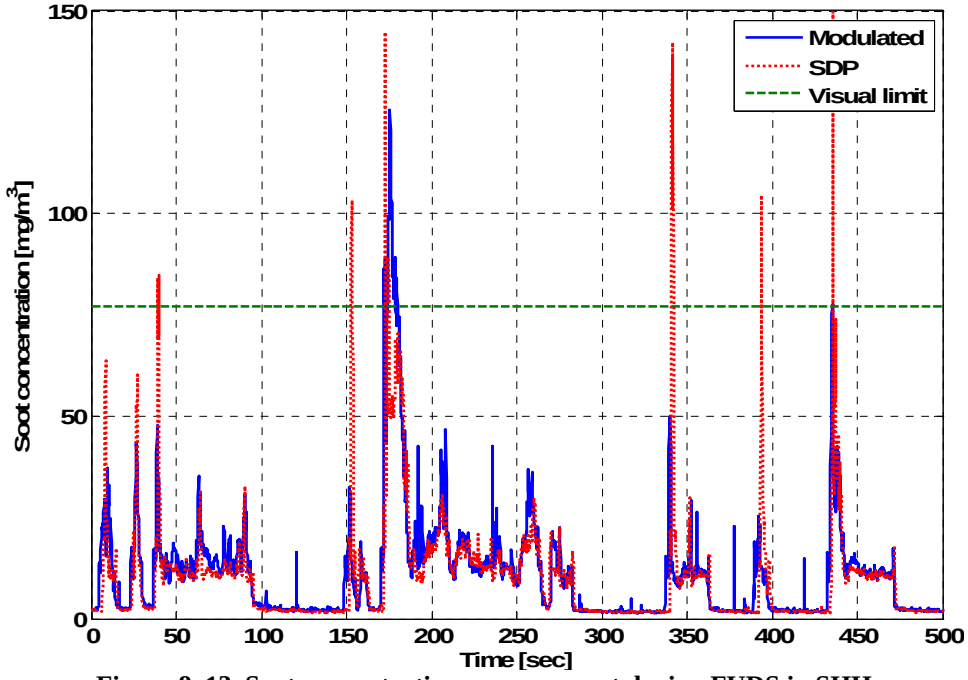

Figure 8. 13. Soot concentration measurement during FUDS in SHH

The integrated fuel-consumption distribution is presented on the engine map in the modulated SOC control case as shown in Figure 8. 14 and with SDP control in Figure 8. 15. The fuel consumed on the minimum BSFC line clearly shows that for the same engine power, engine operation points moved to the low speed and high load area where the fuel efficiency is better in comparison with the conventional vehicle case.

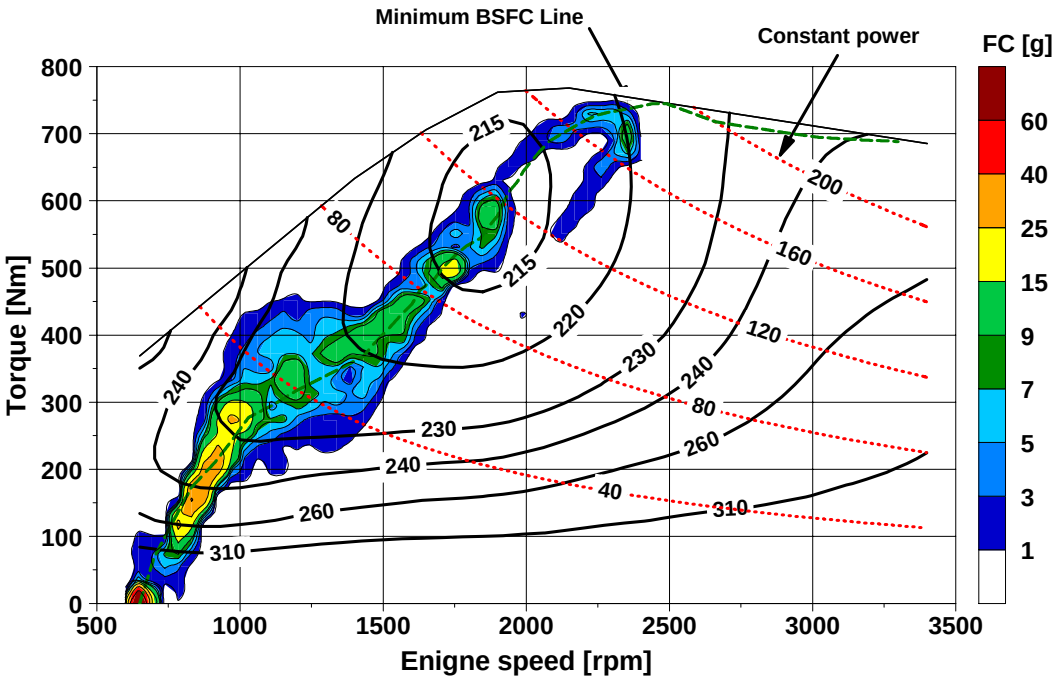

Figure 8. 14. Integrated fuel consumption of SHH with modulated SOC control in EIL test

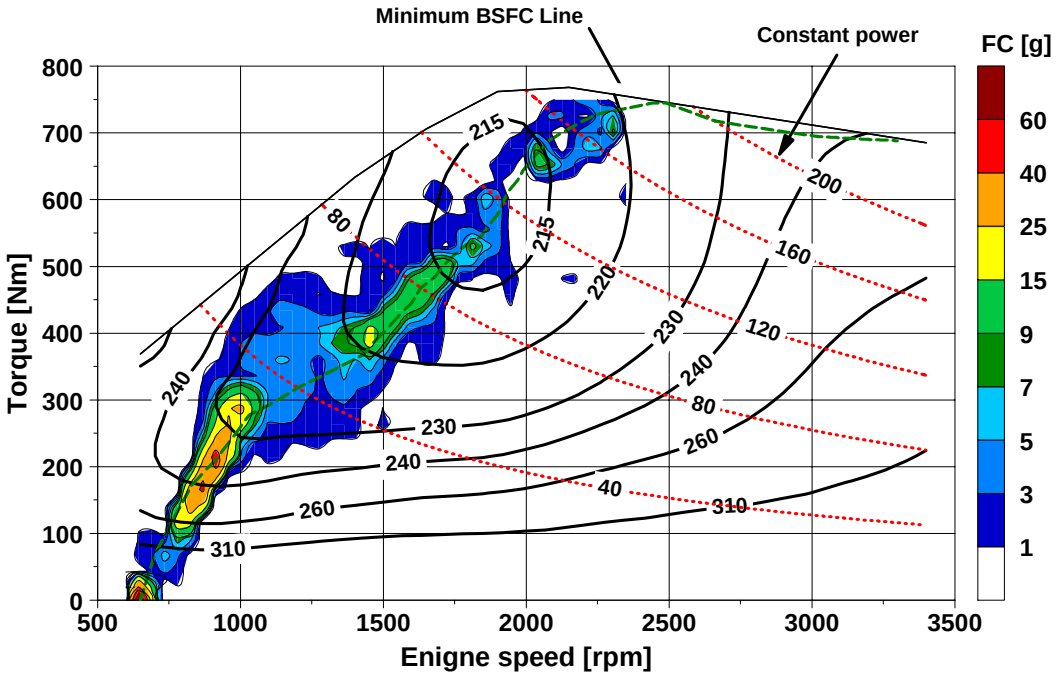

Figure 8. 15. Integrated fuel consumption of SHH with SDP control in EIL test

However, in the EIL test, more transient engine operations cause engine operation points to distribute in broader area around the minimum BSFC line. In comparison with the pure simulation results for both power managements, there exist system delays in the EIL setup including the turbo-lag. Even though the relatively simple engine model in the

simulation is enough for the optimization process and the parametric studies of hydraulic hybrid systems, actual engine tests in the EIL setup show that real world-phenomena are composed of transient operations and raise many control issues in the actual engine application.

8.2.4. Power-Split Hydraulic Hybrid System Result

The PSHH system with optimized design and power managements, described in Chapter 7, is used for the EIL test. In addition to basic EIL setup challenges, e.g., operating the engine safely and achieving the full functionality of test equipments and models [34], [105], there are integration issues for the PSHH system for the EIL setup.

First, the connection causality in the power-split hybrid system needs to be determined. As described in Chapter 5, the reversed causality for the stable system control is also applied to the PSHH EIL setup. The engine speed is calculated in the power-split drivetrain model and used as an input to the dynamometer controller. As a result, the engine-speed control model with a P/M_{gen} exists in the simulation part in the EIL setup in contrast with the SHH EIL case. Therefore, the PSHH EIL setup does not need an inversed P/M model. The engine torque is calculated by the engine power demand from the power management and is interpreted to the rack position of the engine. The throttle position signal is an input to the engine control unit (ECU) of the real engine. The engine torque measured from the dynamometer is given to the power-split drivetrain model, so each hydraulic P/M's power can be calculated from the vehicle power demand and actual engine power measurement.

Second, for the PSHH system, inertias of the engine and hydraulic devices make significant effects on the transient behavior of the system and the high inertia of the dynamometer may cause differences from pure simulation results. Thus, it is critical that the dynamometer inertia cancellation is guaranteed for the EIL test of the PSHH system and the current EIL setup in this study has the dynamometer-inertia cancellation function up to 70% of the dynamometer inertia.

Third, in contrast to simulation results, high rate of the engine power demand from SDP controller in the EIL setup overshoot and undershoot the engine speed and torque because of system delays and unsynchronized speed and torque controls of a real engine. Because the part of the engine power is directly transferred to the wheel without any

buffer in the PSHH system, the vehicle power demand from the driver model becomes sensitive to the rate of the engine power demand. Thus, the total system control becomes unstable during the EIL test. As a countermeasure, the smoothing of the SDP controller is applied for the safety and controllability of the engine and dynamometer system (see in Figure 8. 16). The smoothing of the SDP controller makes the engine power rate lower and the engine control becomes more stable and smoother.

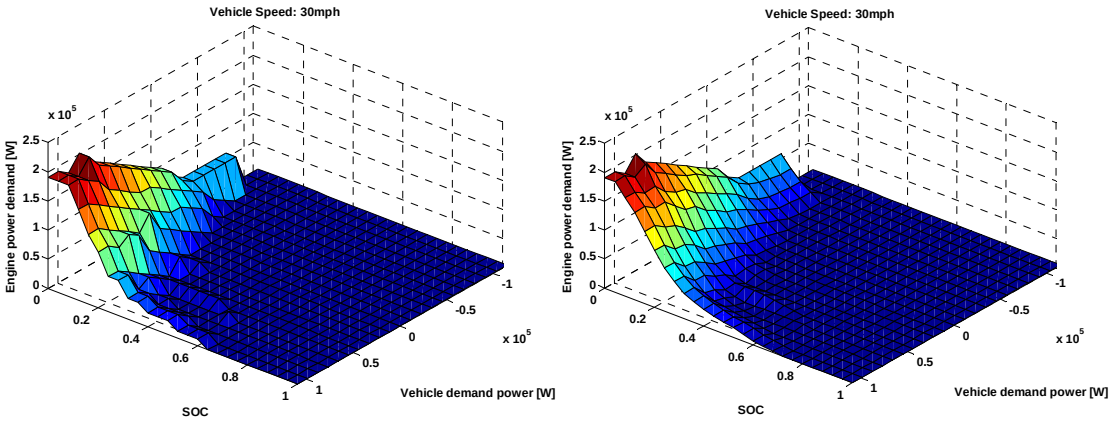

(a) before smoothing **(b) after smoothing**

Figure 8. 16. Before and after smoothing of the PSHH SDP controller

The EIL test results are represented in Table 8. 6. The idle-stop and start capability is applied as the same way as the PHH and SHH systems in the previous sections.

Table 8. 6. EIL test result of PSHH with modulated SOC control and SDP control

(without / with idle-stop)	Modulated Control, V8	SDP, V8
Fuel economy [mpg]	17.7 / 19.7 (61 / 79 %↑)	17.5 / 19.0 (59 / 73 %↑)
NO_x [g/km]	2.65 / 2.29 (22 / 32 %↓)	2.67 / 2.36 (21 / 30 %↓)
Soot [g/km]	0.0454 / 0.0426 (69 / 71 %↓)	0.0525 / 0.0493 (64 / 66 %↓)

The optimized PSHH super-HMMWV with modulated SOC control shows the fuel economy improvement of 61 % without idle-stop and 79 % with idle-stop in comparison with the conventional vehicle case. The fuel economy improvement of the SDP control is about 2 % less than that of the modulated SOC control without idle-stop in the EIL test but, in pure simulation, the SDP control case shows slightly higher fuel economy than the modulated SOC control case (see Table 7. 8). It seems that system delays in the EIL setup including turbo-lag make engine operations more transient in the case of the SDP control. As a result, the transient fuel consumption increases in comparison with

relatively smooth engine operations by the modulated SOC control. In the case with idle-stop, the fuel economy gap between the SDP control and modulated SOC control increases because the smoothed SDP control decreases the total idle time. In the EIL test, total idle-stop time of the modulated SOC control is 632 second and, in the case of the SDP control, total idle-stop time is 562 seconds.

The NO_x emissions reduction depends on the trade-offs between the total burned fuel reduction and the combustion efficiency increased by using the high load and fuel-efficient engine operation. Therefore, the NO_x emissions reduction is not proportional to the fuel economy improvement. For both power managements, NO_x decreases about 21 % without idle-stop and around 30 % with idle-stop. Even though the fuel economy is lower in the case of the SDP control, the transient engine operation visits more high load points, so NO_x emissions is slightly higher in the SDP control case than the modulated SOC control case. Exhaust soot emissions decrease significantly by around 70% in the modulated SOC control case and by around 65 % in the case of the SDP control. Even with smoothing, the transient effect still increase soot emissions in the SDP control case than in the modulated SOC control case. In addition, the idle-stop capability does not decrease soot so much as NO_x because the starting soot amount is net negligible.

System behaviors of simulation and EIL test results during FUDS are shown for the modulated SOC control case in Figure 8. 17. In the modulated SOC control case, the simulation and EIL test results are close except for soot emissions. This closeness shows that the modulated SOC control restrains transient engine operations and the simulation using the static engine map can predict the actual engine behavior so closely. The similarity of SOC predictions between the simulation and EIL test results also proves that the dynamometer controls engine power as well as the simulation does. As a result, the fuel consumption of EIL test results is similar with simulation results because it corresponds to the engine power demand that is similar with simulation data.

As for exhaust emissions, NO_x emission data of the EIL test are also similar to the simulation results with the integrated emission responses described in Chapter 5. However, exhaust soot predictions based on the quasi-static engine test, even with smooth engine operations, show significant differences between the simulation and EIL test results. This fact implies that even though engine operations are close to the

simulation results, the soot emission mechanism highly depends on the transient engine operation. As a result, the EIL test is needed to predict actual exhaust soot emissions in the real PSHH vehicle application.

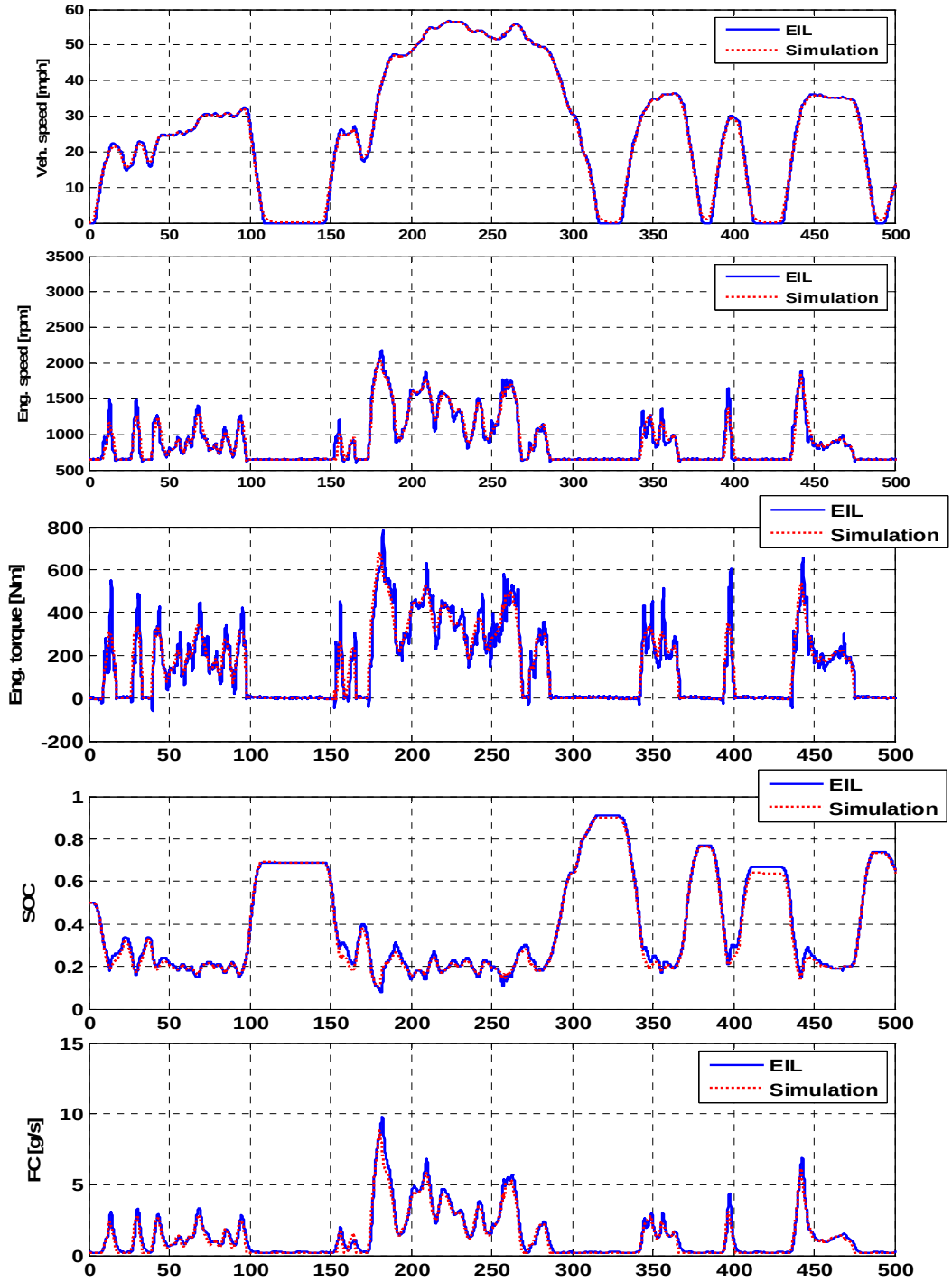

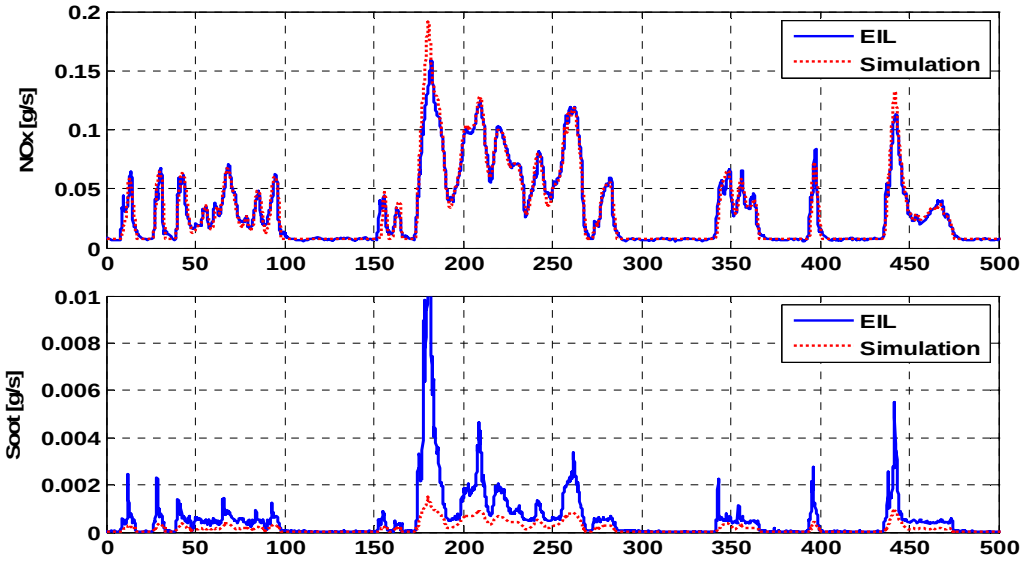

Figure 8. 17. Comparison between simulation and EIL test with modulated SOC control in PSHH

Contrary to the closeness between the simulation and EIL test data in the modulated SOC control case, the engine speed and torque measurement of the real engine does not synchronize well with simulation results when the SDP control is used as shown in Figure 8. 18. However, the resultant SOC prediction in the EIL test is similar with pure simulation data, which means that the engine power measurements in the EIL test are similar in both cases. That is why the EIL test is needed to validate simulation result especially when the system operates very transiently by the power management. Thus, the fuel consumption predictions are similar with each other.

As for exhaust emissions, NO_x and soot emission data of the EIL test show high peaks when the engine kicks in with high rate power demand. Except the points of the engine-kick-in, NO_x emission data of the EIL test shows similar results with simulation data. However, exhaust soot predictions show significant differences between the simulation and EIL test results

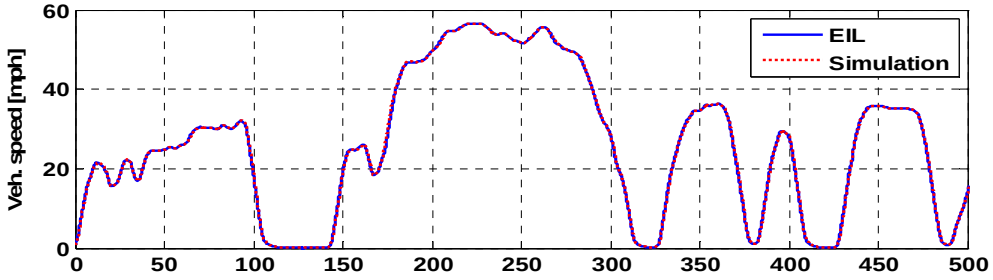

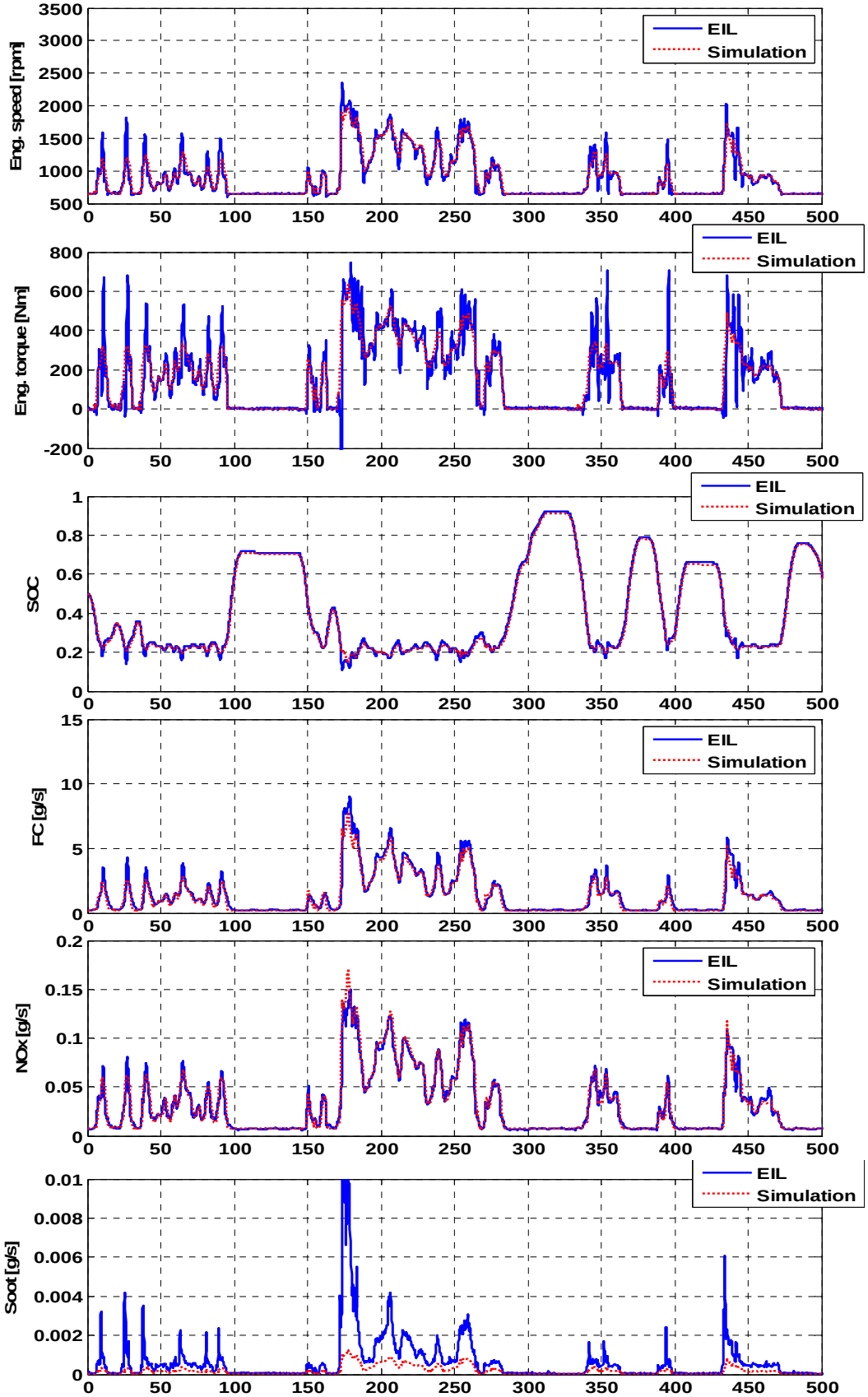

Figure 8. 18. Comparison between simulation and EIL test with SDP control in PSHH

The modulated SOC control shows better performance in suppressing the visual signature than SDP control by passing visual limits only 2 times during FUDS and reduces the chances of visual signatures by 95 %. The smoothed SDP control also reduced visual signatures significantly by 74 % with smooth engine operations in comparison with conventional vehicle case as shown in Table 8. 7.

Table 8. 7. The number of times over the visibility limit during FUDS in PSHH

	Number of times
Modulated SOC control	2
SDP control	10

The soot concentration is compared between the modulated SOC control and SDP control in Figure 8. 19. The soot concentration of the SDP case has higher peaks than the modulated SOC control case with more frequent visual signatures.

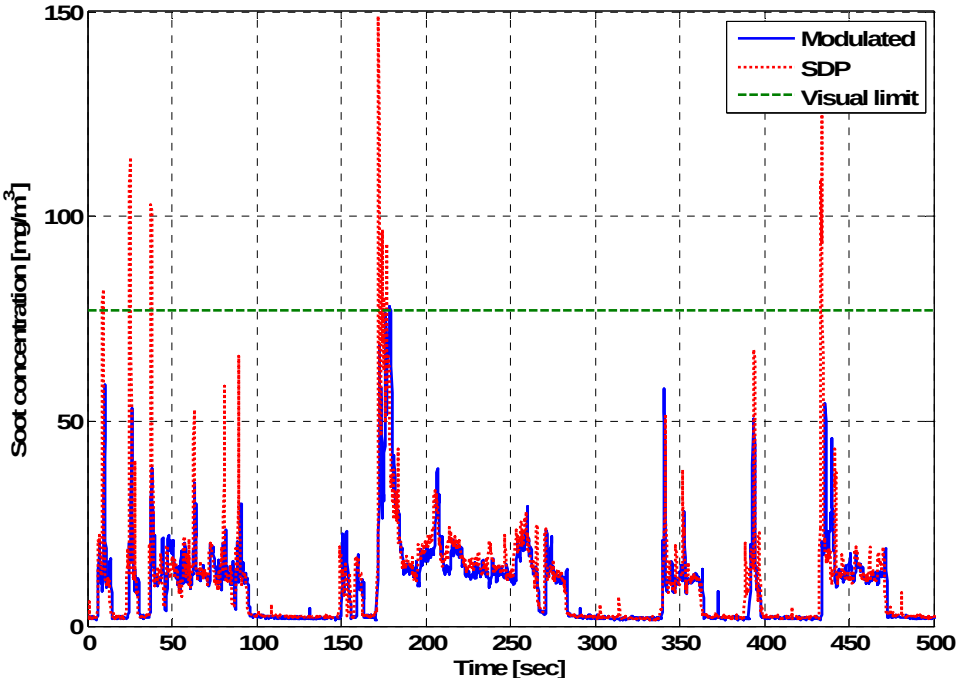

Figure 8. 19. Soot concentration measurement during FUDS in PSHH

The integrated fuel-consumption distribution is presented on the engine map with modulated SOC control in Figure 8. 20 and with SDP control in Figure 8. 21. The fuel consumed on the minimum BSFC line in the PSHH system clearly shows that for the same engine power, the engine operation points moved to the low speed and high load area where the fuel efficiency is better in comparison with the conventional vehicle case.

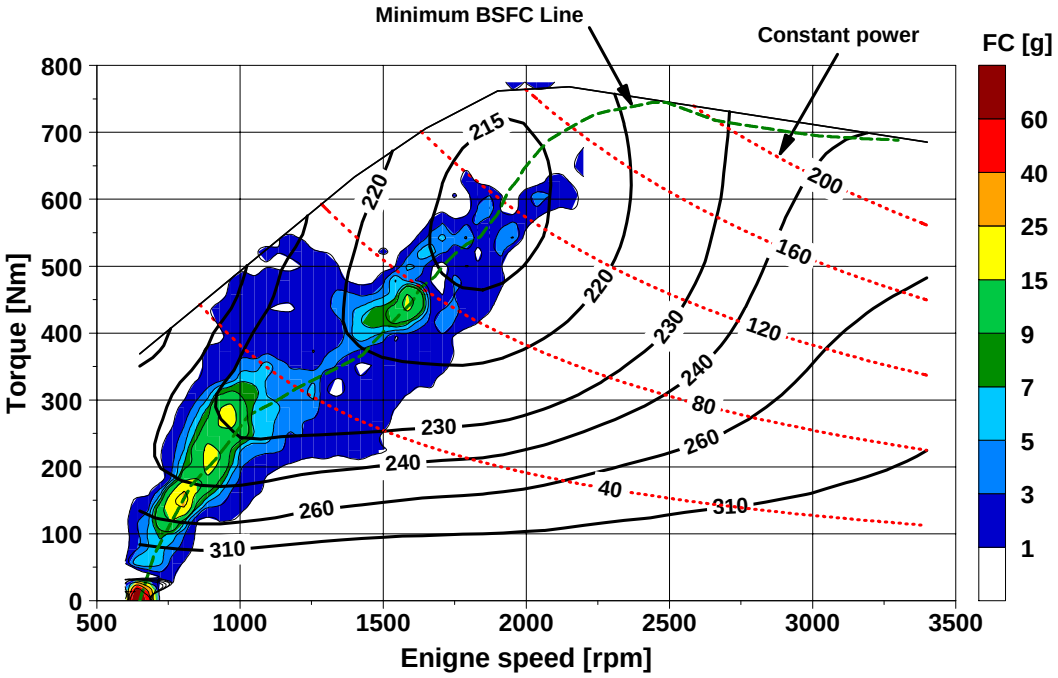

Figure 8. 20. Integrated fuel consumption of PSHH with modulated SOC control in EIL test

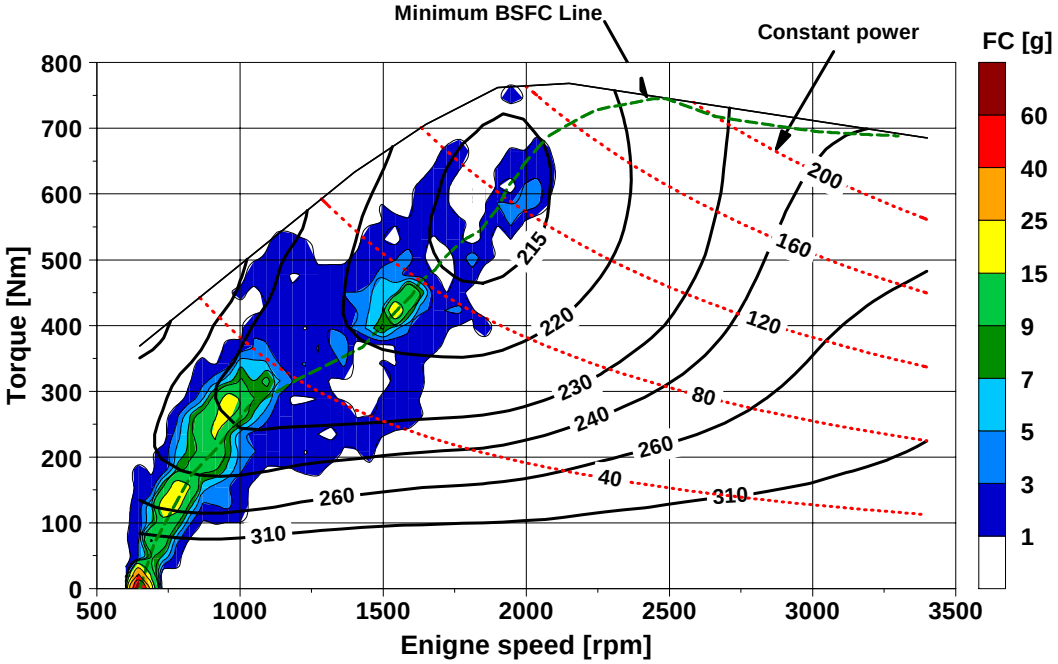

Figure 8. 21. Integrated fuel consumption of PSHH with SDP control in EIL test

However, in the EIL test, transient engine operations cause engine operation points to distribute on broader area in comparison with the pure simulation case for both power managements. Because system delays exist in the EIL setup including the turbo-lag. Even though the relatively simple engine model in the simulation is enough for the optimization process and the parametric studies of hydraulic hybrid systems, actual

engine tests in the EIL setup show that real world-phenomena are composed of transient operations and raise many control issues in the actual engine application. Especially, severely transient system behaviors disappear with the smoothed SDP control, even though more scattered engine operations at the high load area is obvious than the modulated SOC control case.

8.3. Summary of Engine-in-the-Loop Tests of Three Hybrid Systems

As a summary of the EIL test, comparisons of fuel economy, NO_x and soot emissions for each vehicle system and power management are presented in Figure 8. 22 and the relative amounts in comparison with the conventional vehicle case are shown in Figure 8. 23.

In Figure 8. 22(a), the PSHH system is the highest in fuel economy and SHH and PHH systems follow it. Even though the PHH system has the similar fuel economy with the SHH system between pure simulation results, transient effects cause the SHH system to have better fuel economy than the PHH system. Interestingly, the higher fuel economy gain of the SDP control over modulated SOC control in simulation results disappears in the EIL test in SHH system and the modulated SOC control case shows better fuel economy due to smoother engine operations reducing overshoots of the engine speed and torque. Most SDP control cases except the PHH-system case, show disadvantages in the fuel economy improvement in real engine tests because of transient fuel consumptions. In the PHH case, the sub-optimal rule-based control demands the higher engine kick-in power in comparison with the SDP control case. If the sequential 4x4 operation is used in the SHH system, around 5~10% of the fuel economy gain is expected in comparison with the simultaneous 4x4 operation case as predicted in Chapter 4.

In Figure 8. 22(b), the PHH system with the sub-optimal rule-based control shows the least NO_x emissions even though the fuel economy is not the best. It seems that transient engine operations cause incomplete combustions. As a result, exhaust soot emissions increase and the gas temperature decrease with reducing NO_x emissions.

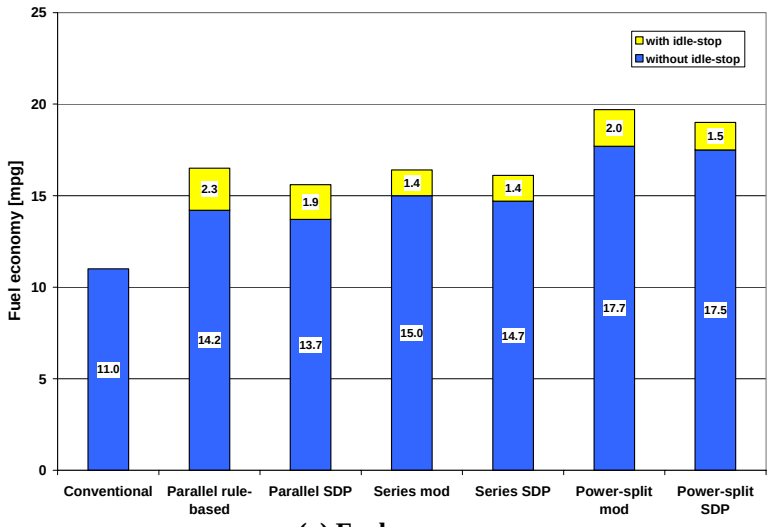

(a) Fuel economy

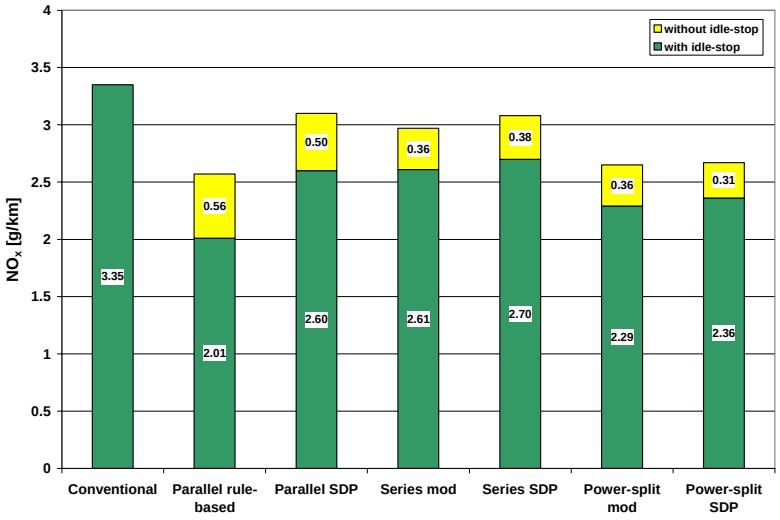

(b) NO_x

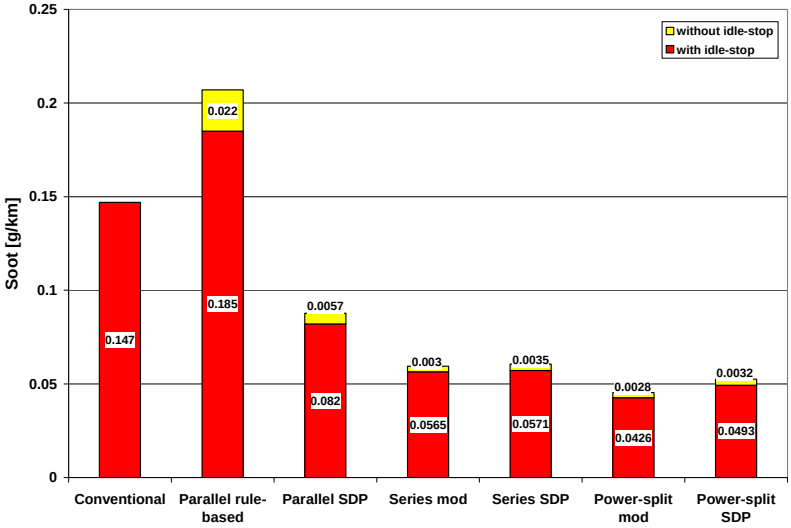

(c) Soot

Figure 8. 22. Fuel economy, NO_x, Soot for each hydraulic hybrid system and power management

With the less fuel consumption, NO_x emissions of the PSHH system are lower than SHH system case because the engine operation area is almost the same in both systems. As for NO_x emissions, SDP control cases shows less NOx emission reductions than modulated SOC control cases in real engine tests because of visiting the high speed and high load area by transient engine operations.

In Figure 8. 22(c), the PSHH system is the most advantageous in reducing soot emissions with the least fuel consumption and smooth engine operations. Both the SHH and PSHH systems reduce exhaust soot emissions with smooth engine operations but the PHH system with the rule-based power management dramatically increases soot emissions even far more than conventional vehicle case. In contrast with fuel economy and NO_x emission cases, the EIL tests prove that transient effects are the most dominant in the exhaust soot-emission generation.

With exclusive operations of the engine and hydraulic P/M according to semi-optimized power management, engine power rates are largest in PHH system when the engine kicks in. As a result, the engine emits significant exhaust soot emissions. In addition, the EIL test proves that transient engine operations may cause vibration and durability problems and aggravates the driver's comfort in real vehicle applications even though the sub-optimal rule-based power management shows the best fuel economy improvement in the pure simulation of the PHH system.

In Figure 8. 23(a), the PSHH system improves fuel economy about 80% and 60% without- and with idle-stop, respectively in comparison with conventional vehicle case. The SHH system improves about 50% and 35% and the PHH system improves about 45% and 25% of the fuel economy without- and with idle-stop, respectively. For all systems, SDP control cases have less gain in fuel economy and it seems to be transient effects except the PHH system case.

In Figure 8. 23(b), the PHH system reduces NO_x about 40% and 25% with the rule-based control and reduces NO_x about 23% and 8% with the SDP control without- and with idle-stop, respectively. The PSHH system reduces about 30% and 20% and the SHH system reduces about 20% and 10% of NO_x emissions without- and with idle-stop, respectively. For all systems, SDP control cases have less reduction in NO_x emissions that seems to be derived from transient effects.

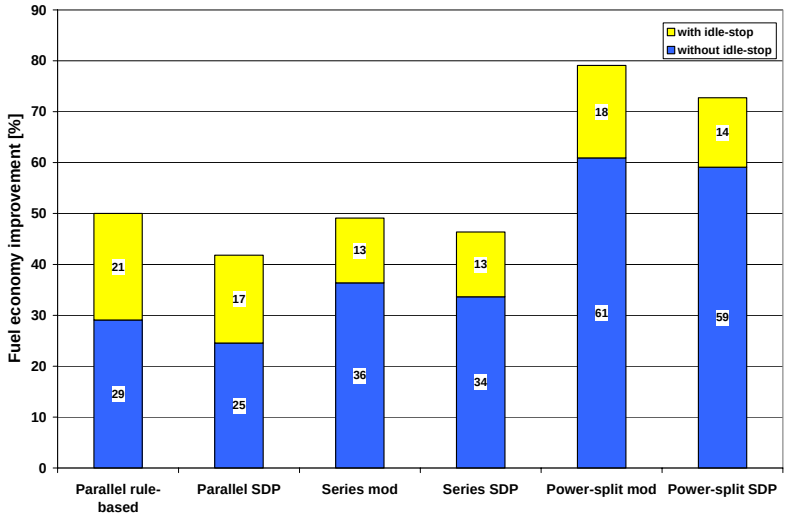

(a) Fuel economy improvement

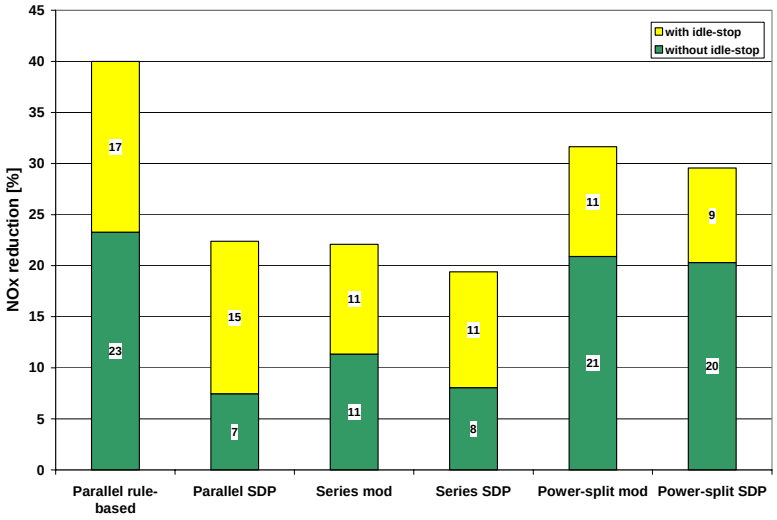

(b) NO_x reduction

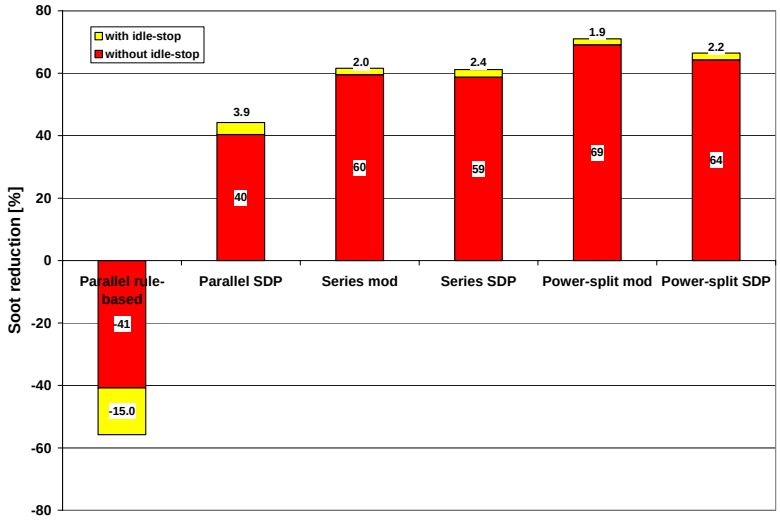

(c) Soot

Figure 8. 23. Fuel economy improvement and NO_x and soot reduction for each hybrid system

In Figure 8. 23(c), the PSHH system reduces soot emissions about 75% and 65% without- and with idle-stop, respectively. The SHH system reduces soot emissions 60% for both without- and with idle-stop, respectively. Because of the significant amount of starting soot emissions, the idle-stop capability does not reduce the total soot emissions in the case of with idle-stop. As for PHH system, soot emissions increase 55% and 40% with rule-based control because of transient engine operations and decrease 45% and 40% with the SDP control without- and with idle-stop, respectively. As for the soot emission, the EIL test results prove that reducing transient engine operations is the key to lower exhaust soot emissions and it depends on how exclusively the power management uses the engine and hydraulic power.

The comparison of simulation and EIL test results is represented in Table 8. 8 and in Figure 8. 24. As for fuel economy, simulation results overestimate about 10% for the most of cases even though the gap between pure simulation and EIL test results increases as the engine operation becomes transient by the system characteristics or power managements. Simulations predict NO_x emissions so closely in the case of the SHH and PSHH systems by less than 4% but underestimates up to 30% in the case of conventional and PHH vehicle systems. As for soot emissions, simulation predictions are almost impossible. Especially, in the case of the PHH system with the rule-based control, the simulation predicts the reduction of soot emissions but EIL tests show the dramatic increase even much more than the conventional vehicle case.

Table 8. 8. Comparison of EIL test and simulation without idle-stop

	Fuel economy (EIL-sim)/sim [%]	NO_x (EIL-sim)/sim [%]	Soot (EIL-sim)/sim [%]
Conventional	-11.3	19.6	374
Parallel rule-based	-12.9	13.7	820
Parallel SDP	-9.9	30.3	258
Series mod	-8.5	-3.6	265
Series SDP	-12.0	2.3	276
Power-split mod	-8.3	-0.4	234
Power-split SDP	-9.3	0.4	286

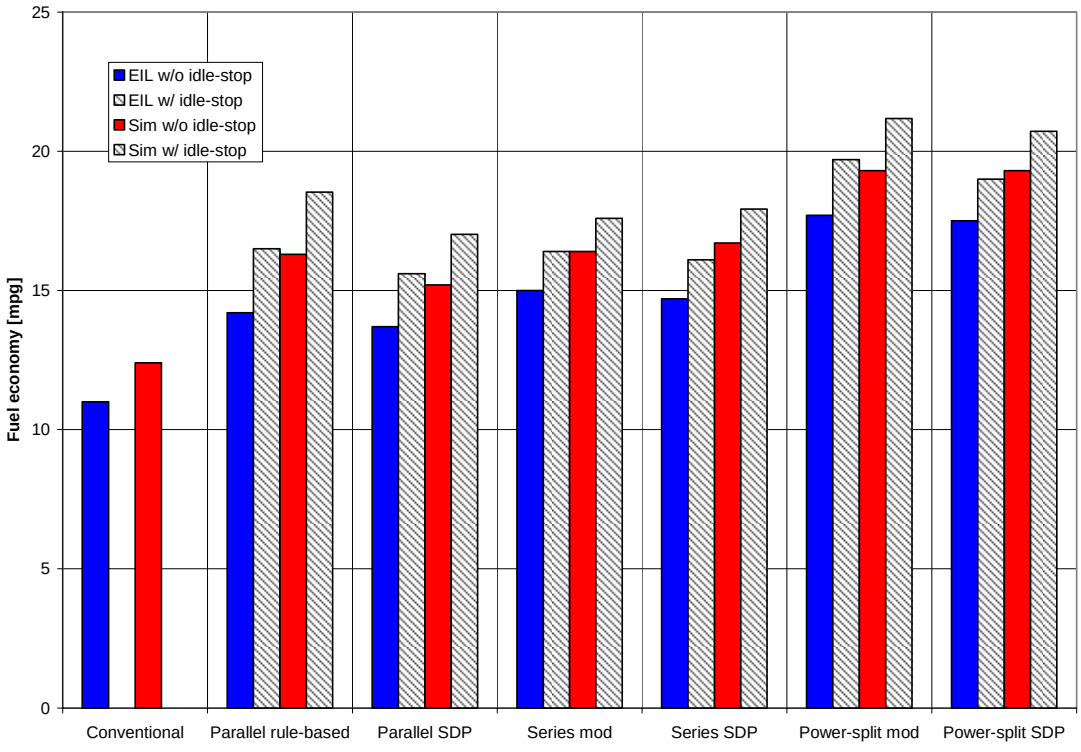

(a) Fuel economy

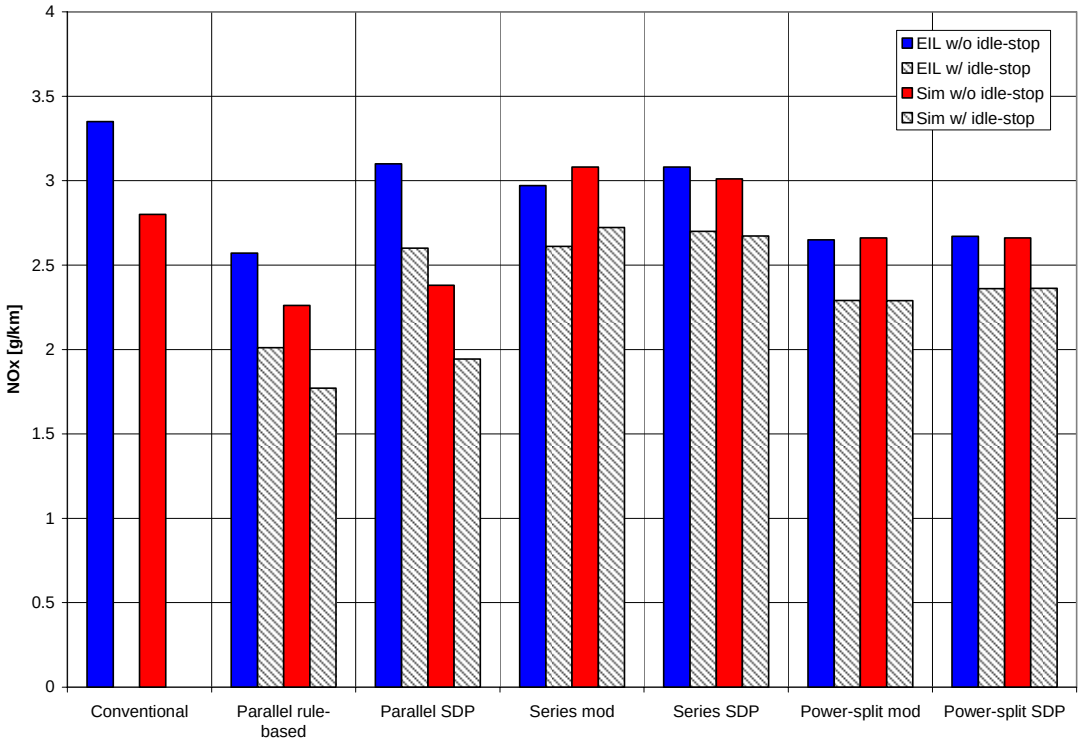

(b) NO_x

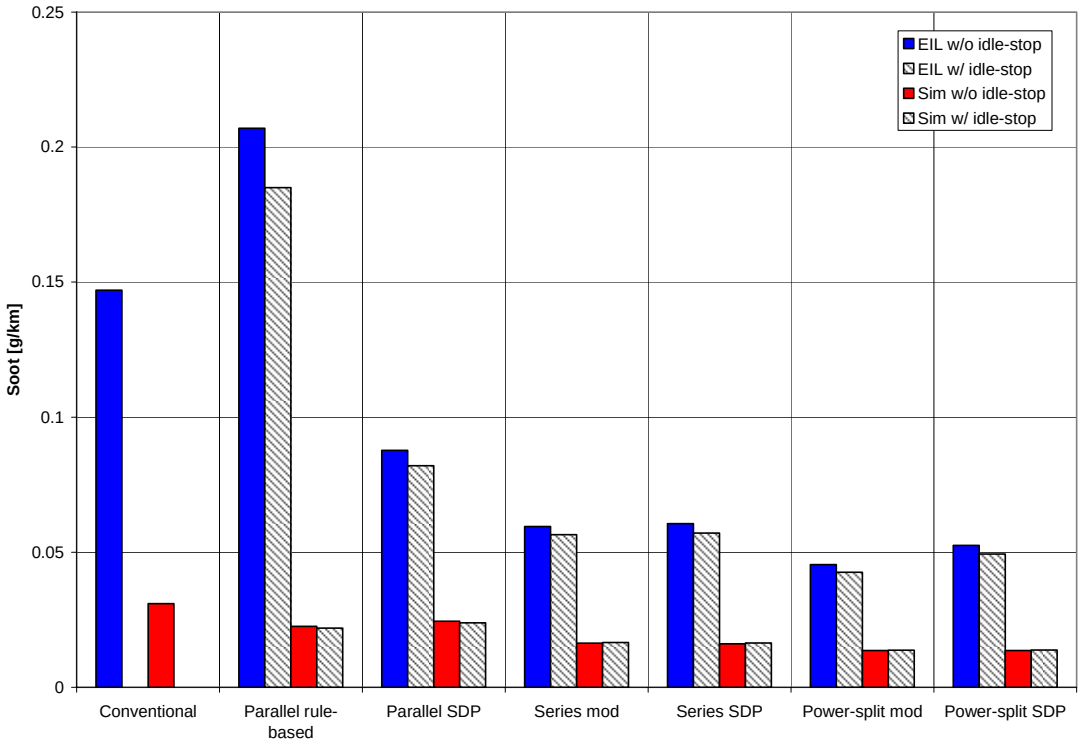

(c) Soot

Figure 8. 24. Comparison of EIL test and simulation for each vehicle system and supervisory control

CHAPTER 9
CONCLUSIONS AND FUTURE WORK

9.1. Conclusions

In this dissertation, a comprehensive methodology for up-front strategic assessment of the best hybrid system for a given vehicle platform has been developed and demonstrated. The methodology combines optimization of the design and power management of the hybrid propulsion system to determine the ultimate potential of any given architecture and selection of energy conversion and storage components. In addition, the methodology considers a range of driving schedules, or duty cycles, to yield guidance related to selection of the preferred hybrid system for a different dominant mission. Finally, the modeling-simulation work is extended to develop the Engine-in-the-Loop capability for testing the real diesel engine coupled with a virtual hybrid driveline, including parallel, power-split and series configurations. This enables considering real-life transient particulate and nitric oxide emissions when optimizing any given configuration and supervisory control. The 4x4 on- and off- road truck weighing 5 tons has been used as a platform for case studies that demonstrate all aspects of the methodology. The hydraulic energy conversion and storage option was selected due to the potential benefits in heavy vehicle applications stemming from high power-density and conversion efficiency of hydraulic devices.

Several original contributions were essential for accomplishing the goals of the study. Physics based simulations of the relevant hybrid propulsion configurations are developed in MATLAB/Simulink. The modeling and system integration includes a unique power-split configuration suitable for a hydraulic hybrid vehicle. Power-split systems have so far been studied extensively in the context of electric hybrids, but the use of hydraulic devices poses unique challenges related to limited speed ranges of motors and relatively small energy density of the hydro-pneumatic energy storage. The results indicate that power-split systems can be very advantageous in the case of hydraulic hybrids too if their design is carefully tailored within the constraints defined by component characteristics.

The dynamic programming algorithm for determining the optimal benchmark for a hybrid supervisory control strategy has been successfully applied to a hydraulic power-split and series system. The previous work includes only the applications to a parallel system, and a completely different problem statement was required for power-split and series system. In case of the latter, the complete mechanical decoupling of the engine from the wheels fundamentally changes the objective of the supervisory control, as the strategy does not coordinate the operation of multiple power sources but rather the engine operation and state-of-charge management. The study provides an in-depth look at this issue and highlights the lessons learned that in many ways challenge the simplified conventional wisdom often applied to series systems.

Finally, the second stage of the optimal supervisory control work demonstrated for the first time application of the stochastic programming algorithm for the development of implementable strategies for controlling the hydraulic parallel, power-split and series systems. The optimal design and supervisory control were initially developed using the fuel economy as the main objective. Predicting the exhaust emission at the system level using simulations is impractical and problematic, as the models with sufficient fidelity require extremely long computational times. Hence, the Engine-in-the-Loop capability was deemed necessary to be able to include exhaust emissions into the propulsion-system optimization process. The methodology for the integration of the virtual hydraulic hybrid driveline was developed and demonstrated for all three major configurations. The results provide a first ever in-depth look at the interplay between the hybrid system design, supervisory control, diesel engine control and transient emissions of soot and nitric oxides. They also validate the predictions of vehicle system simulations. Finally, the application of the multi-step methodology and synthesis of main findings provides a clear guidance for the selection of a hydraulic hybrid configuration and design depending on the pre-dominant vehicle mission.

A detailed summary of the dissertation contents is as follows. Forward-looking VESIM models for three hydraulic hybrid systems were developed and integrated in the MATLAB/Simulink environment. Through the design optimization study, the optimal size-based hydraulic devices and vehicle parameters were selected and 4x4 drive options were explored in the SHH system. With optimized baseline designs, optimization of the

supervisory controls were carried out for three hybrid systems with DDP and SDP techniques. EIL test capabilities for three hydraulic hybrid systems were developed and simulation results were validated by capturing transient effects on fuel consumption, NO_x and soot emissions according to various hydraulic hybrid systems and power managements.

In Chapter 2, a high fidelity hydraulic accumulator and P/M model were introduced. Volumetric and torque loss coefficients of the hydraulic P/M model were calibrated according to experiment data of the current hydraulic P/M which was developed for the vehicle propulsion. The mass estimation of hydraulic devices and powertrain components were based on prototype hydraulic-hybrid vehicle data and effects of the total vehicle mass were reflected on simulation results.

In Chapter 3, a SHH model of a light-duty truck was integrated in the MATLAB/Simulink environment. The low-level engine-control strategy, 4x4 options and a simple 2-speed transmission with the gearshift logic were presented with the traditional thermostatic control and alternative modulated SOC control. The modulated SOC control scheme is based on the analysis of modes of hybrid system operations and prioritized opportunities to improve the system efficiency, e.g., preventing engine from charging the accumulator and managing the SOC to guarantee to capture the regenerative braking energy effectively. Design optimization with an original and downsized engine showed the potential of the fuel economy improvement of the SHH system without degrading the performance of the conventional vehicle.

In Chapter 4, the power management optimization of the SHH system was carried out with dynamic programming techniques. With the optimized baseline design, DDP technique was applied to find benchmark power management during FUDS and SDP technique was applied to find an implementable sub-optimal power management, respectively. The benchmark power management improved the system efficiency with transient engine operations in the simulation and the engine operation points coincided with the minimum combined-BSFC line. With an engine acceleration constraint, the fuel economy gain of the benchmark control was around 6 % over that of the SDP control. SDP control showed slightly better fuel economy than the optimized modulated SOC control case and a reliable charge-sustaining capability.

In Chapter 5, the development of the SHH EIL capability was presented. In addition to general EIL challenges, an inverse P/M model had to be applied because of the unstable engine control problems. In other word, from speed and torque measurements with the dynamometer system, fluid flows to and from the P/M were calculated. After validating simulation results with the diesel engine in the loop, the traditional thermostatic control and the alternative modulated SOC control were tested with the original and downsized engines. As a result, fuel economy improvements were verified as about 50 % in FUDS and 10% in HWFET without the idle-stop. As for exhaust emissions, NO_x decreases by 14% and soot decreases by 63% from conventional vehicle data. In the case of an engine downsizing from V8 to V6 and with the idle-stop capability, up to 70% of the fuel economy improvement was possible.

In Chapter 6, a PHH modeling of a light duty truck was presented. With the sub-optimal rule-based power management, the design optimization was carried out. With the optimized design, power management optimization with DDP techniques was applied. The benchmark supervisory control prediction suggested exclusive engine and P/M operations to improve fuel economy in the simulation. With a gearshift constraint, the benchmark power management shows about 5% fuel economy gain over that of the semi-optimized rule-based power management. With relatively smooth operations of the engine and hydraulic devices, SDP control case showed about 7 % lower fuel economy than the sub-optimal rule-based power management case.

In Chapter 7, a modeling of the PSHH system of a light duty truck was presented. In addition to general challenges from the low density of the hydraulic accumulator, speed reduction for P/Ms was indispensable for the PSHH system. An alternative modulated SOC control showed smooth engine operations with reliable vehicle driveability. The systematic design optimization with the alternative modulated SOC control was carried out and the optimized design was used for the power management optimization.

The benchmark supervisory control that derived from the DDP technique showed that transient engine operations improved the system efficiency in the simulation. The implementable SDP control showed almost the same fuel economy as the modulated SOC control case.

In Chapter 8, aggressiveness effects of the driving schedules on fuel economy were tested for three hybrid systems with the SDP control. The PSHH system showed the best fuel economy in most cycles and the fuel economy improvement of the hybrid systems highly depended on the combination of the average vehicle speed, the number of vehicle-stops and total idle time.

Validations of simulation results were carried out using a real diesel engine in the loop for three hydraulic hybrid systems with optimized designs and various power managements, respectively. The PSHH system was the best in terms of the fuel economy improvement and emission reduction. Even though the parallel system with semi-optimized rule-based power management showed lowest NO_x emissions, it was proven that extremely exclusive usages of the engine and hydraulic power were not suitable in the actual vehicle application because of the huge increase in transient soot emissions.

On the contrary, the SDP control in the PHH system showed exhaust soot emission reduction even though the fuel economy improvement was slightly lower than the rule-based control. Due to smooth engine operations, EIL test results of the SHH and PSHH systems were close to the simulation results, which were based on the static engine maps, in the fuel consumption and NO_x emissions. As for exhaust soot-emission predictions, considerable gaps existed between simulation and EIL setup results. In addition, SDP control results showed slightly less fuel economy improvements than modulated SOC control cases in both SHH and PSHH systems because of more transient engine operations. As a result, it was proven that the EIL test should be used to validate simulation results in real world and the capturing of the transient engine behavior was significantly useful for the evaluation of respective hybrid systems and power managements.

9.2. Future Work

The following are the opportunities for future research in the area of optimization of hydraulic hybrid propulsion for light and medium trucks

- Refine the integrated hydraulic hybrid engine-vehicle simulation models with additional powertrain sub-models and control strategies, for example, a detailed engine cold start model or clutch model for the gearshift.

- Explore the optimal benchmark power managements with constraints or objective function terms for exhaust emission derived from the EIL test.
- Integrate more hardware into the test cell setup and create a complete powertrain-in-the-loop setup for further studies using real propulsion and energy storage hardware, and real actuators.
- Improve and calibrate individual models based on findings obtained with EIL setup to better capture the transient behavior and increase the fidelity of optimal power management techniques.

APPENDICES

The following numerical values are used as input data for all test runs and calculation for the simulation.

A. 1. Hydraulic Vehicle System Specification

Table A. 1. Super-HMMWV diesel engine specifications

System	Conventional and Hybrid	Hybrid
Configuration	V8, 4 Overhead Valves	V6 , virtual engine
Bore x Stroke [mm]	95 x 105	-
Displacement [Liter]	6.0	4.5
Rated Power [kW] @3300 rpm	238	178.5
Maximum Torque [Nm] @2100 rpm	774	580.5
Compression Ratio	18.0 : 1	-
Aspiration	Variable Geometry Turbine(VGT)/Intercooler	-
Fuel Injection System	Generation 2 Hydraulic Electronic Unit Injector (HEUI), Up to 2000bar	-

Table A. 2. Super-HMMWV driveline specifications

	Conventional and parallel hybrid
T/C Turbine inertia [kgm^2]	0.2
Transmission 1st gear ratio	3.42
Transmission 2nd gear ratio	2.26
Transmission 3rd gear ratio	1.5
Transmission 4th gear ratio	1.0
Transmission 1st gear efficiency	0.94
Transmission 2nd gear efficiency	0.96
Transmission 3rd gear efficiency	0.97
Transmission 4th gear efficiency	0.97
Differential gear ratio	3.56
Differential gear efficiency	0.94

Table A. 3. Super-HMMWV vehicle specifications

Number of wheels [-]	4
Sprung mass [kg]	4672
Unsprung mass front [kg]	220
Unsprung mass rear [kg]	220
Wheel inertia [kgm^2]	32.0
Brake viscous damping [Nms/rad]	170
Wheel radius [m]	0.4412
Wheel viscous damping [Nms/rad]	4.0
Aerodynamic drag coefficient (Cd)	0.7
Frontal area [m^2]	3.58
Road/tire friction coefficient [-]	0.7

Table A. 4. Baseline hydraulic component specifications

Foam specific heat [kJ/kgK]	2.3
Thermal time constant [sec]	100
Frictional loss	4% of input energy
Fluid bulk modulus of elasticity, b [MPa]	1660
Coefficient of laminar leakage-motor, Cs_m	10.11 x 10-9
Coefficient of turbulent leakage-motor, Cst_m	3.0 x 10-5
Coefficient of viscous drag-motor, Cv_m	34270
Coefficient of friction-motor, Cf_m	2.16 x 10-3
Coefficient of hydrodynamic loss-motor, Ch_m	34.92
Coefficient of laminar leakage-pump, Cs_p	1.123 x 10-9
Coefficient of turbulent leakage-pump, Cst_p	6.0 x 10-5
Coefficient of viscous drag-pump, Cv_p	34270
Coefficient of friction-pump, Cf_p	2.16 x 10-3
Coefficient of hydrodynamic loss-pump, Ch_p	34.92

A. 2. Engine Maps (BSFC, $BSNO_x$ and BSsoot)

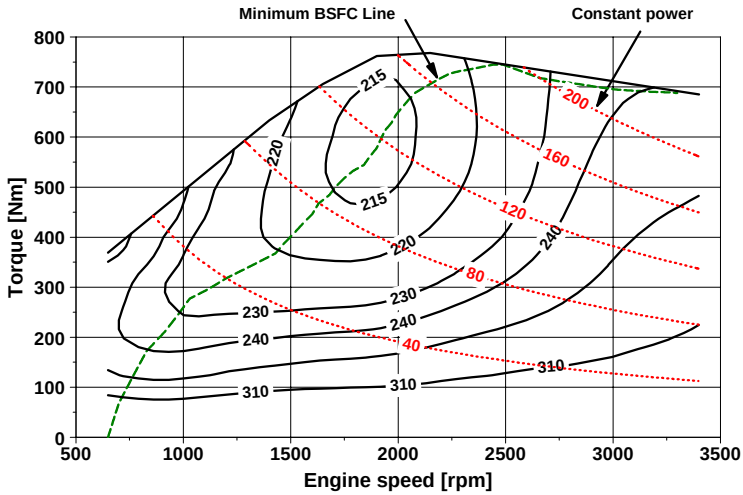

(a) BSFC [g/kWh], V8

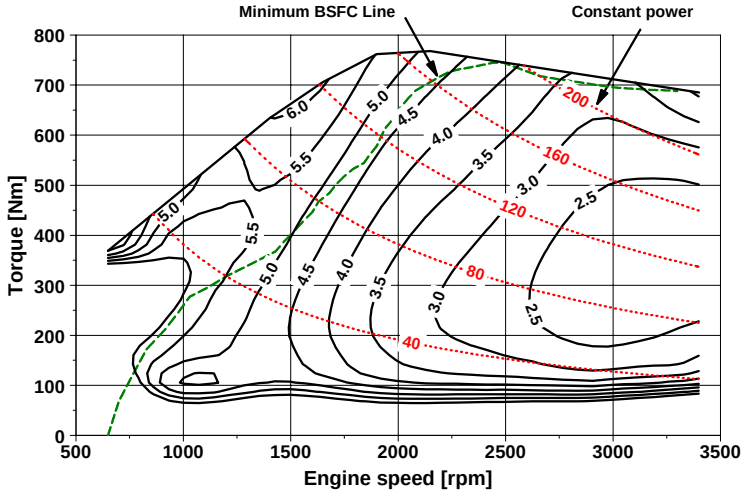

(b) $BSNO_x$ [g/kWh], V8

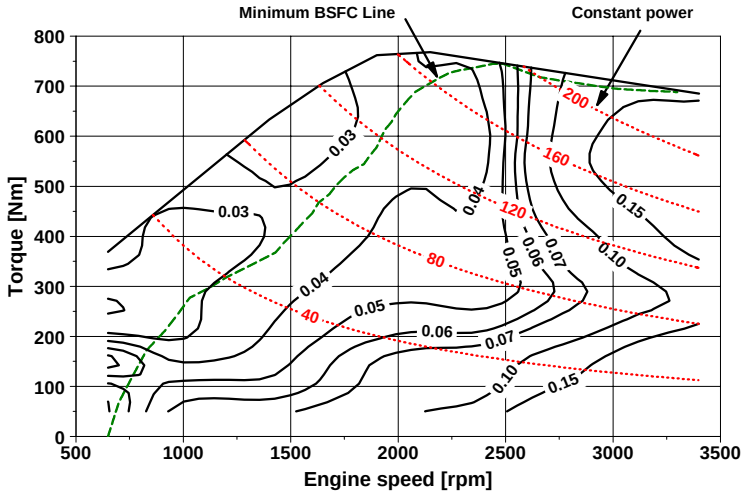

(c) BSsoot [g/kWh], V8

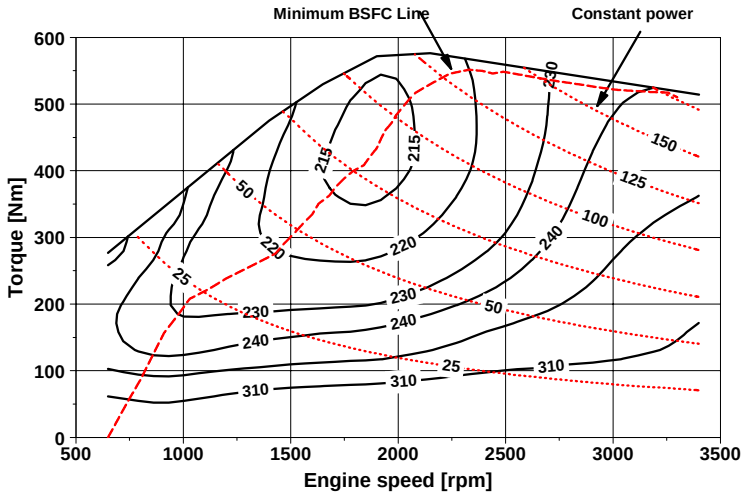

(d) BSFC [g/kWh], V6

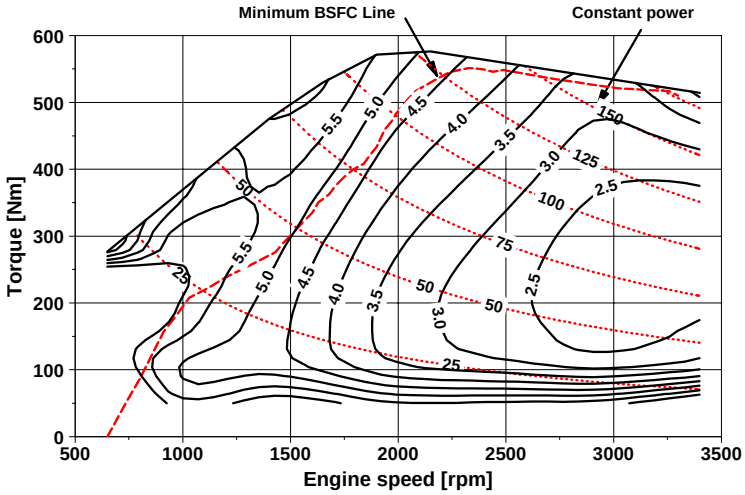

(e) $BSNO_x$ [g/kWh], V6

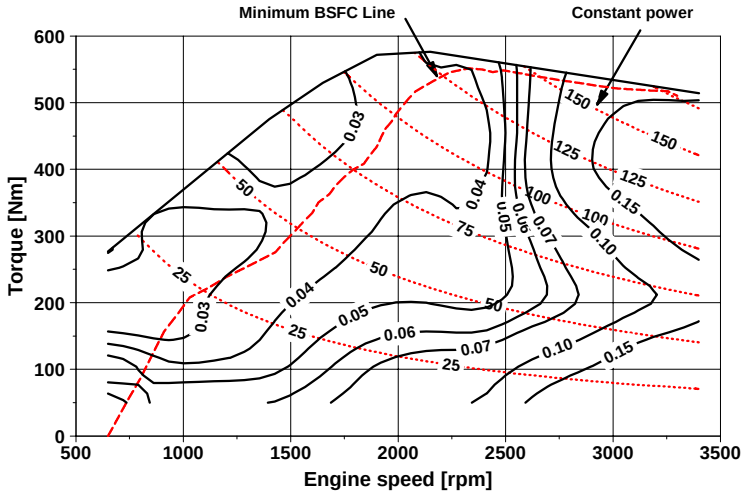

(f) BSsoot [g/kWh], V6

Figure A. 1. Engine maps

A. 3. P/M Efficiency Maps (maximum displacement: 150cc/rev)

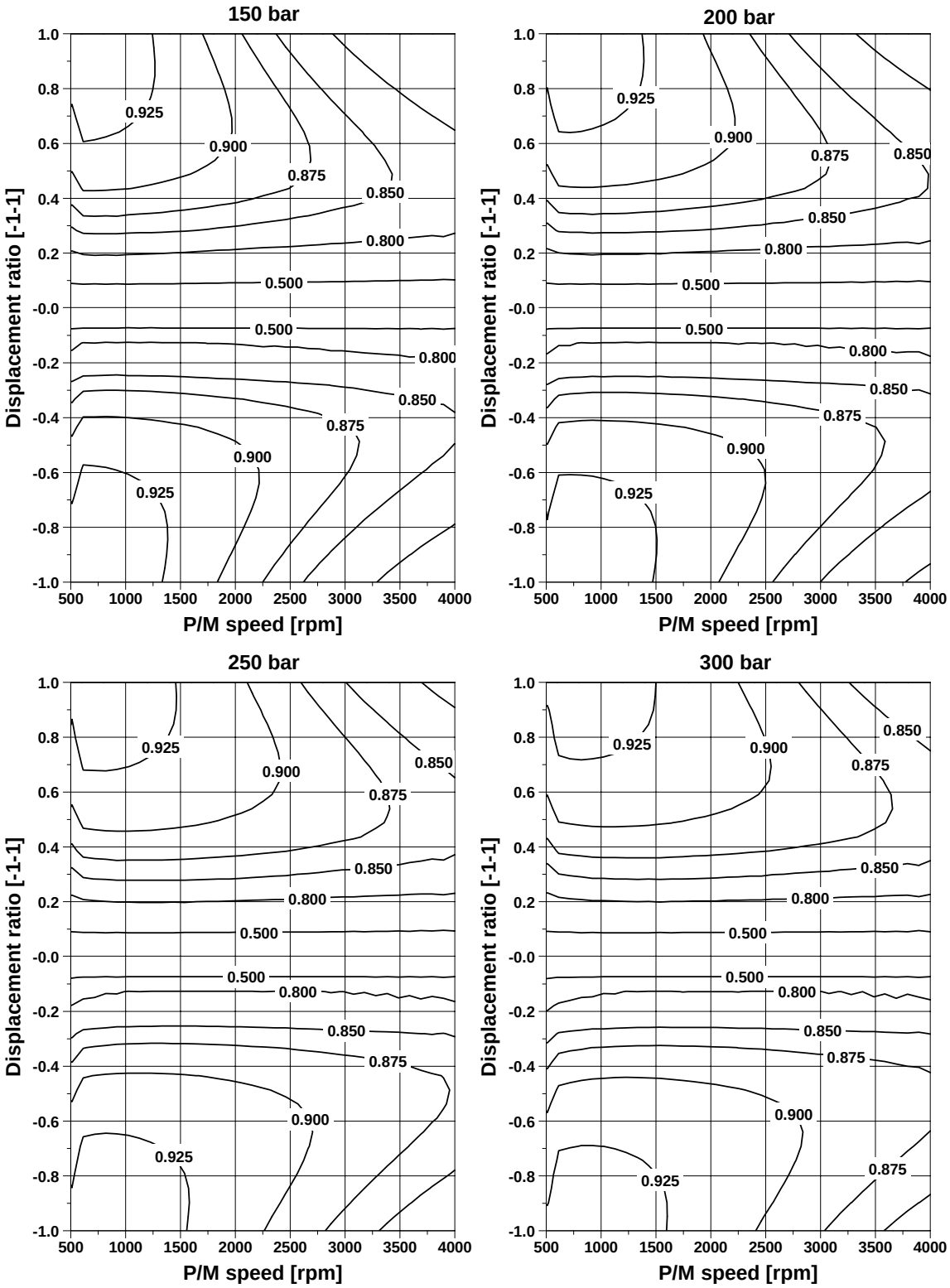

Figure A. 2. P/M maps (*D*=150cc/rev)

A. 4. Hydraulic Accumulator and Pump/Motor Characteristics

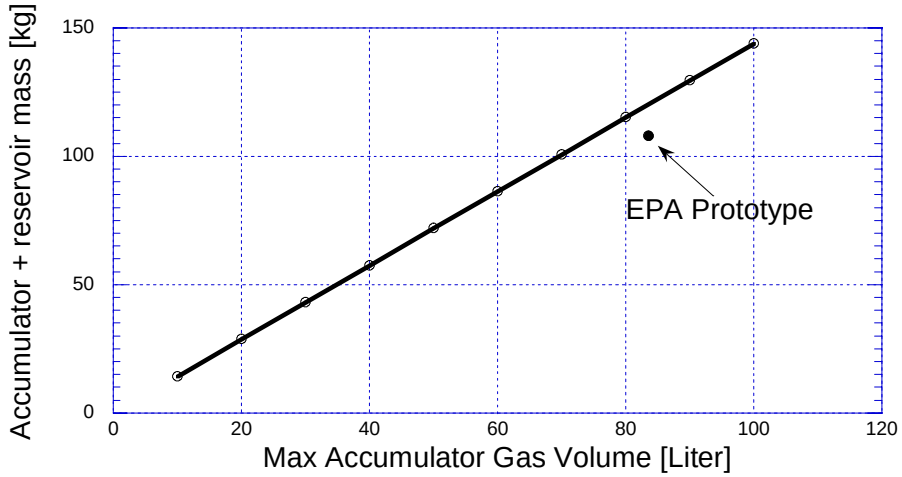

(a) Energy storage mass and volume relation

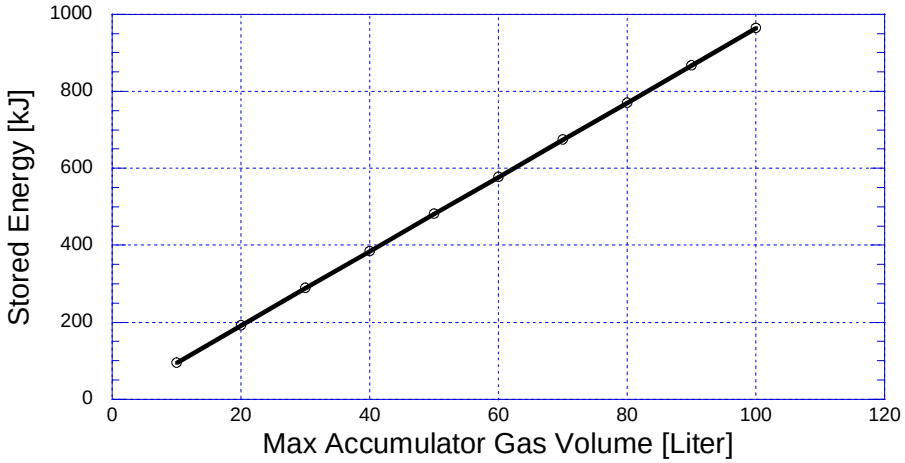

(b) Energy storage energy capacity and volume relation

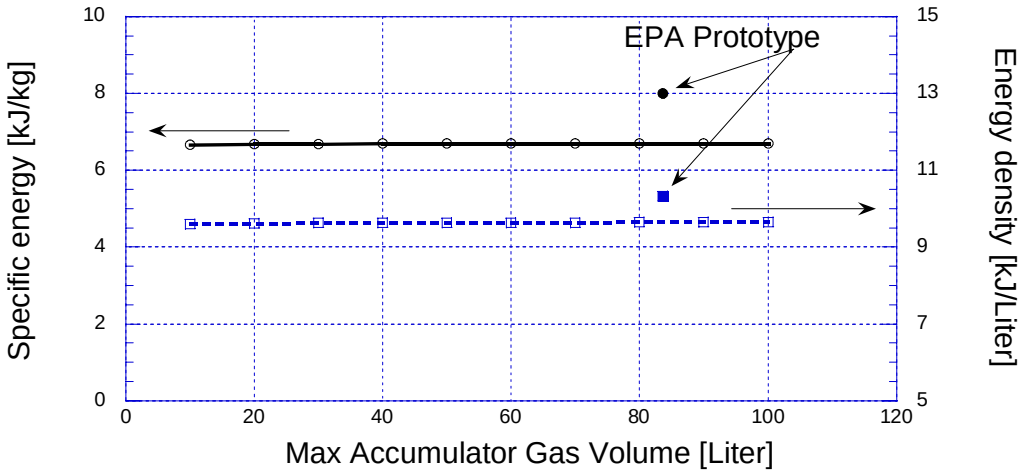

(c) Energy storage specific energy and energy density with volume relation

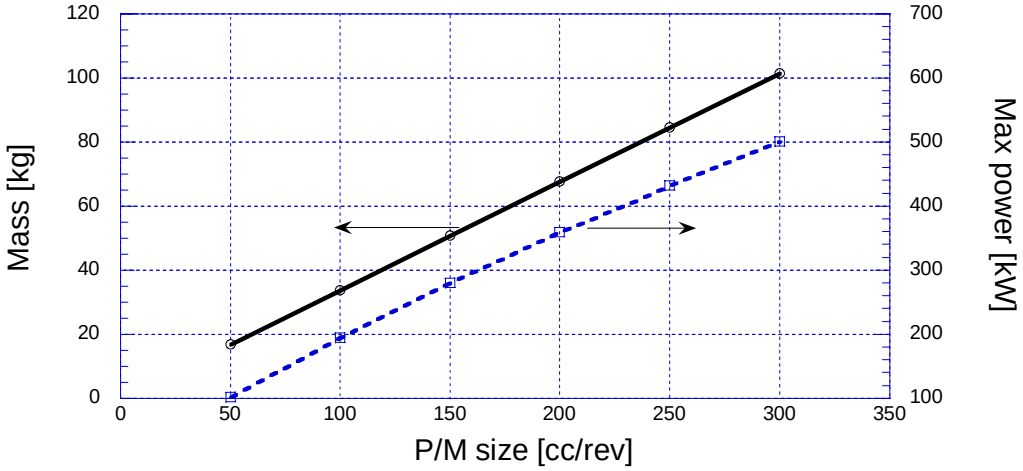

(d) P/M mass and max power vs. P/M size

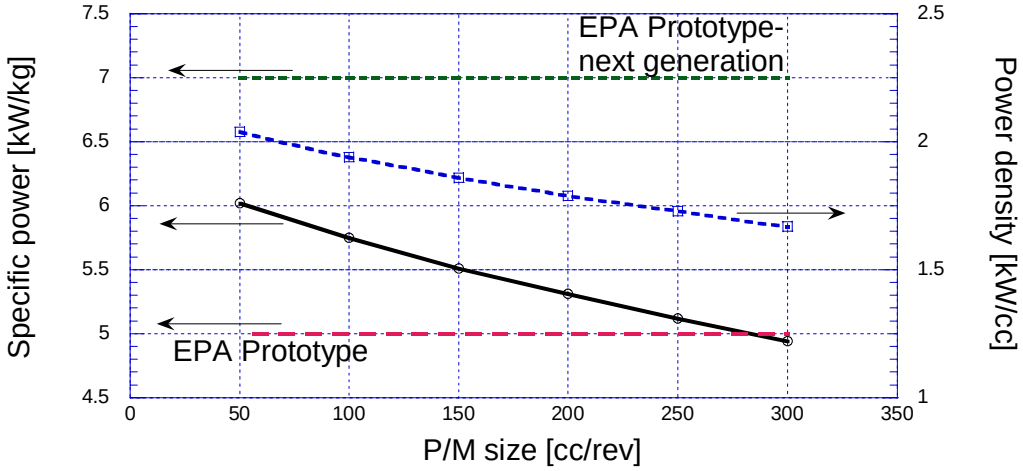

(e) P/M specific power and power density vs. P/M size

Figure A. 3. Hydraulic P/M characteristics at 350bar, 4000rpm

***from the EPA prototype, the size and pressure condition, rotational speed is not provided [17]**

A. 5. General Solution of $ax^3 + bx + c = 0$

$$x_1 = \frac{1}{6a}\sqrt[3]{\left(\left(-108c + 12\sqrt{3}\right)\sqrt{\frac{4b^3 + 27ac^3}{a}}\right)a^2} - \frac{2b}{\sqrt[3]{\left(\left(-108c + 12\sqrt{3}\right)\sqrt{\frac{4b^3 + 27ac^3}{a}}\right)a^2}}$$

$$x_2 = -\frac{1}{2}\left(\frac{1}{6a}\sqrt[3]{\left(\left(-108c + 12\sqrt{3}\right)\sqrt{\frac{4b^3 + 27ac^3}{a}}\right)a^2} - \frac{2b}{\sqrt[3]{\left(\left(-108c + 12\sqrt{3}\right)\sqrt{\frac{4b^3 + 27ac^3}{a}}\right)a^2}}\right) +$$

$$-\frac{\sqrt{3}i}{2}\left(\frac{1}{6a}\sqrt[3]{\left(\left(-108c + 12\sqrt{3}\right)\sqrt{\frac{4b^3 + 27ac^3}{a}}\right)a^2} + \frac{2b}{\sqrt[3]{\left(\left(-108c + 12\sqrt{3}\right)\sqrt{\frac{4b^3 + 27ac^3}{a}}\right)a^2}}\right)$$

$$x_3 = -\frac{1}{2}\left(\frac{1}{6a}\sqrt[3]{\left(\left(-108c + 12\sqrt{3}\right)\sqrt{\frac{4b^3 + 27ac^3}{a}}\right)a^2} - \frac{2b}{\sqrt[3]{\left(\left(-108c + 12\sqrt{3}\right)\sqrt{\frac{4b^3 + 27ac^3}{a}}\right)a^2}}\right) -$$

$$-\frac{\sqrt{3}i}{2}\left(\frac{1}{6a}\sqrt[3]{\left(\left(-108c + 12\sqrt{3}\right)\sqrt{\frac{4b^3 + 27ac^3}{a}}\right)a^2} + \frac{2b}{\sqrt[3]{\left(\left(-108c + 12\sqrt{3}\right)\sqrt{\frac{4b^3 + 27ac^3}{a}}\right)a^2}}\right)$$

BIBLIOGRAPHY

[1] Davis, S. C., Diegel, S.W., "Transportation Energy Data Book: Edition 24", Center for Transportation Analysis Engineering Science & Technology Division, Oak Ridge National Laboratory, 2004.

[2] Environmental Protection Agency, "World's First Full-Size Hydraulic Hybrid SUV Presented at 2004 SAE World Congress", EPA420-F-04-019, 2004.

[3] Pourmovahed, A., "Vehicle propulsion systems with hydraulic energy storage. A literature survey", International Journal of Vehicle Design, Vol. 12, No. 4, 1991, pp. 378-403.

[4] Backe, W., "The present and future of fluid power", Proceedings of the Institution of Mechanical Engineers. Part I, Journal of Systems & Control Engineering, Vol. 207, No 4, 1993, pp. 193-212.

[5] Miller, J. M., "Propulsion systems for hybrid vehicles", Stevenage, UK, Institution of Electrical Engineers, 2004.

[6] Williamson, S.S., Emadi, A.,Rajashekara, K., "Comprehensive Efficiency Modeling of Electric Traction Motor Drives for Hybrid Electric Vehicle Propulsion Applications", IEEE Transactions on Vehicular Technology, Vol.56, No.4, July 2007.

[7] Buchwald, P., Christensen, H., Larsen, H., Pedersen, P. S., "Improvement of City bus Fuel Economy Using a Hydraulic Hybrid Propulsion System-a Theoretical and Experimental Study", SAE Paper 790305, Warrendale, PA, USA, 1979.

[8] Tollefson, S. W., Beachley, N. H. and Fronczak, F. J., "Studies of an accumulator energy storage automobile design with a single pump/motor", SAE Paper 851677, Warrendale, PA, USA, 1985.

[9] Wu, P., Luo, N. C., Fronczak, F. J. and Beachley, N. H., "Fuel Economy and Operating Characteristics of a Hydropneumatic Energy Storage Automobile", SAE Paper 851678, Warrendale, PA, USA, 1985.

[10] Park, J., Raju, B., Emadi, A., "Effects of an Ultra-Capacitor and Battery Energy Storage System in a Hybrid Electric Vehicle", SAE paper 2005-01-3452, Warrendale, PA, USA, 2005.

[11] Wu, B., Lin, C. C., Filipi, Z., Peng, H., Assanis, D, "Optimization of Power Management Strategies for a Hydraulic Hybrid Medium Truck", Vehicle System Dynamics, Vol. 42, Nos. 1-2, 2004, pp.23-40.

[12] Filipi, Z., Louca, L., Daran, B., Lin, C. C., Yildir, U., Wu, B., Kokkolaras, M., Assanis, D., Peng, H., Papalambros, P., Stein, J., Szkubiel, D., Chapp, R., "Combined optimization of design and power management of the hydraulic hybrid propulsion system for the 6 x 6 medium truck", International Journal of Heavy Vehicle Systems, Vol. 11, No 3-4, 2004, pp. 372-402.

[13] Kapellen, D. R., Jamzadeh, F., Frank, A. A. and Wang, S., "Analysis of energy-storage concepts for refuse collection trucks", SAE Paper 840056, Warrendale, PA, USA, 1984.

[14] Beachley, N. H. and Otis, D. R., "Study of accumulator passenger cars based on the Ifield hydrostatic pump/motor unit", UCRL-15390, Aug., NTIS, 1981.

[15] Beachley, N. H., "Comparison of accumulator and flywheel energy storage for motor vehicle applications", 20th IECEC, Aug 1985.

[16] Beachley, N. H. and Fronczak, F. J. "Control of an accumulator energy-storing automobile using a single hydrostatic pump/motor", Proc. Int. Conf. Fluid Power Trans. and Control, Hangzhou, China, Sep 1985.

[17] Alson, J., Barba, D., Bryson, J., Doorag, M., Haugen, D., Kargul, J., McDonald, J., Newman, K., Platte, L., Wolcott, M., "Progress Report on clean and Efficient Automotive Technologies Under Development at EPA", EPA420-R-04-002, 2004.

[18] Pourmovahed, A., Baum, S. A., Fronczak, F. J., Beachley, N. H., "Experimental Evaluation of Hydraulic Accumulator Efficiency with and without Elastomeric Foam", Journal of Propulsion and Power, Vol. 4, No 2, 1988, pp. 185-192.

[19] Brahma, A., Guezennec, Y., Rizzoni, G., "Optimal energy management in series hybrid electric vehicles", American Automotive Control Council, Vol. 1, 2000, pp. 60-64.

[20] Caratozzolo, P., Serra. M., Riera. J., "Energy management strategies for hybrid electric vehicles", IEMDC'03. IEEE International Electric Machines and Drives Conference, Vol. 1, 2003, pp. 241-248.

[21] Paganelli, G., Guezennec, Y., Rizzoni, G., "Optimizing Control Strategy for Hybrid Fuel Cell Vehicle", SAE Paper 2002-01-0102, Warrendale, PA, USA, 2002.

[22] Konev, A., Lezhnev, L., Kolmanovsky, I., "Control Strategy Optimization for a Series Hybrid Vehicle", SAE Paper 2006-01-0663, Warrendale, PA, USA, 2006.

[23] Jalil, N., Kheir, N. A., Salman, M., "A rule-based energy management strategy for a series hybrid vehicle", American Automotive Control Council, Vol. 1, 1997, pp. 689-693.

[24] Kokkolaras, M., Louca, L. S., Delagrammatikas, G. J., Michelena, N. F., Filipi, Z. S., Papalambros, P. Y., Stein, J. L. and Assanis, D. N., "Simulation-based optimal design of heavy trucks by model-based decomposition: An extensive analytical target cascading case study", International Journal of Heavy Vehicle Systems, Vol. 11, no 3-4, 2004, pp. 403-433.

[25] Beachley, N. H., "Control Strategies for an Internal Combustion Engine/Accumulator Automobile", Proceedings, Symposium on Advanced and Hybrid Vehicles, University of Strathclyde, Glasgow, Scotland, Sep. 1984, pp 72-82.

[26] Rahman, Z., Butler, K. L., Ehsani, M., "Design studies of a series hybrid heavy-duty transit bus using V-ELPH 2.01", IEEE, 49th Vehicular Technology Conference, Vol.3, 1999, pp. 2268-2272.

[27] Otis, D. R., Pourmovahed, A., "Algorithm for Computing Non flow Gas Processes in Gas Springs and Hydro pneumatic Accumulators", Journal of Dynamic Systems, Measurement and Control, Transactions ASME, Vol. 107, No.1, 1985, pp. 53-59.

[28] Pourmovahed, A., Beachley, N. H., Fronczak, F. J., "Modeling of a hydraulic energy regeneration system-Part I: Analytical treatment", Journal of Dynamic Systems, Measurement and Control, Transactions of the ASME, Vol. 114, No 1, 1992, pp. 155-159.

[29] Pourmovahed, A., Beachley, N. H., Fronczak, F. J., "Modeling of a hydraulic energy regeneration system-Part II: Experimental Program", Journal of Dynamic Systems, Measurement and Control, Transactions of the ASME, Vol. 114, No 1, 1992, pp. 160-165.

[30] Pourmovahed, A., and Otis, D. R., "An Experimental Thermal Time-Constant Correlation for Hydraulic Accumulators", ASME Journal of Dynamic Systems, Measurement and Control, Vol. 112, No. 1, 1990, pp. 116-121.

[31] Wiegman, H. L. N., Vandenput, A.J.A., "Battery State Control Techniques for Charge Sustaining Applications", SAE Paper 981129, Warrendale, PA, USA, 1998.

[32] Hydraulics & Pneumatics Magazine, http://www.hydraulicspneumatics.com/ , "Hydraulic motors - part 2".

[33] Lin, C. C., Filipi, Z., Wang, Y., Louca, L., Peng, H., Assanis, D., Stein, J, "Integrated, feed-forward hybrid electric vehicle simulation in SIMULINK and its use for power management studies", SAE Paper 2001-01-1334, Warrendale, PA, USA, 2001.

[34] Louca, L., Yildir, U. B., "Modeling and Reduction Techniques for Studies of Integrated Hybrid Vehicle Systems", Mathematical and Computer Modeling of Dynamical Systems, Vol. 12, No. 2-3, April-June 2006, pp. 203-218(16).

[35] Fathy, H. K., Ahlawat, R., and Stein, J. L., "Proper Powertrain Modeling for Engine-in-the-Loop Simulation", Proceedings of the ASME International Mechanical Engineering Congress and Exposition, November 5-11 2005, Orlando, Florida, 2005.

[36] Filipi, Z., Fathy, H., Hagena, J., Knafl, A., Ahlawat, R., Liu, J., Jung, D., Assanis, D., Peng, H., Stein, J., "Engine-in-the-Loop Testing for Evaluating Hybrid Propulsion Concepts and Transient Emissions – HMMWV Case Study", SAE Paper 2006-01-0443, Warrendale, PA, USA, 2006.

[37] Franklin, G. F., Powell, J. D., and Emami-Naeini, A., "Feedback Control of Dynamic Systems", 3rd edition, Addison-Wesley, 1994.

[38] Skogestad, S., and Postlethwaite, I., "Multivariable Feedback Control: Analysis and Design", John Wiley & Sons, 1997.

[39] Transportation and Regional Programs Division, "IM240 & Evap Technical Guidance", EPA420-R-00-007, Office of Transportation and Air Quality, U.S. Environmental Protection Agency, April 2000.

[40] Hagena, J., Filipi, Z., Assanis, D., "Transient Diesel Emissions: Analysis of Engine Operation During a Tip-In", SAE Paper 2006-01-1151, Warrendale, PA, USA, 2006.

[41] Assanis, D., Filipi. Z., Gravante, S., Grohnke, D., Gui. X., Louca, L., Rideout. G., Stein, J., Wang, Y., "Validation and use of SIMULINK integrated, high fidelity, engine-in-vehicle simulation of the international class VI truck", SAE Paper 2000-01-0288, Warrendale, PA, USA, 2000.

[42] Assanis, D., Delagrammatikas, G., Fellini, R., Filipi, Z., Liedtke, J., Michelena, N., Papalambros, P., Reyes, D., Rosenbaum, D., Sales, A., Sasena, M., "Optimization approach to hybrid electric propulsion system design", Mechanics of Structures and Machines, Vol. 27, No. 4, 1999, pp. 393-421.

[43] Lin, C. C., Kang, J. M., Grizzle, J. W., Peng, H., "Energy management strategy for a parallel hybrid electric truck", IEEE, Proceedings of the American Control Conference, Vol. 4, 2001, pp. 2878-2883.

[44] Lin, C. C., Kang, J. M., Grizzle, J. W., Peng, H., "Power management strategy for a parallel hybrid electric truck", IEEE, transactions on control systems technology, Vol. 11, No. 6, Nov. 2003, pp. 839- 849.

[45] NEUGART, http://www.neugartusa.com/. "Planetary gear ratios & Rating"

[46] Papalambros, P. Y. Wilde, D. J., "Principles of optimal design : modeling and computation", Cambridge University Press, 1991.

[47] McKay, M. D., Beckman, R. J., Conover, W. J., "Comparison of three methods for selecting values of input variables in the analysis of output from a computer code", Technometrics, Vol. 42, No. 1, 2000, pp. 55-61.

[48] Koch, P. N., Evans, J. P., Powell, D., “Interdigitation for effective design space exploration using iSIGHT”, Structural and Multidisciplinary Optimization, Vol. 23, No. 2, 2002, pp. 111-126.

[49] Ng, H., Anderson, J., Duoba, M. J., Larsen, R., “Engine Start Characteristics of Two Hybrid Electric Vehicles (HEVs) – Honda Insight and Toyota Prius”, SAE Paper 2001-01-2492, Warrendale, PA, USA, 2001.

[50] Partridge W. P., Storey, J. M. E., Lewis, S. A., Smithwick, R. W., DeVault, G. L., Cunningham, M. J., Currier, N. W., Yonushonis, T. M., “Time-Resolved Measurements of Emission Transients by Mass Spectrometry”, SAE Paper 2000-01-2592, Warrendale, PA, USA, 2000.

[51] Reavell, K., Hands, T., Collings, N., “A fast-response particulate spectrometer for combustion aerosols”, SAE Paper 2002-01-2714, Warrendale, PA, USA, 2002.

[52] Park, K., Cao, F., Kittelson, D. B., McMurry, P. H., “Relationship between particle mass and mobility for diesel exhaust particle”, Environmental Science and Technology, Vol. 37, No. 3, 2003, pp. 577-583.

[53] Christian, V. R., Knopf, F., Jaschek, A., Schindler, W., “Eine neue Messmethodik der Bosch-Zahl mit erhoehter Empfindlichkeit”, MTZ, Vol. 54, 1993, pp. 16-22.

[54] Fleming, M., Leng, G., Stryker, P., “Design and Construction of a University-Based Hybrid Electric Power train Test Cell”, SAE Paper 2000-01-3106, Warrendale, PA, USA, 2000.

[55] Tartt, C. J. and Moskwa, J. J., “A hardware-in-the-loop transient diesel engine test system for control and diagnostic development”, Proceedings of ASME International Mechanical Engineering Congress and Exposition, Vol. 2, 2001, pp. 1207-1213.

[56] Gelb, G. H., Richardson, N. A., Wang, T. C., Berman, B., “An Electromechanical Transmission for Hybrid Vehicle Power Trains - Design and Dynamometer Testing”, SAE Paper 710235, Warrendale, PA, USA, 1971.

[57] Sasaki, S. “Toyota’s newly developed hybrid power train”, Proceedings of the 1998 10th IEEE International Symposium on Power Semiconductor Devices & ICs, Kyoto, Japan, 1998, pp. 17-22.

[58] Harada, O., Yamaguchi, K., Shibata, Y., “Power output apparatus and method of controlling the same”, U.S. Patent number 6,067,801, issued May. 30, 2000.

[59] Morisawa, K., Shiori, H., Iwase, Y., Itoh, H., Nagashima N., Umeyama, M. Taga, Y., “Hybrid Drive System”, U.S. Patent number 6,306,057, issued Oct. 23, 2001.

[60] Holmes, A. G., Klemen, D., Schmidt, M. R., “Electrically Variable Transmission with Selective Input Split, Compound Split, Neutral and Reverse Modes”, U.S. Patent number 6,527,658, issued May. 4, 2003.

[61] Holmes, A. G., Schmidt, M. R., “Hybrid Electric Power train Including a Two-Mode Electrically Variable Transmission”, U.S. Patent number 6,478,705 B1, issued Nov. 12, 2002.

[62] Duoba, M., Ng, H., Larsen, R., “In-Situ Mapping and Analysis of the Toyota Prius HEV Engine”, SAE Paper 2000-01-3096, Warrendale, PA, USA, 2000.

[63] Duoba, M., Ng, H., Larsen, R., “Characterization and Comparison of Two Hybrid Electric Vehicles (HEVs) - Honda Insight and Toyota Prius”, SAE Paper 2001-01-1335, Warrendale, PA, USA, 2001.

[64] Markel, T., Brooker, A., Hendricks, T., Johnson, V., Kelly, K., Kramer, B., O’Keefe, M., Sprik, S., Wipke, K., “ADVISOR: A systems analysis tool for advanced vehicle modeling”, Journal of Power Sources, Vol.110, No. 2, 2002, pp. 255-266.

[65] Rousseau, A., Sharer, P., Pasquier, M., “Validation Process of a HEV System Analysis Model: PSAT”, SAE Paper 2001-01-0953, Warrendale, PA, USA, 2001.

[66] Liu, J., Peng, H., Filipi, Z., “Modeling and analysis of the Toyota hybrid system”, 2005 IEEE/ASME International Conference on Advanced Intelligent Mechatronics, Vol. 1, 2005, pp. 134-139.

[67] “Toyota Hybrid system THS II”, http://www.toyota.co.jp/en/tech/environment/ths2/SpecialReports_12.pdf

[68] Gillespie, T. D., “Fundamentals of vehicle dynamics”, Society of Automotive Engineers, Inc., 400 Commonwealth Drive, Warrendale, PA, 2001.

[69] Haapala, K., Thul, A., Andrasko, S., Muehlfield, C., Bloss, B., Nesbitt, R., Beard, J. E., “Design and Development of the 2001 Michigan Tech Future Truck, a Power-Split Hybrid Electric Vehicle”, SAE Paper 2002-01-1212, Warrendale, PA, USA, 2002.

[70] Bertsekas, D. P., “Dynamic Programming and Optimal Control”, Athena Scientific, Vol. I, 2nd edition, 2001.

[71] Bellman, R. E., “Dynamic Programming”, Princeton University Press, 1962.

[72] Puterman, M. L., “Markov Decision Processes: Discrete Stochastic Dynamic Programming”, New York, J. Wiley, 1994.

[73] Han, Z., Yuan, Z., Guangyu, T., Quanshi, C., Yaobin, C., “Optimal Energy Management Strategy for Hybrid Electric Vehicles”, SAE Paper, Warrendale, PA, USA, 2004-01-0576, 2004.

[74] Rizoulis, D., Burl, J., Beard, J., “Control Strategies for a Series-Parallel Hybrid Electric Vehicle”, SAE paper, 2001-01-1354, Warrendale, PA, USA, 2001.

[75] Dai, J., “Isolated Word Recognition Using Markov Chain Models”, IEEE Transactions on speech and audio processing, Vol. 3, No. 6, Nov. 1995, pp. 458-463.

[76] He, B., Yang, M., “Optimization-based energy management of series hybrid vehicles considering transient behavior”, Int. J. Alternative Propulsion, Vol. 1, No.1, 2006, pp. 79~96.

[77] Kang, J., Kolmanovsky, I., Grizzle, J. W., “Dynamic Optimization of Lean Burn Engine Aftertreatment”, ASME J. of Dynamic Systems, Measurement and Controls, Vol. 123, No. 2, 2001, pp. 153-160.

[78] Paganelli, G., Delprat, S., Guerra, T. M., Rimaux, J., Santin, J., “Equivalent consumption minimization strategy for parallel hybrid power trains”, IEEE Vehicular Technology Conference, Vol. 4, 2002, pp. 2076-2081.

[79] Lin, C. C., Peng, H., Grizzle, J. W., “A Stochastic Control Strategy for Hybrid electric Vehicle”, Proceeding of the 2004 American Control conference, Boston, Massachusetts, Vol.5, 2004, pp. 4710- 4715.

[80] Kolmanovsky, I., Siverguina, I., Lygoe, B., “Optimization of Power train Operation Policy for Feasibility Assessment and Calibration: Stochastic Dynamic Programming Approach”, Proceedings of American Control Conference, Anchorage, AK, May 2002, pp. 1425-1430.

[81] Schouten, N. J., Salman, M. A., Kheir, N. A., “Fuzzy Logic Control for Parallel Hybrid Vehicles”, IEEE Transactions on control systems technology, Vol. 10, No. 3, 2002, pp. 460-468.

[82] Musardo, C., Rizzoni, G, Staccia, B., “A-ECMS: An Adaptive Algorithm for Hybrid Electric Vehicle Energy Management”, Proceedings of the 44th IEEE Conference on Decision and Control, and the European Control Conference, Seville, Spain, Dec 2005, pp. 1816- 1823.

[83] Liu, J., Peng, H., “Control Optimization for a Power-Split Hybrid Vehicle”, Proceedings of the 2006 American Control Conference, Minneapolis, June 2006, pp. 461-471.

[84] Sciarretta, A., Back, M., Guzzella, L., “Optimal Control of Parallel Hybrid Electric Vehicles”, IEEE Transactions on control systems technology, Vol. 12, No. 3, 2004, pp. 352- 363.

[85] Pisu, P., Rizzoni, G., “A Supervisory Control Strategy for Series Hybrid Electric Vehicles with Two Energy Storage Systems”, Vehicle Power and Propulsion, IEEE Conference, Sep 2005, pp. 65-72.

[86] Barsali, S., Ceraolo, M., Possenti, A., “Techniques to Control the Electricity Generation in a Series Hybrid Electrical Vehicle”, IEEE Transactions on energy conversion, Vol. 17, No. 2, 2002, pp. 260-266.

[87] Barsali, S., Miulli, C., Possenti, A., “A Control Strategy to Minimize Fuel Consumption of Series Hybrid Electric Vehicles”, IEEE Transactions on energy conversion, Vol. 19, No. 1, 2004, pp. 187- 195.

[88] Niasar, A. H., Moghbelli, H., Vahedi, A., “Design Methodology of Drive Train for a Series-Parallel Hybrid Electric Vehicle (SP-HEV) and its Power Flow control Strategy”, IEEE International Conference on Electric Machines and Drives, 2005, pp. 1549-1554.

[89] Perez, L. V., Bossio, G. R., Moitre, D., Garcia, G. O., “Optimization of power management in an hybrid electric vehicle using dynamic programming”, Mathematics and Computers in simulation, Vol. 73, 2006, pp. 244-254.

[90] Kleimaier, a., Schroder, D., “An Approach for the Online optimized control of a hybrid Powertrain”, Advanced Motion Control, 2002. 7th IEEE International Workshop, 2002, pp. 215- 220.

[91] Paganelli, G, Ercole, G., Brahma, a., Guezennec, Y., Rizzoni, G., “General supervisory control policy for the energy optimization of charge-sustaining hybrid electric vehicles”, JSAE Review, Vol. 22, No. 4, 2001, pp. 511-518.

[92] Johnson, V. H., Wipke, K. B., Rausen, D. J., “HEV control Strategy for Real-Time Optimization of Fuel Economy and Emissions”, SAE paper 2000-01-1543, 2000.

[93] Kolmanovsky, I., Nieuwstadt, M., Sun, J., “Optimization of complex Powertrain systems for Fuel Economy and emissions”, Proceedings of the 1999 IEEE, International Conference on Control applications, Vol. 1, 1999, pp. 833-839.

[94] Liang, C., Weihua, W., Qingnian W., “Energy Management Strategy and Parametric Design for Hybrid Electric Military Vehicle”, SAE paper 2003-01-0086, Warrendale, PA, USA, 2003.

[95] Piccolo, A., Ippolito, L., zo Galdi, V. Vaccaro, A., “Optimization of energy Flow Management in Hybrid Electric Vehicles via Genetic Algorithms”, IEEE/ASME International Conference on Advanced Intelligent Mechatronics Proceedings, Vol. 1, 2001, pp. 434-439.

[96] Miller, J. M., Everett, M., “An Assessment of Ultra-capacitors as the Power Cache in Toyota THS-II, GM-Allison AHS-2 and Ford FHS hybrid propulsion systems”, APEC 2005. Twentieth Annual IEEE Applied Power Electronics Conference and Exposition, Vol. 1, 2005, pp. 481-490.

[97] Beachley, N. H., “Hydromechanical transmission saves fuel”, Hydraulics and Pneumatics, June 1981, pp. 73-76.

[98] Hochgraf, C. G., Ryan M. J., Wiegman, H. L., “Engine control Strategy for a Series Hybrid Electric Vehicle Incorporating Load-leveling and Computer Controlled Energy Management”, SAE paper 960230, 1996.

[99] Rahman, Z., Butler, K. L., Ehsani, M., “A Comparison Study Between Two Parallel hybrid Control Concept”, SAE paper 2000-01-0994, Warrendale, PA, USA, 2000.

[100] Fellini, R., Michelena, N., Papalambros, P., Sasena, M., “Optimal Design of Automotive Hybrid Powertrain Systems”, Environmentally Conscious Design and Inverse Manufacturing, 1999. Proceedings. EcoDesign '99: First International Symposium, Feb, Tokyo, Japan, 1999, pp.400-405.

[101] Lin, C. C., Peng, H., Grizzle, J. W., “Control system Development for an Advanced-Technology Medium-duty Hybrid Electric Truck”, SAE paper, 2003-01-3369, Warrendale, PA, USA, 2003.

[102] Muta, K., Yamazaki, M., Tokieda, J., “Development of New-Generation Hybrid system THS II –Drastic Improvement of Power Performance and Fuel Economy”, SAE paper, 2004-01-0064, Warrendale, PA, USA, 2004.

[103] Hewko, L. O., Weber, T. R., “Hydraulic Energy Storage Based Hybrid Propulsion System for a Terrestrial Vehicle”, Energy Conversion Engineering Conference, 1990. IECEC-90. Proceedings of the 25th Intersociety, Vol.4, 1990, pp. 99-105.

[104] Wu, B., Lin, C. C., Filipi, Z., Peng, H., Assanis, D, “Optimal Power Management for a Hydraulic Hybrid Delivery Truck”, Vehicle System Dynamics, Vol. 42, No. 1-2, 2004, pp. 23-40.

[105] Fathy, H. K., Filipi, Z. S., Hagena J., Stein, J. L., “Review of Hardware-in-the-Loop Simulation and Its Prospects in the Automotive Area”, Modeling and Simulation for Military Applications. Proceedings of the SPIE, Vol. 6228, 2006, pp. 62280E.

[106] Isermann, R., Schaffnit, J. and Sinsel, S., "Hardware-in-the-Loop Simulation for the Design and Testing of Engine-Control Systems", Control Engineering Practice, Vol. 7, pp. 643-653, 1999.

[107] Zhang, R. and Alleyne, A. G., "Dynamic Emulation Using an Indirect Control Input", Journal of Dynamic Systems, Measurement and Control, Vol. 127, pp. 114-124, 2005.

[108] Deppe, M., Robrecht, M., Zanella, M. and Hardt, W., "Rapid Prototyping of Real-Time Control Laws for Complex Mechatronic Systems", Proceedings of the 12th IEEE International Workshop on Rapid System Prototyping, June, 25-27 2001, pp. 188-193, Institute of Electrical and Electronics Engineers Computer Society, Monterrey, CA, 2001.

[109] Liu, J. W., Real-Time Systems, Prentice-Hall, Upper Saddle River, New Jersey, USA, 2000.

[110] Hagiwara, K., Terayama, S., Takeda, Y., Yoda, K. and Suzuki, S., "Development of Automatic Transmission Control System Using Hardware-in-the-Loop Simulation System", JSAE Review, Vol. 23, pp. 55-59, 2002.

[111] Howe, R. M. , "Real-time Multi-rate Asynchronous Simulation with Single and Multiple Processors", Enabling Technology for Simulation Science II, April 14-16 1998, vol. 3369, pp. 331-342, The International Society for Optical Engineering, Orlando, FL, United States, 1998.

[112] Lane, D. M., Falconer, G. J., Randall, G. and Edwards, I. , "Interoperability and Synchronisation of Distributed Hardware-in-the-Loop Simulation for Underwater Robot Development: Issues and Experiments", Proceedings of the 2001 IEEE International Conference on Robotics and Automation, 21-26 May 2001, Vol.1, pp. 909-14, IEEE, Seoul, South Korea, 2001.

[113] Terwiesch, P., Keller, T. and Scheiben, E., "Rail Vehicle Control System Integration Testing Using Digital Hardware-in-the-Loop Simulation", IEEE Transactions on Control System Technology, Vol. 7, pp. 352-62, 1999.

[114] Ersal, T., Fathy, H. K., Stein, J. L., and Louca, L. S., “Automated Proper Modeling: Theoretical Developments and Applications”, Proceedings of the SPIE Modeling and Simulation Symposium, Society of Optical Engineering, Kissimee, FL, United States, 2006.

[115] Kozaki, T., Mori, H., Fathy, H. K., and Gopalswamy, S., “Balancing the Speed and Fidelity of Automotive Powertrain Models Through Surrogation”, Proceedings of the ASME International Mechanical Engineering Congress and Exposition, Nov. 16-20, 2004, Anaheim, California, 2004.

[116] Hong, S.-Ch., Rutland, C., Reitz, R., “Development of an Integrated Spray and Combustion Model for Diesel Simulations”, SAE paper 2001-30-0012, Warrendale, PA, USA, 2001.

[117] Hong, S., Assanis, D., Wooldridge, M., “Multi-dimensional modeling of NO and soot emissions with detailed chemistry and mixing in a direct injection natural gas engine”, SAE paper 2002-01-1112, Warrendale, PA, USA, 2002.

[118] Nabi, S., Balike, M., Allen, J., and Rzemien, K., “An Overview of Hardware-in-the-Loop Testing Systems at Visteon”, Proceedings of the SAE World Congress and Exhibition, March 8-11 2004, SAE paper 2004-01-1240, Warrendale, PA, USA, 2004.

[119] Fleming, M., Len, G., and Stryker, P., “Design and Construction of a University-Based Hybrid Electric Powertrain Test Cell”, SAE Paper 2000-01-3106, Warrendale, PA, USA, 2000.

[120] Shidore, N., and Pasquier, M., “Interdependence of System Control and Component Sizing for a Hydrogen-Fueled Hybrid Vehicle”, SAE Paper 2005-01-3457. Proc. of SPIE Vol. 6228 62280E-19, Warrendale, PA, USA, 2005

[121] “Diesel Hybridization and Emissions”, Argonne National Laboratory Center for Transportation Research, Report to the DOE from the ANL Vehicle Systems and Fuels Team, http://www.osti.gov/bridge.

[122] Liu, J., Peng, H., Hagena, J., Filipi, Z., “Engine-in-the-loop study of the stochastic dynamic programming optimal control design for a hybrid electric HMMWV”, in press, International Journal of Heavy Vehicle Systems, 2007